Westfälische
Wilhelms-Universität
Münster

Singular Regularization of Inverse Problems

Bregman Distances and their Applications to Variational Frameworks with Singular Regularization Energies

Martin Benning

12.05.2011

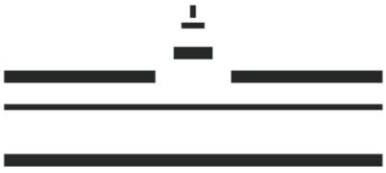

Westfälische
Wilhelms-Universität
Münster

› Singular Regularization of Inverse Problems

Bregman Distances and their Applications to Variational Frameworks

with Singular Regularization Energies

Fach: Mathematik

Inaugural-Dissertation zur Erlangung des
Doktorgrades der Naturwissenschaften
im Fachbereich Mathematik und
Informatik der Mathematisch-
Naturwissenschaftlichen Fakultät
der Westfälischen Wilhelms-Universität
Münster

wissen.leben
WWU Münster

vorgelegt von
Martin Benning
aus Rhede
- Mai 2011 -

Dekan:	Prof. Dr. Matthias Löwe
Erster Gutachter:	Prof. Dr. Martin Burger
Zweite Gutachterin:	Dr. Elena Resmerita
Tag der mündlichen Prüfung:	28.06.2011
Tag der Promotion:	

Abstract

This thesis comments on the use of Bregman distances in the context of singular regularization schemes for inverse problems. According to previous works the use of Bregman distances in combination with variational frameworks, based on singular regularization energies, leads to improved approximations of inverse problems solutions. The Bregman distance has become a powerful tool for the analysis of these frameworks, and has brought iterative algorithms to life that enhance the quality of solutions of existing frameworks significantly. However, most works have yet considered Bregman distances in the context of variational frameworks with quadratic fidelity only.

One of the goals of this thesis is to extend analytical results to more general, nonlinear fidelity terms arising from applications as e.g. medical imaging. Moreover, the concept of Eigenfunctions of linear operators is transferred to nonlinear operators arising from the optimality conditions of the variational frameworks.

From a computational perspective, a novel compressed sensing algorithm based on an inverse scale space formulation is introduced. Furthermore, important concepts related to Bregman distances are carried over to non-quadratic frameworks arising from the applications of dynamic Positron Emission Tomography and Bioluminescence Tomography.

Key Words: Singular Regularization Energies, Error Estimation, Bregman Distance, Discrepancy Principle, Eigenfunction Theory, Regularization Theory, Imaging, Image Processing, Sparsity, Compressed Sensing, Inverse Scale Space, Adaptivity, Greedy Methods, Total Variation Regularization, Infimal Convolution Regularization, Dynamic Positron Emission Tomography, Bioluminescence Tomography

Acknowledgments

I want to thank

Martin Burger, for giving me the opportunity to work on an interesting and challenging topic in one of the nicest workgroups on this planet. For giving interesting insights into the Austrian culture and language. For having special discussions about football, and for the mandatory disagreements which team is best. For being a mentor who always takes care of what is best for his students. And – of course – for supervising this thesis.

Elena Resmerita, for co-reviewing this thesis. For being a wonderful host during my stay at the RICAM in Linz and for arousing my interest in sparse regularization energies.

Stanley Osher, for giving me the opportunity to visit him and his workgroup at UCLA, and to attend IPAMs 10th anniversary. And for having the chance for an interesting discussion during lunch at the UCLA Faculty Center.

My colleagues

- Jahn Müller – for being one of my best friends and for being the living proof that too much hair is overrated
- Alex Sawatzky – for being my travel mate; if you can share the same bed you can share everything
- Marzena Franek – for being the better half of the office of bad jokes
- Christoph Brune – for lots of fruitful discussions; and for making a hilarious impression while puncturing balloons at his wedding
- Bärbel Schlake – for superb cake and for a face at the skiseminar no one could ever imitate
- Frank Wübbeling – for wise advice and for having a laughter worse than mine
- Michael Möller – for all the interesting discussions, for spontaneously giving me a home while I was lost in LA, and for the cocktail unmixing
- Bahne Christiansen – for organizing all those amazing skiseminars
- Ralf Engbers – for working on the dynamic PET stuff for which I do not find the time any more; and for demonstrating that the alternative to little hair is gray hair
- Thomas Kösters – for various variants of EM-code, and for still finishing his thesis despite all my mean comments

- Marcisse Fouego – for belonging to one of the few people laughing about my jokes
- Jan Hegemann – for intending to get acknowledged by correcting just a few words of this thesis
- Felix Albrecht – for organizing the institute to buy its own Wii
- Louise Reips – for having the patience of still reminding me whenever I am talking too fast
- Martin Drohmann – for sharing the BVB-enthusiasm
- Chantal Oberson-Ausoni – for subtle humor and sarcasm, which is probably not meant this way
- Kathrin Smetana – for all the football discussions and the neverending stories of which club is having the best players and the best fans
- Patrick Henning – for still keeping track despite all the obstacles on his desk
- Rene Milk – for often being in a fit of laughter, when Felix did something terribly wrong

and all of you that I forgot to mention, or for which I could not find the right words: You are simply the best!

My student assistant Pia Heins, for lots of interesting questions and discussions. For being better organized than me, and for helping me out with Martins notes when I had lost mine. And for being annoyed in a friendly way whenever I have to make another Heins-Ketchup joke again.

Xiaoqun Zhang, for interesting discussions, and for introducing me to BLT.

My proof-readers Michael Möller, Jahn Müller, Ralf Engbers and Christoph Brune, for preserving this thesis from having even more mistakes than the ones that are already contained.

Antje Brackemeyer, for being the sweetest distraction from work. For always being patient with me for the last couple of months. For listening to my thoughts and doubts. For giving me advice and a perspective I needed when things did not work out. And for always being there. I love you.

My family, Frank, Marie-Theres and Maximlian Benning, Sabrina, Torsten and Sophia Majert, and Nero. For the best family I could ever imagine. For all the support, and for never loosing faith in me and in what I am doing. You gave me more than I could ever give back to you. Thank you!

My friends, Markus, Alex, Matthias, Hendrik, Marion, Antje, all those Martins, Ben, Christian, Andree, all those Steffis, Daniel, Fabian, Felix, Jan, Jens, Julia, Vanessa, Stephan, Michael, Philipp, Eric, Nick, Shemra, Allison, Olga, Thomas, Tobias, Ute, and many many more, for having turned the last three years into very special ones.

The German Research Foundation DFG for supporting me through the project *Regularization with singular energies*.

And all those that deserve to be mentioned here but have been forgotten. Sorry for that!

Contents

List of Figures

List of Tables

Nomenclature

$\mathbb{N}$	The set of natural numbers
$\mathbb{N}_0$	The set of natural numbers and zero
$\mathbb{Z}$	The set of integer numbers
$\mathbb{R}$	The set of real numbers
$\mathbb{R}_{>0}$	The set of positive real numbers
$\mathbb{R}_{\geq 0}$	The set of nonnegative real numbers
$\mathbb{R}^n$	The n-dimensional vector space with elements in $\mathbb{R}$
S^{n-1}	The n-dimensional unit sphere
$\theta^\perp$	The set of vectors orthogonal to θ
$\mathcal{T}_k(\mathbb{R}^n)$	The vector space of k-tensors
$\mathrm{Sym}^k(\mathbb{R}^n)$	The vector space of symmetric k-tensors
$\mathcal{X}$	A (real) Banach space
$\mathcal{X}^*$	The dual space of $\mathcal{X}$
$\mathcal{L}(\mathcal{X}, \mathcal{Y})$	The space of all linear operators $K : \mathcal{X} \to \mathcal{Y}$
$L^p(\Omega)$	The space of Lebesgue measurable functions such that $\|u\|_{L^p(\Omega)} < \infty$ holds
$L^p_{\geq 0}(\Omega)$	All positive functions $u \in L^p(\Omega)$
$L^p_{\mathrm{loc}}(\Omega)$	The space of Lebesgue measurable functions such that $\|u\|_{L^p(\Psi)} < \infty$ holds for every compact $\Psi \subset \Omega$
$L^p(\Omega, \mathrm{Sym}^k(\mathbb{R}^n))$	The space of Lebesgure measurable symmetric k-tensor fields
ℓ^p	The space of sequences with $\sum_x \|u(x)\|^p$ converging in $\mathbb{R}$
$\ell^p_{\geq 0}$	The space of nonnegative sequences in ℓ^p
$W^{k,p}(\Omega)$	The space of Sobolev functions
$W^{k,p}(\Omega, \mathrm{Sym}^l(\mathbb{R}^n))$	The Sobolev space of k-differentiable k-symmetric fields that are in L^p

$C^l(\Omega)$	The space of l-differentiable functions
$C_0^l(\Omega)$	The space of l-differentiable functions with compact support
$C^l(\Omega, \mathrm{Sym}^k(\mathbb{R}^n))$	The space of l-differentiable k-symmetric tensor fields
$\mathcal{D}'(\Omega)$	The space of distributions over $\mathcal{D}(\Omega) = C_0^\infty(\Omega)$
$\mathrm{BV}(\Omega)$	The space of functions with bounded variation
$\rightharpoonup$	Convergence in the weak topology
$\rightharpoonup^*$	Convergence in the weak-* topology
$A \succeq 0$	The matrix A is positive semidefinite
D^α	The α-th (weak) partial derivative
$\mathrm{dom}(G)$	The effective domain of a functional $G : \mathcal{X} \to \mathbb{R} \cup \{+\infty\}$
$d_v G(u)$	The directional derivative of G at u in direction v
$d^2_{v,w} G(u)$	The second directional derivative of G at u in direction w
$dG(u)$	The Gâteaux-derivative of G
G'	The Fréchet-derivative of G
$DG(u)$	The Jacobi matrix of the operator G
$D^2G(u)$	The Hesse matrix of the functional G
G^*	The convex conjugate of G
G^{**}	The biconjugate of G
$D_G(u, v)$	The Bregman Distance between u and v
$D_G^\zeta(u, v)$	The Bregman Distance between u and v for a particular subgradient ζ
$D_G^{\mathrm{symm}}(u, v)$	The symmetric Bregman Distance between u and v
$\partial G(u)$	The subdifferential of a convex functional G at u
$\|u\|_{\mathcal{X}}$	The norm mapping for $u \in \mathcal{X}$
$\langle p, u \rangle_{\mathcal{X}}$	The dual product, see equation (2.1)
$\mathrm{TV}(u)$	The total variation of u, see equation (2.19)
$\mathrm{TV}^l(u)$	The total variation of u of order l, see equation (2.20)
$\mathrm{ICTV}_\beta(u)$	The infimal convolution of $\mathrm{TV}(u)$ and $\mathrm{TV}^2(u)$
GTV_β	The generalized total variation of u, see equation (4.11)
$\mathrm{KL}(f, Ku)$	The Kullback-Leibler fidelity, see equation (4.22)
iff	If and only if
$\mathcal{R}(K)$	The range of an operator K

Chapter 1

Introduction

The basic goal of this thesis is to explore further capabilities of Bregman distances in the context of regularizing inverse problems with singular regularization energies.

In inverse problems one aims at solving an operator equation for the input argument. These operator equations arise from the modeling of a specific process; e.g. a physical process that can be described by partial differential equations (PDE). In many applications, as for instance material inspection, ocean acoustic tomography, or seismic as well as medical imaging, data is measured that can be interpreted as the output of such a model. The goal is to identify input parameters of the particular model that produce the measured output data. Thus, the particular model needs to be inverted.

However, these models are usually not invertible, and in addition very sensitive to measurement errors in the data. Consequently, mathematical tools are needed to replace the non invertible inverse problem by an invertible approximation of that problem. One major concept for finding approximate solutions is the construction of functionals that ideally posses one existing, unique stationary point, close to the unknown solution of the original non-invertible inverse problem in some error measure. These functionals usually consist of two parts: a fidelity term that controls the deviation between the measured output data and the model applied to input parameters, and a regularization term that allows to force the input parameters to satisfy certain properties.

Standard choices for regularization energies are usually differentiable functionals; however, depending on the type of application considered it can be of interest to investigate regularization energies with singularities that are no longer differentiable in the common sense. In the course of this work we mainly want to focus on applications that involve the use of singular regularization energies.

As one may expect, from a mathematical point of view singular regularization energies are more difficult to handle than regular regularization energies. For example, the question of estimating the difference between the solution of the non-invertible and of the approximate inverse problem with respect to the measurement error in the measured data has been a mathematical issue until the beginning of the previous decade, due to the lack of an appropriate error measure when using singular regularization energies.

In terms of error estimation the introduction of the Bregman distance as an error measure has marked a turning point in the analysis of at least convex singular regularization energies and moreover has laid the foundation for a unified error estimation framework for both convex regular and singular regularization energies.

Bregman distances of convex, singular regularization energies have not only become a tool for the mathematical analysis of error propagation but also a tool for the development of iterative

schemes and efficient algorithms, yielding improved approximations. In case of singular, convex and one-homogeneous regularization energies with large multivalued subdifferentials these schemes have led to improved solutions while still suppressing the measurement noise.

However, though the introduction of the Bregman distance to various fields of inverse problems is now more than a decade ago, still numerous related issues wait to be explored. As for instance, Bregman distances in terms of error estimation are well established when dealing with quadratic fidelities. Nevertheless, many important applications like Positron Emission Tomography (PET) or Synthetic Aperture Radar (SAR) imply the use of different, nonlinear fidelities.

One major contribution of this thesis is the derivation of error estimates for convex singular regularization energies in connection with various (possibly nonlinear or even non-differentiable) fidelity terms other than the standard quadratic fidelities.

Another major contribution is the extension of the mathematical analysis of variational schemes with singular regularization terms to a general Eigenfunction theory. The use of the Bregman distance allows the computation of analytical solutions for data given in terms of an Eigenfunction, even in the presence of noise.

In addition we want to modify and apply existing concepts of algorithms based on Bregman distances to solve the large-scale application of parameter identification for dynamic PET reconstruction quantitatively. Moreover, we will present a novel algorithmic approach based on inverse scale space theory for the efficient and stable solution of problems arising in compressed sensing, as for instance the application of Bioluminescence Tomography (BLT).

In the following section we want to recall the basic motivations for this work, while afterwards we are going to outline the contributions of this thesis. Finally, we will give a sketch of how this work is organized.

1.1 Motivation

Mathematically, linear inverse problems can be modeled as computing a function $\tilde{u}$ from the operator equation

$$K\tilde{u} = g$$

for measured data g. However, usually K^{-1} does not exist, and in addition, the data g is corrupted by measurement noise, i.e. there exists an operator $\mathcal{N}$ that transfers g to a function $f = \mathcal{N}(g)$ corrupted by noise.

A common approach for finding approximate solutions close to $\tilde{u}$ is to compute the minimizer of a convex functional of the type

$$\underbrace{H_f(Ku)}_{\text{Fidelity Term}} + \alpha \underbrace{J(u)}_{\text{Regularization Term}},$$

with both $H_f(Ku)$ and J being convex functionals, and for a regularization parameter $\alpha > 0$. If, for instance, the measured data f is given in terms of $g = f + n$ for n being a Gaussian random variable with mean zero and variance σ, the common approach is to consider the quadratic fidelity term $H_f(Ku) = 1/2\|Ku - f\|_2^2$. Thus, in case of this particular fidelity, the approximate solution of $\tilde{u}$ can be obtained via

$$\hat{u} = \arg\min_u \left\{ \frac{1}{2} \|Ku - f\|_2^2 + \alpha J(u) \right\}. \tag{1.1}$$

Typical convex regularization terms are quadratic energies of the form $J(u) = \|Bu\|_2^2$, for a linear operator B, since they are easy to analyze and make the computation of (1.1) fairly easy. Nevertheless, the choice of a particular regularization term is obviously dependent on the application and the related a-priori information on the solution. If for instance a solution is assumed to be smooth the use of $J(u) = \|Bu\|_2^2$ with $B = \nabla$ (or even with higher order derivatives) appears to be reasonable. If however a solution is assumed to have sharp edges (which is the case for many applications in imaging or image processing) the choice of this regularization energy would represent a bad choice, since the functions with discontinuities are not smooth at these discontinuities. A regularization energy that is suitable for the recovery of functions with discontinuities is the total variation (TV) seminorm

$$J(u) = \sup_{\substack{\varphi \in C_0^\infty(\Omega;\mathbb{R}^n) \\ \|\varphi\|_\infty \leq 1}} \int_\Omega u \, \mathrm{div}\varphi \, dx \approx \|\nabla u\|_1 \, .$$

In contrast to $J(u) = \|\nabla u\|_2^2$ the above regularization is not differentiable in the common sense, which is easily visible by considering the informal optimality condition of (1.1) with J being the total variation seminorm regularization, i.e.

$$K^* \left(f - Ku\right) = \mathrm{div}\left(\frac{\nabla u}{|\nabla u|}\right) \, .$$

Obviously for homogeneous parts of a function u (which means $\nabla u = 0$ at these parts) the above equation is undefined.

Considering solutions $\hat{u}$ of (1.1) as approximations for $\tilde{u}$ again, the basic question that arises is: how close is $\hat{u}$ to $\tilde{u}$, with respect to the error in the data f? For convex and subdifferentiable regularization energies the question has been answered in terms of the Bregman distance. The Bregman distance is the difference between a functional evaluated at the point u and its linearization at a point v, i.e. the Bregman distance between u and v for the corresponding functional J is defined as

$$D_J^p(u, v) = J(u) - J(v) - \langle p, u - v \rangle \, ,$$

for $p \in \partial J(v)$, with $\partial J(v)$ denoting the subdifferential of J at v. For this particular measure it has been shown that the difference between $\hat{u}$ and $\tilde{u}$ is bounded by

$$D_J^p(\hat{u}, \tilde{u}) \leq \frac{\sigma^2}{2\alpha} + \alpha \frac{\|q\|_2^2}{2} \, ,$$

for an element q satisfying $K^*q = p \in \partial J(\tilde{u})$.

The discovery of the Bregman distance as an adequate error measure brings up another question: can the application of Bregman distances be useful in the context of variational frameworks with singular regularization energies aside from error estimation? The answer that has been found is yes. The replacement of the regularization term by its corresponding Bregman distance leads to an iterative scheme

$$\hat{u}_k = \arg\min_u \left\{ \frac{1}{2} \|Ku - f\|_2^2 + \alpha D_J^{p_{k-1}}(u, u_{k-1}) \right\} \, ,$$

which has been named iterative refinement method or Bregman iteration. In connection with singular regularization terms as e.g. the TV seminorm the Bregman iteration is a powerful tool

that allows to compensate drawbacks of (1.1) (e.g. loss of contrast in case of TV regularization) while effectively suppressing the noise up to large amount of iterations.

The successful use of the Bregman distance in the context of regularization of inverse problems with singular energies is the overall motivation of this thesis. Based on this we want to summarize the contributions of this thesis in the following section.

1.2 Contributions

The concept of error estimation with Bregman distances as an error measure is well understood in case of quadratic fidelity only recently. Nevertheless, in many relevant applications the use of a quadratic fidelity is insufficient, for instance to describe the behavior of the measurement noise, and likely should be replaced by a different fidelity. For example, in PET the Kullback-Leibler fidelity

$$\mathrm{KL}(f, Ku) = \int_\Sigma \left[f(y) \ln \left(\frac{f(y)}{(Ku)(y)} \right) - f(y) + (Ku)(y) \right] \, d\mu(y)$$

appears to be a much more suitable fidelity to incorporate the fact that the noise in the data obeys a Poisson process. However, error estimates in the Bregman distance setting for a solution $\hat{u}$ of

$$\hat{u} = \arg\min_u \{\mathrm{KL}(f, Ku) + \alpha J(u)\}$$

have to our knowledge not yet been analyzed and established. One of the main contributions of this thesis therefore is the derivation of error estimates in the Bregman distance setting for various fidelities other than the quadratic fidelities.

Besides the question of how close to $\tilde{u}$ a solution $\hat{u}$ of a variational framework can be in terms of the Bregman distance we want to raise the issue of when and under which circumstances $\tilde{u}$ can exactly be recovered, even in the presence of noise. For that reason the notion of Eigenfunctions is transferred to subdifferentiable functionals. For functions $u \neq 0$ that satisfy the property

$$\lambda K^* K\tilde{u} \in \partial J(\tilde{u})$$

for a constant $\lambda \in \mathbb{R}$ the contribution of this thesis is the analytical computation of solutions $\hat{u}$ of (1.1) for $f = K\tilde{u}$. Moreover, for data f given in terms of an Eigenfunction we provide analytical solutions of the Bregman iteration scheme and its time-continuous analogue, the inverse scale space.

Another contribution of this thesis is the development of a novel algorithm for compressed sensing applications. In case of $J(u) = \|u\|_{\ell^1}$ the inverse scale space formulation allows the development of an algorithm that reduces the compressed sensing setting to an iterative sequence of low dimensional least squares problems.

Finally, in applied mathematics theoretical results are only as good as they are capable to applications. As a further contribution, in this thesis computational realizations of synthetic examples to support the theoretical contributions are developed and analyzed. Moreover, tools based on Bregman distances are used for the first time for the quantitative solution of the large-scale application of dynamic PET, as well as for an efficient solution of a BLT example.

1.3 Organization of this Work

In Chapter 2 we want to provide the mathematical tools needed in the course of this work. A short review of the recent impact of Bregman distances in the context of inverse problems is given in Chapter 3. To conclude the providing chapters, in Chapter 4 a collection of singular regularization energies and typical fidelities arising from various applications is presented.

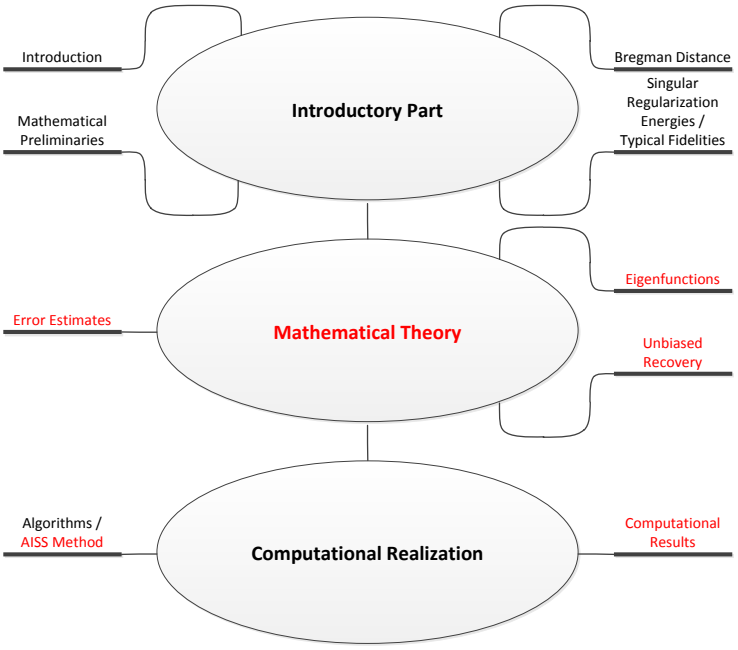

Figure 1.1: Organization of this work. The red coloured parts indicate the contributions.

In Chapter 5 the first major contribution of this thesis follows, which is the development of error estimates in the Bregman distance setting for the fidelities presented in Chapter 4. Subsequently, in the Chapters 6 and 7 the mathematical theory passes over from the question of finding reconstructions close to the unknown exact solution (with respect to an estimate depending on the measurement noise) to the question of how to analytically compute the exact solution in the absence and presence of noise. The Chapters 5, 6 and 7 represent the mathematical-theory-block of this thesis.

The last two chapters of this thesis are concerned with computational issues. In Chapter 8 a collection of algorithms needed for the applications considered in Chapter 9 is presented. As a major contribution, Section 8.2 provides a novel algorithm for compressed sensing applications. Finally, Chapter 9 is divided into three parts. In the first part, computational results on synthetic data are generated to support theoretical results of the Chapters 5, 6 and 7. The second part deals with the issue of the quantitative identification of physiological parameters in the dynamic PET setup. Last but not least, in the third part results of this work are transferred to the application of BLT.
An overview of how the work is organized is given in Figure 1.1.

Chapter 2

Mathematical Preliminaries

This chapter provides the mathematical background needed in the course of this work. We want to give a brief overview on Banach spaces and their dual spaces first. Afterwards we define linear inverse problems, while subsequently motivating approximate solutions by considering a Bayesian framework. This naturally leads to the questions of variational calculus and of appropriate function spaces. Finally, we are going to recall basic tools of convex analysis.

2.1 Banach and Dual Spaces

Throughout this work Banach spaces and duality between Banach spaces will play an important role. Consequently, we briefly want to recall the definition of a Banach space and its dual in the following (based on [67]).

Definition 2.1 (Banach Space)**.** *Let $\mathcal{X}$ be a real vector space.*

- *A mapping $\|\cdot\|_{\mathcal{X}} : \mathcal{X} \to [0, \infty[$ is a norm on $\mathcal{X}$ if*
  1. $\|u\|_{\mathcal{X}} = 0 \Leftrightarrow u = 0 \ \forall u \in \mathcal{X}$,
  2. $\|\lambda u\|_{\mathcal{X}} = |\lambda| \|u\|_{\mathcal{X}} \ \forall u \in \mathcal{X}, \lambda \in \mathbb{R}$,
  3. $\|u + v\|_{\mathcal{X}} \leq \|u\|_{\mathcal{X}} + \|v\|_{\mathcal{X}} \ \forall u, v \in \mathcal{X}$.
- *A normed real vector space $\mathcal{X}$ is called (real) Banach space if it is complete, i.e. if any Cauchy sequence $(u_n)_{n \in \mathbb{N}}$ has a limit $u \in \mathcal{X}$. More precisely, if $\lim_{m,n \to \infty} \|u_m - u_n\|_{\mathcal{X}} = 0$ holds, then there exists a function $u \in \mathcal{X}$ with $\lim_{n \to \infty} \|u_n - u\|_{\mathcal{X}} = 0$.*

In order to define the dual space of a Banach space, we need to define the space of linear mappings first.

Definition 2.2 (Space of Linear Mappings)**.** *Let $\mathcal{L}(\mathcal{X}, \mathcal{Y})$ denote the space of all linear operators $K : \mathcal{X} \to \mathcal{Y}$ that are bounded in the sense that*

$$\|K\|_{\mathcal{X},\mathcal{Y}} := \sup_{\|u\|_{\mathcal{X}}=1} \|Ku\|_{\mathcal{Y}} < \infty$$

holds. The space $\mathcal{L}(\mathcal{X}, \mathcal{Y})$ is a normed space with operator norm $\|\cdot\|_{\mathcal{X},\mathcal{Y}}$.

In this context we want to recall the following important result.

Theorem 2.1. *If $\mathcal{Y}$ is a Banach space then $\mathcal{L}(\mathcal{X}, \mathcal{Y})$ is a Banach space.*

Now we can continue defining the dual space of a Banach space.

Definition 2.3 (Dual Space)**.** *Let $\mathcal{X}$ be a Banach space. The space $\mathcal{X}^* := \mathcal{L}(\mathcal{X}, \mathbb{R})$ of linear functionals on $\mathcal{X}$ is called dual space of $\mathcal{X}$. Due to Theorem 2.1 we know that $\mathcal{X}^*$ is a Banach space equipped with the operator norm*

$$\|p\|_{\mathcal{X}^*} := \sup_{\|u\|_{\mathcal{X}}=1} |p(u)| = \sup_{u\in\mathcal{X}\setminus\{0\}} \frac{|p(u)|}{\|u\|_{\mathcal{X}}} = \sup_{\|u\|_{\mathcal{X}}\leq 1} |p(u)|\,, \tag{2.1}$$

for $p(u)$ defined as the functional

$$\langle p, u\rangle_{\mathcal{X}^*\times\mathcal{X}} := p(u)\,. \tag{2.2}$$

The functional (2.2) is called dual product. For simplicity, we are going to write $\langle p, u\rangle_{\mathcal{X}}$ respectively $\langle u, p\rangle_{\mathcal{X}^*}$ instead of $\langle p, u\rangle_{\mathcal{X}^*\times\mathcal{X}}$ throughout this work.

Remark 2.1. Note that the definition of the dual product implies the estimate

$$\langle p, u\rangle_{\mathcal{X}} \leq |\langle p, u\rangle_{\mathcal{X}}| \leq \|p\|_{\mathcal{X}^*}\|u\|_{\mathcal{X}}\,.$$

The definition of dual spaces also suggests the definition of dual operators.

Definition 2.4 (Dual Operator)**.** *Let $\mathcal{X}$ and $\mathcal{Y}$ be Banach spaces. For an operator $K \in \mathcal{L}(\mathcal{X}, \mathcal{Y})$ the dual or adjoint operator $K^* \in \mathcal{L}(\mathcal{X}^*, \mathcal{Y}^*)$ is defined via the relation*

$$\langle K^* v, u\rangle_{\mathcal{X}} = \langle v, Ku\rangle_{\mathcal{Y}}\,,$$

for all $v \in \mathcal{Y}^*$ and $u \in \mathcal{X}$. Furthermore, it is easy to see that $\|K^*\|_{\mathcal{Y}^*,\mathcal{X}^*} = \|K\|_{\mathcal{X},\mathcal{Y}}$ is satisfied.

2.2 Inverse Problems

When dealing with applications that involve the reconstruction of parameters from certain measurements, as it is the case e.g. in imaging science, the mathematical modeling of these applications usually leads to inverse problems. In inverse problems the goal is to compute a function $\tilde{u} \in \mathcal{U}(\Omega)$ from the operator equation

$$K\tilde{u} = g\,, \tag{2.3}$$

with given data $g \in \mathcal{V}(\Sigma)$. Here $\mathcal{U}(\Omega)$ and $\mathcal{V}(\Sigma)$ are Banach spaces of functions on bounded sets Ω respectively Σ, and K denotes an operator $K : \mathcal{U}(\Omega) \to \mathcal{V}(\Sigma)$ that maps from one Banach space to the other one. In the course of this work we want to call g the *exact data* and $\tilde{u}$ the *exact solution.*

For simplicity, we are going to consider only linear operators throughout this work, since all applications that are going to be considered involve only linear operators. Nevertheless, many of the theoretical results that will be presented are adaptable to general operators.

Due to the situation of discrete measurements encountered in practice we shall also allow Σ to be discrete with point measures.

The challenge of solving (2.3) lies in the ill-posedness of most inverse problems. The following definition goes back to [63].

Definition 2.5. *A problem is called well-posed, if*

- *there exists a solution to the problem*
- *the solution is unique*
- *the solution depends continuously on the input data*

If a problem is not well-posed, it is called ill-posed.

In most inverse problems the third condition is violated. Usually, the operator K cannot be inverted continuously due to the compactness of K (cf. [51]). Even if the considered inverse problem is not ill-posed (as e.g. if K is the identity operator) solving (2.3) can be impossible due to measurement errors, i.e. the exact data g are usually not available. Hence, we face to solve the inverse problem

$$Ku = f \tag{2.4}$$

instead of (2.3), with $u \in \mathcal{U}(\Omega)$ and $f \in \mathcal{V}(\Sigma)$, while g and f differ from each other in a certain amount. This difference is referred to as being *noise* (or systematic and modeling errors, which we shall not consider here). In applications for which the measurement error can be described as a Gaussian random variable with mean zero and standard deviation σ the difference between g and f is bounded in the L^2-sense, i.e.

$$\|g - f\|_{L^2(\Sigma)} \leq \sigma \,.$$

Since f in comparison to g is corrupted by measurement errors, we want to refer to f as being the *noisy data*.

The question that arises for inverse problems is how to find a robust approximation $\hat{u}$ of $\tilde{u}$, despite the ill-posedness of the inverse problem and its underlying measurements corrupted by noise?

In the following we are going to give a short motivation based on Bayesian modeling in order to suggest the use of variational regularization schemes to achieve this robust approximation.

2.3 Bayesian Modeling and Gibbs Priors

In order to find solutions of (2.4) close to the true solution $\tilde{u}$ of (2.3) with additional knowledge on how the noise of the data f is distributed, the approach of Bayesian modeling is very popular for computing approximate solutions of $\tilde{u}$. The idea is to maximize the a-posteriori probability (MAP) of a probability distribution obeying Bayes' formula, i.e. we look for a function u that fulfills

$$u \in \arg\max_u P(u|f) = \arg\min_u -\log\left(P(u|f)\right) \,, \tag{2.5}$$

with P denoting the a-posteriori probability density of u for given data f. In the following we want to investigate a discrete analogue of (2.4), i.e.

$$\overline{K}u = f \,, \tag{2.6}$$

for $\overline{K} : \mathcal{U}^p \to \mathcal{V}^q$ being a linear operator operating on finite dimensional Banach spaces $\mathcal{U}^p$ and $\mathcal{V}^q$. $\overline{K}$ is usually the concatenation of K with a sampling or local averaging.

In a discrete setup Bayes' formula states that the discrete a-posteriori (or conditional) probability distribution $P(u|f)$ of a function u for given data f can be expressed by the a-posteriori probability distribution $P(f|u)$ and the a-priori probability distributions $P(u)$ and $P(f)$, i.e.

$$P(u|f) = \frac{P(f|u)P(u)}{P(f)} .$$

The a-priori probability distribution is most frequently modeled via a Gibbs-prior, i.e.

$$P(u) = c \exp\left(-\alpha J(u)\right) ,$$

for a positive constant α, a normalization constant c and a regularization energy J, which is often supposed to be convex.

2.3.1 Gaussian Noise

If the discrete data f is perturbed by additive Gaussian noise n with mean zero, we can rewrite (2.6) to

$$\overline{K}\tilde{u} + n = f ,$$

with $\tilde{u}$ denoting the exact discrete solution of $\overline{K}\tilde{u} = g$ for exact, non-perturbed discrete data g. The noise n is unknown, but the distribution of n is supposed to be normal with mean zero. Hence, we have

$$P(n) = c(q) \exp\left(-\frac{\|n\|_2^2}{2\sigma^2}\right) = c(q) \exp\left(-\frac{\|\overline{K}\tilde{u} - f\|_2^2}{2\sigma^2}\right)$$

for given noise variance σ^2 and a normalization constant $c(q)$ depending on the dimension q. In order to find u close to $\tilde{u}$, a reasonable choice as a model for $P(u|f)$ and $P(f|u)$ would therefore be

$$P(u|f) = P(f|u) = c(q) \exp\left(-\frac{\|\overline{K}u - f\|_2^2}{2\sigma^2}\right) .$$

Inserting these probabilities into Bayes' formula and subsequently computing the negative log-likelihood, i.e. $-\log\left(P(u|f)\right)$, in order to maximize $P(u|f)$ yields

$$\begin{aligned} \hat{u} \in & \operatorname*{arg\,min}_{u \in \mathrm{dom}(J)} \left\{ -\log\left(P(u|f)\right) \right\} \\ = & \operatorname*{arg\,min}_{u \in \mathrm{dom}(J)} \left\{ \frac{1}{2}\|\overline{K}u - f\|_2^2 + \alpha J(u) \right\} , \end{aligned} \tag{2.7}$$

where we have neglected all constants that do not affect the minimizer. Note that the argmin can be multivalued (e.g. if $\overline{K}$ has a non-trivial nullspace and if J is not strictly convex), and thus we have an inclusion instead of an equality.

With (2.7) we have derived a variational model that allows us to compute an estimate $\hat{u}$ of $\tilde{u}$ by abusing the fact that the noise is Gaussian and by incorporating a-priori knowledge on $\hat{u}$ via a regularization functional $J(u)$.

Obviously, in order to model different noise distributions we can derive different variational frameworks by computing the MAP estimate for different choices of $P(u|f)$ and $P(f|u)$, according to the distribution of the noise. We are going to present numerous fidelities in Chapter 4 for which a motivation in terms of Bayesian modeling could be given, which is however not our goal in this thesis.

Nevertheless, the MAP estimates naturally lead to the questions of existence, uniqueness, and computation of minimizers of functionals, which is part of variational calculus. Before we are going to discuss the variational calculus in detail in the upcoming Chapter 2.4, we want to make sure that we are also able to consider variational models in an analytical framework.

2.3.2 From Discrete to Continuous Variational Frameworks

A-priori knowledge on a solution can usually be incorporated by restricting the functional space in which the solution has to lie in. For example, if we know that the solution is supposed to be bounded in the ℓ^2-sense, we can simply choose $J(u) = 1/2\|u\|_{\ell^2}^2$. In that case we are going to discover that the solution of (2.7) is

$$0 = (\overline{K})^T \left(\overline{K}u - f\right) + \alpha u\,,$$

with $(\overline{K})^T$ denoting the transpose of $\overline{K}$. If $\overline{K}$ is indeed the concatenation of K and a sampling operator in the limiting case $p, q \to \infty$ of infinite samples we therefore have

$$0 = K^* \left(K\hat{u} - f\right) + \alpha\hat{u}\,,$$

with K^* denoting the adjoint operator of K, which is – as we will point out in the following chapter – the solution of

$$\hat{u} \in \operatorname*{arg\,min}_{u\in\mathrm{dom}(J)} \left\{ \frac{1}{2}\|Ku - f\|_{L^2(\Sigma)}^2 + \alpha\|u\|_{L^2(\Omega)}^2 \right\}.$$

Hence, though the derivation of the variational model is discrete, we can also study the continuous L^2-variational framework

$$\hat{u} \in \operatorname*{arg\,min}_{u\in\mathrm{dom}(J)} \left\{ \frac{1}{2}\|Ku - f\|_{L^2(\Sigma)}^2 + \alpha J(u) \right\} \tag{2.8}$$

instead of the discrete setup. Moreover, if we allow the measures on which we integrate to be point measures, the discrete and the continuous setup can be written in a unified way.

We want to mention that in terms of random variables the transition from discrete to continuous frameworks is not straight forward. However, although we have motivated the derivation of variational frameworks via Bayes' formula, which would imply our variables to be random variables, we are going to deal with deterministic variables only. The derivation via Bayes' formula has only been done for motivation purposes. Any limiting cases that are going to be considered are limiting cases for deterministic variables. We neither want to address the question of finding a continuous analogue to Bayes' formula, nor do we want to attempt defining a continuous analogue of randomly distributed noise.

2.4 Variational Calculus

The idea of Bayesian modeling in Section 2.3 has led to the idea of considering variational minimization schemes of the type

$$\hat{u} \in \underset{u \in \mathrm{dom}(J)}{\arg\min} \left\{ H_f(Ku) + \alpha J(u) \right\}, \tag{2.9}$$

with $H_f : \mathcal{V}(\Sigma) \to \mathbb{R} \cup \{+\infty\}$ and $J : \mathrm{dom}(J) \to \mathbb{R} \cup \{+\infty\}$ and $\alpha \in \mathbb{R}_{>0}$, in order to find approximate solutions $\hat{u}$ close to $\tilde{u}$ satisfying (2.3).

Variational calculus mainly deals with the questions of existence, uniqueness, and computation of stationary points of functionals in Banach spaces (in particular function spaces). Finding existent (unique) global minima is one of the important goals when considering variational frameworks like (2.9). We only want to give a short overview on variational calculus here; more information can be found in e.g. [50].

In order to minimize confusion on the use of operators and functionals we make the following definition first.

Definition 2.6. *Let $G : (\mathcal{X}, \tau_1) \to (\mathcal{Y}, \tau_2)$ denote a mapping from a Banach space $\mathcal{X}$ with topology τ_1 to a Banach space $\mathcal{Y}$ with topology τ_2. Then G is called an operator. If $\mathcal{Y}$ – as a special case of a Banach space – is a field, G is called a functional.*

To investigate only functionals with non-empty domain we assume every considered functional to be proper.

Definition 2.7. *A functional $G : \mathcal{X} \to \mathbb{R} \cup \{\infty\}$ is called proper, if the effective domain*

$$\mathrm{dom}(G) := \{u \in \mathcal{X} \mid G(u) < \infty\}$$

is not empty.

The calculus of variations can be seen as a generalization of the computation of extreme values of functions. For that reason, we want to derive a concept of derivatives and gradients for functionals and operators, similar to the one for functions in $\mathbb{R}^n$.

Definition 2.8. *Let $G : \mathcal{X} \to \mathcal{Y}$ be a functional or operator. The directional derivative (also called first variation) at position $u \in \mathcal{X}$ in direction $v \in \mathcal{Y}$ is defined as*

$$d_v G(u) := \lim_{t \downarrow 0} \frac{G(u + tv) - G(u)}{t}, \tag{2.10}$$

if that limit exists.

If we define the function $\varphi_v(\tau) := G(u + \tau v)$, the directional derivative of G is equivalent to $\varphi_v'(\tau)|_{\tau=0}$. Note that by definition the direction v has to lie within the same space as the argument u.

Example 2.1. Let $f \in L_2(\Omega)$ with $\Omega \subset \mathbb{R}^n$ compact and bounded, $K : L_2(\Omega) \to L_2(\Omega)$ be a compact and linear operator and let $G : L_2(\Omega) \to \mathbb{R}_{\geq 0} \cup \{+\infty\}$ be defined as

$$\begin{aligned} G(u) &:= \frac{1}{2} \left\| Ku - f \right\|_{L_2(\Omega)}^2 \\ &= \frac{1}{2} \int_\Omega (Ku - f)^2 dx \,. \end{aligned}$$

We define $\varphi_v(\tau) := H_f(K(u+\tau v))$ for $v \in L_2(\Omega)$ and obtain

$$\begin{aligned}\varphi_v'(\tau)|_{\tau=0} &= \frac{1}{2}\frac{d}{d\tau}\int_\Omega (K(u+\tau v)-f)^2 dx\Big|_{\tau=0} \\ &= \int_\Omega Kv\,(Ku-f)\,dx = \langle Kv, Ku-f\rangle_{L_2(\Sigma)} \\ &= \langle v, K^*(Ku-f)\rangle_{L_2(\Omega)}\,,\end{aligned}$$

with K^* denoting the adjoint operator of K. The permutation of integration and differentiation is justified, due to [56, Chapter 11, Theorem 2]. Thus, we have obtained

$$d_v G(u) = \langle v, K^*(Ku-f)\rangle_{L_2(\Omega)}$$

as the first variation of H_f at position u in direction v.

Similar to the definition of the first variation (2.10) we are able to define higher variations. Only the first and second variation will be of further interest for us.

Definition 2.9. *Let $G : \mathcal{X} \to \mathcal{Y}$ be a functional or an operator and let $d_v G(u)$ exist. The second directional derivative (also called second variation) at position u in direction w is defined as*

$$d^2_{v,w} G(u) := \lim_{t \downarrow 0} \frac{d_v G(u+tw) - d_v G(u)}{t},$$

if that limit exists.

Furthermore we want to summarize two important and interesting cases of differentiability.

Definition 2.10. *Let $G : \mathcal{X} \to \mathcal{Y}$ be a functional or an operator. The set*

$$dG(u) = \{d_v G(u) < \infty \mid v \in \mathcal{U}\} \tag{2.11}$$

is called Gâteaux-derivative. G is called Gâteaux-differentiable, if (2.11) is not empty.

Henceforth we want to explore for which cases the Gâteaux-derivative consists of only one element. This will lead to the notion of Fréchet-differentiability.

Definition 2.11. *Let $G : \mathcal{X} \to \mathcal{Y}$ be a functional or operator, $\mathcal{X}$ and $\mathcal{Y}$ Banach spaces, and suppose $d_v G(u)$ exists for all $v \in \mathcal{X}$. If there exists a continuous linear functional $G'(u) : \mathcal{X} \to \mathcal{Y}$ such that*

$$G'(u)\,v = d_v G(u) \quad \forall v \in \mathcal{X}, \tag{2.12}$$

and

$$\frac{\|G(u+v) - G(u) - G'(u)\,v\|_{\mathcal{Y}}}{\|v\|_{\mathcal{X}}} \longrightarrow 0\,,\ \textit{for}\ \|v\|_{\mathcal{X}} \to 0$$

hold, then G is called Fréchet-differentiable in u and G' is called Fréchet-derivative.

Note that $G'(u)$ does not need to be linear in u. In our definition u is fixed and the linearity – since we want to derive an analogous expression to classical differentiability – is a restriction to v only.

The functional G is called twice Fréchet-differentiable, if the properties of Definition 2.11 hold for $d^2_{v,v}G(u)$ as well. In that case, we are also going to write $G''(u)(v,v)$ instead of $d^2_{v,v}G(u)$.

Example 2.2. Consider again Example 2.1. The functional is Fréchet-differentiable with the Fréchet-derivative

$$G'(u) = K^*(Ku - f)\,.$$

In analogy to standard calculus we can define partial Fréchet-derivatives, Jacobi- and Hesse-operators for Fréchet-differentiable functionals with multiple arguments.

Definition 2.12. *Let $G : \mathcal{X}_1 \times \mathcal{X}_2 \times \cdots \times \mathcal{X}_n \to \mathcal{Y}_1 \times \mathcal{Y}_2 \times \cdots \times \mathcal{Y}_m$ be a functional or operator that is Fréchet-differentiable with respect to $u_i \in \mathcal{X}_i$, $i \in \{1,\dots,n\}$. Then, G is called partial Fréchet-differentiable in u_i. The partial Fréchet-derivative is denoted with $\partial_{u_i} G_j(u)$, $G_j(u) \in \mathcal{Y}_j$, for $j \in \{1,\dots,m\}$. If G is partial Fréchet-differentiable in every argument, then G is called partial Fréchet-differentiable.*

Definition 2.13 (Jacobian)**.** *Let $G : \mathcal{X}_1 \times \mathcal{X}_2 \times \cdots \times \mathcal{X}_n \to \mathcal{Y}_1 \times \mathcal{Y}_2 \times \cdots \times \mathcal{Y}_m$ be a functional or operator that is partial Fréchet-differentiable. Then, the Jacobi matrix of G is defined as*

$$DG(u) := (\partial_{u_i} G_j(u))_{i\in\{1,\dots,n\}, j\in\{1,\dots,m\}}\,.$$

Definition 2.14 (Hessian)**.** *Let $G : \mathcal{X}_1 \times \mathcal{X}_2 \times \cdots \times \mathcal{X}_n \to \mathcal{Y}$ be an operator or functional that is twice partial Fréchet-differentiable. Then, the Hesse matrix is defined as*

$$D^2G(u) := \left(\partial^2_{u_i,u_j} G(u)\right)_{i,j\in\{1,\dots,n\}}\,.$$

Besides computing potential extremal functions the question of existence and uniqueness arises. The question of existence can be answered via the fundamental theorem of optimization. First, we have to define the term of lower semi-continuity in the special case of a Banach space.

Definition 2.15. *Let $\mathcal{U}$ be a Banach space with topology τ. The functional $G : (\mathcal{U},\tau) \to \mathbb{R}\cup\{+\infty\}$ is called lower semi-continuous at $u \in \mathcal{U}$ if*

$$G(u) \le \liminf_{k\to\infty} G(u_k)\,,$$

for all $u_k \to u$ in the topology τ.

Together with compactness this leads to the fundamental theorem (see [138]).

Theorem 2.2 (Fundamental Theorem of Optimization)**.** *Let $\mathcal{U}$ be a Banach space with topology τ and let $G : (\mathcal{U},\tau) \to \mathbb{R}\cup\{+\infty\}$ be lower semi-continuous. Furthermore, let the level set*

$$\{u \in \mathcal{U} \,|\, G(u) \le M\}$$

be non-empty and compact in the topology τ for some $M \in \mathbb{R}$. Then there exists a global minimum of

$$G(u) \to \min_{u\in\mathcal{U}}\,.$$

Proof. Let $\tilde{G} = \inf_{u \in \mathcal{U}} G(u)$. Then a sequence $(u_k)_{k \in \mathbb{N}}$ exists with $G(u_k) \to \tilde{G}$ for $k \to \infty$. For k sufficiently large, $G(u_k) \leq M$ holds and hence, $(u_k)_{k \in \mathbb{N}}$ is contained in a compact set. As a consequence, a subsequence $(u_{k_l})_{l \in \mathbb{N}}$ exists with $u_{k_l} \to \tilde{u}$, for $l \to \infty$, for some $\tilde{u} \in \mathcal{U}$. From the lower semicontinuity of G we obtain

$$\tilde{G} \leq G(\tilde{u}) \leq \liminf_{k \to \infty} G(u_k) \leq \tilde{G} \,,$$

consequently $\tilde{u}$ is a global minimizer. □

In finite dimensional optimization, compactness is usually caused by boundedness, which is not the case in infinite-dimensional optimization. To still conclude compactness from boundedness, we need a weaker topology. Since we are dealing with Banach spaces and their dual spaces, which contain the Fréchet-derivatives, we can use the so-called weak and weak-* topology, which are defined as follows.

Definition 2.16. *Let $\mathcal{X}$ be a Banach space, with $\mathcal{X}^*$ denoting its dual space. Then the weak topology is defined as*

$$u_k \rightharpoonup u :\Leftrightarrow \langle v, u_k \rangle_{\mathcal{X}} \to \langle v, u \rangle_{\mathcal{X}} \,,$$

for all $v \in \mathcal{X}^*$, and the weak- topology is defined as*

$$v_k \rightharpoonup^* v :\Leftrightarrow \langle u, v_k \rangle_{\mathcal{X}^*} \to \langle u, v \rangle_{\mathcal{X}^*} \,,$$

for all $u \in \mathcal{X}$.

The weak-* topology is weaker than the weak topology on $\mathcal{X}^*$, since we have $\mathcal{X} \subset \mathcal{X}^{**}$. For a reflexive Banach space ($\mathcal{X} = \mathcal{X}^{**}$), weak and weak-* topology are the same. According to the theorem of Banach-Alaoglu, the set $\{v \in \mathcal{X}^* \mid \|v\|_{\mathcal{X}^*} \leq C\}$, for $C \in \mathbb{R}_{>0}$, is compact in the weak-* topology.

Theorem 2.3 (Theorem of Banach-Alaoglu)**.** *Let $\mathcal{X}$ be a Banach space with dual space $\mathcal{X}^*$. Then the set*

$$\{v \in \mathcal{X}^* \mid \|v\|_{\mathcal{X}^*} \leq C\} \,,$$

for $C > 0$, is compact in the weak- topology.*

Hence, we could conclude existence of a global minimum for a given infinite dimensional optimization problem, if we were able to prove lower semi-continuity in the weak-* topology. In that case, we could simply compute the Fréchet-derivative to obtain the desired minimum. Unfortunately, in most cases proving lower semi-continuity in the weak-* topology is not trivial.

2.5 Function Spaces

In inverse problems and especially in variational calculus the function spaces that underly the particular functionals are of significant importance. In the following we want to recall the most important function spaces and tools that will be of major interest throughout this work. We want to start with considering Lebesgue and Sobolev spaces first. This review is based on the introduction of [67], which in turn refers to [1, 75, 104, 132, 137]. Subsequently we want to recall the basic concepts of the space of bounded variation (see e.g. [29, 113]) and a generalization under the aspect of symmetric tensor fields based on [12, 18].

2.5.1 Lebesgue Spaces

In this section we want to briefly summarize the function spaces of Lebesgue-integrable functions. We start considering Lebesgue-measurable functions first, and subsequently are going to define the Lebesgue integral as the foundation for the Lebesgue spaces.

Definition 2.17 (σ-Algebra)**.** *A collection $\mathcal{S}$ of subsets of $\mathbb{R}^n$ is called σ-algebra on $\mathbb{R}^n$ if this collection satisfies the following properties:*

- $\emptyset, \mathbb{R}^n \in \mathcal{S}$,
- $A \in \mathcal{S}$ *implies* $\mathbb{R}^n \setminus A \in \mathcal{S}$,
- *If* $(A_k)_{k\in\mathbb{N}} \subset \mathcal{S}$ *is true, then* $\bigcup_{k=1}^{\infty} A_k \in \mathcal{S}$ *is valid as well.*

With the help of σ-algebras we can define measures as follows.

Definition 2.18 (Measure)**.** *A measure $\mu : \mathcal{S} \to [0, \infty]$ is a mapping with the following properties:*

- $\mu(\emptyset) = 0$,
- *If* $(A_k)_{k\in\mathbb{N}} \subset \mathcal{S}$ *is a sequence of pairwise disjoint sets, then the measure is σ-additive, i.e.*

$$\mu\left(\bigcup_{k=1}^{\infty} A_k\right) = \sum_{k=1}^{\infty} \mu(A_k)\,. \qquad (\sigma\text{-additivity})$$

With these definitions we can establish the notions of Lebesgue-measurable sets and corresponding Lebesgue measures.

Theorem 2.4. *There exists the σ-algebra $\mathcal{B}_n$ of Lebesgue measurable sets on $\mathbb{R}^n$ and the Lebesgue-measure $\mu : \mathcal{B}_n \to [0, \infty]$ with properties:*

- *$\mathcal{B}_n$ contains all open sets (and thus, all closed sets),*
- *μ is a measure on $\mathcal{B}_n$,*
- *If B is any ball in $\mathbb{R}^n$, then we obtain $\mu(B) = |B|$, with $|B|$ denoting the volume of the ball,*
- *If $A \subset B$ is valid, with $B \in \mathcal{B}_n$ and $\mu(B) = 0$, then it follows that $A \in \mathcal{B}_n$ and $\mu(A) = 0$ hold, which means that $(\mathbb{R}^n, \mathcal{B}_n, \mu)$ is a complete measure space.*

The sets $A \in \mathcal{B}_n$ are called Lebesgue measurable.

The existence of Lebesgue measurable sets and Lebesgue measures brings us closer to the function spaces of Lebesgue-integrable functions. Prior to that, we want to define the notion of Lebesgue measurable functions.

Definition 2.19 (Lebesgue Measurable Function)**.** *A function $u : \mathbb{R}^n \to [-\infty, \infty]$ is called Lebesgue measurable if we have*

$$\{x \in \mathbb{R}^n \ : \ f(x) > \alpha\} \in \mathcal{B}_n\,,$$

for all $\alpha \in \mathbb{R}$. If we furthermore have $A \in \mathcal{B}_n$, the function $f : A \to [-\infty, \infty]$ is called Lebesgue measurable on A if $f1_A$ is Lebesgue measurable, with 1_A denoting the indicator function, i.e. $f1_A = f$ on A and $f1_A = 0$ otherwise.

With these definitions we can extend the standard integral-theory to Lebesgue-measurable functions.

Definition 2.20. *The set of non-negative elementary functions is defined by*

$$E_+(\mathbb{R}^n) := \left\{ u = \sum_{k=1}^{m} \alpha_k 1_{A_k} \;\middle|\; (A_k)_{1\le k\le m} \subset \mathcal{B}_n \text{ pairwise disjoint, } \alpha_k \ge 0, m \in \mathbb{N} \right\}.$$

The Lebesgue integral of $u \in E_+(\mathbb{R}^n)$ is defined via

$$\int_{\mathbb{R}^n} u(x)\ d\mu(x) := \sum_{k=1}^{m} \alpha_k \mu(A_k)\,.$$

The following Lemma will allow us to extend the Lebesgue-integral term to general Lebesgue measurable functions.

Lemma 2.1. *For any sequence (u_k) of Lebesgue measurable functions*

- $\sup_k u_k$,
- $\inf_k u_k$,
- $\limsup_{k\to\infty} u_k$,
- $\liminf_{k\to\infty} u_k$,

are also Lebesgue measurable functions. Furthermore, for any Lebesgue measurable function $u \ge 0$ there exists a monotone increasing sequence $(u_k)_{k\in\mathbb{N}} \subset E_+(\mathbb{R}^n)$ with $u = \sup_k u_k$.

These facts motivate the following definition of the Lebesgue integral for arbitrary Lebesgue integrable functions.

Definition 2.21 (Lebesgue Integral)**.**

- *For a non-negative Lebesgue measurable function $u : \mathbb{R}^n \to [0,\infty]$ we define the Lebesgue integral of u as*

$$\int_{\mathbb{R}^n} u(x)\ d\mu(x) := \sup_k \int_{\mathbb{R}^n} u_k(x)\ d\mu(x)\,,$$

  with $(u_k)_{k\in\mathbb{N}} \subset E_+(\mathbb{R}^n)$ being a monotone increasing sequence with $u = \sup_k u_k$.

- *For a Lebesgue measurable function $u : \mathbb{R}^n \to [-\infty,\infty]$ we define the Lebesgue integral via*

$$\int_{\mathbb{R}^n} u(x)\ d\mu(x) := \int_{\mathbb{R}^n} u^+(x)\ d\mu(x) - \int_{\mathbb{R}^n} u^-(x)\ d\mu(x)\,, \tag{2.13}$$

  with $u^+ := \max(u,0)$ and $u^- := \max(-u,0)$, if the right-hand side of (2.13) is finite. In this case u is called integrable.

- *If we have $A \in \mathcal{B}_n$ and a function $u : A \to [-\infty,\infty]$ such that $u1_A$ is integrable, then we define the integral on A as*

$$\int_A u(x)\ d\mu(x) := \int_{\mathbb{R}^n} u(x)1_A(x)\ d\mu(x)\,.$$

In the following we are often going to write dx instead of $d\mu(x)$, for the sake of simplicity. The notion of the Lebesgue integral allows us to define the (Banach) spaces of Lebesgue integrable functions, which are of crucial importance for the remainder of this work.

Definition 2.22 (Lebesgue Spaces L^p)**.** *For $\Omega \in \mathcal{B}_n$ and $1 \leq p \leq \infty$ we define the spaces of Lebesgue integrable functions, the Lebesgue spaces, via*

$$L^p(\Omega) := \left\{ u : \Omega \to \mathbb{R} \text{ Lebesgue measurable} \mid \|u\|_{L^p(\Omega)} < \infty \right\} ,$$

with the semi-norm $\|u\|_{L^p(\Omega)}$ defined as

$$\|u\|_{L^p(\Omega)} := \left(\int_\Omega |u(x)|^p \, dx \right)^{1/p}$$

for $p \in [1, \infty[$, and

$$\|u\|_{L^\infty(\Omega)} := \operatorname*{ess\,sup}_{x \in \Omega} |u(x)| := \inf \left\{ \alpha \geq 0 \mid \mu\left(\{ |u| > \alpha \} \right) = 0 \right\} .$$

The Lebesgue spaces are not normed spaces, since there exist Lebesgue measurable functions $u : \Omega \to \mathbb{R}$ with $u \neq 0$ but $\|u\|_{L^p(\Omega)} = 0$. If we use the equivalence relation $u \sim v$ in $L^p(\Omega)$ defined as

$$u \sim v \text{ in } L^p(\Omega) :\Leftrightarrow \|u - v\|_{L^p(\Omega)} = 0 \Leftrightarrow u = v \text{ a.e.}$$

to replace $L^p(\Omega)$ by $L^p(\Omega)/\sim$ (which, for simplicity, will again be denoted by $L^p(\Omega)$), the spaces of Lebesgue measurable functions become normed Banach spaces with norm $\|\cdot\|_{L^p(\Omega)}$.
Moreover, we can define the spaces of locally Lebesgue integrable functions $L^p_{\text{loc}}(\Omega)$ via

$$L^p_{\text{loc}}(\Omega) := \{ u : \Omega \to \mathbb{R} \text{ Lebesgue measurable} \mid u \in L^p(\Psi) \text{ for all } \Psi \subset \Omega \text{ compact} \} .$$

As for the standard Lebesgue spaces we equip $L^p_{\text{loc}}(\Omega)$ with the above equivalence relation and denote $L^p_{\text{loc}}(\Omega)/\sim$ simply as $L^p_{\text{loc}}(\Omega)$.

An interesting class of Lebesgue spaces for a particular σ-algebra and a specific measure are the sequence spaces ℓ^p.

2.5.2 Sequence Spaces ℓ^p

Following [73, Section 1.7], we want to consider the particular σ-algebra $\mathcal{P}_n := \{A \mid A \subset \mathbb{R}^n\}$ of all subsets of $\mathbb{R}^n$ (which is the power set of $\mathbb{R}^n$). Moreover, we define the *counting measure* $\mu : \mathcal{P}_n \to [0, \infty]$ by

$$\mu(A) := \begin{cases} |A| & \text{if } A \subset \mathbb{R}^n \text{ is finite} \\ \infty & \text{otherwise} \end{cases} .$$

For this particular measure, $\emptyset$ is the only set of measure zero and there is no difference between $L^p(\Omega)$ and $L^p(\Omega)/\sim$. We want to denote this particular space by $\ell^p(\mathbb{R}^n)$, for $0 < p \leq \infty$. The spaces can be characterized as follows. The space $\ell^\infty(\mathbb{R}^n)$ is the space of all bounded functions $u : \mathbb{R}^n \to \mathbb{R}$. The space is equipped with the norm

$$\|u\|_{\ell^\infty} := \sup_{x \in \mathbb{R}^n} |u(x)|$$

for all $u \in \ell^\infty(\mathbb{R}^n)$. For $0 < p < \infty$ functions $u : \mathbb{R}^n \to \mathbb{R}$ belong to $\ell^p(\mathbb{R}^n)$ iff the set $S := \{x \in \mathbb{R}^n \mid u(x) \neq 0\}$ is countable and $\sum_{x\in S} |u(x)|^p$ converges in $\mathbb{R}$. We define $\sum_{x\in\mathbb{R}^n} |u(x)|^p := \sum_{x\in S} |u(x)|^p$ and have the ℓ^p-norms

$$\|u\|_{\ell^p} := \left(\sum_{x\in\mathbb{R}^n} |u(x)|^p \right)^{1/p}$$

for all $u \in \ell^p(\mathbb{R}^n)$. In the following we often want to denote $\ell^p(\mathbb{R}^n)$ by ℓ^p.

2.5.3 Sobolev Spaces

Having the approximation of the solution $\tilde{u}$ of (2.3) in mind, Lebesgue spaces supply a broad class of functions as potential solutions for these inverse problems. However, functions with high oscillations can also belong to classes of Lebesgue functions, as long as these functions are Lebesgue integrable. Unfortunately, in practical applications high oscillations usually correspond to noise. Since, we want to get rid of noise in the data, Lebesgue spaces therefore do not represent a suitable function space in terms of filtering noise. In order to reduce high oscillations we want to investigate the Lebesgue spaces of derivatives of Lebesgue integrable functions in the following.

As derivatives are indicators of the smoothness of functions, it is natural to consider Lebesgue spaces of derivatives of functions. Let us therefore recall the concept of weak derivatives.

Definition 2.23 (Weak Derivative)**.** *Let $\Omega \subset \mathbb{R}^n$ be open and let $u \in L^1_{\text{loc}}(\Omega)$ be locally L^1 integrable. If there exists a function $w \in L^1_{\text{loc}}(\Omega)$ such that*

$$\int_\Omega w\varphi \, dx = (-1)^{|\alpha|} \int_\Omega u D^\alpha \varphi \, dx$$

holds, for all $\varphi \in C_0^\infty(\Omega)$, then w is called the α-th weak partial derivative of u.

In order to easily identify the weak derivative w of u with u we are going to denote w by $D^\alpha u$, for the sake of simplicity.

Note that Definition 2.23 is only valid for $u \in L^1_{\text{loc}}(\Omega)$. However, since the Hölder inequality states that

$$\|uv\|_{L^1(\Omega)} \leq \|u\|_{L^p(\Omega)} \|v\|_{L^q(\Omega)}$$

holds, for all $u \in L^p(\Omega)$, $v \in L^q(\Omega)$ and $uv \in L^1(\Omega)$ with $p, q \in [0, \infty]$ such that $1/p + 1/q = 1$ is valid, we easily see that for the indicator function 1_Ψ – with $\Psi \subset \Omega$ being compact – we obtain

$$\|u\|_{L^1(\Psi)} \leq \|u\|_{L^p(\Omega)} \|1_\Psi\|_{L^q(\Omega)} \,. \tag{2.14}$$

If $u \in L^p(\Omega)$, the right-hand side of (2.14) is finite and hence, we obtain $u \in L^1(\Psi)$ for compact $\Psi \subset \Omega$. As a consequence it is sufficient to define weak derivatives for functions in $L^1_{\text{loc}}(\Omega)$ only, in order to consider them for functions $u \in L^p(\Omega)$ in general.

We are now going to define the so-called Sobolev spaces of L^p-functions, for which the weak derivatives $D^\alpha u$, for $|\alpha| \leq k$, are L^p-functions as well.

Definition 2.24. *Let $\Omega \subset \mathbb{R}^n$ be open. For $k \in \mathbb{N}_0$ and $p \in [1, \infty]$ the Sobolev space $W^{k,p}(\Omega)$ is defined as*

$$W^{k,p}(\Omega) = \{u \in L^p(\Omega) \mid u \text{ has weak derivatives } D^\alpha u \in L^p(\Omega) \text{ for all } |\alpha| \leq k\} \,.$$

The Sobolev spaces are equipped with the norm

$$\|u\|_{W^{k,p}(\Omega)} := \left(\sum_{|\alpha| \leq k} \|D^\alpha u\|^p_{L^p(\Omega)} \right)^{1/p}$$

for $p \in [1, \infty[$, *and*

$$\|u\|_{W^{k,\infty}(\Omega)} := \sum_{|\alpha| \leq k} \|D^\alpha u\|_{L^\infty(\Omega)} \, .$$

Let us briefly investigate an example of a function that is in $L^1_{\text{loc}}(\Omega)$ but not in $W^{k,1}(\Omega)$.

Example 2.3. If we consider $u(x) : \mathbb{R}_{\geq 0} \to \mathbb{R}_{\geq 0}$ defined as $u(x) := \sin(1/x)$ we immediately see that we have $u \in L^1_{\text{loc}}(\mathbb{R}^n)$ because u is bounded on any compact set $\Psi \subset \mathbb{R}_{\geq 0}$, even for $x \to 0$ since the sine is bounded by one. This is no longer valid for the derivative of u for which we obtain $u'(x) = -\cos(1/x)/(x^2)$. In case of $x \to 0$ it follows that $u'(x) \to \infty$ and hence, $\|u'\|_{L^1([0,a])}$ for $0 < a < \infty$ is not finite.

From this brief example we see that Sobolev spaces seem to be more suitable function spaces for finding appropriate solutions to inverse problems in contrast to Lebesgue spaces. Unfortunately, for many applications Sobolev spaces appear to be too restrictive in contrast to the Lebesgue spaces. As for example piecewise constant functions, which are subject of many important applications (e.g. in image processing), do not belong to Sobolev spaces as we are going to see with the following example.

Example 2.4. We are going to see that for the Heaviside function $H(x) : \mathbb{R} \to \{0, 1\}$ with

$$H(x) = \begin{cases} 1 & \text{for } x \geq 0 \\ 0 & \text{else} \end{cases}$$

a weak derivative does not exist. For this particular function we see that for any subset $[a, b] \subset \mathbb{R}$ with $-\infty < a < 0 < b < \infty$ we obtain

$$\int_{-a}^{b} u\varphi' \, dx = \int_{0}^{b} 1\varphi' \, dx = \varphi(0) \, ,$$

for $\varphi \in C^\infty_0([a, b])$. A function $w \in L^1_{\text{loc}}([a, b])$ with $\int_{-a}^{a} w\varphi \, dx = \varphi(0)$ cannot exist and as a consequence, the Heaviside function H is not weakly differentiable and, moreover, not a Sobolev space function.

The last example shows the need for a function space different than the Sobolev spaces. In the following section we are going to recall the space of functions of bounded variation (BV) in order to find this space being more suitable with respect to the applications that are going to be considered. Prior to that we are going to extend the Lebesgue and Sobolev spaces from function spaces to spaces of symmetric tensor fields.

2.5.4 Spaces of Symmetric Tensor Fields

In order to systematically define function spaces for n-dimensional higher-order derivatives, we want to briefly introduce spaces of symmetric tensor fields. This section is a short summary of parts of [12, Chapter 2] and [18, Section 2].
We want to start with a very basic definition of tensor spaces.

Definition 2.25. *Let $\mathcal{V}$ be a vector space. The scalar-valued multilinear functions with variables all in either $\mathcal{V}$ or $\mathcal{V}^*$ are called tensors over $\mathcal{V}$, and the vector spaces they form are called tensor spaces over $\mathcal{V}$. The number of variables from $\mathcal{V}^*$ is called contravariant degree, the number of variables from $\mathcal{V}$ covariant degree. We denote the contravariant degree by r, the covariant degree by k, and the corresponding tensor space by $\mathcal{T}_k^r(\mathcal{V})$. Moreover, a tensor of degree $(0,0)$ is defined to be a scalar, i.e. $\mathcal{T}_0^0(\mathcal{V}) := \mathbb{R}$. A tensor of degree $(1,0)$ is called contravariant vector, while a tensor of degree $(0,1)$ is named covariant vector. In analogy to this terminology, a tensor of type $(r,0)$ is called contravariant tensor, while a tensor of degree $(0,k)$ is called covariant tensor.*

Example 2.5. A specific multilinear function $u : \mathcal{V}^* \times \mathcal{V} \times \mathcal{V} \to \mathcal{V}$ mapping from $\mathcal{V}^* \times \mathcal{V} \times \mathcal{V}$ to $\mathcal{V}$ is of degree $(1,2)$, i.e. $u \in \mathcal{T}_2^1(\mathcal{V})$.

Throughout this work we are only interested in symmetric covariant tensors on the vector space $\mathcal{V} = \mathbb{R}^n$. Suppressing the contravariant degree in the notation, we find out that for this setup the vector space of k-tensors $\mathcal{T}_k(\mathbb{R}^n)$ reads as

$$\mathcal{T}_k(\mathbb{R}^n) = \left\{ \xi : \underbrace{\mathbb{R}^n \times \cdots \times \mathbb{R}^n}_{k\text{-times}} \to \mathbb{R} \mid \xi \text{ } k\text{-linear} \right\},$$

for $k \in \mathbb{N}$, and with k-linearity denoting linearity in every component. In case of $k = 0$ we have $\mathcal{T}_0(\mathbb{R}^n) = \mathbb{R}$.

Definition 2.26. *A tensor $\xi \in \mathcal{T}_k(\mathbb{R}^n)$ is called symmetric, if $\xi(a_1, \ldots, a_k) = \xi(\pi(a_1), \ldots, \pi(a_k))$ for all $\pi \in S_k$, with S_k representing the permutation group of $\{1, \ldots, k\}$. The vector space of symmetric k-tensors is defined as*

$$\mathrm{Sym}^k(\mathbb{R}^n) := \left\{ \xi : \underbrace{\mathbb{R}^n \times \cdots \times \mathbb{R}^n}_{k\text{-times}} \to \mathbb{R} \mid \xi \text{ } k\text{-linear and symmetric} \right\}.$$

Basic operations for tensors are the tensor product, the trace and symmetrization.

Definition 2.27. *For $\xi \in \mathcal{T}_k(\mathbb{R}^n)$ and $\eta \in \mathcal{T}_l(\mathbb{R}^n)$ the tensor product $(\xi \otimes \eta) \in \mathcal{T}_{k+l}(\mathbb{R}^n)$ is defined as*

$$(\xi \otimes \eta)(a_1, \ldots, a_{k+l}) = \xi(a_1, \ldots, a_k)\eta(a_{k+1}, \ldots, a_{k+l}).$$

The trace $\mathrm{tr}(\xi) \in \mathcal{T}_{k-2}(\mathbb{R}^n)$ of $\xi \in \mathcal{T}_k(\mathbb{R}^n)$ for $k \geq 2$ is defined as

$$\mathrm{tr}(\xi)(a_1, \ldots, a_{k-2}) = \sum_{i=1}^{n} \xi(e_i, a_1, \ldots, a_{k-2}, e_i),$$

with e_i denoting the i-th canonical basis vector. Furthermore, every k-tensor $\xi \in \mathcal{T}_k(\mathbb{R}^n)$ can be symmetrized by

$$(|||\,\xi)(a_1, \ldots, a_k) = \frac{1}{k!} \sum_{\pi \in S_k} \xi(a_{\pi(1)}, \ldots, a_{\pi(k)}). \tag{2.15}$$

Note that the symmetrization is a projection, i.e. $|||^2 \xi = ||| \xi$. The trace-operation can be iterated by applying the trace to a tensor product, e.g. $\mathrm{tr}^l(\xi \otimes \eta) \in \mathrm{Sym}^k(\mathbb{R}^n)$ for $\xi \in \mathrm{Sym}^{k+l}(\mathbb{R}^n)$ and $\eta \in \mathrm{Sym}^l(\mathbb{R}^n)$.

Example 2.6. Let us consider the case $k = 1$, i.e. we map from $\mathbb{R}^n$ to $\mathbb{R}$. We can define a tensor $\xi^1 : \mathbb{R}^n \to \mathbb{R}$ via $\xi^1(a^1)$ with $\xi^1(a^1_1, a^1_2, \ldots, a^1_n) = \sum_{i=1}^n a^1_i \xi_i$, for constants $\xi_i \in \mathbb{R}$. As an example, for $n = 2$ and constants $\xi_1 = 1$ and $\xi_2 = -1$ we obtain $\xi^1(a^1_1, a^1_2) = a^1_1 - a^1_2$.

Now we want to investigate the case $k = 2$. Since in that case ξ is a bilinear form, we expect that ξ can be represented in terms of a vector-matrix-vector multiplication. Indeed we can write tensors $\xi^2 : \mathbb{R}^n \times \mathbb{R}^n \to \mathbb{R}$ as

$$\xi^2(a^1, a^2) = (a^2)^T \begin{pmatrix} \xi_{1,1} & \cdots & \xi_{1,n} \\ \vdots & \ddots & \vdots \\ \xi_{n,1} & \cdots & \xi_{n,n} \end{pmatrix} a^1 ,$$

for constants $\xi_{i,j} \in \mathbb{R}$ and vectors $a^1, a^2 \in \mathbb{R}^n$. Let us consider the constants

$$\begin{pmatrix} \xi_{1,1} & \xi_{1,2} \\ \xi_{2,1} & \xi_{2,2} \end{pmatrix} = \begin{pmatrix} 1 & -2 \\ -2 & 0 \end{pmatrix}$$

as an particular example for $n = 2$. The matrix of coefficients is symmetric and thus, the tensor is symmetric and we have $\left(||| \xi^2\right)(a^1, a^2) = \xi^2(a^1, a^2)$. The trace computes as

$$\begin{aligned} \mathrm{tr}(\xi^2) &= \xi^2(e_1, e_1) + \xi^2(e_2, e_2) \\ &= (1,0) \begin{pmatrix} 1 & -2 \\ -2 & 0 \end{pmatrix} \begin{pmatrix} 1 \\ 0 \end{pmatrix} + (0,1) \begin{pmatrix} 1 & -2 \\ -2 & 0 \end{pmatrix} \begin{pmatrix} 0 \\ 1 \end{pmatrix} \\ &= 1 \end{aligned}$$

and indeed equals the trace of the matrix of constants $\xi_{i,j}$.

The spaces $\mathcal{T}_k(\mathbb{R}^n)$ and $\mathrm{Sym}^k(\mathbb{R}^n)$ can be equipped with the scalar product

$$\xi \cdot \eta = \mathrm{tr}^k(\overline{\xi} \otimes \eta) = \sum_{p \in \{1,\ldots,n\}^k} \xi\left(e_{p_1}, \ldots, e_{p_k}\right) \eta\left(e_{p_1}, \ldots, e_{p_k}\right) ,$$

for $\overline{\xi}(a_1, \ldots, a_k) = \xi(a_k, \ldots, a_1)$. This scalar product induces the norm $|\xi| = \sqrt{\xi \cdot \xi}$.

If we now assume to have a fixed domain $\Omega \subset \mathbb{R}^n$ we can furthermore define *symmetric k-tensor fields* as mappings $\xi : \Omega \to \mathrm{Sym}^k(\mathbb{R}^n)$ and define Lebesgue-spaces in analogy to Section 2.5.1, but based on symmetric k-tensor fields. The Lebesgue-spaces then are defined as

$$L^p(\Omega, \mathrm{Sym}^k(\mathbb{R}^n)) := \left\{ \xi : \Omega \to \mathrm{Sym}^k(\mathbb{R}^n) \text{ Lebesgue measurable} \mid \|\xi\|_{L^p(\Omega)} < \infty \right\} ,$$

with

$$\|\xi\|_{L^p(\Omega)} := \left(\int_\Omega |\xi(x)|^p \, dx \right)^{1/p}$$

for $1 \leq p < \infty$, and

$$\|\xi\|_{L^\infty(\Omega)} := \operatorname*{ess\,sup}_{x\in\Omega} |\xi(x)| .$$

Note that the usual duality relation $L^p(\Omega, \mathrm{Sym}^k(\mathbb{R}^n))^* = L^q(\Omega, \mathrm{Sym}^k(\mathbb{R}^n))^*$ for $1 \leq p < \infty$ and $1/p + 1/q = 1$ holds, since the vector norm in $\mathrm{Sym}^k(\mathbb{R}^n)$ is induced by a scalar product.
We can also extend the Banach space of continuous functions to symmetric k-tensor fields, via

$$C(\Omega, \mathrm{Sym}^k(\mathbb{R}^n)) := \left\{ \xi \in C(\overline{\Omega}), \xi \in \mathrm{Sym}^k(\mathbb{R}^n) \mid \operatorname{supp} \xi \subsetneq \Omega \right\} .$$

For the spaces of differentiable functionals the generalization to symmetric k-tensor fields is more complicated, since a differential tensor in general is not symmetric. However, we can symmetrize these tensors via (2.15). For a differential tensor we are going to use the notation

$$\left(\nabla^l \otimes \xi\right)(x)(a_1, \ldots, a_{k+l}) = \left(D^l \xi(x)(a_1, \ldots, a_l)\right)(a_{l+1}, \ldots, a_{k+l}) , \tag{2.16}$$

with $D^l\xi : \Omega \to \mathcal{L}^l\left(\mathbb{R}^n, \mathrm{Sym}^k(\mathbb{R}^n)\right)$ denoting the l-th Fréchet-derivative of ξ and $\mathcal{L}^l(X, Y)$ being the space of l-linear and continuous mappings $X^l \to Y$.

Example 2.7. For $k = 1$ and $l = 1$ we obtain the bilinear form

$$(\nabla \otimes \xi)(x)(a_1, a_2) = a_2^T (D\xi) a_1 ,$$

with $D\xi$ being the Jacobi-matrix of ξ (note that $D\xi \in \mathbb{R}^{n\times n}$ for $\xi : \Omega \subset \mathbb{R}^n \to \mathbb{R}^n$).
For $k = 0$ and $l = 2$ we have $\xi : \Omega \subset \mathbb{R}^n \to \mathbb{R}$ and again obtain a bilinear form via

$$\left(\nabla^2 \otimes \xi\right)(x)(a_1, a_2) = a_2^T \left(D^2\xi\right) a_1 ,$$

with $D^2\xi$ being the Hesse-matrix. Note that the application of the trace operation therefore yields

$$\operatorname{tr}\left(\left(\nabla^2 \otimes \xi\right)(x)(a_1, a_2)\right) = \Delta\xi .$$

The symmetrization of the differential tensor (2.16) is denoted by $\mathcal{E}$, i.e.

$$\mathcal{E}^l(\xi) = |||\left(\nabla^l \otimes \xi\right) .$$

This particular definition of differential tensors and subsequent symmetrization allows the extension of the space of differentiable functions to symmetric k-tensor fields via

$$C^l(\overline{\Omega}, \mathrm{Sym}^k(\mathbb{R}^n)) := \left\{ \xi : \overline{\Omega} \to \mathrm{Sym}^k(\mathbb{R}^n) \mid \nabla^m \otimes \xi \text{ continuous on } \overline{\Omega},\ m = 0, \ldots, l \right\} ,$$

with the norm defined as

$$\|\xi\|_{l,\infty} = \max_{m=0,\ldots,l} \|\mathcal{E}^m(\xi)\|_\infty .$$

Moreover, we can define the l-divergence for elements of $C^l(\overline{\Omega}, \mathrm{Sym}^k(\mathbb{R}^n))$ as

$$\left(\mathrm{div}^l \xi\right) := \mathrm{tr}^l \left(\nabla^l \otimes \xi\right) .$$

Example 2.8. Again, we want to consider the case $k = 1$ and $l = 1$. According to Example 2.7 in that case the 1-divergence reads as

$$\begin{aligned}\operatorname{tr}(\nabla \otimes \xi) &= \sum_{i=1}^{n} (\nabla \otimes \xi)(x)(e_i, e_i) \\ &= \sum_{i=1}^{n} e_i^T (D\xi)\, e_i \\ &= \sum_{i=1}^{n} \frac{\partial \xi_i}{\partial x_i},\end{aligned}$$

and thus equals the standard divergence. In case of second-order derivatives the divergence for $l = 2$ and $k = 2$ reads as

$$\begin{aligned}&\operatorname{tr}(\operatorname{tr}((\nabla \otimes \xi)(x)(a_1, a_2, a_3, a_4))(a_2, a_4)) \\ &= \sum_{i=1}^{n} \operatorname{tr}((\nabla \otimes \xi)(x)(a_1, a_2, a_3, a_4))(e_i, e_i) \\ &= \sum_{i=1}^{n}\sum_{j=1}^{n} (\nabla \otimes \xi)(x)(e_j, e_i, e_i, e_j) \\ &= \sum_{i=1}^{n}\sum_{j=1}^{n} \left(\left(D^2\xi\right)(x)(e_j, e_i)\right)(e_i, e_j). \qquad (2.17)\end{aligned}$$

In case of $i = j$ we see that $\left(\left(D^2\xi\right)(x)(e_i, e_i)\right)(e_i, e_i)$ simply equals $\frac{\partial^2 \xi_{i,i}}{\partial x_i^2}$, while for $i \neq j$ we obtain mixed derivatives $\frac{\partial^2 \xi_{i,j}}{\partial x_i \partial x_j}$ and $\frac{\partial^2 \xi_{i,j}}{\partial x_j \partial x_i}$, respectively. Since $\frac{\partial^2 \xi_{i,j}}{\partial x_i \partial x_j} = \frac{\partial^2 \xi_{i,j}}{\partial x_j \partial x_i}$ we can rewrite (2.17) to

$$\operatorname{div}^2 \xi = \sum_{i=1}^{n} \frac{\partial^2 \xi_{i,i}}{\partial x_i^2} + \sum_{i<j} 2 \frac{\partial^2 \xi_{i,j}}{\partial x_i \partial x_j}.$$

This second-order divergence term will be the foundation for functionals incorporating higher-order derivatives presented in Section 4.1.

After having introduced the space of continuous symmetric tensor fields we can extend the definitions of Sobolev spaces as presented in Section 2.5.3 to symmetric tensor fields. In case of the Sobolev spaces we obtain

$$W^{k,p}(\Omega, \operatorname{Sym}^l(\mathbb{R}^n)) := \left\{ \xi \in L^p(\Omega, \operatorname{Sym}^l(\mathbb{R}^n)) \mid \mathcal{E}^m(\xi) \in L^p(\Omega, \operatorname{Sym}^{l+m}(\mathbb{R}^n)), m = 0, \ldots, k \right\},$$

with the norm

$$\|\xi\|_{W^{k,p}(\Omega, \operatorname{Sym}^l(\mathbb{R}^n))} = \left(\sum_{m=0}^{k} \|\mathcal{E}^m(\xi)\|^p_{L^p(\Omega, \operatorname{Sym}^{l+m}(\mathbb{R}^n))} \right)^{1/p}$$

for $1 \leq p < \infty$, and with

$$\|\xi\|_{W^{k,\infty}(\Omega, \operatorname{Sym}^l(\mathbb{R}^n))} = \max_{m=0,\ldots,k} \|\mathcal{E}^m(\xi)\|_{L^\infty(\Omega, \operatorname{Sym}^l(\mathbb{R}^n))}.$$

2.5.5 The Space of Functions with Bounded Variation

Finally, we want to define the space of functions with bounded variation (BV). Motivation for this function space is the consideration of the L^1-norm of the gradient, i.e.

$$\|\nabla u\|_{L^1(\Omega;\mathbb{R}^n)} = \int_\Omega \|\nabla u\|_{\ell^p} \; dx \,, \tag{2.18}$$

for $1 \leq p < \infty$. The functional is called total variation (TV) seminorm, since it measures the absolute deviation of the gradient of a function. Due to the definition of (2.18) the function u is supposed to satisfy $u \in W^{1,1}\big(\Omega, \mathbb{R}^d\big)$. The problem with $u \in W^{1,1}\big(\Omega, \mathbb{R}^d\big)$ is, that it does not contain functions with discontinuities such that $\|\nabla u\|_{L^1(\Omega)}$ is not finite any more, as we have already pointed out in Section 2.5.3. Hence, the definition of (2.18) needs to be carried over to suit well also for discontinuous functions by considering the distributional definition of the L^1-norm of the gradient. The distributional derivative is defined as

$$\frac{\partial}{\partial x_i} T_u[\varphi] := -T_u\left[\frac{\partial \varphi}{\partial x_i}\right] ,$$

for $T_u \in \mathcal{D}'(\Omega)$ being the distribution $T_u[\varphi] = \int_\Omega u\varphi \; dx$ and for $\varphi \in C_0^\infty\big(\Omega; \mathrm{Sym}^1(\mathbb{R}^n)\big) = C_0^\infty(\Omega;\mathbb{R}^n)$ being the testfunction. Since $\frac{\partial \varphi}{\partial x_i} \in C_0^\infty(\Omega;\mathbb{R}^n)$ the derivative is well-defined. In analogy, the distributional gradient can be defined as

$$\nabla T_u[\varphi] := -\int_\Omega u \; \mathrm{div}\varphi \; dx \,,$$

for $\varphi \in C_0^\infty(\Omega;\mathbb{R}^n)$, since the divergence is the dual operator of the gradient, i.e. $(\nabla)^* = -\mathrm{div}$. Moreover, from the duality relation (2.2) of Section 2.1 and the definition of the dual norm (2.1) it seems to be natural to define

$$\mathrm{TV}(u) := \sup_{\substack{\varphi \in C_0^\infty(\Omega;\mathbb{R}^n) \\ \|\varphi\|_\infty \leq 1}} \int_\Omega u \; \mathrm{div}\varphi \; dx \,. \tag{2.19}$$

For functions $u \in W^{1,1}\big(\Omega, \mathbb{R}^d\big)$ the definitions (2.18) and (2.19) fall together; however, for discontinuous functions (2.19) is also finite.

Example 2.9. If we consider the one-dimensional function $u(x) = \mathrm{sign}(x)$ on the interval $\Omega = [-1, 1]$ again, we see that the value of the total variation is

$$\begin{aligned} \mathrm{TV}(u) &= \sup_{\substack{\varphi \in C_0^\infty(\Omega;\mathbb{R}) \\ \|\varphi\|_\infty \leq 1}} \int_{-1}^{1} u\varphi' \; dx = \sup_{\substack{\varphi \in C_0^\infty(\Omega;\mathbb{R}) \\ \|\varphi\|_\infty \leq 1}} \left(-\int_{-1}^{0} \varphi' \; dx + \int_0^1 \varphi' \; dx \right) \\ &= \sup_{\substack{\varphi \in C_0^\infty(\Omega;\mathbb{R}) \\ \|\varphi\|_\infty \leq 1}} -2\varphi(0) = 2 < \infty \,, \end{aligned}$$

since it is easy to construct a function $\varphi \in C_0^\infty(\Omega;\mathbb{R})$ with $\|\varphi\|_\infty = 1$ and $\varphi(0) = -1$.

The space of functions for which (2.19) is finite is denoted as the space of functions of bounded variation (BV), i.e.

$$\mathrm{BV}(\Omega) := \big\{ u \in L^1(\Omega) \mid \mathrm{TV}(u) < \infty \big\} \,.$$

Finally, we want to note that we can define higher-order BV-spaces by allowing the divergence to be of order $l > 1$. For the derivation of the total variation semi-norm we have considered testfunctions $\varphi \in C_0^\infty(\Omega;\mathbb{R}^n) = C_0^\infty\big(\Omega;\mathrm{Sym}^1(\mathbb{R}^n)\big)$ and the divergence $\mathrm{div}\varphi = \mathrm{tr}^1(\nabla^1 \otimes \varphi)$. Obviously we can extend (2.19) to arbitrary symmetric tensor fields by replacing the divergence term with the divergence for symmetric tensor fields of order l and thus, we can consider

$$\mathrm{TV}^l(u) := \sup_{\substack{\varphi \in C^l(\Omega;\mathrm{Sym}^l(\mathbb{R}^n)) \\ \|\varphi\|_\infty \leq 1}} \int_\Omega u \ \mathrm{div}^l \varphi \ dx \tag{2.20}$$

instead. This naturally leads to the more general class of spaces of bounded variations in terms of

$$\mathrm{BV}^l(\Omega) := \Big\{ u \in L^1(\Omega) \mid \mathrm{TV}^l(u) < \infty \Big\} .$$

2.6 Convex Analysis

In this section we are going to review basic concepts of convex analysis, including subdifferential calculus and Legendre-Fenchel duality, which will be of high relevance with respect to the introduction of Bregman distances in the upcoming chapter. For detailed information on convex analysis we refer to [50, 108].

2.6.1 Subdifferential Calculus

In the following we assume $\mathcal{X}$ to be a Banach space. Moreover, we assume every considered functional to be proper. Let us recall the definition of a convex set and the definition of a convex functional on a convex set.

Definition 2.28 (Convex Set)**.** *Let $\mathcal{X}$ be a Banach space. A subset $\mathcal{C} \subseteq \mathcal{X}$ is called convex, if*

$$\lambda u + (1-\lambda)v \in \mathcal{C} ,$$

for all $\lambda \in [0,1]$ and all $u, v \in \mathcal{C}$.

In analogy we can define (strictly) convex functionals on convex sets.

Definition 2.29 (Convex Functional)**.** *Let $\mathcal{C}$ be a convex set. A functional $G : \mathcal{C} \to \mathbb{R} \cup \{\infty\}$ is called convex, if*

$$G(\lambda u + (1-\lambda)v) \leq \lambda G(u) + (1-\lambda)G(v) \tag{2.21}$$

for all $\lambda \in [0,1]$ and all $u, v \in \mathcal{C}$. The functional J is called strictly convex, if the equality of (2.21) only holds for $u = v$ or $\alpha \in \{0,1\}$.

Example 2.10 (Absolute Value Function)**.** For $\mathcal{C} = \mathbb{R}$ and $G : \mathbb{R} \to \mathbb{R}_{\geq 0}$ the absolute value function $G(u) = |u|$ is convex, since the absolute value function is a metric, and the triangular inequality yields $|\lambda u + (1-\lambda)v| \leq \lambda|u| + (1-\lambda)|v|$. Obviously, the absolute value function is not strictly convex.

In the following we want to recall first- and second-order conditions for convexity of a Fréchet-differentiable functional.

Lemma 2.2. *Let $G : \mathcal{C} \to \mathbb{R} \cup \{\infty\}$ be Fréchet-differentiable, for convex $\mathcal{C} \subseteq \mathcal{X}$. Then, G is convex iff*

$$G(v) \geq G(u) + \langle DG(u), v - u \rangle_{\mathcal{C}} \,, \tag{2.22}$$

for all $u, v \in \mathcal{C}$.

Hence, for convex G a first-order approximation, i.e. a first-order Taylor-linearization, provides a global underestimate of G. If G is twice Fréchet-differentiable we can give another equivalent condition to convexity of G.

Lemma 2.3. *Let $G : \mathcal{C} \to \mathbb{R} \cup \{\infty\}$ be twice Fréchet-differentiable, for convex $\mathcal{C} \subseteq \mathcal{X}$. Then, G is convex iff its Hessian is positive semidefinite, i.e.*

$$D^2 G(u) \succeq 0 \,, \tag{2.23}$$

for all $u \in \mathcal{C}$.

Example 2.11. If we consider $G(u) := 1/2 \|Ku - f\|^2_{L^2(\Sigma)}$ as an example again, the Jacobian and Hessian simply reduce to the first and second Fréchet-derivative, respectively. Hence, condition (2.22) of Lemma 2.2 reads as

$$\frac{1}{2}\|Kv - f\|^2_{L^2(\Sigma)} \geq \frac{1}{2}\|Ku - f\|^2_{L^2(\Sigma)} + \langle K^*(Ku - f), v - u \rangle_{L^2(\Omega)} \,,$$

which can be rewritten to

$$\frac{1}{2}\|Kv - Ku\|^2_{L^2(\Sigma)} \geq 0 \,.$$

Obviously, condition (2.22) is always satisfied for any operator K and hence, G is convex. Alternatively we can look at condition (2.23) of Lemma 2.3 that simply reads as $K^*K\mathbf{1} \geq 0$, which is always fulfilled for any operator K.

Example 2.12. For $\mathcal{C} = \mathbb{R} \times \mathbb{R}_{>0}$ the function $G : \mathbb{R} \times \mathbb{R}_{>0} \to \mathbb{R}_{\geq 0}$ with $G(u, v) = u^2/v$ is convex, which can easily be verified by

$$D^2 G(u, v) = \frac{2}{v^3} \begin{pmatrix} v^2 & -uv \\ -uv & u^2 \end{pmatrix} = \frac{2}{v^3} \begin{pmatrix} v \\ -u \end{pmatrix} \begin{pmatrix} v \\ -u \end{pmatrix}^T \succeq 0 \,,$$

for all $v > 0$. As a consequence of Lemma 2.3 G is convex.

Lemma 2.2 and 2.3 are nice tools to check once or twice Fréchet-differentiable functionals for convexity. Nevertheless, throughout this work we are going to investigate mainly non-differentiable, convex functionals. In order to characterize derivatives of non-differentiable functionals, we want to introduce the notion of subdifferential calculus.

Definition 2.30 (Subdifferential)**.** *Let $\mathcal{X}$ be a Banach space with dual space $\mathcal{X}^*$, and let the functional $G : \mathcal{X} \to \mathbb{R} \cup \{\infty\}$ be convex. Then, G is called subdifferentiable at $u \in \mathcal{X}$, if there exists an element $p \in \mathcal{X}^*$ such that*

$$G(v) - G(u) - \langle p, v - u \rangle_{\mathcal{X}} \geq 0$$

holds, for all $v \in \mathcal{X}$. Furthermore, we call p a subgradient at position u. The collection of all subgradients at position u, i.e.

$$\partial G(u) := \{p \in \mathcal{X}^* \mid G(v) - G(u) - \langle p, v - u \rangle_{\mathcal{X}} \geq 0 \,, \forall v \in \mathcal{X}\} \subset \mathcal{X}^* \,,$$

is called subdifferential of G at u.

If a convex functional G is Fréchet-differentiable, its Fréchet-derivative is the only subgradient, i.e. $\partial G(u) = \{G'(u)\}$.

For non-differentiable functionals the subdifferential is multivalued; we want to consider the subdifferential of the absolute value function as an illustrative example.

Example 2.13. Let $\mathcal{X} = \mathbb{R}$, and let $G : \mathbb{R} \to \mathbb{R}_{\geq 0}$ be the absolute value function $G(u) = |u|$. Then, the subdifferential of G at u is given by

$$\partial G(u) = \operatorname{sign}(u) := \begin{cases} \{1\} & \text{for } u > 0 \\ [-1, 1] & \text{for } u = 0 \\ \{-1\} & \text{for } u < 0 \end{cases} .$$

This can easily be verified by case differentiation. For $u = 0$ the inequality $|v| \geq pv$ is obviously fulfilled for any $v \in \mathbb{R}$ iff $p \in [-1, 1]$. For $u > 0$ the inequality $|v| \geq pv + (1 - p)u$ is fulfilled for every $v \in \mathbb{R}$ iff $p = 1$. In analogy, $p = -1$ has to hold for $u < 0$ in order to guarantee $|v| \geq pv - (1 + p)u$ for each $v \in \mathbb{R}$.

When considering variational frameworks like (2.9) it will be of importance not just to handle subdifferentials of functionals but also sums of functionals. With additional restrictions to the corresponding functionals, the following theorem will allow us to split up a subdifferential.

Theorem 2.5. *Let $H_f : \mathcal{Y} \to \mathbb{R} \cup \{\infty\}$ and $J : \mathcal{Z} \to \mathbb{R} \cup \{\infty\}$ be proper, convex and lower semi-continuous functionals, for Banach spaces $\mathcal{Y}$ and $\mathcal{Z}$. Let furthermore $K : \mathcal{X} \to \mathcal{Y}$ be a linear operator between Banach spaces $\mathcal{X}$ and $\mathcal{Y}$. Then, if there exists a u' with $Ku' \in \operatorname{dom}(H_f)$ and $u' \in \operatorname{dom}(J)$ such that H_f is continuous at Ku', the following equality for the particular subdifferentials holds:*

$$\partial H_f(Ku) + \partial J(u) = \partial(H_f(Ku) + J(u)) .$$

Proof. Since there exists a u' with $Ku' \in \operatorname{dom}(H_f)$ and $u' \in \operatorname{dom}(J)$ such that H_f is continuous at Ku', we can apply [50, Chapter 1, Section 5, Proposition 5.6] in order to obtain the desired result. □

Throughout this work we are particularly interested in convex, non-differentiable and one-homogeneous functionals (like the absolute value function), i.e. we want to consider functionals G for which $G(cu) = |c|G(u)$ is satisfied, for every $c \in \mathbb{R}$. We therefore characterize the subdifferential of one-homogeneous functionals with the following lemma.

Lemma 2.4 (Subdifferential for One-Homogeneous Functionals)**.** *Let $G : \mathcal{X} \to \mathbb{R} \cup \{\infty\}$ be a convex and one-homogeneous functional. Then, the subdifferential of G at u can equivalently be written as*

$$\partial G(u) = \{p \in \mathcal{X}^* \mid \langle p, u\rangle_{\mathcal{X}} = G(u), \langle p, v\rangle_{\mathcal{X}} \leq G(v), \forall v \in \mathcal{X}\} .$$

Proof. If we consider $v = 0 \in \mathcal{X}$ in the definition of the subdifferential we immediately see

$$\langle p, u\rangle_{\mathcal{X}} \geq G(u) ,$$

while for $v = 2u \in \mathcal{X}$ we obtain

$$\langle p, u\rangle_{\mathcal{X}} \leq G(2u) - G(u) = 2G(u) - G(u) = G(u) ,$$

due to the one-homogeneity of G. Thus, $\langle p, u\rangle_{\mathcal{X}} = G(u)$ follows. Moreover, if we insert $\langle p, u\rangle_{\mathcal{X}} = G(u)$ in the definition of the subdifferential we get

$$\langle p, v\rangle_{\mathcal{X}} \leq G(v)\,,$$

for all $v \in \mathcal{X}$. □

Example 2.14. If we consider the one-homogeneous absolute value function $G : \mathbb{R} \to \mathbb{R}_{\geq 0}$ with $G(u) = |u|$ again, we see that $up = |u|$ implies $p = \operatorname{sign}(u)$. Moreover, we discover that for arguments v with the same sign as u we obtain $vp = |v|$, while e.g. for $v > 0$, having the opposite sign as u, we get $vp = -|v| < |v|$.

Theorem 2.6 (Subdifferential Calculus and Optimality)**.** *Let $G : \mathcal{X} \to \mathbb{R} \cup \{\infty\}$ be a proper, convex functional. An element $u \in \mathcal{X}$ is a minimizer of G iff $0 \in \partial G(u)$.*

Proof. For $0 \in \partial G(u)$ by definition of the subdifferential we have

$$0 = \langle 0, v - u\rangle_{\mathcal{X}} \leq G(v) - G(u)$$

for all $v \in \mathcal{X}$and thus, u is a global minimizer of G.
If $0 \notin \partial G(u)$ holds, then there exists at least one $v \in \mathcal{X}$ such that

$$G(v) - G(u) < \langle 0, v - u\rangle_{\mathcal{X}} = 0\,,$$

and hence, u cannot be a minimizer of G. □

2.6.2 Legendre-Fenchel Duality

Finally we want to review specific duality properties of convex functionals that are going to be of further interest in the course of this work. In particular we want to recall a transformation called *convex conjugate*, which is a generalization of the Legendre transformation and also known as *Legendre-Fenchel transformation*, named after Adrien-Marie Legendre and Werner Fenchel. For further information on Legendre-Fenchel duality we refer to [50, 108], [109, Chapter 11], [15, Chapter 3] or [17, Section 3.3 and Section 5].

Definition 2.31 (Convex Conjugate)**.** *Let $\mathcal{X}$ be a Banach space with dual space $\mathcal{X}^*$. For a functional $G : \mathcal{X} \to \mathbb{R} \cup \{\infty\}$ the convex conjugate $G^* : \mathcal{X}^* \to \mathbb{R} \cup \{\infty\}$ is defined as*

$$G^*(p) := \sup_{u \in \mathcal{X}} \left\{\langle p, u\rangle_{\mathcal{X}} - G(u)\right\}\,.$$

The biconjugate $G^{**} : \mathcal{X} \to \mathbb{R} \cup \{\infty\}$ of G is defined as

$$G^{**}(u) := \sup_{p \in \mathcal{X}^*} \left\{\langle u, p\rangle_{\mathcal{X}^*} - G^*(p)\right\}.$$

Example 2.15. Let us consider the characteristic functional $G : \mathcal{X} \to \mathbb{R} \cup \{\infty\}$ of a convex set $\mathcal{C} \subset \mathcal{X}$, i.e.

$$G(u) = \chi_{\mathcal{C}}(u) := \begin{cases} 0 & \text{if } u \in \mathcal{C} \\ +\infty & \text{else} \end{cases}\,.$$

The convex conjugate of G simply is

$$\begin{aligned} G^*(p) &= \sup_{u \in \mathcal{X}} \left\{ \langle p, u \rangle_{\mathcal{X}} - \chi_{\mathcal{C}}(u) \right\} \\ &= \sup_{u \in \mathcal{C}} \left\{ \langle p, u \rangle_{\mathcal{C}} \right\} . \end{aligned}$$

The convex conjugate and the biconjugate inhere some very interesting properties, few of which we want to review very briefly.

Lemma 2.5. *Let $G : \mathcal{X} \to \mathbb{R} \cup \{\infty\}$ be a functional with underlying Banach space $\mathcal{X}$. Then, $G^* : \mathcal{X}^* \to \mathbb{R} \cup \{\infty\}$ is convex and lower semi-continuous.*

Proof. See [91, Section 2.3, Lemma 2.1]. □

Lemma 2.6. *Let $G : \mathcal{X} \to \mathbb{R} \cup \{\infty\}$ be a functional, for which the underlying Banach space $\mathcal{X}$ is reflexive. Then, $G = G^{**}$ iff G is convex and lower semi-continuous.*

Proof. See [91, Section 2.3, Theorem 2.3]. □

Example 2.16. If we again consider the characteristic functional $\chi_{\mathcal{C}}$ from Example 2.15, it is easy to see that $\chi_{\mathcal{C}}$ is convex, since we have

$$\chi_{\mathcal{C}}(\lambda u + (1-\lambda)v) = \begin{cases} 0 & \text{if } \lambda u + (1-\lambda)v \in \mathcal{C} \\ +\infty & \text{else} \end{cases}$$

and

$$\lambda \chi_{\mathcal{C}}(u) + (1-\lambda)\chi_{\mathcal{C}}(v) = \begin{cases} 0 & \text{if } u, v \in \mathcal{C} \\ +\infty & \text{else} \end{cases} ,$$

for $\lambda \in [0,1]$. Due to the convexity of $\mathcal{C}$ we have $\chi_{\mathcal{C}}(\lambda u + (1-\lambda)v) = \lambda\chi_{\mathcal{C}}(u) + (1-\lambda)\chi_{\mathcal{C}}(v)$. According to Lemma 2.6 and Example 2.15 the convex conjugate of $G(u) := \sup_{p \in \mathcal{X}^*} \{\langle p, u \rangle_{\mathcal{C}}\}$ therefore is $G^*(p) = \chi_{\mathcal{C}}(p)$.
More examples of convex conjugates for some specific functionals can be found in Table 2.1.

$G(u)$	$G^*(p)$
$\|u\|_{L^2(\Omega)}$	$\chi_{\{p \mid \|p\|_{L^2(\Omega)} \leq 1\}}$
$\frac{\alpha}{2}\|u\|^2_{L^2(\Omega)}$	$\frac{1}{2\alpha}\|p\|^2_{L^2(\Omega)}$
$\|u\|_{L^1(\Omega)}$	$\chi_{\{p \mid \|p\|_{L^\infty(\Omega)} \leq 1\}}$
$\|u\|_{L^\infty(\Omega)}$	$\chi_{\{p \mid \|p\|_{L^1(\Omega)} \leq 1\}}$
$\max(u)$	$\chi_{\{p \mid p \geq 1 \wedge \|p\|_{L^1(\Omega)} = 1\}}$

Table 2.1: An overview of functionals G and their corresponding convex conjugates G^*.

For Fréchet-differentiable functionals G with invertible Fréchet-derivative G' the Fréchet-derivative of the convex-conjugate equals $(G')^{-1}$.

Lemma 2.7. *Let $G : \mathcal{X} \to \mathbb{R}$ be a Fréchet-differentiable functional G with invertible Fréchet-derivative G', i.e. $(G')^{-1}(v)$ exists for all $v \in \mathcal{X}$. Then, this invertible Fréchet-derivative is the derivative of the convex conjugate of G, i.e. $(G^*)'(v) = (G')^{-1}(v)$.*

Proof. For a Fréchet-differentiable functional G with invertible Fréchet-derivative G' the convex conjugate reads as

$$G^*(v) = \left\langle v, \left(G'\right)^{-1}(v) \right\rangle_{\mathcal{X}} - G\left(\left(G'\right)^{-1}(v)\right) .$$

Computing the Fréchet derivative of $G^*(v)$ therefore yields

$$\begin{aligned}(G^*)'(v) &= \left(G'\right)^{-1}(v) + v\left(\left(G'\right)^{-1}\right)'(v) - \left(\left(\left(G'\right)^{-1}\right)'(v)\, \underbrace{G'\left(\left(G'\right)^{-1}(v)\right)}_{=v}\right) , \\ &= \left(G'\right)^{-1}(v) ,\end{aligned}$$

and thus, the assertion holds. □

A remarkable result for the biconjugate of a functional is that the biconjugate represents the convex hull of the related functional.

Lemma 2.8. *Let $G : \mathcal{X} \to \mathbb{R} \cup \{+\infty\}$ be a functional on the Banach space $\mathcal{X}$. Then, $G^{**} : \mathcal{X} \to \mathbb{R} \cup \{+\infty\}$ is the convex hull of G, i.e. we have*

$$G^{**}(u) \leq G(u) \ \forall u \in \mathcal{X} ,$$

and for any convex functional H satisfying $H(u) \leq G(u)$ for all $u \in \mathcal{X}$ we observe

$$G^{**}(u) \geq H(u) \ \forall u \in \mathcal{X} .$$

Proof. See [24, Section 5.2.1, Proposition 5.2.3]. □

Example 2.17. As a brief example we want to compute the convex hull of the function $G_{\alpha,f} : \mathbb{R} \to \mathbb{R}_{\geq 0}$ with

$$G_{\alpha,f}(u) := \frac{1}{2}(u - f)^2 + \alpha |u|^0 ,$$

for $f \in \mathbb{R}$ and $\alpha \in \mathbb{R}_{>0}$. We start considering the convex conjugate of $G_{\alpha,f}$, which computes as

$$\begin{aligned}G^*_{\alpha,f}(q) &:= \sup_v \{qv - G_{\alpha,f}(v)\} \\ &= \sup_v \left\{ qv - \frac{1}{2}(v - f)^2 - \alpha |v|^0 \right\} .\end{aligned}$$

In case of $v = 0$ we simply have

$$\sup_v \{qv - G_{\alpha,f}(v)\} = -\frac{1}{2} f^2 ,$$

otherwise we obtain

$$\sup_v \{qv - G_{\alpha,f}(v)\} = \frac{1}{2}(q+f)^2 - \frac{1}{2}f^2 - \alpha\,.$$

It is easy to see that $\frac{1}{2}(q+f)^2 - \frac{1}{2}f^2 - \alpha > -\frac{1}{2}f^2$ is true only if $|q+f| > \sqrt{2\alpha}$ holds. Hence, we end up with

$$G^*_{\alpha,f}(q) = \begin{cases} \frac{1}{2}(q+f)^2 - \frac{1}{2}f^2 - \alpha & \text{if } |q+f| > \sqrt{2\alpha} \text{ holds} \\ -\frac{1}{2}f^2 & \text{otherwise} \end{cases}.$$

Now we want to continue computing the convex hull of $G_{\alpha,f}$, i.e. $G^{**}_{\alpha,f}$ via

$$G^{**}_{\alpha,f}(u) = \sup_q \{uq - G^*(q)\}\,.$$

If we consider the case $|q+f| > \sqrt{2\alpha}$ we have

$$\sup_q \left\{ uq - \frac{1}{2}(q+f)^2 + \frac{1}{2}f^2 + \alpha \right\}.$$

The optimality condition is $q = u - f$, which also implies that this case is only valid for $|u| > \sqrt{2\alpha}$. Inserting the optimality condition yields

$$\frac{1}{2}(u-f)^2 + \alpha$$

as a supremum for $|u| > \sqrt{2\alpha}$.
If we consider $|q+f| \leq \sqrt{2\alpha}$, we need to focus on

$$\sup_q \left\{ u\left(\pm\sqrt{2\alpha} - f\right) + \frac{1}{2}f^2 \right\}.$$

It is easy to see that $u\left(\sqrt{2\alpha} - f\right) + \frac{1}{2}f^2 > u\left(-\sqrt{2\alpha} - f\right) + \frac{1}{2}f^2$ is true if u is non-negative. Therefore we end up with

$$G^{**}_{\alpha,f}(u) = \begin{cases} \frac{1}{2}(u-f)^2 + \alpha & \text{if } |u| > \sqrt{2\alpha} \\ |u|\sqrt{2\alpha} - uf + \frac{1}{2}f^2 & \text{else} \end{cases}. \tag{2.24}$$

A plot for $G^{**}_{\alpha,f}$ in comparison to the function $H_{\alpha,f} : \mathbb{R} \to \mathbb{R}_{\geq 0}$ defined as

$$H_{\alpha,f}(u) := \frac{1}{2}(u-f)^2 + \frac{\alpha^2}{2}|u| \tag{2.25}$$

for exemplary input values can be seen in Figure 2.1. It can be seen that for $f = 1$ and $\alpha = 4/10$ the minima of both functions are slightly shifted; the minimum of $G^{**}_{\alpha,f}$ is at $u = f = 1$, while for $H_{\alpha,f}(u)$ the minimum is at $u = f - \alpha^2/2 = 0.92$.

With regard to optimality of variational frameworks the Fenchel duality theorem allows a nice relation between a functional and its convex conjugate.

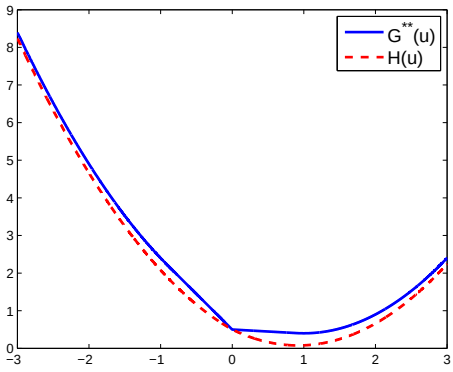

Figure 2.1: The computed convex hull $G^{**}_{\alpha,f}$ for $u = -3$ to 3, $f = 1$ and $\alpha = 0.4$, and in comparison the function $H_{\alpha,f}(u)$ as defined in (2.25).

Theorem 2.7 (Fenchel's Duality Theorem)**.** *Let $F : \mathcal{Y} \to \mathbb{R} \cup \{\infty\}$ and $J : \mathcal{Z} \subseteq \mathcal{X} \to \mathbb{R} \cup \{\infty\}$ be proper, lower semi-continuous and convex functionals for reflexive Banach spaces $\mathcal{X}$, $\mathcal{Y}$ and $\mathcal{Z}$, such that $\mathrm{dom}(F) \cap \mathrm{dom}(J) \neq \emptyset$, and let $K : \mathcal{X} \to \mathcal{Y}$ be a continuous linear operator. Then, the primal-dual identities*

$$\inf_{u \in \mathcal{Z}} \left\{ \frac{1}{\alpha} F(Ku - f) + J(u) \right\} = \sup_{p \in \mathcal{Y}^*} \left\{ -\frac{1}{\alpha} F^*(\alpha p) - J^*(-K^* p) - \langle p, f \rangle_{\mathcal{Y}} \right\} \tag{2.26}$$

and

$$\inf_{u \in \mathcal{Z}} \left\{ \frac{1}{\alpha} F(Ku - f) + J(u) \right\} = - \inf_{p \in \mathcal{Y}^*} \left\{ \frac{1}{\alpha} F^*(-\alpha p) + J^*(K^* p) - \langle p, f \rangle_{\mathcal{Y}} \right\} \tag{2.27}$$

are satisfied.

Proof. We only want to give a sketch of a proof. A fully detailed proof is given in [50, Chapter 3, Section 1 - 4]. Formally, we can rewrite

$$\inf_{u \in \mathcal{Z}} \left\{ \frac{1}{\alpha} F(Ku - f) + J(u) \right\} \tag{2.28}$$

in terms of a Lagrange functional to

$$\inf_{u \in \mathcal{Z}, z \in \mathcal{Y}} \sup_{p \in \mathcal{Y}^*} \left\{ \frac{1}{\alpha} F(z) + J(u) + \langle p, Ku - f - z \rangle_{\mathcal{Y}} \right\}$$

Due to the assumptions we are allowed to exchange inf and sup to obtain

$$\sup_{p \in \mathcal{Y}^*} \left\{ \underbrace{\inf_{z \in \mathcal{Y}} \left\{ \frac{1}{\alpha} \left(F(z) - \langle \alpha p, z \rangle_{\mathcal{Y}} \right) \right\}}_{= -\frac{1}{\alpha} F^*(\alpha p)} + \underbrace{\inf_{u \in \mathcal{Z}} \left\{ J(u) - \langle -K^* p, u \rangle_{\mathcal{Z}} \right\}}_{= -J^*(-K^* p)} - \langle p, f \rangle_{\mathcal{Y}} \right\},$$

and thus, we have derived (2.26). Alternatively, we can rewrite (2.28) in terms of the Lagrange functional

$$\inf_{u\in\mathcal{Z},z\in\mathcal{Y}}\sup_{p\in\mathcal{Y}^*}\left\{\frac{1}{\alpha}F(z)+J(u)+\langle p,z-Ku+f\rangle_{\mathcal{Y}}\right\}.$$

Analogous reasoning as in the previous case yields (2.27). □

Chapter 3

Bregman Distances

The major tool in the course of this work is the so-called *Bregman distance* for general convex, but not necessarily differentiable functionals. The Bregman distance is named after L. M. Bregman and has been introduced in [20] first, as a tool for an iterative method in order to find common points of convex sets.

However, the Bregman distance has probably attracted most of its attention during the last decade since it has been established as a major tool in the context of variational image processing and inverse problems in theoretical as well as in computational terms.

Due to the lack of error estimates for the ROF-model (cf. [110]) in an appropriate error distance measure, capturing the individual features of the L^1-type regularization on the gradient, in [28] Burger and Osher have proposed the use of the Bregman distance as an error measure to derive error estimates for convex and subdifferentiable functionals. Furthermore, they have unified already existing estimates for quadratic as well as for nonlinear fidelities and the novel estimates, also applicable to non-differentiable functionals, to an overall framework. Up to now many works deal with the consideration of error estimates in the context of Bregman distances, see for instance [30, 31, 68, 84, 86, 107]. However, most works still focus on a setup with quadratic fidelity; in Chapter 5 we are going to generalize results of [28] to various other important fidelities.

The use of Bregman distances in the context of variational frameworks with singular regularization energies has not been limited to theoretical purposes only. In [95] the regularization term of the ROF model, the Total Variation seminorm $\mathrm{TV}(u)$ as introduced in Section 2.5.5, has been replaced by the Bregman distance $D_{\mathrm{TV}}^{p_k}(u, u_k)$, for $p_k \in \partial \mathrm{TV}(u_k)$ and $u_k \in \mathrm{BV}(\Omega)$, in order to generate an iterative refinement method that allows to overcome the usual loss of contrast of a standard ROF reconstruction while still suppressing the noise. The method is very related to iterated Tikhonov regularization (cf. [83, 78, 55]); however, the specific combination of Bregman distances and singular regularization energies with multivalued subdifferentials has made the iterated refinement method very successful. Yet, many singular regularization functionals with multivalued subdifferential have been replaced by the iterated refinement scheme, respectively a linearized version of it, see for instance [136, 33, 32].

In [26] the concept of the iterated refinement method has been generalized to a time-continuous inverse scale space (ISS) method. The ISS method has been studied and analyzed, especially in the context of Total Variation regularization. In the latter case it can be observed from computational tests that the ISS evolution has a discrete nature, a fact that has partly been supported by theoretical results (cf. [26, 25, 23]).

Moreover, the Bregman distance has been used to derive existing algorithms from a different perspective, see for instance [59]. However, the exploration of this relation is not our goal in this

chapter; we briefly focus on that in Chapter 8.

In the following we want to define Bregman distances and highlight some of the specific properties they inhere. Subsequently, we want to recall the application of Bregman distances in deriving error estimates for variational schemes with quadratic fidelity. Afterwards we will introduce the concept of Bregman iteration and the Inverse Scale Space method, since they will represent important tools throughout this work. In addition, we want to briefly recall some of their important properties.

3.1 Definition and Properties

The Bregman distance for general convex, but not necessarily differentiable functionals is defined as follows.

Definition 3.1 (Bregman Distance)**.** *Let $\mathcal{X}$ be a Banach space and $G : \mathcal{X} \to \mathbb{R} \cup \{\infty\}$ be a convex functional with non-empty subdifferential ∂G. Then, the Bregman distance is defined as*

$$D_G(u, v) := \{G(u) - G(v) - \langle p, u - v\rangle_{\mathcal{X}} \mid p \in \partial G(v)\} \ . \tag{3.1}$$

The Bregman distance for a specific subgradient $\zeta \in \partial G(v)$, $v \in \mathcal{X}$, is defined as $D_G^\zeta : \mathcal{X} \times \mathcal{X} \to \mathbb{R}_{>0}$ with

$$D_G^\zeta(u, v) := G(u) - G(v) - \langle \zeta, u - v\rangle_{\mathcal{X}} \ . \tag{3.2}$$

Note that the Bregman distance basically measures the difference between a functional and its linearization.

In the following we want to consider three particular examples of functions (or functionals) and their corresponding Bregman distances. More examples can be discovered in Table 3.1.

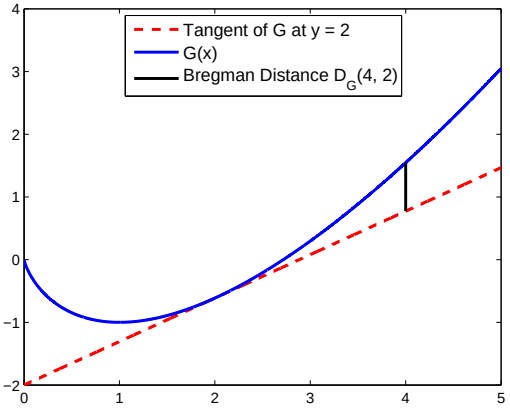

Figure 3.1: The function $G(x) = x\log(x) - x$ and its tangent at $y = 2$. The Bregman distance $D_G(4, 2)$ equals the length of the perpendicular from $G(x)$ to this tangent at $x = 4$.

Example 3.1. Let us consider the quadratic functional $G : L^2(\Omega) \to \mathbb{R}_{>0}$ with $G(u) := \frac{1}{2}\|Bu\|^2_{L^2(\Omega)}$, for a linear operator $B : \mathcal{W}(\Omega) \to L^2(\Omega)$. Since G is Fréchet-differentiable

with Fréchet-derivative $G'(u) = B^*Bu$, the subdifferential $\partial G(v)$ reads as $\partial G(v) = \{B^*Bv\}$. If we insert $p = B^*Bv$ into the definition of the Bregman distance we therefore obtain

$$\begin{aligned} D_G(u,v) &= \frac{1}{2}\|Bu\|^2_{L^2(\Omega)} - \frac{1}{2}\|Bv\|^2_{L^2(\Omega)} - \langle B^*Bv, u-v\rangle_{L^2(\Omega)} \\ &= \frac{1}{2}\|Bu\|^2_{L^2(\Omega)} - \langle Bv, Bu\rangle_{L^2(\Omega)} + \frac{1}{2}\|Bv\|^2_{L^2(\Omega)} \\ &= \frac{1}{2}\|B(u-v)\|^2_{L^2(\Omega)} \,. \end{aligned}$$

Hence, for quadratic L^2-terms the corresponding Bregman distance simply equals the quadratic L^2-distance between u and v with respect to the operator B.

Example 3.2. We want to investigate the function $G : \mathbb{R}_{\geq 0} \to \mathbb{R}$ with $G(x) := x\log(x) - x$ under the additional assumption $0\log(0) \equiv 0$. As in the previous example the subdifferential consists of the derivative only, which is $G'(x) = \log(x)$. Inserting the derivative into the definition of the Bregman distance yields

$$\begin{aligned} D_G(x,y) &= x\log(x) - x - y\log(y) + y - \log(y)(x-y) \\ &= x\log\left(\frac{x}{y}\right) + y - x \,, \end{aligned}$$

for $y \neq 0$. In Figure 3.1 the function G as well as the Bregman distance D_G for exemplary points x and y is shown.

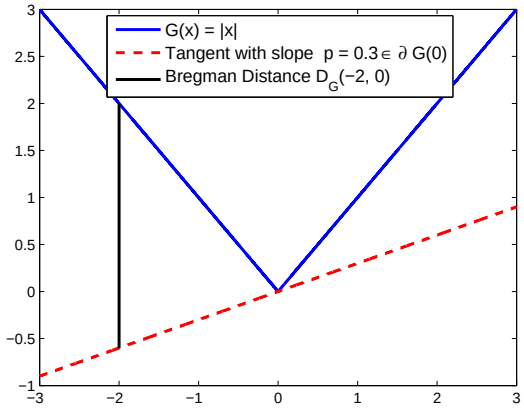

Figure 3.2: The function $G(x) = |x|$ and one specific tangent at $y = 0$ with slope $p = 3/10 \in \partial|0|$. The Bregman distance $D_G(-2, 0)$ equals the length of the perpendicular from $G(x)$ to this tangent at $x = -2$.

Example 3.3. As a third example we want to consider the absolute value function again, i.e. $G : \mathbb{R} \to \mathbb{R}_{\geq 0}$ with $G(x) = |x|$. Due to Example 2.13 the subdifferential reads as $\partial G(y) = \operatorname{sign}(y)$. The Bregman distance simplifies to

$$\begin{aligned} D_G(x,y) &= |x| - |y| - \operatorname{sign}(y)(x-y) \\ &= (\operatorname{sign}(x) - \operatorname{sign}(y))\, x \,. \end{aligned}$$

Hence, the Bregman distance is only larger than zero if x and y have a different sign. In Figure 3.1 we can see an illustrative example of the Bregman distance $D_{|\cdot|}(2, 0)$ for the subgradient $p = 3/10$.

Function Name	$G(x)$	$\mathrm{dom}(G)$	$D_G(x,y)$
Bit Entropy	$x\log(x)+(1-x)\log(1-x)$	$[0,1]$	$x\log\left(\frac{x}{y}\right)+(1-x)\log\left(\frac{1-x}{1-y}\right)$
Burg Entropy	$-\log(x)$	$]0,\infty[$	$\frac{x}{y}-\log\left(\frac{x}{y}\right)-1$
Hellinger	$-\sqrt{1-x^2}$	$[-1,1]$	$(1-xy)(1-y^2)^{-1/2}-(1-x^2)^{1/2}$
ℓ^p Quasi Norm	$-x^p$ $(0<p<1)$	$[0,\infty[$	$-x^p+pxy^{p-1}-(p-1)y^p$
ℓ^p Norm	$\lvert x\rvert^p$ $(1<p<\infty)$	$]-\infty,\infty[$	$\lvert x\rvert^p-px\mathrm{sign}(y)\lvert y\rvert^{p-1}+(p-1)\lvert y\rvert^p$
Exponential	$\exp(x)$	$]-\infty,\infty[$	$\exp(x)-(x-y+1)\exp(y)$
Inverse	$1/x$	$]0,\infty[$	$1/x+x/y^2-2/y$

Table 3.1: An overview of functions and their corresponding Bregman distances, see [7].

The Bregman distance is no distance in the usual sense; at least $D_G^\zeta(u,u)=0$ and $D_G^\zeta(u,v)\geq 0$ hold for all $\zeta\in\partial G(v)$, the latter due to the convexity of G. If G is strictly convex, we even obtain $D_G^\zeta(u,v)>0$ for $u\neq v$ and $\zeta\in\partial G(v)$.

Moreover, between the Bregman distance for a specific functional G and the Bregman distance for the convex conjugate G^* as introduced in Section 2.6.2 is an interesting connection.

Lemma 3.1. *Let $G:\mathcal{X}\to\mathbb{R}\cup\{+\infty\}$ be a convex functional and let G^* denote its convex conjugate as defined in Definition 2.31. Then, the relation*

$$\sup_v D_G^p(u,v)=\sup_q D_{G^*}^u(p,q)$$

holds.

Proof. The statement follows immediately by applying the Legendre-Fenchel transform twice for $p\in\partial G(v)$ and $u\in\partial G^*(q)$. □

In general, no triangular inequality nor symmetry holds for the Bregman distance. The latter can be achieved by introducing the so-called symmetric Bregman distance.

Definition 3.2 (Symmetric Bregman Distance)**.** *Let $\mathcal{X}$ be a Banach space and $G:\mathcal{X}\to\mathbb{R}\cup\{\infty\}$ be a convex functional with non-empty subdifferential ∂G. Then, a symmetric Bregman distance is defined as $D_G^{\mathrm{symm}}:\mathcal{X}\times\mathcal{X}\to\mathbb{R}_{\geq 0}$ with*

$$D_G^{\mathrm{symm}}(u_1,u_2):=D_G^{p_1}(u_2,u_1)+D_G^{p_2}(u_1,u_2)=\langle u_1-u_2,p_1-p_2\rangle_{\mathcal{X}^*}\,, \tag{3.3}$$

with

$$p_i\in\partial G(u_i)\quad\textit{for}\quad i\in\{1,2\}\,. \tag{3.4}$$

Obviously, the symmetric Bregman distance depends on the specific selection of the subgradients p_i, which will be suppressed in the notation for simplicity throughout this work.

In the coarse of this work the Bregman distance will be a major tool for considering the differences of functions with respect to their Bregman distance. In the next section we briefly want to recall error estimates that can be derived in the Bregman distance setting. As already mentioned in the introduction, Bregman distances can also be used to improve variational schemes like (2.8) in order to develop superior algorithms. The replacement of the regularization term in (2.8) leads to the concept of Bregman iteration, which will be part of Section 3.3. Subsequently, we will consider the transition from discrete Bregman iteration to time-continuous ISS methods.

3.2 Error Estimates

In [28] the Bregman distance has been introduced to derive error estimates in case of quadratic fidelity and subdifferentiable regularization term, comparable to error estimates for quadratic regularization schemes. In order to obtain error estimates a so-called source condition is needed, which reads

$$\exists\, \xi \in \partial J(\tilde{u}),\, \exists\, q \in L^2(\Sigma) \setminus \{0\} : \quad \xi = K^* q\,. \tag{SCL^2}$$

In case that (SCL^2) is satisfied the main result of [28] is the following estimate.

Theorem 3.1. *Let $\tilde{u}$ denote the exact solution of the inverse problem (2.3). Furthermore assume that the standard deviation of f and g is bounded, i.e. $\|f - g\|_{L^2(\Sigma)} \leq \delta$, and that the source condition (SCL^2) is fulfilled. Then, for every existing minimizer of (2.8) denoted by $\hat{u}$ we obtain the error estimate*

$$D_J^{\xi}(\hat{u}, \tilde{u}) \leq \frac{\delta^2}{2\alpha} + \alpha \frac{\|q\|^2_{L^2(\Sigma)}}{2}\,.$$

Proof. See [28, Theorem 2] or alternatively [30, Theorem 3.1]. □

In Chapter 5 we want to transfer the concept of error estimation with Bregman distances to various other fidelities arising from specific applications.

3.3 Bregman Iteration

In [95] the use of the Bregman distance for a particular regularization energy instead of the energy itself has been proposed in order to overcome the loss of contrast in comparison to the standard reconstruction. Many publications have followed in which Bregman distances have been applied to general singular regularization energies (cf. [136, 33, 32]). The idea of the Bregman iteration is to replace the regularization term of (2.8) with the corresponding Bregman distance. This yields the following iterative scheme, assuming $u_0 = 0 \in \mathrm{dom}(K) \cap \mathrm{dom}(J)$ and $p_0 \in \partial J(0)$:

$$u_{k+1} \in \operatorname*{arg\,min}_{u \in \mathrm{dom}(J)} \left\{ \frac{1}{2} \|Ku - f\|^2_{L^2(\Sigma)} + \alpha D_J^{p_k}(u, u_k) \right\}, \tag{3.5}$$

with J being a singular, one-homogeneous regularization energy.

For the particular case of $J(u) = \mathrm{TV}(u)$ in [95] it has been shown that the optimality condition of (3.5), i.e.

$$0 = K^*(Ku_{k+1} - f) + \alpha(p_{k+1} - p_k)\,, \tag{3.6}$$

can be rewritten as

$$0 = K^*(Ku_{k+1} - (f + v_k)) + \alpha p_{k+1} \tag{3.7}$$

for $p_k := \frac{1}{\alpha} K^* v_k$. In order to satisfy (3.6) we then obtain

$$v_{k+1} = v_k - (Ku_{k+1} - f)\,. \tag{3.8}$$

Obviously the considerations can be carried out on any convex and subdifferentiable functional J. Consequently we end up with the following iterative algorithm that we are going to refer to as Bregman iteration.

Algorithm 1 Bregman Iteration

1. **Parameters:** $K,\ f,\ v_0,\ \text{maxiter} \in \mathbb{N},\ \alpha \in \mathbb{R}_{>0}$
for $k \leq \text{maxiter}$ **do**
Compute $u_k = \arg\min_{u \in \text{dom}(J)} \left\{ \frac{1}{2} \|Ku - (f + v_{k-1})\|^2_{L^2(\Sigma)} + \alpha J(u) \right\}$
Compute $v_k = v_{k-1} - (Ku_k - f)$
end for
return u_{maxiter}

In [95] it has been stated that in case of $J(u) = \text{TV}(u)$ the iterates of Algorithm 1 are well-defined.

Lemma 3.2. *Let $J(u) = TV(u)$ hold and let $u_0 = 0$ and $p_0 \in \partial J(u_0)$ be guaranteed. Then, for each $k \in \mathbb{N}$ there exists a subgradient $p_k \in \partial J(u_k)$ such that*

$$\alpha p_k + K^* (Ku_k - f) = \alpha p_{k-1}$$

is true. If, in addition, K has only the trivial null space, then the minimizer u_k is unique.

Proof. See [95, Section 3.2, Proposition 3.1]. □

In case of a general regularizer J it can furthermore be stated that the iterates are monotonically non-increasing.

Proposition 3.1. *With the same assumptions as in Lemma 3.2, but for general convex J, the sequence of iterates of Algorithm 1 is monotonically non-increasing; precisely we have*

$$\frac{1}{2} \|Ku_k - f\|^2_{L^2(\Sigma)} \leq \frac{1}{2} \|Ku_k - f\|^2_{L^2(\Sigma)} + \alpha D_J^{p_{k-1}}(u_k, u_{k-1}) \leq \frac{1}{2} \|Ku_{k-1} - f\|^2_{L^2(\Sigma)} .$$

Moreover, for u with $TV(u) < \infty$ we obtain

$$\alpha D_J^{p_k}(u, u_k) + \alpha D_J^{p_{k-1}}(u_k, u_{k-1}) + \frac{1}{2} \|Ku_k - f\|^2_{L^2(\Sigma)} \leq \frac{1}{2} \|Ku_{k-1} - f\|^2_{L^2(\Sigma)} .$$

Proof. See [95, Section 3.2, Proposition 3.2]. □

In [30] the convergence properties of the Bregman iteration scheme have been investigated in case of general subdifferentiable regularization terms J. Under the additional assumption that (SCL^2) is fulfilled the following important results can be verified.

Theorem 3.2. *Let $\tilde{u}$ denote the exact solution of the inverse problem (2.3) and assume (SCL^2) to be satisfied. Then, we obtain in case of noise-free data $f = g$ the estimate*

$$D_J^{p_k}(\tilde{u}, u_k) \leq \alpha \frac{\|q\|^2_{L^2(\Sigma)}}{2k} = \mathcal{O}\left(\frac{1}{k}\right) ,$$

for the iterates u_k of Algorithm 1, and for all $k \in \mathbb{N} \setminus \{1\}$.

Proof. See [30, Theorem 4.1]. □

Note that for $k \to \infty$ the iterates are guaranteed to converge to the true solution. In the course of this work we are going to present setups for which we will be able to even prove convergence in a finite number of Bregman iterations.

In case of noisy data the Bregman iteration scheme obviously does not converge to $\tilde{u}$ but rather has to be stopped at some optimal iterate.

Theorem 3.3. *Let $\tilde{u}$ denote the exact solution of the inverse problem (2.3) and assume (SCL^2) to be satisfied. Moreover, the standard deviation of f and g is bounded, i.e. $\|f - g\|_{L^2(\Sigma)} \leq \delta$. Then, we obtain the estimate*

$$D_J^{p_k}(\tilde{u}, u_k) \leq \alpha \frac{\|q\|_{L^2(\Sigma)}}{2k} + \delta \|q\|_{L^2(\Sigma)} + \frac{\delta^2 k}{\alpha} \text{ , for all } k \in \mathbb{N} .$$

Proof. See [30, Theorem 4.3]. □

Note that for an a-priori choice $k^* \approx 1/\delta$ we have $D_J^{p_k}(\tilde{u}, u_{k^*}) = \mathcal{O}(\delta)$.

In the following section we want to briefly investigate the interesting transition from discrete Bregman iteration to time-continuous ISS methods and recall some of the interesting properties.

3.4 Inverse Scale Space Flow

The optimality condition (3.6) for $\alpha \to \infty$ can also be seen as the backward Euler discretization of the evolution equation

$$\frac{\partial}{\partial t} p(t) = K^* \left(f - K u(t) \right) , \tag{3.9}$$

which has been termed nonlinear inverse scale space method (ISS) (cf. [26, 25]) in analogy to previous work on inverse scale space methods by Scherzer and Groetsch [114]. The inverse scale space flow is a differential inclusion, which can also be formulated as a dual gradient flow using the relation $p = A^* q$ for some q. This allows us to write

$$\frac{\partial}{\partial t} q(t) = f - K u(t), \qquad u(t) \in \partial_p J^*(K^* q),$$

thus we have

$$\frac{\partial}{\partial t} q(t) \in -\partial E^*(q),$$

with the dual energy functional

$$E^*(q) = J^*(K^* q) - \langle f, q \rangle,$$

where J^* denotes the convex conjugate of J as defined in Section 2.6.2. As a consequence of Proposition 3.1 we find

$$\|Ku(t) - f\|_{L^2(\Sigma)} \leq \|Ku(s) - f\|_{L^2(\Sigma)}, \qquad \forall\ t \geq s.$$

A second useful property concerns the decrease of the Bregman distance and the dissipation of the least-squares functional. If $\tilde{u}$ is a solution of $Ku = f$ that minimizes J then taking the duality product with $u - \tilde{u}$ reveals

$$\frac{\partial}{\partial t} D_J^{p(t)}(\tilde{u}, u(t)) = -\|Ku(t) - f\|^2_{L^2(\Sigma)}.$$

From this inequality we can infer the major convergence properties of the inverse scale space method, namely

$$\|Ku(t) - f\| = \mathcal{O}(t^{-1/2})$$

and – under appropriate conditions on J – the weak or weak-* convergence of $u(t)$ to solutions of $Ku = f$ with minimal J along subsequences. Improved convergence properties can be obtained for data satisfying (SCL^2). In that case the following convergence estimates have been proved in [30].

Theorem 3.4. *Let $\tilde{u}$ satisfy* (2.3) *and* (SCL^2). *Moreover, let u be the solution of the ISS* (3.9) *for exact data $f = g$. Then we obtain the convergence rate*

$$D_J^{p(t)}(\tilde{u}, u(t)) \leq \frac{\|q\|^2_{L^2(\Sigma)}}{2t} = \mathcal{O}(t^{-1})\,.$$

Proof. See [30, Theorem 5.1]. □

In analogy to Theorem 3.3 the following convergence estimate has been derived in case of noisy data f.

Theorem 3.5. *Let $\tilde{u}$ satisfy* (2.3) *and* (SCL^2), *and let the standard deviation of $f - g$ be bounded by δ, i.e. $\|f - g\|_{L^2(\Sigma)} \leq \delta$. Moreover, let u be the solution of the ISS* (3.9). *Then we obtain the convergence estimate*

$$D_J^{p(t)}(\tilde{u}, u(t)) \leq \frac{1}{2t}\left(\|q\|^2_{L^2(\Sigma)} + \delta t\right)^2 + \frac{\delta^2 t}{8}\,.$$

Proof. See [30, Theorem 5.2]. □

3.4.1 Regularized Inverse Scale Space Flow

By considering a time-continuous flow on (2.8) instead of the optimality condition of $\frac{1}{2}\|Ku - f\|^2_{L^2(\Sigma)}$ only, we obtain the regularized inverse scale space flow, which is defined as

$$\frac{\partial}{\partial t} p(t) = K^*\left(f - Ku(t)\right) - \alpha p(t)\,, \tag{3.10}$$

for which analogous reasoning as in the case of the unregularized problem can be carried out, respectively some results can even be improved due to the presence of p on the right-hand side. First of all, we obtain a decrease of the objective functional, i.e.

$$\frac{1}{2}\|Ku(t) - f\|^2_{L^2(\Sigma)} + \alpha J(u(t)) \leq \frac{1}{2}\|Ku(s) - f\|^2_{L^2(\Sigma)} + \alpha J(u(s)), \qquad \forall\ t \geq s.$$

Concerning the decrease of the Bregman distance we can show a stronger result.

Proposition 3.2. *Let (u,p) be a solution of (3.10) for $\alpha > 0$. Then, for $\hat{u}_\alpha$ being a minimizer of (2.8), the estimate*

$$D_J^{p(t)}(\hat{u}_\alpha, u(t)) \leq e^{-\alpha t} J(\hat{u}_\alpha)$$

holds.

Proof. Taking the duality product of (3.10) with $u - \hat{u}$ yields

$$\begin{aligned} \frac{d}{dt} D_J^p(\hat{u}, u) &= -\langle K^*(Ku - K\hat{u} + K\hat{u} - f), u - \hat{u}\rangle - \alpha\langle p, u - \hat{u}\rangle \\ &= -\|Ku - K\hat{u}\|^2 - \alpha\langle p - \tilde{p}_\alpha, u - \hat{u}\rangle \\ &\leq -\alpha D_J^p(\hat{u}, u), \end{aligned}$$

where we have inserted the optimality condition for $\hat{u}$ with subgradient $\hat{p}_\alpha \in \partial J(\hat{u}_\alpha)$ in the second line. The Gronwall inequality finally yields the assertion. □

A similar result can be shown for the dual variable q satisfying $p = K^*q$. Using

$$\hat{q} = \frac{1}{\alpha}(f - K\hat{u})$$

one can show

$$\|q(t) - \hat{q}\| \leq e^{-\alpha t}\|\hat{q}\|,$$

which by the continuity of K^* also implies the exponential convergence of $p = K^*q$.

Chapter 4

Typical Fidelities and Singular Regularization Energies

The goal of this thesis is to demonstrate the versatility of Bregman distances in the context of error estimation of approximate solutions $\hat{u}$, arising from variational schemes (2.9), with respect to true solutions $\tilde{u}$ of (2.3), as well as for the analytical and numerical computation of the approximate solutions. This chapter therefore gives an overview on popular regularization and fidelity functionals suitable for the scheme (2.9). The functionals presented are chosen to incorporate necessary a-priori information with respect to relevant applications.

4.1 Singular Regularization Energies

One of the main goals of this work is to focus on regularization functionals that are not differentiable in the conventional sense and to analyze their differences, advantages and disadvantages in comparison to differentiable regularization energies. In this section we want to introduce standard representatives of the class of singular regularization energies.

4.1.1 ℓ^0 Regularization

In the last decade the efficient sampling of datasets with only very few samples has been given a general framework called *compressed sensing* or *compressive sensing*, see for instance [47]. The typical compressed sensing application is to solve (2.3) or (2.4) with a highly under-determined matrix operator $K \in \mathbb{R}^{m\times n}$, i.e. $m \ll n$. However, as an a-priori information the true solution $\tilde{u}$ is assumed to be sparse, i.e. the amount s of non-zero elements of $\tilde{u}$ is much smaller than n. Thus, in order to find an approximate solution $\hat{u}$ of (2.9) close to $\tilde{u}$ the goal is to recover sparse solutions. A reasonable regularization energy for this kind of a-priori information would be the ℓ^0-"norm", i.e.

$$J(u) = \|u\|_{\ell^0} = \sum_{j=1}^{n} |u_j|^0 \,,$$

where we use the convention $0^0 = 0$. The ℓ^0-norm therefore exactly counts the number of non-zero elements. Note that $\|\cdot\|_{\ell^0}$ is not a proper norm, because it is obviously easy to find vectors $u \in \mathbb{R}^n$ and constants $\lambda \in \mathbb{R}_{>0}$ for which $\lambda\|u\|_{\ell^0} \neq \|u\|_{\ell^0} = \|\lambda u\|_{\ell^0}$ holds. Nevertheless $\|\cdot\|_{\ell^0}$ has been

termed norm, since it can be seen as the limit of the ℓ^p-norm for $p \to 0$. If we consider (2.9) in case of $K = I$, i.e.

$$\hat{u} = \arg\min_u \left\{ \frac{1}{2} \|u - f\|_{\ell^2}^2 + \alpha \|u\|_{\ell^0} \right\},$$

we easily discover by case differentiation that $\hat{u}$ is the hard shrinkage of f with threshold $\sqrt{2\alpha}$, i.e.

$$\hat{u}_j = \begin{cases} f_j & \text{for } f_j \geq \sqrt{2\alpha} \\ 0 & \text{else} \end{cases}.$$

However, for an arbitrary matrix K the solution of (2.9) with $J(u) = \|u\|_{\ell^0}$ is difficult (and even NP-hard), since J is highly non-convex. As an alternative, the use of the convex ℓ^1-norm as a sparsity-promoting regularizer will be discussed in the following section, since under appropriate conditions on K it can be proved that the minimizing ℓ^1- and ℓ^0-solutions coincide, see [34, 35, 48, 47].

4.1.2 ℓ^1 Regularization

The standard choice of a convex singular regularization functional to promote sparse solutions in a discrete or semi-discrete setup is the ℓ^1-norm, i.e.

$$J(u) = \|u\|_{\ell^1} = \sum_{j=1}^{n} |u_j|, \tag{4.1}$$

with its subdifferential

$$\partial J(u) = \operatorname{sign}(u) \tag{4.2}$$

being the component wise signum of u (see Example 2.13), which we will also denote by sign. If a discrete or semi-discrete inverse problem is considered for which the solutions can be assumed to be sparse signals, the choice of (4.1) is more natural than the use of a squared ℓ^2-norm. Ifwe compare a sparse signal and a dense signal in the sense of the ℓ^2-norm it is possible to have very different signals but quite similar norm values. If, on the other hand, we compare both signals in the sense of the ℓ^1-norm, the difference in the norm values is quite significant. Figure 4.1 illustrates this property of the two norms. In many compressed sensing applications the ℓ^2-ℓ^1 variational scheme is considered, i.e.

$$u \in \arg\min_{u \in \ell^1} \left\{ \frac{1}{2} \|Ku - f\|_{\ell^2}^2 + \alpha \|u\|_{\ell^1} \right\}. \tag{4.3}$$

One of the advantages of this scheme is that in case of $K = \mathrm{I}$ the solution of (4.3) can easily be computed pointwise via

$$u_j = \operatorname{shrink}(f_j, \alpha),$$

with shrink denoting the soft shrinkage operator

$$\operatorname{shrink}(f_j, \alpha) = \operatorname{sign}(f_j) \max(|f_j| - \alpha, 0).$$

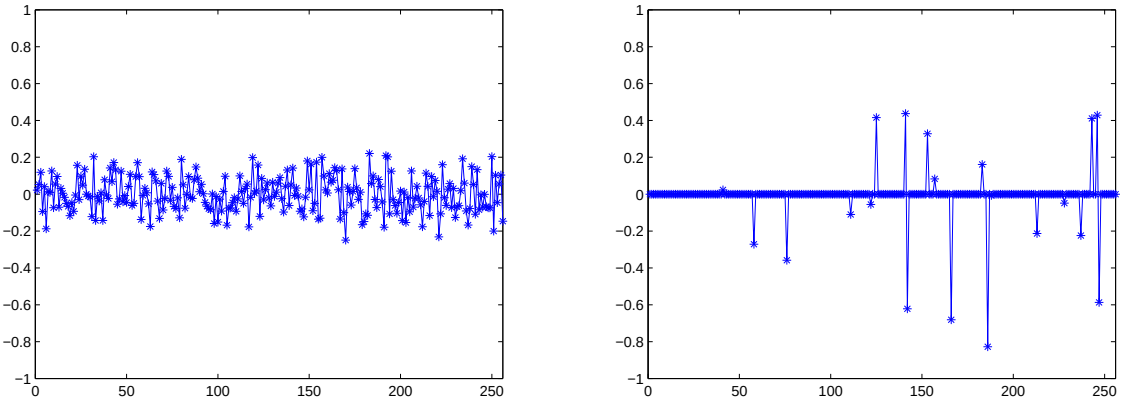

(a) Dense (b) Sparse

Figure 4.1: A dense and a sparse signal. The ℓ^2-norm of signal 4.1(a) is 1.5431, while the ℓ^2-norm of 4.1(b) is 1.7472. The difference in the ℓ^1-norm is much more significant. The ℓ^1-norm of 4.1(a) is 20.0615 and therefore large in comparison to the ℓ^1-norm of 4.1(b), which is 6.2931.

The ℓ^1 norm can be used not just for recovering sparse signals but also for promoting sparse solutions with respect to a certain basis. If a function u can be represented as $u = \sum_{j=1}^{n} \langle u, \varphi_j \rangle \varphi_j$ with respect to the basis $(\varphi_j)_{j \in \{1,\dots,n\}}$ the functional

$$J(u) = \sum_{j=1}^{n} |\langle u, \varphi_j \rangle|$$

would be a reasonable choice for a regularizer if u has a sparse representation with respect to φ.

4.1.3 L^1 Regularization and Regularization with Radon Measures

As the continuous analogue of the discrete ℓ^1 regularization we could consider the L^1 norm as a regularizer, i.e.

$$J(u) = \|u\|_{L^1(\Omega)},$$

for a function $u : \Omega \subset \mathbb{R}^d \to \mathbb{R}$, $d \in \mathbb{N}$, in $L^1(\Omega)$. Similar to ℓ^1 regularization it might be even more reasonable to consider not just the L^1-norm of a signal as a regularizer but also the L^1-norm of a suitable operator applied to that signal, i.e.

$$J(u) = \|Bu\|_{L^1(\Theta)}, \tag{4.4}$$

with $B : \mathcal{U}(\Omega) \to L^1(\Theta)$, for a suitable Banach space $\mathcal{U}(\Omega)$ and suitable sets Ω and Θ. Unfortunately, as we have already discovered in Section 2.5.5, the space L^1 might be too restrictive, depending on the operator B. We have seen that e.g. for $B = \nabla$ the regularization (4.4) only allows functions u to be in $W^{1,1}(\Omega)$, which is not desirable. To overcome this problem we have considered the distributional representation and therefore transferred the L^1-type problem to the space of Radon measures. A general approach for sparsity-promoting regularization in measure spaces has been considered in [19]. In the cited work, linear inverse problems of the form

$$K^* \mu = g$$

have been considered. In this setup, K^* maps continuously from the space of finite vector-valued Radon measures $\mathcal{M}(\Omega, \mathbb{R}^n)$ into a Hilbert space $\mathcal{H}$, for $g \in \mathcal{H}$. The space of Radon measures allows for finite combinations of delta distributions, which are the continuous analogue to sparse patterns in a discrete setup. Thus, in analogy to (4.3) in [19] the Tikhonov minimization scheme

$$\mu \in \operatorname*{arg\,min}_{\mu \in \mathcal{M}(\Omega;\mathbb{R}^n)} \left\{ \frac{1}{2} \|K^*\mu - f\|_{\mathcal{H}}^2 + \alpha \|\mu\|_{\mathcal{M}} \right\}$$

has been proposed and analyzed, for f being a noisy version of g. For more information on the novel concept of regularization with Radon measures we want to refer to [19].

4.1.4 Total Variation Regularization and the ROF-Model

One of the most popular and most extensively studied convex singular regularization functionals is the distributional representation of the L^1-norm of the gradient, as introduced in Section 2.5.5, i.e. $J(u) = \mathrm{TV}(u)$ with the Total Variation seminorm

$$\mathrm{TV}(u) = \sup_{\substack{\varphi \in C_0^\infty(\Omega;\mathbb{R}^n) \\ \|\varphi\|_\infty \leq 1}} \int_\Omega u \, \mathrm{div}\varphi \, dx \, .$$

With the help of Lemma 2.4 the subdifferential of $\mathrm{TV}(u)$ is relatively easy to characterize. Lemma 2.4 states that the subdifferential can be characterized via

$$\partial \mathrm{TV}(u) = \left\{ p \in \mathrm{BV}(\Omega)^* \mid \langle p, u \rangle_{\mathrm{BV}(\Omega)} = \mathrm{TV}(u), \langle p, v \rangle_{\mathrm{BV}(\Omega)} \leq \mathrm{TV}(v), \forall v \in \mathrm{BV}(\Omega) \right\} .$$

The dual norm $\|p\|_{\mathrm{BV}(\Omega)^*}$ therefore is bounded by one, since we easily check

$$\|p\|_{\mathrm{BV}(\Omega)^*} = \sup_{\substack{v \in \mathrm{BV}(\Omega) \\ \mathrm{TV}(v)=1}} \langle p, v \rangle_{\mathrm{BV}(\Omega)} \leq \sup_{\substack{v \in \mathrm{BV}(\Omega) \\ \mathrm{TV}(v)=1}} \mathrm{TV}(v) = 1$$

and consequently we can rewrite the subdifferential of TV to

$$\partial \mathrm{TV}(u) = \left\{ p \in \mathrm{BV}(\Omega)^* \mid \|p\|_{\mathrm{BV}(\Omega)^*} \leq 1, \langle p, u \rangle_{\mathrm{BV}(\Omega)} = \mathrm{TV}(u) \right\} .$$

Due to the characterization of the dual space of BV via

$$\mathrm{BV}(\Omega)^* = \left\{ (c, \mathrm{div}\varphi) \mid c \in \mathbb{R}, \varphi \in C\left(\overline{\Omega}; \mathbb{R}^n\right), \varphi|_{\partial\Omega} \cdot n = 0 \right\}$$

(see [29, Chapter 3]) we know that there has to exist a function $\varphi \in L^\infty(\Omega; \mathbb{R}^n)$ with $p = \mathrm{div}\varphi$. Thus, the subdifferential of TV can be written as

$$\partial \mathrm{TV}(u) = \left\{ \mathrm{div}\varphi \mid \|\varphi\|_{L^\infty(\Omega;\mathbb{R}^n)} \leq 1, \varphi|_{\partial\Omega} \cdot n = 0, \langle \mathrm{div}\varphi, u \rangle_{\mathrm{BV}(\Omega)} = \mathrm{TV}(u) \right\} . \tag{4.5}$$

The use of the Total Variation seminorm has become popular with the introduction as a regularizer in [110] of the much-cited ROF-model, i.e.

$$u \in \operatorname*{arg\,min}_{u \in \mathrm{BV}(\Omega)} \left\{ \frac{\lambda}{2} \|u - f\|_{L^2(\Omega)}^2 + \mathrm{TV}(u) \right\} , \tag{4.6}$$

named after Rudin, Osher and Fatemi. For (4.6) it can be shown that the scheme is lower semi-continuous, coercive and strictly convex (cf. [29, Chapter 3]). Hence, the application of Theorem 2.2 ensures existence of a minimizer of (4.6), while the strict convexity states that this existing minimizer has to be global and unique.

As it has been pointed out in Section 2.5.5 the TV-seminorm can be extended to higher-order derivatives, which can also be useful in terms of regularization as we want to discuss in the following section.

4.1.5 TV^2 and Higher-Order Singular Regularization Energies

In analogy to Section 4.1.4 and Section 2.5.5 the distributional representation of the L^1-norm of higher order differential operators can be considered. In particular, we want to focus on higher order TV, i.e.

$$J(u) = \mathrm{TV}^l(u) = \sup_{\substack{\varphi \in C^l(\Omega;\mathrm{Sym}^l(\mathbb{R}^n)) \\ \|\varphi\|_\infty \leq 1}} \int_\Omega u \ \mathrm{div}^l \varphi \ dx \,,$$

especially in case of $l = 2$. In analogy to the previous section the subdifferential can be characterized by

$$\partial \mathrm{TV}^l(u) = \left\{ \mathrm{div}^l \varphi \mid \|\varphi\|_{L^\infty(\Omega;\mathrm{Sym}^l(\mathbb{R}^n))} \leq 1, \varphi|_{\partial\Omega} \cdot n = 0, \langle \mathrm{div}^l \varphi, u \rangle_{\mathrm{BV}^l(\Omega)} = \mathrm{TV}^l(u) \right\} . \tag{4.7}$$

Usually, promoting sparsity with respect to one particular higher order derivative is not desirable. However, combinations of various derivatives have been subject of recent publications (cf. [117, 18, 118, 80]). Two particular models for combining the TV and higher order TV^l will be presented in the upcoming sections.

4.1.6 Infimal Convolution Regularization

A regularization approach that has been made popular by Chambolle and Lions ([38]) is the use of infimal convolutions as regularization functionals. The infimal convolution of two functionals Φ and Ψ is defined as

$$(\Phi \square \Psi)(u) := \inf_{u=v+w} \Phi(v) + \Psi(v) \,.$$

Though infimal convolution regularization can be used for arbitrary functionals Φ and Ψ (cf. [5, 6, 120]), the particular interest of this work will lie on the infimal convolution of TV and TV^2. Hence, we define

$$\begin{aligned} \mathrm{ICTV}_\beta(u) :=& \left(\mathrm{TV} \square \mathrm{TV}^2\right)(u) = \inf_{u=v+w} \mathrm{TV}(v) + \beta \mathrm{TV}^2(w) \\ =& \inf_{u=v+w} \sup_{\substack{p \in C_0^\infty(\Omega;\mathbb{R}^n) \\ \|p\|_\infty \leq 1}} \int_\Omega v \ \mathrm{div} p \ dx + \beta \sup_{\substack{q \in C_0^\infty\left(\Omega;\mathrm{Sym}^2(\mathbb{R}^n)\right) \\ \|q\|_\infty \leq 1}} \int_\Omega w \ \mathrm{div}^2 q \ dx \,, \end{aligned} \tag{4.8}$$

where we have used $\|\cdot\|_\infty$ as an abbreviation for both $\|\cdot\|_{L^\infty(\Omega;\mathbb{R}^n)}$ as well as $\|\cdot\|_{L^\infty(\Omega;\mathrm{Sym}^2(\mathbb{R}^n))}$. Equation (4.8) can be rewritten to

$$\begin{aligned} \mathrm{ICTV}_\beta(u) =& \inf_w \sup_{\substack{p \in C_0^\infty(\Omega;\mathbb{R}^n) \\ \|p\|_\infty \leq 1}} \int_\Omega (u - w) \ \mathrm{div} p \ dx + \beta \sup_{\substack{q \in C_0^\infty\left(\Omega;\mathrm{Sym}^2(\mathbb{R}^n)\right) \\ \|q\|_\infty \leq 1}} \int_\Omega w \ \mathrm{div}^2 q \ dx \\ =& \sup_{\substack{p \in C_0^\infty(\Omega;\mathbb{R}^n) \\ \|p\|_\infty \leq 1}} \sup_{\substack{q \in C_0^\infty\left(\Omega;\mathrm{Sym}^2(\mathbb{R}^n)\right) \\ \|q\|_\infty \leq 1}} \inf_w \int_\Omega (u - w) \ \mathrm{div} p \ dx + \beta \int_\Omega w \ \mathrm{div}^2 q \ dx \,, \end{aligned}$$

with the infimum for w being attained for $\beta \mathrm{div}^2 q = \mathrm{div} p$. By inserting this relation we end up with

$$\mathrm{ICTV}_\beta(u) = \sup_{\substack{p \in C_0^\infty(\Omega;\mathbb{R}^n) \\ q \in C_0^\infty\left(\Omega;\mathrm{Sym}^2(\mathbb{R}^n)\right) \\ \|p\|_\infty \leq 1 \\ \|q\|_\infty \leq 1 \\ \beta \mathrm{div}^2 q = \mathrm{div} p}} \int_\Omega u \ \mathrm{div} p \ dx = \sup_{\substack{p \in C_0^\infty(\Omega;\mathbb{R}^n) \\ q \in C_0^\infty\left(\Omega;\mathrm{Sym}^2(\mathbb{R}^n)\right) \\ \|p\|_\infty \leq 1 \\ \|q\|_\infty \leq 1 \\ \beta \mathrm{div}^2 q = \mathrm{div} p}} \beta \int_\Omega u \ \mathrm{div}^2 q \ dx \, .$$

If we substitute $q = \beta q$ we obtain

$$\mathrm{ICTV}_\beta(u) = \sup_{\substack{p \in C_0^\infty(\Omega;\mathbb{R}^n) \\ q \in C_0^\infty\left(\Omega;\mathrm{Sym}^2(\mathbb{R}^n)\right) \\ \|p\|_\infty \leq 1 \\ \|q\|_\infty \leq \beta \\ \mathrm{div}^2 q = \mathrm{div} p}} \int_\Omega u \ \mathrm{div}^2 q \ dx \, . \tag{4.9}$$

As in the previous sections we can characterize the subdifferential as

$$\begin{aligned} \partial \mathrm{ICTV}_\beta(u) = \Big\{ \mathrm{div}^2 \varphi \mid \|\psi\|_{L^\infty(\Omega;\mathbb{R}^n)} \leq 1, \|\varphi\|_{L^\infty(\Omega;\mathrm{Sym}^2(\mathbb{R}^n))} \leq \beta, \varphi|_{\partial\Omega} \cdot n = 0, \\ \psi|_{\partial\Omega} \cdot n = 0, \mathrm{div}^2 \varphi = \mathrm{div} \psi, \langle \mathrm{div}^2 \varphi, u \rangle_{L^2(\Omega)} = \mathrm{ICTV}_\beta(u) \Big\} \, . \end{aligned} \tag{4.10}$$

A typical variational setup for denoising is the combination of the L^2 data fidelity and ICTV_β as a regularizer, i.e.

$$u \in \operatorname*{arg\,min}_{u \in \mathrm{BV}^2(\Omega)} \left\{ \frac{1}{2} \|u - f\|_{L^2(\Omega)}^2 + \alpha \mathrm{ICTV}_\beta(u) \right\} .$$

In comparison to Total Variation regularization the infimal convolution of TV and TV^2 is witnessed to reduce the so-called staircasing phenomenon. A solution of the ROF model (4.6) for a piecewise linear input function corrupted by noise is not a linear but a piecewise constant stair-like approximation of the input data, which is not the case for ICTV_β regularization if the regularization parameters are carefully chosen.

However, in higher than one dimension it has been observed that the infimal convolution model does not separate a function into its TV and TV^2 structures properly. Consequently, a modified infimal convolution model has been proposed that we are going to recall in the following section.

4.1.7 Generalized Total Variation

Since the infimal convolution of TV and TV^2 did not yield the desired optimal separations of piecewise constant and piecewise linear regions for two and higher dimensions, modifications of (4.9) have been proposed. In [117] a modification of (4.9) named modified infimal convolution has been developed from a rather algorithmic point of view, while in [18] a generalization and the analytical foundation for this work has been investigated and analyzed under the name Total Generalized Variation. Since the name goes back to a pun on French trains we are going to refer to this model as *Generalized Total Variation* (GTV). In [118] it has been pointed out that in case of TV and TV^2 as regularizers the modified infimal convolution and GTV coincide. The generalized total variation of second order is defined as

$$\mathrm{GTV}_\beta(u) := \sup_{\substack{q \in C_0^\infty(\Omega;\mathbb{R}^n) \\ \|q\|_\infty \leq \beta \\ \|\mathrm{div} q\|_\infty \leq 1}} \int_\Omega u \ \mathrm{div}^2 q \ dx \, . \tag{4.11}$$

The infimal convolution regularization (4.9) and the generalized TV regularization (4.11) therefore coincide if $p = \mathrm{div} q$ holds.
The subdifferential of the second-order generalized total variation reads

$$\begin{aligned}\partial \mathrm{GTV}_\beta(u) = \Big\{ &\mathrm{div}^2 \varphi \mid \|\varphi\|_{L^\infty(\Omega;\mathbb{R}^n)} \leq \beta, \|\mathrm{div}\varphi\|_{L^\infty(\Omega;\mathrm{Sym}^2(\mathbb{R}^n))} \leq 1, \varphi|_{\partial\Omega} \cdot n = 0, \\ &\nabla\varphi|_{\partial\Omega} \cdot n = 0, \langle \mathrm{div}^2 \varphi, u\rangle_{L^2(\Omega)} = \mathrm{GTV}_\beta(u) \Big\} \,.\end{aligned} \tag{4.12}$$

In Chapter 6, Section 6.3, we are going to investigate the different regularization functionals and their properties in recovering functions exactly both in the absence and presence of noise.

4.2 Typical Fidelities

Typically, most inverse problems involve the computation of the least-squares-solution with some additional regularization term, i.e. the data fidelity is assumed to be a squared L^2-norm. The popularity of this fidelity term lies in its computational simplicity, since the optimality condition of the squared L^2-norm yields a linear problem. Moreover, measurement noise can very often be assumed to be normal-distributed, which also suggests the use of the squared L^2-norm as a reasonable data fidelity.

However, in many applications different fidelities than the standard L^2-fidelity are considered, usually to incorporate different a-priori knowledge on the distribution of noise. Exemplary applications are Synthetic Aperture Radar, Positron Emission Tomography or Optical Nanoscopy. In the following, we want to present those fidelities that are of further interest in the course of this work.

4.2.1 Fidelities with Scaling Properties

In order to provide a rather broad class of general fidelities including the popular quadratic fidelities, we want to consider general convex fidelities with scaling property, i.e.

$$H_f(Ku) := F(Ku - f)\,,$$

with $F : \mathcal{V}(\Sigma) \to \mathbb{R}$ being a convex and Fréchet-differentiable functional such that the scaling property

$$\lambda F'(v) = F'(s(\lambda)v) \tag{4.13}$$

is fulfilled, for all $\lambda \in \mathbb{R}_{>0}$ and for a monotone function $s : \mathbb{R}_{>0} \to \mathbb{R}$. The corresponding variational problem reads as

$$\hat{u} \in \underset{u \in \mathrm{dom}(J)}{\arg\min} \left\{ F(Ku - f) + \alpha J(u) \right\} , \tag{4.14}$$

with optimality condition

$$0 = K^* F'(K\hat{u} - f) + \alpha \hat{p}\,,$$

for $\hat{p} \in \partial J(\hat{u})$.

Note that the functionals F are Fréchet-differentiable and therefore continuous, and consequently also lower semi-continuous.

Typical examples for data fidelities fulfilling a scaling property are L^p norms to the power of p (for $p > 1$), as introduced in Section 2.5.1.

L^p Fidelities

If we consider

$$H_f(Ku) := \frac{1}{p} \|(Ku)(y) - f(y)\|^p_{L^p(\Sigma)} = \frac{1}{p} \int_\Sigma |Ku - f|^p \ d\mu(y) \,, \tag{4.15}$$

for $p > 1$, we easily see that $H_f(Ku)$ satisfies a scaling property with $s(\lambda) = \lambda^{\frac{1}{p-1}}$. As a special case the choice $p = 2$ (4.15) yields the most popular among all fidelities,

$$H_f(Ku) = \frac{1}{2} \|Ku - f\|^2_{L^2(\Sigma)} \,, \tag{4.16}$$

with $s(\lambda) = \lambda$. The optimality condition of (4.14) with $H_f(Ku)$ being defined via (4.16) simply equals

$$K^* (K\hat{u} - f) + \alpha\hat{p} = 0 \,, \, \hat{p} \in \partial J(\hat{u}) \,. \tag{4.17}$$

Note that the Fréchet-derivatives of L^p-fidelities to the power of p are continuously invertible for $p > 1$.

4.2.2 General Norm Fidelity

Typical non-quadratic fidelity terms, moreover non-Fréchet-differentiable, are norms in general, i.e.

$$H_f(Ku) := \|Ku - f\|_{\mathcal{V}(\Sigma)} \,,$$

without taking a power of it. The corresponding variational problem is given via

$$\hat{u} \in \operatorname*{arg\,min}_{u \in \mathcal{W}(\Omega)} \left\{ \|Ku - f\|_{\mathcal{V}(\Sigma)} + \alpha J(u) \right\} . \tag{4.18}$$

The optimality condition of (4.18) can be computed as

$$K^*\hat{s} + \alpha\hat{p} = 0 \qquad \hat{s} \in \partial \|K\hat{u} - f\|_{\mathcal{V}(\Sigma)}, \quad \hat{p} \in \partial J(\hat{u}) \,. \tag{4.19}$$

In the following we want to present two special cases of this general class of fidelity terms that have been investigated in several applications.

L^1 Fidelity

A typical norm fidelity term used in applications involving Laplace-distributed or impulsive noise (e.g. Salt'n'Pepper noise), is the L^1-fidelity (see for instance [40, 39, 133]). The related variational problem is given via

$$\hat{u} = \operatorname*{arg\,min}_{u \in \mathcal{W}(\Omega)} \left\{ \int_\Sigma |(Ku)(y) - f(y)| \ d\mu(y) + \alpha J(u) \right\} . \tag{4.20}$$

The optimality condition of (4.20) can easily be computed as

$$K^*\hat{s} + \alpha\hat{p} = 0, \qquad \hat{s} \in \operatorname{sign}(K\hat{u} - f), \quad \hat{p} \in \partial J(\hat{u}) \,, \tag{4.21}$$

with $\operatorname{sign}(x)$ being the signum "function", which is the continuous analogue to the discrete pointwise signum "function" that we have already considered in (4.2).

BV* Fidelity

In order to separate an image into texture and structure, in [90] Meyer proposed a modification of the ROF model (4.6) via

$$F(u,v) := \|v\|_{BV(\Omega)^*} + \frac{1}{2\lambda} \sup_{\substack{q\in C_0^\infty(\Omega;\mathbb{R}^2)\\ \|q\|_\infty\le 1}} \int_\Omega u \ \mathrm{div} q \ dx$$

with respect to u (structure) and v (texture) for a given image $f = u + v$, and with $\|\cdot\|_{BV(\Omega)^*}$ being defined as

$$\|w\|_{BV(\Omega)^*} := \inf_p \left\| \left(|p_1|^2 + |p_2|^2 \right)^{\frac{1}{2}} \right\|_{L^\infty(\Omega)},$$

subject to $\mathrm{div} p = w$. Initially the norm has been introduced as G-norm.
In this context, we are going to consider the variational model

$$u \in \operatorname*{arg\,min}_{u\in\mathcal{W}(\Omega)} \left\{ \|Ku - f\|_{\mathrm{BV}(\Sigma)^*} + \alpha J(u) \right\},$$

with its corresponding optimality condition

$$K^*\hat{s} + \alpha\hat{p} = 0, \qquad \hat{s} \in \partial \|K\hat{u} - f\|_{\mathrm{BV}(\Sigma)^*}, \qquad \hat{p} \in \partial J(\hat{u}).$$

4.2.3 Kullback-Leibler Fidelity

In applications such as Positron Emission Tomography or Optical Nanoscopy, sampled data usually obey a Poisson process. For that reason, other fidelities than the L^2 fidelity have to be incorporated into the variational framework. The most popular fidelity in this context is the Kullback-Leibler divergence (cf. [92]), i.e.

$$H_f(Ku) = \mathrm{KL}(f, Ku) := \int_\Sigma \left[f(y) \ln\left(\frac{f(y)}{(Ku)(y)} \right) - f(y) + (Ku)(y) \right] d\mu(y). \tag{4.22}$$

Note that $\mathrm{KL}(u,v)$ equals the Bregman distance $D_G^{G'(v)}(u,v)$ for $G(u) = \int_\Sigma u \ln(u) - u \ d\mu(y)$, because of Example 3.2. Furthermore, due to the nature of the applications and their data, the function u usually represents a density that needs to be positive. The related variational minimization problem with an additional positivity constraint therefore reads

$$\hat{u} \in \operatorname*{arg\,min}_{\substack{u\in\mathcal{W}(\Sigma)\\ u\ge 0}} \left\{ \int_\Sigma \left[f(y) \ln\left(\frac{f(y)}{(Ku)(y)} \right) - f(y) + (Ku)(y) \right] d\mu(y) + \alpha J(u) \right\}. \tag{4.23}$$

With the natural scaling assumption

$$K^*\mathbf{1} = \mathbf{1}, \tag{4.24}$$

we obtain the complementarity condition

$$\begin{aligned} \hat{u} \ge 0, \qquad & K^*\frac{f}{Ku} - \alpha\hat{p} \le 1, \\ \hat{u}\left(1 - K^*\frac{f}{K\hat{u}} + \alpha\hat{p}\right) = 0, \qquad & \hat{p} \in \partial J(\hat{u}), \end{aligned} \tag{4.25}$$

to find optimal solutions of (4.23). The questions in which spaces the data f and the solution $\hat{u}$ can be considered is not trivial, see for instance [76, Section 4.1.3].

The Kullback-Leibler functional is lower semi-continuous (cf. [106, Section 3]), which is a key property that allows to show well-posedness of the variational framework (4.23) for particular choices of the regularization energy (e.g. for $J(u) = \mathrm{TV}(u)$, see for instance [21, Section 5.4.2]).

4.2.4 Multiplicative Noise Fidelities

In applications such as Synthetic Aperture Radar the data is supposed to be corrupted by multiplicative noise, i.e. $f = (Ku)\, v$, where v represents the noise following a certain probability law and where $Ku \geq 0$ is assumed. In [4], Aubert and Aujol assumed v to follow a gamma law with mean one and derived the data fidelity

$$H_f(Ku) = \int_\Sigma \left[\ln\left(\frac{(Ku)(y)}{f(y)} \right) + \frac{f(y)}{(Ku)(y)} - 1 \right] d\mu(y)\,.$$

Hence, the corresponding variational minimization problem reads as

$$\hat{u} \in \operatorname*{arg\,min}_{u \in \mathcal{W}(\Omega)} \left\{ \int_\Sigma \left[\ln\left(\frac{(Ku)(y)}{f(y)} \right) + \frac{f(y)}{(Ku)(y)} - 1 \right] d\mu(y) + \alpha J(u) \right\}, \tag{4.26}$$

with the formal optimality condition

$$0 = K^* \left(\frac{(K\hat{u})(y) - f(y)}{((K\hat{u})(y))^2} \right) + \alpha \hat{p}\,, \qquad \hat{p} \in \partial J(\hat{u})\,. \tag{4.27}$$

One main drawback of (4.26) is that the fidelity term is not globally convex and therefore will not allow unconditional use of the Bregman-distance based analytical framework we are going to derive in the upcoming sections. In order to convexify this speckle noise removal model, in [69] Huang et al. suggested the substitution $z(y) := \ln((Ku)(y))$ to obtain the entirely convex optimization problem

$$\hat{z} = \operatorname*{arg\,min}_{z \in \mathcal{W}(\Sigma)} \left\{ \int_\Sigma \left[z(y) + f(y) e^{-z(y)} - 1 - \ln(f(y)) \right] d\mu(y) + \alpha J(z) \right\}, \tag{4.28}$$

with optimality condition

$$1 - f(y) e^{-\hat{z}(y)} + \alpha \hat{p} = 0\,, \tag{4.29}$$

for $\hat{p} \in \partial J(\hat{z})$. This model is a special case of the general multiplicative noise model presented in [119]. We mention that in case of total variation regularization a contrast change as above is not harmful, since the structural properties (edges and piecewise constant regions) are preserved.

In ultrasound imaging the use of different data fidelities for incorporating improved a-priori information on the noise structure has recently become of major interest. In [82] the authors have proposed the data fidelity term

$$H_f(Ku) = \int_\Omega \left[\frac{(u - f)^2}{u} \right] d\mu(x)\,, \tag{4.30}$$

which is based on the assumption that the exact data u is corrupted by multiplicative noise of the form $f = u + n\sqrt{u}$, with n being a Gaussian distributed random variable with mean zero and standard deviation σ. In [74] this data fidelity has been combined with total variation regularization, which motivates the general variational minimization problem

$$\hat{u} \in \operatorname*{arg\,min}_{\substack{u \in \mathcal{W}(\Omega) \\ u>0}} \left\{ \int_{\Sigma} \left[\frac{(Ku - f)^2}{Ku} \right] d\mu(y) + \alpha J(u) \right\}, \tag{4.31}$$

with the formal optimality condition

$$0 = K^* \left(\frac{(K\hat{u})^2 - f^2}{(K\hat{u})^2} \right) + \alpha \hat{p}\,, \qquad \hat{p} \in \partial J(\hat{u})\,. \tag{4.32}$$

Chapter 5

Error Estimates

By regularizing the inverse problem (2.4), our goal is to obtain a solution $\hat{u}$ close to $\tilde{u}$ in a robust way with respect to noise. Hence, we are interested in error estimates that describe the behavior of $\hat{u}$ in contrast to $\tilde{u}$ with respect to the "data error" δ, and we are interested in optimal choices for quadratic fitting (see [51]). A major step for error estimates in the case of regularization with singular energies has been the introduction of (generalized) Bregman distances (cf. [20, 79]) as an error measure (cf. [49, 28]), as we have already pointed out in Section 3.2.

Many works yet deal with the analysis and error propagation by considering the Bregman distance between $\hat{u}$ satisfying the optimality condition of a variational regularization method (2.9) and the exact solution $\tilde{u}$ (cf. [30, 31, 68, 84, 86, 107]). The Bregman distance turned out to be an adequate error measure since it seems to control only those errors that can be distinguished by the regularization term. This point of view is supported by the need of so-called source conditions, which are needed to obtain error estimates in the Bregman distance setting.

Most works yet deal with the case of quadratic fitting, with only few exceptions (see e.g. [97]). However, as we have seen in Chapter 4, for many applications, such as Positron Emission Tomography (PET), Microscopy, CCD cameras, or radar, different types of data fidelities appear.

In the following we want to present rather general error estimates for arbitrary fidelities. Then, we are going to apply these basic error estimates for general, convex variational regularization methods to the specific models presented in Chapter 4, Section 4.2. We would also like to mention the parallel development on error estimates for variational models with non-quadratic fidelity in [97], which yields the same results as our paper in the case of L^1 fidelity. Since the analysis in [97] is rather based on fidelities that are powers of a metric instead of the noise models we use here, most approaches appear orthogonal. In particular we base our analysis on convexity and duality and avoid the use of triangle inequalities, which can only be used for a metric. Most of the work that is considered in this chapter is part of [8].

5.1 Estimates for General Fidelities

After having introduced some frequently used non-quadratic variational schemes in Section 4.2, we want to present general error estimates for (convex) variational schemes. These basic estimates will allow us to derive specific error estimates for the specific models. Furthermore we want to explore duality and will discover an error estimate dependent on the convex conjugates of the fidelity and regularization terms.

In order to derive estimates in the Bregman distance setting we need to introduce the so-called

source condition

$$\exists\, \xi \in \partial J(\tilde{u}),\, \exists\, q \in \mathcal{V}(\Sigma)^* \setminus \{0\} : \quad \xi = K^* q\,, \tag{SC1}$$

which can also be written as

$$\mathcal{R}(K^*) \cap \partial J(\tilde{u}) \neq \emptyset\,.$$

The source condition (SC1) in some sense will ensure that a solution $\tilde{u}$ contains features that can be distinguished by the regularization term J, which can be seen by the following lemma.

Lemma 5.1. *The source condition* (SC1) *is equivalent to the existence of a function $h \in \mathcal{V}(\Sigma)$, such that $\tilde{u}$ satisfies*

$$\tilde{u} \in \operatorname*{arg\,min}_{u \in \mathrm{dom}(J)} \left\{ H_h(Ku) + \alpha J(u) \right\}\,, \tag{5.1}$$

for a Fréchet-differentiable functional $H_h : \mathcal{V}(\Sigma) \to \mathbb{R}$ such that $(H_h')^{-1}$ exists.

Proof. "⇐": The fact that $\tilde{u}$ minimizes (5.1) implies optimality; hence, the equation

$$K^* H_h'(K\tilde{u}) + \alpha\xi = 0$$

has to hold, for an existing $\xi \in \partial J(\tilde{u})$. This in turn implies (SC1) with source element $q = -\left(K^* H_h'\left(K\tilde{u}\right)\right)/\alpha \in \mathcal{V}(\Sigma)^*$.
"⇒": The validity of (SC1) implies

$$0 = \alpha\xi - \alpha K^* q\,,$$

which can be rewritten to

$$0 = \alpha\xi + K^* G_h'\left((G_h^*)'(-\alpha q)\right)\,,$$

with $G_h(Ku - h) := H_h(Ku)$ and G_h^* denoting the convex conjugate of G_h, since Lemma 2.7 states that $G_h'\left((G_h^*)'(p)\right) = p$. Hence, by defining $h := K\tilde{u} - (G_h^*)'(-\alpha q)$ we obtain

$$0 = \alpha\xi + K^* G_h'(K\tilde{u} - h)\,.$$

□

Consequently, Lemma 5.1 guarantees the existence of some data $h \in \mathcal{V}(\Sigma)$, such that $\tilde{u}$ minimizes (2.9) with respect to the data h. This is only possible if $\tilde{u}$ contains features that can be distinguished by the regularization term.

Motivated by [105] we can also define a stronger source condition for centered functionals of the type $G_f(Ku - f) := H_f(Ku)$. The stronger source condition then is defined as

$$\exists\, \xi \in \partial J(\tilde{u}),\, \exists\, v \in \mathcal{U}(\Omega) \setminus \{0\} : \quad \xi = -K^* G_f'(Kv)\,, \tag{SC2}$$

for $f \in \mathcal{R}(K)$, which can equivalently be written as

$$\mathcal{R}\left(-K^* G_f'(K\cdot)\right) \cap \partial J(\tilde{u}) \neq \emptyset\,.$$

In Section 5.1.3 we are going to see that for a specific type of functionals, namely the functionals with scaling property (4.13) as defined in Section 4.2.1, the strong source condition (SC2) can be interpreted as a condition that guarantees $\tilde{u}$ to be a minimizer of the variational model (2.9) for some exact data in the range of K.

5.1.1 Basic Estimates

In this section we are going to derive basic error estimates in the Bregman distance measure for general variational regularization methods.

To find a suitable solution of the inverse problem (2.4), close to the unknown exact solution $\tilde{u}$ of (2.3), we consider methods of the form (2.9). We are going to denote a solution of (2.9), which fulfills the optimality condition due to the Karush-Kuhn-Tucker conditions (KKT), by $\hat{u}$.
First of all, we are going to derive a rather general estimate for the Bregman distance $D_J^{\xi}(\hat{u}, \tilde{u})$.

Lemma 5.2. *Let $\tilde{u}$ denote an exact solution of the inverse problem* (2.3) *and let the source condition* (SC1) *be fulfilled. Furthermore, let the functional $J : \mathcal{W}(\Omega) \to \mathbb{R} \cup \{\infty\}$ be convex. If there exists a solution $\hat{u}$ that satisfies* (2.9) *for $\alpha > 0$, then the error estimate*

$$H_f(K\hat{u}) + \alpha D_J^{\xi}(\hat{u}, \tilde{u}) \leq H_f(g) - \alpha \langle q, K\hat{u} - g \rangle_{\mathcal{V}(\Sigma)}$$

holds.

Proof. Since $\hat{u}$ is an existing minimal solution satisfying (2.9) we have

$$H_f(K\hat{u}) + \alpha J(\hat{u}) \leq H_f(\underbrace{K\tilde{u}}_{=g}) + \alpha J(\tilde{u})\,.$$

If we subtract $\alpha \left(J(\tilde{u}) + \langle \xi, \hat{u} - \tilde{u} \rangle_{\mathcal{U}(\Omega)} \right)$ on both sides we end up with

$$\begin{aligned} & H_f(K\hat{u}) + \alpha \underbrace{\left(J(\hat{u}) - J(\tilde{u}) - \langle \xi, \hat{u} - \tilde{u} \rangle_{\mathcal{U}(\Omega)} \right)}_{= D_J^{\xi}(\hat{u}, \tilde{u})} \\ \leq\ & H_f(g) - \alpha \underbrace{\langle \xi, \hat{u} - \tilde{u} \rangle_{\mathcal{U}(\Omega)}}_{= \langle K^* q, \hat{u} - \tilde{u} \rangle_{\mathcal{U}(\Omega)}} \\ =\ & H_f(g) - \alpha \langle q, K\hat{u} - g \rangle_{\mathcal{V}(\Sigma)}\,. \end{aligned}$$

□

Notice that J needs to be convex in order to guarantee the positivity of $D_J^{\xi}(\hat{u}, \tilde{u})$ and therefore to ensure a meaningful estimate. In contrast to that, the data fidelity H_f does not necessarily need to be convex, which makes Lemma 5.2 a very general estimate. Furthermore, the estimate also holds for any $\overline{u}$ for which we can guarantee $H_f(K\overline{u}) + \alpha J(\overline{u}) \leq H_f(K\tilde{u}) + \alpha J(\tilde{u})$ (a property that obviously might be hard to prove for a specific $\overline{u}$), which might be useful to study non-optimal approximations to $\hat{u}$. Nevertheless, we are mainly going to deal with a specific class of convex variational problems that allows us to derive sharper estimates, similar to Lemma 5.2 but for $D_J^{\text{symm}}(\hat{u}, \tilde{u})$. Before we start proving these estimates, we are going to define the following class of problems that we further want to investigate:

Definition 5.1. *We define the class $\mathcal{C}(\Phi, \Psi, \Theta)$ as follows: $(H, J, K) \in \mathcal{C}(\Phi, \Psi, \Theta)$ if*

- *$K : \Theta \to \Phi$ is a linear operator between Banach spaces Θ and Φ*
- *$H : \Phi \to \mathbb{R} \cup \{\infty\}$ is proper, convex and lower semi-continuous*
- *$J : \Psi \to \mathbb{R} \cup \{\infty\}$ is proper, convex and lower semi-continuous*
- *There exists a u' with $Ku' \in dom(H)$ and $u' \in dom(J)$, such that H is continuous at Ku'.*

With this definition we assume more regularity to the considered functionals and are now able to derive the same estimate as in Lemma 5.2, but for $D_J^{\text{symm}}(\hat{u},\tilde{u})$ instead of $D_J^{\xi}(\hat{u},\tilde{u})$.

Theorem 5.1 (Basic Estimate I)**.** *Let $(H_f, J, K) \in \mathcal{C}(\mathcal{V}(\Sigma),\mathcal{W}(\Omega),\mathcal{U}(\Omega))$, for compact and bounded sets Ω and Σ. Then, if the source condition* (SC1) *is fulfilled, the error estimate*

$$H_f(K\hat{u}) + \alpha D_J^{\text{symm}}(\hat{u},\tilde{u}) \leq H_f(g) - \alpha\langle q, K\hat{u} - g\rangle_{\mathcal{V}(\Sigma)} \tag{5.2}$$

holds.

Proof. Since H_f and J are convex, the optimality condition of (2.9) is given via

$$0 \in \partial\left(H_f(K\hat{u}) + \alpha J(\hat{u})\right) .$$

Since both H_f and J are proper, lower semi-continuous and convex, and since there exists u' with $Ku' \in \operatorname{dom}(H_f)$ and $u' \in \operatorname{dom}(J)$, such that H_f is continuous at Ku', we have $\partial H_f(Ku) + \alpha\partial J(u) = \partial\left(H_f(Ku) + \alpha J(u)\right)$ for all $u \in \mathcal{W}(\Omega)$, because of Theorem 2.5. Due to the linear mapping properties of K we furthermore have $\partial H_f(K\cdot)(u) = K^*\partial H_f(Ku)$. Hence, the following equality holds:

$$K^*\hat{\eta} + \alpha\hat{p} = 0\,,$$

for $\hat{\eta} \in \partial H_f(K\hat{u})$ and $\hat{p} \in \partial J(\hat{u})$. If we subtract $\alpha\xi$, with ξ fulfilling (SC1), and if we take the duality product with $\hat{u} - \tilde{u}$, we obtain

$$\langle K^*\hat{\eta}, \hat{u} - \tilde{u}\rangle_{\mathcal{U}(\Omega)} + \alpha\langle \hat{p} - \xi, \hat{u} - \tilde{u}\rangle_{\mathcal{U}(\Omega)} = -\alpha\langle \underbrace{\xi}_{=K^*q}, \hat{u} - \tilde{u}\rangle_{\mathcal{U}(\Omega)}\,,$$

which equals

$$\langle \hat{\eta}, K\hat{u} - \underbrace{K\tilde{u}}_{=g}\rangle_{\mathcal{V}(\Sigma)} + \alpha D_J^{\text{symm}}(\hat{u},\tilde{u}) = -\alpha\langle q, K\hat{u} - \underbrace{K\tilde{u}}_{=g}\rangle_{\mathcal{V}(\Sigma)}\,.$$

Since H_f is convex, the Bregman distance $D_{H_f}^{\hat{\eta}}(g, K\hat{u})$ is non-negative, i.e.

$$D_{H_f}^{\hat{\eta}}(g, K\hat{u}) = H_f(g) - H_f(K\hat{u}) - \langle\hat{\eta}, g - K\hat{u}\rangle_{\mathcal{V}(\Sigma)} \geq 0\,,$$

for $\hat{\eta} \in \partial H_f(K\hat{u})$. Hence, we obtain

$$\langle\hat{\eta}, K\hat{u} - g\rangle_{\mathcal{V}(\Sigma)} \geq H_f(K\hat{u}) - H_f(g)\,.$$

As a consequence, this yields (5.2). □

We can further generalize the estimate of Theorem 5.1 to obtain the second important general estimate in this work.

Theorem 5.2 (Basic Estimate II)**.** *Let $(H_f, J, K) \in \mathcal{C}(\mathcal{V}(\Sigma),\mathcal{W}(\Omega),\mathcal{U}(\Omega))$, for compact and bounded sets Ω and Σ. Then, if the source condition* (SC1) *is fulfilled, the error estimate*

$$\begin{aligned}(1-c)H_f(K\hat{u}) + \alpha D_J^{\text{symm}}(\hat{u},\tilde{u}) \leq\ & (1+c)H_f(g)\\ & - \alpha\langle q, f - g\rangle_{\mathcal{V}(\Sigma)} - cH_f(g)\\ & + \alpha\langle q, f - K\hat{u}\rangle_{\mathcal{V}(\Sigma)} - cH_f(K\hat{u})\end{aligned} \tag{5.3}$$

holds, for $c \in]0,1[$.

Proof. Due to Theorem 5.1 we have

$$H_f(K\hat{u}) + \alpha D_J^{\text{symm}}(\hat{u}, \tilde{u}) \leq H_f(g) - \alpha\langle q, K\hat{u} - g\rangle_{\mathcal{V}(\Sigma)}\,.$$

The left hand side is equivalent to

$$(1-c)H_f(K\hat{u}) + \alpha D_J^{\text{symm}}(\hat{u}, \tilde{u}) + cH_f(K\hat{u})\,,$$

while the right-hand side can be rewritten to

$$(1+c)H_f(g) - \alpha\langle q, K\hat{u} - g\rangle_{\mathcal{V}(\Sigma)} - cH_f(g)\,,$$

for $c \in]0,1[$, without affecting the inequality. The dual product $\langle q, K\hat{u} - g\rangle_{\mathcal{V}(\Sigma)}$ is equivalent to $\langle q, f + K\hat{u} - g - f\rangle_{\mathcal{V}(\Sigma)}$ and hence we have

$$-\alpha\langle q, K\hat{u} - g\rangle_{\mathcal{V}(\Sigma)} = -\alpha\langle q, f - g\rangle_{\mathcal{V}(\Sigma)} + \alpha\langle q, f - K\hat{u}\rangle_{\mathcal{V}(\Sigma)}\,.$$

Subtracting $cH_f(K\hat{u})$ on both sides and replacing $-\alpha\langle q, K\hat{u} - g\rangle_{\mathcal{V}(\Sigma)}$ by $-\alpha\langle q, f - g\rangle_{\mathcal{V}(\Sigma)} + \alpha\langle q, f - K\hat{u}\rangle_{\mathcal{V}(\Sigma)}$ yields (5.3). □

In Section 5.2 these two basic estimates will allow us to easily derive specific error estimates for the fidelities described in Section 4.2.

5.1.2 A Dual Perspective

In the following we provide a formal analysis in terms of Fenchel duality, which highlights a general way to obtain error estimates and provides further insights. In order to make the approach rigorous one needs to check detailed properties of all functionals allowing to pass to dual problems formally (cf. Section 2.6.2), which is however not our goal here.

In order to formulate the dual approach we redefine the fidelity to $G_f(Ku - f) := H_f(Ku)$. Under appropriate conditions, Theorem 2.7 implies the primal-dual relation

$$\inf_{u\in\mathcal{W}(\Omega)} \left[\frac{1}{\alpha}G_f(Ku - f) + J(u)\right] = -\inf_{q\in\mathcal{V}(\Sigma)^*} \left[J^*(K^*q) - \langle q, f\rangle_{\mathcal{V}(\Sigma)} + \frac{1}{\alpha}G_f^*(-\alpha q)\right]$$

as well as a relation between the minimizers $\hat{u}$ of the primal and $\hat{q}$ of the dual problem, namely

$$K^*\hat{q} \in \partial J(\hat{u}), \qquad \hat{u} \in \partial J^*(K^*\hat{q}).$$

More precisely, the optimality condition for the dual problem becomes

$$K\hat{u} - f - r = 0, \qquad r \in \partial G_f^*(-\alpha\hat{q}).$$

If the exact solution $\tilde{u}$ satisfies a source condition with source element d (i.e. $K^*d \in \partial J(\tilde{u})$), then we can use the dual optimality condition and take the duality product with $\hat{q} - d$, which yields

$$\langle K(\hat{u} - \tilde{u}), \hat{q} - d\rangle_{\mathcal{V}(\Sigma)^*} = \frac{1}{\alpha}\langle r, (-\alpha d) - (-\alpha\hat{q})\rangle_{\mathcal{V}(\Sigma)^*} + \langle f - g, \hat{q} - d\rangle_{\mathcal{V}(\Sigma)^*}.$$

One observes that the left hand side equals

$$D_J^{\text{symm}}(\hat{u}, \tilde{u}) = \langle \hat{u} - \tilde{u}, K^*(\hat{q} - d)\rangle_{\mathcal{U}(\Omega)^*},$$

i.e. the Bregman distance we want to estimate. Using $r \in \partial G_f^*(-\alpha\hat{q})$ we find

$$\langle r, (-\alpha d) - (-\alpha\hat{q})\rangle_{\mathcal{V}(\Sigma)^*} \leq G_f^*(-\alpha d) - G_f^*(-\alpha\hat{q}).$$

Under the standard assumption $G_f(0) = 0$ we find that G_f^* is nonnegative and hence in the noise-free case ($f = g$) we end up with the estimate

$$D_J^{\text{symm}}(\hat{u}, \tilde{u}) \leq \frac{1}{\alpha} G_f^*(-\alpha d).$$

Hence the error in terms of α is determined by the properties of the convex conjugate of G_f. For typical smooth fidelities G_f we have $G_f^*(0) = 0$ and $(G_f^*)'(0) = 0$, hence $\frac{1}{\alpha} G_f^*(-\alpha d)$ will at least grow linearly for small α, which will also be confirmed by our results below.

In the applications to specific noise models our strategy will be to estimate the terms on the right-hand side of (5.3) by quantities like $G_f^*(-\alpha d)$ and then work out the detailed dependence on α.

5.1.3 General Estimates with Strong Source Condition

In contrast to Section 5.1.1 we want to consider error estimates for a rather general class of functionals such that the strong source condition (SC2), inspired by [105], has to be satisfied. We therefore consider variational minimization problems like (4.14), such that F fulfills the scaling property (4.13). In case of this specific type of data fidelity (SC2) has a very intuitive interpretation, as the following lemma states.

Lemma 5.3. *Let $F : \mathcal{V}(\Sigma) \to \mathbb{R} \cup \{\infty\}$ satisfy a scaling property* (4.13)*. Then, the strong source condition* (SC2) *is equivalent to the existence of a function $\overline{u} \in \mathcal{U}(\Omega)$ for which $\tilde{u}$, satisfying* (2.3)*, is a valid, existing minimizer of* (4.14) *with data $f = K\overline{u}$, i.e.*

$$\tilde{u} = \operatorname*{arg\,min}_{u \in \mathcal{W}(\Omega)} \left\{ F(Ku - K\overline{u}) + \alpha J(u) \right\} .$$

Proof. "⇐": Since $\tilde{u}$ is supposed to be a minimizer of (4.14) for $f = K\overline{u}$, the optimality condition

$$0 = K^* F'(K\tilde{u} - K\overline{u}) + \alpha\xi \,,\, \xi \in \partial J(\tilde{u})$$

needs to be satisfied. We can rewrite this equation to

$$\xi = -K^* F' \left(s\left(\frac{1}{\alpha}\right) (K\tilde{u} - K\overline{u}) \right) ,$$

which implies that (SC2) is fulfilled, with $v = s(1/\alpha)(\hat{u} - \overline{u})$.
"⇒": If we assume that (SC2) holds, we have

$$K^* F'(Kv) + \xi = 0 \,,\, \xi \in \partial J(\tilde{u})$$

which we can multiply with α to obtain

$$K^* F'(s(\alpha)Kv) + \alpha\xi = 0 \,.$$

Defining $\overline{u} = \tilde{u} - s(\alpha)v$ finally yields

$$K^* F'(K\tilde{u} - K\overline{u}) + \alpha\xi = 0 \,.$$

□

In contrast to Lemma 5.1, Lemma 5.3 states that (SC2) is equivalent to $\tilde{u}$ being a minimizer of (4.14) with some exact data in the range of K, i.e. the input data g can be represented as $K\overline{u}$ with some exact data $\overline{u}$.

Lemma 5.3 will allow us to derive a similar estimate for noise-free data g as in [105, Theorem 2.1] for variational minimization problems of the type (4.14).

Theorem 5.3. *Let $(F, J, K) \in \mathcal{C}(\mathcal{V}(\Sigma), \mathcal{W}(\Omega), \mathcal{U}(\Omega))$ be satisfied, for reflexive Banach spaces $\mathcal{U}(\Omega)$, $\mathcal{W}(\Omega)$ and $\mathcal{V}(\Sigma)$, such that F satisfies a scaling property* (4.13) *with scaling function s, and such that $(F')^{-1}$ exists. Moreover, we assume the regularization functional J to be one-homogeneous. Then, if the strong source condition* (SC2) *is fulfilled and if we have exact, noise-free data $f = g$, the error estimate*

$$D_J^{\xi}(\hat{u}, \tilde{u}) \leq D_J^{\xi}(\tilde{u} + s(\alpha)v, \tilde{u}) \tag{5.4}$$

holds.

Proof. We know that $\hat{u}$ is the solution of

$$\hat{u} = \operatorname*{arg\,min}_{u \in \mathcal{W}(\Omega)} \left\{ \frac{1}{\alpha} F(Ku - g) + J(u) \right\} .$$

Since all underlying Banach spaces are assumed to be reflexive, we can apply Theorem 2.7 to obtain the relation

$$\inf_{u \in \mathcal{W}(\Omega)} \left\{ \frac{1}{\alpha} F(Ku - g) + J(u) \right\} = \sup_{w \in \mathcal{V}(\Sigma)^*} \left\{ -\frac{1}{\alpha} F^*(\alpha w) - J^*(-K^* w) - \langle w, f \rangle_{\mathcal{V}(\Sigma)} \right\}$$

with the convex-conjugates F^* and J^*. Considering the optimality condition of the dual problem yields

$$\begin{aligned} & 0 = -(F^*)'(\alpha\hat{w}) + K\hat{u} - g \,,\ \hat{u} \in \partial J^*(-K^*\hat{w}) \\ \Leftrightarrow\ & 0 = K\hat{u} - K\tilde{u} - s(\alpha)(F^*)'(\hat{w}) \,, \end{aligned} \tag{5.5}$$

since we have

$$(F^*)'(\alpha w) = (F^*)'(\alpha F'((F^*)'(w))) = (F^*)'(F'(s(\alpha)(F^*)'(w))) = s(\alpha)(F^*)'(w) \,,$$

because of Lemma 2.7. Due to Lemma 5.3 we know that (SC2) is equivalent to the existence of a function $\overline{u} \in \mathcal{W}(\Omega)$ such that $\tilde{u}$ satisfying (2.3) is the solution of

$$\tilde{u} = \operatorname*{arg\,min}_{u \in \mathcal{W}(\Omega)} \{ F(Ku - K\overline{u}) + \alpha J(u) \} .$$

In analogy to the previous variational minimization problem we can apply Theorem 2.7 to obtain the dual optimality condition

$$\begin{aligned} & 0 = K\tilde{u} - K\overline{u} + s(\alpha)(F^*)'(\tilde{w}) \,,\ \tilde{u} \in \partial J^*(-K^*\tilde{w}) \\ \Leftrightarrow\ & 0 = s(\alpha)Kv - s(\alpha)(F^*)'(\tilde{w}) \end{aligned} \tag{5.6}$$

with $\overline{u} = \tilde{u} - s(\alpha)v$.

If we subtract (5.6) from (5.5), and if we take the duality product with $\tilde{w} - \hat{w}$, such that $\xi = -K^*\tilde{w} \in \partial J(\tilde{u})$ and $\hat{p} = -K^*\hat{w} \in \partial J(\hat{u})$ holds, we obtain

$$\begin{aligned} 0 &= \langle \tilde{w} - \hat{w}, K(\hat{u} - \tilde{u} - s(\alpha)v)\rangle_{\mathcal{V}(\Sigma)} - s(\alpha)\left\langle \tilde{w} - \hat{w}, (F^*)'(\hat{w}) - (F^*)'(\tilde{w})\right\rangle_{\mathcal{U}(\Omega)^*} \\ \Leftrightarrow\ 0 &= \langle \hat{p} - \xi, \hat{u} - \tilde{u} - s(\alpha)v\rangle_{\mathcal{U}(\Omega)} + s(\alpha)\left\langle \hat{w} - \tilde{w}, (F^*)'(\hat{w}) - (F^*)'(\tilde{w})\right\rangle_{\mathcal{U}(\Omega)^*} . \end{aligned} \tag{5.7}$$

Since F^* is convex (due to Lemma 2.5) we know that $(F^*)'$ is a monotone operator, and therefore

$$\left\langle \hat{w} - \tilde{w}, (F^*)'(\hat{w}) - (F^*)'(\tilde{w})\right\rangle_{\mathcal{U}(\Omega)^*} \geq 0$$

is fulfilled. Together with (5.7) this implies

$$\langle \hat{p} - \xi, \hat{u} - \tilde{u} - s(\alpha)v\rangle_{\mathcal{U}(\Omega)} \leq 0 \tag{5.8}$$

If we consider the Bregman distance $D_J^{\xi}(\hat{u}, \tilde{u})$, we easily see that together with (5.8) we have

$$\begin{aligned} D_J^{\xi}(\hat{u}, \tilde{u}) &= J(\hat{u}) - J(\tilde{u}) - \langle \xi, \hat{u} - \tilde{u}\rangle_{\mathcal{U}(\Omega)} \ , \xi \in \partial J(\tilde{u}) \\ &\leq J(\hat{u}) - J(\tilde{u}) - \langle \xi, \hat{u} - \tilde{u}\rangle_{\mathcal{U}(\Omega)} - \langle \hat{p} - \xi, \hat{u} - \tilde{u} - s(\alpha)v\rangle_{\mathcal{U}(\Omega)} \\ &= J(\hat{u}) - J(\tilde{u}) - \langle \hat{p}, \hat{u} - \tilde{u}\rangle_{\mathcal{U}(\Omega)} + \langle \hat{p} - \xi, s(\alpha)v\rangle_{\mathcal{U}(\Omega)} \\ &\leq \langle \hat{p}, \tilde{u}\rangle_{\mathcal{U}(\Omega)} - J(\tilde{u}) + \langle \hat{p} - \xi, s(\alpha)v\rangle_{\mathcal{U}(\Omega)} \ , \end{aligned}$$

with the last inequality being a consequence of the subdifferential property $J(\hat{u}) - \langle \hat{p}, \hat{u}\rangle_{\mathcal{U}(\Omega)} \leq J(0) = 0$. Hence, we can derive the desired estimate via

$$\begin{aligned} D_J^{\xi}(\hat{u}, \tilde{u}) &\leq \langle \hat{p}, \tilde{u} + s(\alpha)v\rangle_{\mathcal{U}(\Omega)} - J(\tilde{u}) - \langle \xi, s(\alpha)v\rangle_{\mathcal{U}(\Omega)} \\ &\leq J(\tilde{u} + s(\alpha)v) - J(\tilde{u}) - \langle \xi, \tilde{u} + s(\alpha)v - \tilde{u}\rangle_{\mathcal{U}(\Omega)} = D_J^{\xi}(\tilde{u} + s(\alpha)v, \tilde{u}) , \end{aligned}$$

since J is assumed to be one-homogeneous, which implies $\langle \hat{p}, \tilde{u} + s(\alpha)v\rangle_{\mathcal{U}(\Omega)} \leq J(\tilde{u} + s(\alpha)v)$ due to Lemma 2.4. Hence, we have achieved the desired estimate. □

Remark 5.1. Note that for $F(Ku - g) = 1/2\|Ku - g\|^2_{L^2(\Sigma)}$ we have $s(\alpha) = \alpha$ and therefore we end up with

$$D_J^{\xi}(\hat{u}, \tilde{u}) \leq D_J^{\xi}(\tilde{u} + \alpha v, \tilde{u}) , \tag{5.9}$$

which is exactly the result obtained in [105].

5.2 Application to Specific Fidelities

We want to use the basic error estimates derived in Section 5.1 to derive specific error estimates for the fidelities presented in Section 4.2. In the following it will be assumed that the operator K will satisfy the conditions of Theorem 5.1 and Theorem 5.2.

5.2.1 Squared L^2-Fidelity

Error estimates in the context of Bregman distances for the standard fidelity choice of a squared L^2-fidelity have been considered in [28] first, and have been generalized to Bregman iteration- and ISS-schemes in [30]. The estimate that has been established in that case is (cf. [30, Theorem 3.1])

$$\frac{1}{2}\left\|K\hat{u}-g\right\|_{L^2(\Sigma)}^2+\alpha D_J^{\text{symm}}(\hat{u},\tilde{u})\leq\frac{\delta^2}{2}+\frac{\alpha^2}{2}\|q\|_{L^2(\Sigma)}^2\,. \tag{5.10}$$

We are going to see that with the use of Theorem 5.2 we can find a very similar estimate to (5.10) but with the exact data g on the left hand side of (5.10) replaced by the noisy data f. First of all we need to prove the following lemma.

Lemma 5.4. *Let α, φ and γ be real numbers, i.e. $\alpha,\varphi,\gamma\in\mathbb{R}$. Furthermore, let $c\in]0,1[$. Then, the family of functions*

$$h_n(x):=(-1)^n\alpha\gamma(\varphi-x)-\frac{c}{2}\left(\varphi-x\right)^2\,,$$

for $x\in\mathbb{R}$ and $n\in\mathbb{N}$, are strictly concave and have their unique maxima at

$$\overline{x}_n^h=\varphi-(-1)^n\frac{\alpha}{c}\gamma$$

and are therefore bounded by

$$h_n(x)<h_n(\overline{x}_n^h)=\frac{\alpha^2}{2c}\gamma^2\,.$$

Proof. It is easy to see that $h_n^{''}(x)=-c<0$ and hence, h_n is strictly concave for all $n\in\mathbb{N}$. The unique maxima $\overline{x}_n^h$ can be computed via $h_n^{'}(\overline{x}_n^h)=0$. Finally, since h_n is strictly concave for all $n\in\mathbb{N}$, $h_n(\overline{x}_n^h)$ has to be a global maximum. □

We can use Lemma 5.4 to prove the following estimate.

Theorem 5.4. *Let $\hat{u}$ satisfy the optimality condition* (4.17) *and let $\tilde{u}$ denote the exact solution of* (2.3)*. Furthermore, the difference between exact data g and noisy data f is bounded in the L^2-norm, i.e. $\|f-g\|_{L^2(\Sigma)}\leq\delta$ and* (SC1) *holds. Then, for the symmetric Bregman distance $D_J^{\text{symm}}(\hat{u},\tilde{u})$ for a specific regularization functional J, such that*

$$(H_f,J,K)\in\mathcal{C}(L^2(\Sigma),\mathcal{W}(\Omega),\mathcal{U}(\Omega))$$

is satisfied, the estimate

$$\frac{1-c}{2}\left\|K\hat{u}-f\right\|_{L^2(\Sigma)}^2+\alpha D_J^{\text{symm}}(\hat{u},\tilde{u})\leq\frac{1+c}{2}\delta^2+\frac{\alpha^2}{c}\|q\|_{L^2(\Sigma)}^2 \tag{5.11}$$

holds.

Proof. We have $(H_f,J,K)\in\mathcal{C}(L^2(\Sigma),\mathcal{W}(\Omega),\mathcal{U}(\Omega))$ and therefore are allowed to apply Theorem 5.1 and Theorem 5.2, which leads to

$$\begin{aligned}\frac{1-c}{2}\left\|K\hat{u}-f\right\|_{L^2(\Sigma)}^2+\alpha D_J^{\text{symm}}(\hat{u},\tilde{u})\leq\frac{1+c}{2}\delta^2\\ -\alpha\langle q,f-g\rangle_{L^2(\Sigma)}-\frac{c}{2}\left\|g-f\right\|_{L^2(\Sigma)}^2\\ +\alpha\langle q,f-K\hat{u}\rangle_{L^2(\Sigma)}-\frac{c}{2}\left\|K\hat{u}-f\right\|_{L^2(\Sigma)}^2\end{aligned}\,.$$

The pointwise application of Lemma 5.4 on the functionals of the right-hand side yields

$$-\alpha\langle q, f-g\rangle_{L^2(\Sigma)} - \frac{c}{2}\|g-f\|^2_{L^2(\Sigma)} \leq \frac{\alpha^2}{2c}\|q\|^2_{L^2(\Sigma)}\,,$$

and

$$\alpha\langle q, f-K\hat{u}\rangle_{L^2(\Sigma)} - \frac{c}{2}\|K\hat{u}-f\|^2_{L^2(\Sigma)} \leq \frac{\alpha^2}{2c}\|q\|^2_{L^2(\Sigma)}\,.$$

Substitution of these estimates yields the overall estimate (5.11). □

Remark 5.2. Note that in the limiting case $c \to 1$ the right-hand side of estimate (5.11) equals the right-hand side of estimate (5.10) up to a factor of two. The estimate (5.11) therefore is not as sharp as (5.10), but at least reveals the same asymptotic behavior. Furthermore, a significant difference between the estimates is that in the left hand side of (5.10) the L^2-norm between $K\hat{u}$ and the exact data g has been considered, while the estimate (5.11) only involves considering the L^2-norm between $K\hat{u}$ and the noisy data f.

5.2.2 General Norm Fidelity

With the use of Theorem 5.1 we can – in analogy to the error estimates for the exact penalization model in [28] – obtain the following estimate for $H_f(Ku) := \|Ku-f\|_{\mathcal{V}(\Sigma)}$, with $\hat{u}$ satisfying the optimality condition (4.19) and $\tilde{u}$ being the exact solution of (2.3).

Theorem 5.5. *Let $\hat{u}$ satisfy the optimality condition* (4.19) *and let $\tilde{u}$ denote the exact solution of* (2.3)*. Furthermore, the difference between exact data g and noisy data f is bounded in the $\mathcal{V}$-norm, i.e. $\|f-g\|_{\mathcal{V}(\Sigma)} \leq \delta$, and* (SC1) *holds. Then, for the symmetric Bregman distance $D_J^{\mathrm{symm}}(\hat{u},\tilde{u})$ for a specific regularization functional J, such that*

$$(H_f, J, K) \in \mathcal{C}(\mathcal{V}(\Sigma), \mathcal{W}(\Omega), \mathcal{U}(\Omega))$$

is satisfied, the estimate

$$\left(1-\alpha\|q\|_{\mathcal{V}(\Sigma)^*}\right) H_f(K\hat{u}) + \alpha D_J^{\mathrm{symm}}(\hat{u},\tilde{u}) \leq \left(1+\alpha\|q\|_{\mathcal{V}(\Sigma)^*}\right)\delta \tag{5.12}$$

holds. Furthermore, for $\alpha < \frac{1}{\|q\|_{\mathcal{V}(\Sigma)^*}}$, we obtain

$$D_J^{\mathrm{symm}}(\hat{u},\tilde{u}) \leq \delta\left(\frac{1}{\alpha} + \|q\|_{\mathcal{V}(\Sigma)^*}\right). \tag{5.13}$$

Proof. Since we have $(H_f, J, K) \in \mathcal{C}(\mathcal{V}(\Sigma), \mathcal{W}(\Omega), \mathcal{U}(\Omega))$, we obtain (due to Theorem 5.1)

$$\begin{aligned}
H_f(K\hat{u}) + \alpha D_J^{\mathrm{symm}}(\hat{u},\tilde{u}) &\leq \underbrace{H_f(g)}_{\leq\delta} - \alpha\langle q, K\hat{u}-g\rangle_{\mathcal{V}(\Sigma)} \\
&\leq \delta - \alpha\langle q, K\hat{u}-f+f-g\rangle_{\mathcal{V}(\Sigma)} \\
&= \delta - \alpha\big(\langle q, K\hat{u}-f\rangle_{\mathcal{V}(\Sigma)} \\
&\quad + \langle q, f-g\rangle_{\mathcal{V}(\Sigma)}\big) \\
&\leq \delta + \alpha\|q\|_{\mathcal{V}(\Sigma)^*}\Big(\|K\hat{u}-f\|_{\mathcal{V}(\Sigma)} \\
&\quad + \|f-g\|_{\mathcal{V}(\Sigma)}\Big) \\
&\leq \delta + \alpha\|q\|_{\mathcal{V}(\Sigma)^*}\Big(\|K\hat{u}-f\|_{\mathcal{V}(\Sigma)} + \delta\Big)\,,
\end{aligned}$$

which leads to (5.12). If we insert $H_f(K\hat{u}) = \|K\hat{u} - f\|_{\mathcal{V}(\Sigma)}$ and set $\alpha < \frac{1}{\|q\|_{\mathcal{V}(\Sigma)^*}}$ we can subtract $\|K\hat{u} - f\|_{\mathcal{V}(\Sigma)}$ on both sides. If we divide by α we obtain (5.13). □

As expected from the dual perspective above, we obtain in case of exact data ($\delta = 0$) for α sufficiently small

$$D_J^{\text{symm}}(\hat{u}, \tilde{u}) = 0, \qquad H_g(K\hat{u}) = 0.$$

For larger α no useful estimate is obtained. In the noisy case we can choose α small but independent of δ and hence obtain

$$D_J^{\text{symm}}(\hat{u}, \tilde{u}) = \mathcal{O}(\delta).$$

We remark on the necessity of the source condition (SC1). In usual converse results one proves that a source condition needs to hold if the distance between the reconstruction and the exact solution satisfies a certain asymptotic in δ (cf. [94]). Such results so far exist only for quadratic fidelity and special regularizations and cannot be expected for general Bregman distance estimates – even less with non-quadratic fidelity models. We shall therefore only look at the asymptotics of H_f in the noise free case and argue that for this asymptotic the source condition is necessary (at least in some sense). In case of a general norm fidelity this is particularly simple due to the asymptotic exactness for α small. The optimality condition $K^*\hat{s} + \alpha\hat{p} = 0$ can be rewritten as

$$\hat{p} = K^*q, \qquad \hat{p} \in \partial J(\hat{u}), q \in \mathcal{V}(\Sigma)^*,$$

with $q = -\frac{1}{\alpha}\hat{s}$. Since $\hat{u}$ is a solution minimizing J for α sufficiently small, we see that if the asymptotic in α holds, there exists a solution of $Ku = g$ with minimal J satisfying (SC1).

5.2.3 Kullback-Leibler Fidelity

In case of Poisson noise the source condition can be written as

$$\exists\, \xi \in \partial J(\tilde{u}),\, \exists\, q \in L^\infty(\Sigma): \quad \xi = K^*q\,. \tag{SCL^1}$$

and we have the Kullback-Leibler fidelity

$$H_f(Ku) = \int_\Sigma \left[f(y) \ln\left(\frac{f(y)}{(Ku)(y)}\right) - f(y) + (Ku)(y) \right] d\mu(y)\,,$$

and a positivity constraint $u \geq 0$. Theorem 5.2 will allow us to derive an error estimate of the same order as known for quadratic fidelities. Before that, we have to prove the following lemma.

Lemma 5.5. *Let α and φ be positive, real numbers, i.e. $\alpha, \varphi \in \mathbb{R}^+$. Furthermore, let $\gamma \in \mathbb{R}$ be a real number and $c \in]0,1[$. Then, the family of functions*

$$h_n(x) := (-1)^n\alpha\gamma(\varphi - x) - c\left(\varphi \ln\left(\frac{\varphi}{x}\right) - \varphi + x\right)\,,$$

for $x > 0$ and $n \in \mathbb{N}$, are strictly concave and have their unique maxima at

$$\overline{x}_n^h = \frac{\varphi}{1 + (-1)^n\frac{\alpha}{c}\gamma}$$

and are therefore bounded by

$$h_n(x) < h_n(\overline{x}_n^h) = (-1)^n\alpha\gamma\varphi - c\varphi \ln\left(1 + (-1)^n\frac{\alpha}{c}\gamma\right)\,,$$

for $\frac{\alpha}{c}|\gamma| < 1$ and $x \neq \overline{x}_n^h$.

Proof. It is easy to see that $h_n''(x) = -c\frac{\varphi}{x^2} < 0$ and hence, h_n is strictly concave for all $n \in \mathbb{N}$. The unique maxima $\overline{x}_n^h$ can be computed via $h_n'(\overline{x}_n^h) = 0$. Finally, since h_n is strictly concave for all $n \in \mathbb{N}$, $h_n(\overline{x}_n^h)$ has to be a global maximum. □

Furthermore, we have to ensure the existence of $u' \geq 0$ with $Ku' \in \mathrm{dom}(H_f)$ and $u' \in \mathrm{dom}(J)$, such that H_f is continuous at Ku'. If e.g. $\mathrm{dom}(J) = \mathrm{BV}(\Omega)$, we do not obtain continuity of H_f at Ku' if K maps to e.g. $L^1(\Sigma)$. Therefore we restrict K to map to $L^\infty(\Sigma)$. However, we still keep (SCL^1) to derive the error estimates, which corresponds to an interpretation of K mapping to L^1. This implies more regularity than needed, since one usually uses q in the dual of the image space, which would mean $q \in L^\infty(\Sigma)^*$. For the latter we are not able to derive the same estimates. Note however that the assumption of K mapping to $L^\infty(\Sigma)$ is used only to deal with the positivity of K. With the help of Lemma 5.5 and the restriction of K, we are able to prove the following error estimate.

Theorem 5.6. *Let $\hat{u}$ satisfy the optimality condition (4.25) with $K : \mathcal{U}(\Omega) \to L^\infty(\Sigma)$ satisfying $\mathcal{N}(K) = \{0\}$, let $\tilde{u}$ denote the exact solution of (2.3) and let f be a probability density measure, i.e. $\int_\Sigma f \, d\mu(y) = 1$. Furthermore, the difference between noisy data f and exact data g is bounded in the Kullback-Leibler measure, i.e.*

$$\int_\Sigma \left[f \ln\left(\frac{f}{g}\right) - f + g \right] \, d\mu(y) \leq \delta$$

and (SCL^1) holds. Then, for $c \in]0,1[$ and $\alpha < \frac{c}{\|q\|_{L^\infty(\Sigma)}}$, the symmetric Bregman distance $D_J^{\mathrm{symm}}(\hat{u}, \tilde{u})$ for a specific regularization functional J, such that

$$(H_f, J, K) \in \mathcal{C}(L^1(\Sigma), \mathcal{W}(\Omega), \mathcal{U}(\Omega))$$

is satisfied, is bounded via

$$(1-c)H_f(K\hat{u}) + \alpha D_J^{\mathrm{symm}}(\hat{u}, \tilde{u}) \leq (1+c)\delta - c\ln\left(1 - \frac{\alpha^2}{c^2}\|q\|_{L^\infty(\Sigma)}^2\right). \tag{5.14}$$

Proof. We have $(H_f, J, K) \in \mathcal{C}(L^1(\Sigma), \mathcal{W}(\Omega), \mathcal{U}(\Omega))$. Using an analogous proof as in Theorem 5.2 with the non-negativity of $\hat{u}$ being incorporated in a variational inequality, we can still derive (5.3) in this case. Hence, we have to investigate $-\alpha\langle q, f-g\rangle_{L^1(\Sigma)} - cH_f(g)$ and $\alpha\langle q, f - K\hat{u}\rangle_{L^1(\Sigma)} - cH_f(K\hat{u})$. If we consider both functionals pointwise and force $\alpha^2 < \left(\frac{c}{q}\right)^2$, we can use Lemma 5.5 to estimate

$$-\alpha\langle q, f-g\rangle_{L^1(\Sigma)} - cH_f(g) \leq \int_\Sigma f\left(-\alpha q - c\ln\left(1 - \frac{\alpha}{c}q\right)\right) d\mu(y)$$

and

$$\alpha\langle q, f - K\hat{u}\rangle_{L^1(\Sigma)} - cH_f(K\hat{u}) \leq \int_\Sigma f\left(\alpha q - c\ln\left(1 + \frac{\alpha}{c}q\right)\right) d\mu(y).$$

Adding these terms together yields the estimate

$$\begin{aligned}(1-c)H_f(K\hat{u}) + \alpha D_J^{\mathrm{symm}}(\hat{u}, \tilde{u}) \leq{}& (1+c)\underbrace{H_f(g)}_{\leq\delta} \\ &+ \int_\Sigma f\left(-c\ln\left(1 - \frac{\alpha^2}{c^2}q^2\right)\right) d\mu(y).\end{aligned}$$

It is easy to see that for $\alpha < \frac{c}{\|q\|_{L^\infty(\Sigma)}}$ we have
$-\ln\left(1-\frac{\alpha^2}{c^2}q^2\right) \leq -\ln\left(1-\frac{\alpha^2}{c^2}\|q\|^2_{L^\infty(\Sigma)}\right)$. Hence, for positive f we obtain

$$\begin{aligned}(1-c)H_f(K\hat{u}) + \alpha D_J^{\text{symm}}(\hat{u},\tilde{u}) \leq &(1+c)\delta \\ &+ \int_\Sigma f\left(-c\ln\left(1-\frac{\alpha^2}{c^2}\|q\|^2_{L^\infty(\Sigma)}\right)\right)d\mu(y) \\ =&(1+c)\delta - c\ln\left(1-\frac{\alpha^2}{c^2}\|q\|^2_{L^\infty(\Sigma)}\right)\underbrace{\int_\Sigma f\,d\mu(y)}_{=1}\end{aligned}$$

and hence, (5.14) holds. □

One observes from a Taylor approximation of the second term on the right-hand side of (5.14) around $\alpha = 0$ that

$$H_f(K\hat{u}) = \mathcal{O}\left(\delta+\alpha^2\right), \qquad D_J^{\text{symm}}(\hat{u},\tilde{u}) = \mathcal{O}\left(\frac{\delta}{\alpha}+\alpha\right)$$

for small α, which is analogous to the quadratic case.

Remark 5.3. The assumption $\mathcal{N}(K) = \{0\}$ is very strict. If $\mathcal{N}(K)$ is larger, the error estimate is still satisfied since H_f is convex (no longer strictly convex) and the terms $-\alpha\langle q, f-g\rangle_{L^1(\Sigma)} - cH_f(g)$ and $\alpha\langle q, f-K\hat{u}\rangle_{L^1(\Sigma)} - cH_f(K\hat{u})$ are concave (instead of being strictly concave). Hence, Lemma 5.5 can still be applied to find an upper estimate, the only difference is that there can be more than just one maximum.

5.2.4 Multiplicative Noise Fidelities

In the case of multiplicative noise we are going to examine model (4.28) instead of (4.26), since (4.28) is convex for all z and therefore allows the application of Theorem 5.2. The source condition slightly differs, since there is no operator in (4.28). Therefore we get

$$\exists\,\xi \in \partial J(\tilde{z}),\ \exists\, q \in L^\infty(\Sigma): \quad \xi = q\,. \tag{$z\text{SC}L^1$}$$

In analogy to the Poisson case we have to prove the following lemma first, to derive qualitative and quantitative error estimates the case of multiplicative noise.

Lemma 5.6. *Let α and φ be positive, real numbers, i.e. $\alpha, \varphi \in \mathbb{R}^+$. Furthermore, let $\gamma \in \mathbb{R}$ be a real number and $c \in]0,1[$. Then, the family of functions*

$$k_n(x) := (-1)^n\alpha\gamma(\varphi - x) - c(x + \varphi e^{-x} - 1 - \ln(\varphi))\,,$$

for $x > 0$ and $n \in \mathbb{N}$, are strictly concave and have their unique maxima at

$$\overline{x}_n^k = -\ln\left(\frac{c+(-1)^n\alpha\gamma}{c\varphi}\right),$$

for $\frac{\alpha}{c}|\gamma| < 1$. *Hence,* k_n *is bounded via*

$$k_n(x) < k_n(\overline{x}_n^k) = \alpha\gamma\left((-1)^n\left(\varphi + \ln\left(\frac{c+(-1)^n\alpha\gamma}{c\varphi}\right)\right) - 1\right) + c\ln\left(\frac{c+(-1)^n\alpha\gamma}{c}\right),$$

for $x \neq \overline{x}_n^k$.

Proof. Similarly to Lemma 5.5, it can easily be shown that $k_n''(x) = -c\varphi e^{-x} < 0$ for all $x \in \mathbb{R}^+$ and hence, the k_n are strictly concave for all $n \in \mathbb{N}$. The arguments $\overline{x}_n^k$ are computed to satisfy $k_n'(\overline{x}_n^k) = 0$. Since the k_n are strictly concave, $k_n(\overline{x}_n^k)$ has to be a global maximum for all $n \in \mathbb{N}$. □

With the help of Lemma 5.6 we are able to prove the following error estimate.

Theorem 5.7. *Let* $\hat{z}$ *satisfy the optimality condition* (4.29) *and let* $\tilde{z}$ *denote the solution of* $\tilde{z} = \ln(K\tilde{u}) = \ln(g)$, *with* $\tilde{u}$ *being the exact solution of* (2.3). *Furthermore, the difference between noisy data* f *and exact data* g *is bounded in the measure of* (4.26), *i.e.*

$$\int_\Sigma \left[\ln\left(\frac{g}{f}\right) + \frac{f}{g} - 1\right] d\mu(y) \leq \delta$$

and ($z\mathrm{SC}L^1$) *holds. Then, for* $c \in]0,1[$ *and* $\alpha < \frac{c}{\|q\|_{L^\infty(\Sigma)}}$, *the symmetric Bregman distance* $D_J^{\mathrm{symm}}(\hat{z},\tilde{z})$ *for a specific regularization functional* J *such that*

$$(H_f, J, Id) \in \mathcal{C}(L^1(\Sigma), \mathcal{W}(\Sigma), \mathcal{U}(\Sigma))$$

is satisfied, is bounded via

$$(1-c)H_f(\hat{z}) + \alpha D_J^{\mathrm{symm}}(\hat{z},\tilde{z}) \leq (1+c)\delta + \alpha|\Sigma|\,\|q\|_{L^\infty(\Sigma)} \ln\left(\frac{c+\alpha\|q\|_{L^\infty(\Sigma)}}{c-\alpha\|q\|_{L^\infty(\Sigma)}}\right). \tag{5.15}$$

Proof. First of all we have $H_f \in \mathcal{C}(L^1(\Sigma), \mathcal{W}(\Sigma), \mathcal{U}(\Sigma))$. Furthermore, there exists u' with $Ku' \in \mathrm{dom}(H_f)$ and $u' \in \mathrm{dom}(J)$, such that H_f is continuous at Ku'. Hence, we can apply Theorem 5.2 to obtain (5.3). Therefore, we have to consider the functionals $-\alpha\langle q, f-g\rangle_{L^1(\Sigma)} - cH_f(g)$ and $\alpha\langle q, f-\hat{z}\rangle_{L^1(\Sigma)} - cH_f(\hat{z})$ pointwise. Due to Lemma 5.6 we have

$$\begin{aligned}
&-\alpha\langle q, f-g\rangle_{L^1(\Sigma)} - cH_f(g) + \alpha\langle q, f-\hat{z}\rangle_{L^1(\Sigma)} - cH_f(\hat{z}) \\
&\leq \int_\Sigma \alpha q\left(1 - f - \ln\left(\frac{c-\alpha q}{cf}\right)\right) + c\ln\left(\frac{c-\alpha q}{c}\right) d\mu(y) \\
&\quad + \int_\Sigma \alpha q\left(f + \ln\left(\frac{c-\alpha q}{cf}\right) - 1\right) + c\ln\left(\frac{c+\alpha q}{c}\right) d\mu(y) \\
&\quad = \alpha\int_\Sigma q\underbrace{\left(\ln\left(\frac{c+\alpha q}{cf}\right) - \ln\left(\frac{c-\alpha q}{cf}\right)\right)}_{=\ln\left(\frac{c+\alpha q}{c-\alpha q}\right)} d\mu(y) \\
&\qquad + c\int_\Sigma \underbrace{\left(\ln\left(\frac{c+\alpha q}{c}\right) + \ln\left(\frac{c-\alpha q}{c}\right)\right)}_{=\ln\left(1-\frac{\alpha^2}{c^2}q^2\right)} d\mu(y),
\end{aligned}$$

for $\alpha < \frac{c}{q}$. It is easy to see that $q \ln\left(\frac{c+\alpha q}{c-\alpha q}\right) \leq \|q\|_{L^\infty(\Sigma)} \ln\left(\frac{c+\alpha\|q\|_{L^\infty(\Sigma)}}{c-\alpha\|q\|_{L^\infty(\Sigma)}}\right)$. Furthermore, it can also easily be verified that the function $l(x) := \ln\left(1-\frac{\alpha^2}{c^2}x^2\right)$ is strictly concave and has its unique global maximum $l(\overline{x}) = 0$ at $\overline{x} = 0$. Hence, if we consider $\ln\left(1-\frac{\alpha^2}{c^2}q^2\right)$ pointwise, $c\int_\Sigma \ln\left(1-\frac{\alpha^2}{c^2}q^2\right) d\mu(y) \leq 0$ has to hold. Inserting these estimates into (5.3) yields (5.15). □

Again a Taylor approximation of the second term on the right-hand side of (5.15) around $\alpha = 0$ yields the asymptotic behavior

$$H_f(K\hat{u}) = \mathcal{O}\left(\delta + \alpha^2\right), \qquad D_J^{\text{symm}}(\hat{u}, \tilde{u}) = \mathcal{O}\left(\frac{\delta}{\alpha} + \alpha\right).$$

For the multiplicative noise model (4.31) we can assume the considered functions to be L^1 functions, and hence, the source condition for this particular model again is (SCL^1). In order to prove an error estimate via Theorem 5.2 we need the following Lemma.

Lemma 5.7. *Let α, φ and γ be positive, real numbers, i.e. $\alpha, \varphi, \gamma \in \mathbb{R}_{>0}$. Furthermore, let c be a real number with $c \in]0,1[$. Then, the function*

$$h_1(x) := -\alpha\gamma(\varphi - x) - c\left(\frac{(x-\varphi)^2}{x}\right)$$

for $x > 0$ and $0 < \gamma < c/\alpha$ is strictly concave and has its unique maximum at

$$\overline{x}_1^h = -\frac{\varphi}{\sqrt{1-\frac{\alpha}{c}\gamma}}$$

and is therefore bounded by

$$h_1(x) < h_1(\overline{x}_1^h) = \frac{\varphi\left(\sqrt{1-\frac{\alpha}{c}\gamma}+1\right)\left(c\left(\sqrt{1-\frac{\alpha}{c}\gamma}+1\right)-\alpha\gamma\right)}{\sqrt{1-\frac{\alpha}{c}\gamma}}. \tag{5.16}$$

Moreover, the function

$$h_2(x) := \alpha\gamma(\varphi - x) - c\left(\frac{(x-\varphi)^2}{x}\right)$$

for $x > 0$ and $0 < \gamma < c/\alpha$ is strictly concave and has its unique maximum at

$$\overline{x}_2^h = \frac{\varphi}{\sqrt{1+\frac{\alpha}{c}\gamma}}$$

and is globally bounded by

$$h_2(x) < h_2(\overline{x}_2^h) = \frac{-\varphi\left(\sqrt{1+\frac{\alpha}{c}\gamma}-1\right)\left(c\left(\sqrt{1+\frac{\alpha}{c}\gamma}-1\right)-\alpha\gamma\right)}{\sqrt{1+\frac{\alpha}{c}\gamma}}.$$

Proof. We immediately see that h_1 and h_2 are strictly concave, since we have $h_1''(x) = h_2''(x) = -(2c\varphi^2)/(x^3) < 0$ for $\varphi \neq 0$, $c > 0$ and $x > 0$. Solving the optimality condition $h_1(\overline{x}_{1,2}) = 0$ actually yields $\overline{x}_{1,2} = \pm\varphi/\sqrt{1-(\alpha q)/c}$. Inserting $\overline{x}_{1,2}$ into h_1 leads to the two options

$$h_1(\overline{x}_{1,2}) = \begin{cases} -\frac{\varphi\left(\sqrt{1-\frac{\alpha}{c}\gamma}-1\right)\left(c\left(\sqrt{1-\frac{\alpha}{c}\gamma}-1\right)+\alpha\gamma\right)}{\sqrt{1-\frac{\alpha}{c}\gamma}} \\ \frac{\varphi\left(\sqrt{1-\frac{\alpha}{c}\gamma}+1\right)\left(c\left(\sqrt{1-\frac{\alpha}{c}\gamma}+1\right)-\alpha\gamma\right)}{\sqrt{1-\frac{\alpha}{c}\gamma}} \end{cases} .$$

For $\gamma < c/\alpha$ and φ we can compute that

$$\begin{aligned} &-\varphi\left(\sqrt{1-\frac{\alpha}{c}\gamma}-1\right)\left(c\left(\sqrt{1-\frac{\alpha}{c}\gamma}-1\right)+\alpha\gamma\right) \\ &<\varphi\left(\sqrt{1-\frac{\alpha}{c}\gamma}+1\right)\left(c\left(\sqrt{1-\frac{\alpha}{c}\gamma}+1\right)-\alpha\gamma\right) \end{aligned}$$

is always satisfied and hence, (5.16) is the global maximum. The proof for the estimate of h_2 can be done in a completely analogous way. □

The use of Lemma 5.7 allows us to prove the following theorem.

Theorem 5.8. *Let $\hat{u}$ satisfy the optimality condition* (4.32) *with $K : \mathcal{U}(\Omega) \to L^\infty(\Sigma)$ satisfying $\mathcal{N}(K) = \{0\}$, let $\tilde{u}$ denote the exact solution of* (2.3) *and let f be a probability density measure, i.e. $\int_\Sigma f \, d\mu(y) = 1$. Furthermore, the difference between noisy data f and exact data g is bounded in the terms of the fidelity* (4.30)*, i.e.*

$$\int_\Sigma \left[\frac{(g-f)^2}{g}\right] \, d\mu(y) \leq \delta$$

and (SCL^1) *holds. Then, for $c \in]0,1[$ and $\alpha < \frac{c}{\|q\|_{L^\infty(\Sigma)}}$, the symmetric Bregman distance $D_J^{\text{symm}}(\hat{u},\tilde{u})$ for a specific regularization functional J, such that*

$$(H_f, J, K) \in \mathcal{C}(L^1(\Sigma), \mathcal{W}(\Omega), \mathcal{U}(\Omega))$$

is satisfied, is bounded via

$$(1-c)H_f(K\hat{u}) + \alpha D_J^{\text{symm}}(\hat{u},\tilde{u}) \leq (1+c)\delta + 2c\left(2 + \sqrt{1+\frac{\alpha}{c}\|q\|_{L^\infty(\Sigma)}} - \sqrt{1-\frac{\alpha}{c}\|q\|_{L^\infty(\Sigma)}}\right) . \tag{5.17}$$

Proof. Similar to the proof of Theorem 5.6 we have $(H_f, J, K) \in \mathcal{C}(L^1(\Sigma), \mathcal{W}(\Omega), \mathcal{U}(\Omega))$. Again, we can use an analogous proof as in Theorem 5.2 with the non-negativity of $\hat{u}$ being incorporated in a variational inequality, and therefore we are still able to derive (5.3). Hence, we have to investigate $-\alpha\langle q, f-g\rangle_{L^1(\Sigma)} - cH_f(g)$ and $\alpha\langle q, f-K\hat{u}\rangle_{L^1(\Sigma)} - cH_f(K\hat{u})$ again. We consider both functionals pointwise and force $\alpha < \frac{c}{q}$ in order to use Lemma 5.7 to estimate

$$-\alpha\left\langle q, f-g\right\rangle_{L^1(\Sigma)} - cH_f(g) \leq \int_\Sigma f\left(\frac{\left(\sqrt{1-\frac{\alpha}{c}q}+1\right)\left(c\left(\sqrt{1-\frac{\alpha}{c}q}+1\right)-\alpha q\right)}{\sqrt{1-\frac{\alpha}{c}q}}\right) \, d\mu(y)$$

and

$$\alpha \langle q, f - K\hat{u}\rangle_{L^1(\Sigma)} - cH_f(K\hat{u}) \leq -\int_\Sigma f\left(\frac{\left(\sqrt{1+\frac{\alpha}{c}q}-1\right)\left(c\left(\sqrt{1+\frac{\alpha}{c}q}-1\right)-\alpha q\right)}{\sqrt{1+\frac{\alpha}{c}q}}\right)\,d\mu(y)\,.$$

If we add both terms together we obtain the estimate

$$(1-c)H_f(K\hat{u}) + \alpha D_J^{\text{symm}}(\hat{u},\tilde{u}) \leq (1+c)\delta + 2c\int_\Sigma f\left(2+\sqrt{1+\frac{\alpha}{c}q}+\sqrt{1-\frac{\alpha}{c}q}\right)\,d\mu(y)\,.$$

Since for $-c/\alpha < q < c/\alpha$ we can estimate $\sqrt{1+(\alpha q)/c}+\sqrt{1-(\alpha q)/c} \leq \sqrt{1+\left(\alpha\|q\|_{L^\infty(\Sigma)}\right)/c}+\sqrt{1-\left(\alpha\|q\|_{L^\infty(\Sigma)}\right)/c}$ the estimate for the Bregman distance simplifies to

$$\begin{aligned}(1-c)H_f(K\hat{u}) + \alpha D_J^{\text{symm}}(\hat{u},\tilde{u}) \leq (1+c)\delta \\ + 2c\left(2+\sqrt{1+\frac{\alpha}{c}\|q\|_{L^\infty(\Sigma)}}+\sqrt{1-\frac{\alpha}{c}\|q\|_{L^\infty(\Sigma)}}\right)\underbrace{\int_\Sigma f\,d\mu(y)}_{=1}\,,\end{aligned}$$

and thus, equals (5.17). □

As for the last two estimates a Taylor approximation of the second term on the right-hand side of (5.15) around $\alpha = 0$ yields the asymptotic behavior

$$H_f(K\hat{u}) = \mathcal{O}\left(\delta+\alpha^2\right), \qquad D_J^{\text{symm}}(\hat{u},\tilde{u}) = \mathcal{O}\left(\frac{\delta}{\alpha}+\alpha\right).$$

Remark 5.4. Like in case of the Kullback-Leibler fidelity the assumption $\mathcal{N}(K) = \{0\}$ is not really necessary. If $\mathcal{N}(K)$ is larger, the error estimate is still satisfied because H_f is yet convex and the upper bounds for the terms $-\alpha\langle q, f-g\rangle_{L^1(\Sigma)} - cH_f(g)$ and $\alpha\langle q, f-K\hat{u}\rangle_{L^1(\Sigma)} - cH_f(K\hat{u})$ are not affected. Hence, Lemma 5.7 can still be applied in order to prove Theorem 5.8.

5.3 A-posteriori Parameter Choice

Before we start discussing the question of how to recover a function $\tilde{u}$ exactly, we want to shortly consider a-posteriori parameter choices for variational problems. A typical a-posteriori parameter choice rule is the discrepancy principle. For a general norm fidelity $\|Ku-f\|_{\mathcal{V}(\Sigma)}$ the discrepancy principle states that for a given noise bound $\|f-g\|_{\mathcal{V}(\Sigma)} \leq \delta$ the solution $\hat{u}$ of a regularized variational problem should satisfy $\|K\hat{u}-f\|_{\mathcal{V}(\Sigma)} \leq \delta$, i.e.

$$\hat{u} \in \operatorname*{arg\,min}_{u\in\mathcal{W}(\Omega)}\{J(u)\}\,, \tag{5.18}$$

subject to

$$\|Ku-f\|_{\mathcal{V}(\Sigma)} \leq \delta\,. \tag{5.19}$$

We can reformulate this problem to

$$\hat{u} \in \operatorname*{arg\,min}_{u\in\mathcal{W}(\Omega)}\left\{\mathcal{X}_\delta\left(\|Ku-f\|_{\mathcal{V}(\Sigma)}\right)+J(u)\right\}\,, \tag{5.20}$$

with $\mathcal{X}_\delta$ being the characteristic function

$$\mathcal{X}_\delta(v) := \begin{cases} 0 & \text{if } v \leq \delta \\ +\infty & \text{else} \end{cases},$$

as introduced in Example 2.15 and Example 2.16. With the use of the triangular inequality of the norm and the monotonicity and convexity of the characteristic function it can easily be seen that $\mathcal{X}_\delta\left(\|Ku - f\|_{\mathcal{V}(\Sigma)}\right)$ is convex and by setting $H_f(Ku) = \mathcal{X}_\delta\left(\|Ku - f\|_{\mathcal{V}(\Sigma)}\right)$ we can apply Lemma 5.2 to obtain the following theorem.

Theorem 5.9. *Let $\tilde{u}$ denote the exact solution of* (2.3) *and let the source condition* (SC1) *be fulfilled. If there exists a minimal solution $\hat{u}$ satisfying* (5.18) *subject to* (5.19) *and if $\|f - g\|_{\mathcal{V}(\Sigma)}$ is also bounded by δ, the error estimate*

$$D_J^\xi(\hat{u}, \tilde{u}) \leq 2\delta \|q\|_{\mathcal{V}(\Sigma)^*}$$

holds.

Proof. If we apply Lemma 5.2 to the variational problem (5.20) we obtain

$$\begin{aligned} \underbrace{\mathcal{X}_\delta\left(\underbrace{\|K\hat{u} - f\|_{\mathcal{V}(\Sigma)}}_{\leq\delta}\right)}_{=0} + D_J^\xi(\hat{u}, \tilde{u}) &\leq \underbrace{\mathcal{X}_\delta\left(\underbrace{\|f - g\|_{\mathcal{V}(\Sigma)}}_{\leq\delta}\right)}_{=0} - \langle q, K\hat{u} - g\rangle_{\mathcal{V}(\Sigma)} \\ &= -\left(\langle q, K\hat{u} - f\rangle_{\mathcal{V}(\Sigma)} + \langle q, f - g\rangle_{\mathcal{V}(\Sigma)}\right) \\ &\leq \|q\|_{\mathcal{V}^*(\Sigma)} \left(\underbrace{\|K\hat{u} - f\|_{\mathcal{V}(\Sigma)}}_{\leq\delta} + \underbrace{\|f - g\|_{\mathcal{V}(\Sigma)}}_{\leq\delta}\right) \\ &= 2\delta \|q\|_{\mathcal{V}(\Sigma)^*} \end{aligned}$$

□

Remark 5.5. Obviously a discrepancy principle can also be considered for general fidelities, not only for norm fidelities, i.e. we replace $\|Ku - f\|_{\mathcal{V}(\Sigma)}$ in (5.19) by a general fidelity $H_f(Ku)$. In that case we can add and subtract the terms $cH_f(K\hat{u})$ and $cH_f(g)$ for $c > 0$ in order to compute estimates for $\langle q, f - g\rangle_{\mathcal{V}(\Sigma)} - cH_f(g)$ and $\langle q, f - K\hat{u}\rangle_{\mathcal{V}(\Sigma)} - cH_f(K\hat{u})$ similar as in Lemma 5.5 and Lemma 5.6), and in addition make us of the estimate $cH_f(K\hat{u}) + cH_f(g) \leq 2c\delta$. For the Kullback-Leibler fidelity we therefore would obtain the estimate

$$D_J^\xi(\hat{u}, \tilde{u}) \leq 2c\delta - c\ln\left(1 - \frac{\|q\|_{L^\infty(\Sigma)}^2}{c^2}\right),$$

for $c > 0$ and $\|q\|_{L^\infty(\Sigma)} < c$. For the multiplicative-noise fidelities the corresponding error estimates would read as

$$D_J^\xi(\hat{u}, \tilde{u}) \leq 2c\delta + |\Sigma|\|q\|_{L^\infty(\Sigma)} \ln\left(\frac{c + \|q\|_{L^\infty(\Sigma)}}{c - \|q\|_{L^\infty(\Sigma)}}\right),$$

or respectively

$$D_J^{\xi}(\hat{u},\tilde{u}) \leq 2c\left(\delta + 2 + \sqrt{1+\frac{\|q\|^2_{L^\infty(\Sigma)}}{c}} - \sqrt{1-\frac{\|q\|^2_{L^\infty(\Sigma)}}{c}}\right),$$

also for $c > 0$ and $\|q\|_{L^\infty(\Sigma)} < c$.

Chapter 6

Ground States and Eigenfunctions

In this chapter we want to move beyond error estimates, and address the question of exact recovery. In the previous Chapter 5 we have focused our attention on estimating upper bounds for the Bregman distance between the true but unknown solution $\tilde{u}$ and the solution $\hat{u}$ of the variational framework (2.9), for arbitrary input data f. In this chapter, we want to focus on particular input data. We assume that the input data is given as the operator K of the inverse problem (2.3) applied to an Eigenfunction of a specific regularization functional. Throughout this chapter, we are going to show that with the use of the Bregman distance we will be able to prove that the solution of the variational framework (2.8) with this specific input data is the Eigenfunction itself, up to a constant factor. The chapter is organized as follows. First of all, we are going to introduce the terminology of Eigenfunctions, and present numerous examples of Eigenfunctions for the regularization functionals presented in Section 4.1. Subsequently, we will prove that for data given in terms of an Eigenfunction, the Eigenfunction can be recovered up to a constant factor by the use of (2.8), even in the presence of noise.

6.1 Ground States

In the context of variational schemes like (2.8), we are particularly interested in non-trivial Ground States of the regularization energy. Therefore we define Ground States as follows.

Definition 6.1. *Let $J : \mathrm{dom}(J) \subseteq L^2(\Omega) \to \mathbb{R} \cup \{+\infty\}$ be a proper functional and $K : L^2(\Omega) \to L^2(\Sigma)$ a linear operator. Then, a Ground State u_0 is defined as*

$$u_0 = \operatorname*{arg\,min}_{\substack{u \in \mathrm{dom}(J) \\ \|Ku\|_{L^2(\Sigma)}=1}} \{J(u)\} \ . \tag{6.1}$$

Note that Ground States may not be unique. In the following we want to give some examples of Ground States for the regularization energies of Chapter 4, Section 4.1. For simplicity we assume $K = \mathrm{I}$.

Example 6.1. In case of $J(u) = \|u\|_{\ell^1}$ every basis element of the canonical basis $(e_j)_{j\in\{1,\dots,N\}}$, with $e_j = (0, 0, \dots, 0, 1, 0, \dots, 0)^T$ having a single one at j-th position and zeros everywhere else, is a Ground State of J.

Example 6.2. In case of Total Variation regularization, i.e $J(u) = \mathrm{TV}(u)$, it is easy to see that u_0 can be determined as the constant function $u_0 \equiv 1/|\Omega|$, with $|\Omega|$ denoting the cardinality of the underlying set Ω, since $\mathrm{TV}(u) \equiv 0$ iff u is constant.

Example 6.3. For regularization energies that incorporate second-oder derivatives, as e.g. TV^2 or second-order ICTV_β and GTV_β, every affine-linear function yields $J(u) \equiv 0$. Hence, the Ground States u_0 are all functions $u_0(x) = ax + b$ for which the constants a and b are chosen such that

$$a = \frac{1 - b|\Omega|}{\int_\Omega x \, dx}$$

holds.

6.2 Eigenfunctions

Similar to the characterization of Eigenfunctions of linear operators as in case of quadratic variational schemes we want to define Eigenfunctions for the scheme (2.8), especially in case of singular and one-homogeneous regularization energies.

Definition 6.2. *Let $J : \mathrm{dom}(J) \subseteq L^2(\Omega) \to \mathbb{R} \cup \{+\infty\}$ be a convex functional with non-empty subdifferential ∂J and let $K : L^2(\Omega) \to L^2(\Sigma)$ be a linear operator. Then, every function $u \neq 0$ that satisfies*

$$\lambda K^* K u \in \partial J(u)$$

is called Eigenfunction of J with corresponding Eigenvalue λ.

Remark 6.1. The Ground State is a trivial Eigenfunction, a fact that can be seen from a Lagrange multiplier point of view. If we rewrite condition (6.1) in terms of the Lagrange multiplier

$$\mathcal{L}(u; \lambda) = J(u) + \frac{\lambda}{2} \left(1 - \|Ku\|^2_{L^2(\Omega)}\right) ,$$

then we obtain

$$\lambda K^* K u \in \partial J(u) \, ,$$

as the equation for the optimality condition $\partial_u \mathcal{L} = 0$. Moreover, taking a dual product with u yields the general Eigenvalue relation

$$\lambda = \frac{J(u)}{\|Ku\|^2_{L^2(\Omega)}}$$

in case of a one-homogeneous functional J. Hence, a Ground State u_0 is an Eigenfunction with Eigenvalue $\lambda_0 = J(u_0)/\|Ku_0\|^2_{L^2(\Omega)} = J(u_0)$; moreover, we immediately see that for any other Eigenvalue we have $\lambda \geq J(u_0)$. Furthermore, Eigenvalues measure the ratio between $J(u)$ and $\|Ku\|^2_{L^2(\Omega)}$ and are therefore a global measure of scale.

In order to point out the connection to standard Eigenfunction-theory and to present interesting and revealing examples of Eigenfunctions, we are discussing examples of Eigenfunctions for the regularization energies introduced in Section 4.1.

6.3 Examples

To highlight the connection to standard Eigenfunction theory, we want to consider the quadratic functional $J(u) = 1/2\|\nabla u\|^2_{L^2(\Omega)}$ as a regularizer first. Since J is Fréchet-differentiable the subdifferential consists of the Fréchet-derivative only, and the Eigenvalue Definition 6.2 in that case reads as

$$\lambda K^* K u \in \partial J(u) = \{-\Delta u\}\,.$$

For the choice of $K = I$ we therefore end up with the classical Eigenfunction-problem of the Laplace operator, i.e.

$$-\lambda u = \Delta u$$

with its solutions

$$u(x) = \sum_{n=1}^{\infty} a_n \cos(b_n x)\,,$$

if $\sum_{n=1}^{\infty} b_n^2$ exists and $\lambda = \sum_{n=1}^{\infty} b_n^2$ holds, due to the Neumann-boundary conditions implied by the optimality condition of (2.8) for $J(u) = 1/2\|\nabla u\|^2_{L^2(\Omega)}$. Hence, Definition 6.2 is a generalization of standard Eigenfunction-theory to subdifferential calculus.

In the following we want to show some typical non-trivial examples of Eigenfunctions for the specific variational models consisting of an L^2 fidelity and the regularization functionals introduced in Chapter 4.

6.3.1 ℓ^1 Regularization

In the context of discrete ℓ^1-regularization as introduced in Section 4.1.2, the subgradient simply reads as

$$\partial\|u\|_{\ell^1} = (\operatorname{sign}(u_n))_{n\in\{1,\dots,n\}}\,,$$

as it has been shown in Section 2.6, Example 2.13. Hence, we basically need to find functions for which K^*Ku is in their signum.

Example 6.4 (Dante's Peak)**.** In Example 6.1 we have already seen that Kronecker delta-functions are Ground States of the ℓ^1-functional for $K = I$. Moreover, we know from Remark 6.1 that these Ground States are also Eigenfunctions with Eigenvalue $\lambda = 1$. If we consider a semi-discrete operator $K : \ell^2 \to L^2(\Sigma)$, or a fully discrete operator $\overline{K} : \ell^2 \to \ell^2$, the following theorem will state the logical consequence that any Kronecker δ multiplied by a factor $1/\lambda$ is an Eigenfunction of the ℓ^1-norm with Eigenvalue λ.

Theorem 6.1. *Let $K : \ell^1 \to L^2(\Sigma)$ be a linear operator with $|\langle K^* e_i, K e_j\rangle_{\ell^2}| \leq 1$ for all $i \in \{1,\dots,n\}$ and $j \in \{1,\dots,n\}$, such that $i \neq j$, and with $|\langle K^* e_j, K e_j\rangle_{\ell^2}| = 1$. Then, $\tilde{u} = \delta_j/\lambda$, with $\lambda \in \mathbb{R}\setminus\{0\}$ and δ representing the Kronecker-δ-function, i.e.*

$$\delta_j = \begin{cases} 1 & \text{if } i = j \\ 0 & \text{else} \end{cases}\,,$$

is an Eigenfunction of the ℓ^1-norm with Eigenvalue λ.

Proof. If we evaluate $\tilde{q}_n := (K^*K\tilde{u})_n = 1/\lambda\,(K^*K\delta_j)_n$ we easily see that $\lambda\tilde{q}_n \in \operatorname{sign}(\tilde{u}_n)$ holds, if $|\langle K^*e_j, Ke_j\rangle_{\ell^2}| = 1$ and $|\langle K^*e_i, Ke_j\rangle_{\ell^2}| \leq 1$, for $i \in \{1,\dots,n\}$ with $i \neq j$.

□

Remark 6.2. Consequently, for a fully discrete linear operator or matrix $\overline{K} : \ell^2 \to \ell^2$ this implies that the ℓ^2-norms of the columns have to be less or equal to one; the ℓ^2-norm of the j-th column needs to be exactly one.

6.3.2 Total Variation Regularization

In case of total variation regularization as introduced in Section 4.1.4 we have figured out that the subdifferential of TV can be written as (4.5).

In the following, we assume $K = I$ for the sake of simplicity and are going to present some functions $\tilde{u}$ for which we will prove that they are Eigenfunctions of TV, i.e. $\lambda\tilde{u} \in \partial\mathrm{TV}(\tilde{u})$ for $\lambda \in \mathbb{R} \setminus \{0\}$. In order to prove that a function $\tilde{u}$ is an Eigenfunction with Eigenvalue λ, we need to find a function q such that the subdifferential conditions are satisfied, i.e.

1. $\operatorname{div} q = \lambda\tilde{u}$, (in a weak sense)
2. $q|_{\partial\Omega} = 0$,
3. $\|q\|_{L^\infty(\Omega)} = 1$,
4. $\langle \operatorname{div} q, \tilde{u}\rangle_{L^2(\Omega)} = \mathrm{TV}(\tilde{u})$.

If such a particular function q exists, then $\lambda\tilde{u} \in \partial\mathrm{TV}(\tilde{u})$ holds.

The One-Dimensional Setting

In order to get familiar with Eigenfunctions of the ROF model we want to start considering examples in one dimension. The subdifferential in 1D simplifies to

$$\partial\mathrm{TV}(u) = \left\{ p' \mid p \in L_0^\infty([a,b]),\ \|p\|_\infty = 1,\ \ \langle p', u\rangle_{L^2([a,b])} = \mathrm{TV}(u) \right\},$$

for $x \in [a,b]$, $a, b \in \mathbb{R}$ with $b > a$. In the following, we are going to consider symmetric intervals, i.e. $b = -a$, $b \in \mathbb{R}_{>0}$. Here and throughout this chapter $L_0^\infty(\Omega)$ denotes the space of all functions in $L^\infty(\Omega)$ that vanish at the boundary in direction of the normals.

Example 6.5 (The Edge)**.** As a first example we want to show that the function

$$\tilde{u}(x) = \operatorname{sign}(x)$$

on the interval $\Omega = [-L, L]$, $L > 0$, is an Eigenfunction of TV with Eigenvalue $\lambda = 1/L$. Therefore, we define the function

$$q(x) := (|x| - L)/L\,.$$

It is easy to see that q satisfies the subgradient properties, since we have

- $q'(x) = \operatorname{sign}(x)/L = \lambda\tilde{u}$,
- $q(L) = q(-L) = 0$,

- $\|q\|_{L^\infty([-L,L])} = |q(0)| = 1$,
- $\langle q', \tilde{u}\rangle_{L^2([-L,L])} = 1/L \int_{-L}^{L} 1 \, dx = 2 = \mathrm{TV}(\mathrm{sign}) = \mathrm{TV}(\tilde{u})$.

Therefore, $\tilde{u}(x) = \mathrm{sign}(x)$ is an Eigenfunction of TV with Eigenvalue $1/L$. Figure 6.1 shows a plot of $\tilde{u}$ and the corresponding dual variable q.

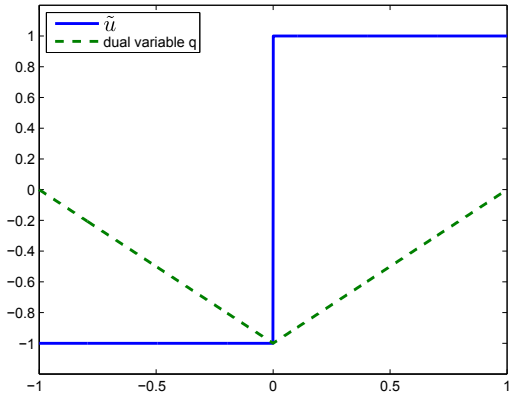

Figure 6.1: The Eigenfunction $\tilde{u} = \mathrm{sign}(x)$ and its corresponding dual variable $q \in \partial \mathrm{TV}(\tilde{u})$ on the interval $[-1, 1]$.

Example 6.6 (The Cylinder)**.** As a second intuitive example we want to consider the function

$$\tilde{u}(x) = 2H(L/2 - |x|) - 1\,,$$

with H denoting the Heaviside function, on the interval $[-L, L]$. We are going to show that $\tilde{u}$ is an Eigenfunction of TV with Eigenvalue $\lambda = 2/L$. Defining q with

$$q(x) := \frac{2}{L} \begin{cases} x & x \in [-L/2, L/2[\\ L - x & x \in [L/2, L] \\ -L - x & x \in [-L, -L/2[\end{cases}$$

will allow us to prove this assumption. Considering the subdifferential properties yields

- $q'(x) = (4H(L/2 - |x|))/L - 2/L = \lambda \tilde{u}$,
- $q(L) = q(-L) = 0$,
- $\|q\|_{L^\infty([-L,L])} = |q(-L/2)| = q(L/2) = 1$,
- $\langle q', \tilde{u}\rangle_{L^2([-L,L])} = 2/L \int_{-L}^{L} 1 \, dx = 4 = \mathrm{TV}(\tilde{u})$,

and hence, $\tilde{u}$ is an Eigenfunction of TV with Eigenvalue $\lambda = 2/L$. A plot of $\tilde{u}$ and q can be found in Figure 6.2.

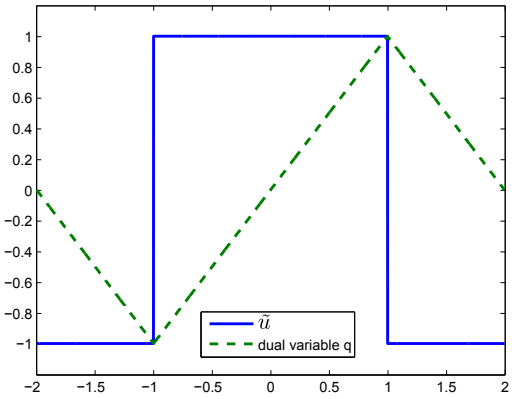

Figure 6.2: The function $\tilde{u} = 2H(1 - |x|) - 1$ and the corresponding dual variable $q \in \partial \mathrm{TV}(\tilde{u})$ on the interval $[-2, 2]$.

Example 6.7 (The Hat)**.** Finally, to conclude this section on the one-dimensional TV-setting, we want to consider a function that is no TV-Eigenfunction. Let us therefore investigate the function

$$\tilde{u}(x) = \frac{L}{2} - |x| \,.$$

It is easy to see that a function q satisfying $q'(x) = \lambda \tilde{u}$ for some constant λ needs to be of the form

$$q(x) = \lambda \left(\frac{L}{2} x - \frac{1}{2} \mathrm{sign}(x)|x|^2 \right)$$

in order to be continuous and to fulfill $q(L) = q(-L) = 0$. The trouble lies in matching the subdifferential conditions 3 and 4. On the one hand, we have

$$\langle q', \tilde{u} \rangle_{L^2([-L,L])} = \lambda \int_L^L \left(\frac{L}{2} - |x| \right)^2 dx = \lambda \frac{L^3}{6}$$

and $\mathrm{TV}(\tilde{u}) = 2L$, which leads to the conclusion $\lambda = 12/\left(L^2\right)$. On the other hand, we would therefore obtain $\|q\|_{L^\infty([-L,L])} = q\left(L/2\right) = \left(12\left(L^2/4 - L^2/8\right)\right)/\left(L^2\right) = 3/2 > 1$, which is a violation of subdifferential condition 3. Due to this contradiction in constructing a unique function q such that q satisfies the subdifferential properties, $\tilde{u}$ is not an Eigenfunction of TV. The functions $\tilde{u}$ and q can be seen in Figure 6.3. Nevertheless, the function q gives us a good intuition of how a ROF-minimizer with input data $f = \tilde{u}$ should look like. If we consider $\tilde{q}$ with

$$\begin{aligned} \tilde{q}(x) &= \max\left(\min\left(\frac{6}{L} x - \frac{6}{L^2} \mathrm{sign}(x)|x|^2, 1 \right), -1 \right) \\ &= \begin{cases} 1 & x \in [L/2 - L/\sqrt{12}, L/2 + L/\sqrt{12}] \\ -1 & x \in [-L/2 - L/\sqrt{12}, -L/2 + L/\sqrt{12}] \\ \frac{6}{L} x - \frac{6}{L^2} \mathrm{sign}(x)|x|^2 & \text{else} \end{cases}, \end{aligned}$$

then from the optimality condition of the ROF-model $p = (\tilde{u} - u)/\alpha$ we can intuitively guess that in regions where $|\tilde{q}| = 1$ holds the functions $\tilde{u}$ and the ROF minimizer coincide. In the regions

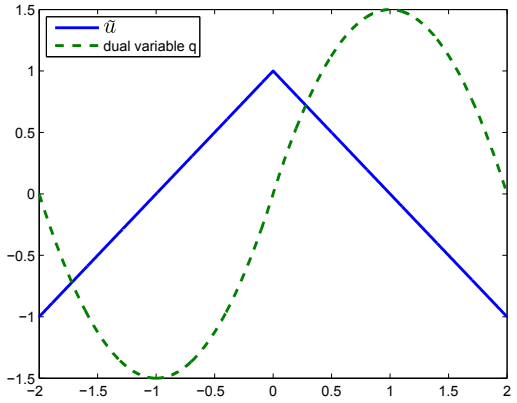

Figure 6.3: The function $\tilde{u} = 1 - |x|$ and the dual variable $q \in \partial \mathrm{TV}(\tilde{u})$ on the interval $[-2, 2]$.

where $\tilde{q}$ is not constant, we expect the ROF minimizer to be constant, such that the overall function is continuous; an intuition that is also supported by the relation between the ROF-model and the taut string algorithm (cf. [61]). The solution of the dual variable for the ROF-model with this particular input function indeed is

$$q(x) = \frac{1}{\alpha} \begin{cases} \sqrt{2\alpha}x - \frac{1}{2}\mathrm{sign}(x)|x|^2 & x \in [-\sqrt{2\alpha}, \sqrt{2\alpha}] \\ \alpha & x \in [-L + \sqrt{2\alpha}, -\sqrt{2\alpha}[\\ -\alpha & x \in]\sqrt{2\alpha}, L - \sqrt{2\alpha}] \\ (L - \sqrt{2\alpha})x + \frac{1}{2}x^2 + \frac{1}{2}L^2 - \sqrt{2\alpha}L & x \in [-L, -L + \sqrt{2\alpha}[\\ (L - \sqrt{2\alpha})x - \frac{1}{2}x^2 - \frac{1}{2}L^2 + \sqrt{2\alpha}L & x \in]L - \sqrt{2\alpha}, L] \end{cases},$$

for $L > \sqrt{2\alpha}$.

The Anisotropic Two-Dimensional Setting

What is special about the total variation semi-norm is that in two or higher dimensions there are different classes of Eigenfunctions of the semi-norm, depending on the particular choice of vector norm for the supremum of the dual variable. In this context, we basically want to differ between two important cases; the isotropic and the anisotropic TV-setting. If we take a look at the formal definition of the TV-semi-norm, i.e.

$$\mathrm{TV}(u) = \int_\Omega \|\nabla u\|_p \, dx \,,$$

we see that we can use different choices for the inner vector norm $\|\cdot\|_p$. In literature, the most popular cases are $p = 1$ (anisotropic TV) and $p = 2$ (isotropic TV); in this thesis, we are going to focus on Eigenfunctions for two-dimensional anisotropic TV only, for the sake of simplicity.
The subifferential in the anisotropic case can be written as

$$\partial \mathrm{TV}(u) = \left\{ \mathrm{div} p \mid p \in L_0^\infty(\Omega; \mathbb{R}^2), \ \max(|p_x|, |p_y|) = 1, \ \langle \mathrm{div} p, u \rangle_{L^2(\Omega)} = \mathrm{TV}(u) \right\},$$

with $p = (p_x, p_y)$.
In the following, we want to extend the one-dimensional Example 6.6 to two dimensions.

Example 6.8 (The Checkerboard)**.** Let $\tilde{u}$ be defined as

$$\tilde{u}(x,y) := \begin{cases} \frac{4}{L} & (x,y) \in [-L/2, L/2]^2 \\ 0 & ((|x| > 1) \wedge (|y| \leq 1)) \vee ((|x| \leq 1) \wedge (|y| > 1)) \\ -\frac{4}{L} & \text{else} \end{cases}, \tag{6.2}$$

for $(x,y) \in [-L, L]^2$. We are going to show that $\tilde{u}$ is an Eigenfunction of anisotropic TV with Eigenvalue $\lambda = 1$. Let us therefore consider q with

$$q_x(x,y) := \frac{2}{L} \begin{cases} x & x \in [-L/2, L/2[\\ L - x & x \in [L/2, L] \\ -L - x & x \in [-L, -L/2[\end{cases},$$

and

$$q_y(x,y) := \frac{2}{L} \begin{cases} y & y \in [-L/2, L/2[\\ L - y & y \in [L/2, L] \\ -L - y & y \in [-L, -L/2[\end{cases}.$$

With q defined as $q = (q_x, q_y)$ we can prove the subdifferential properties of q in order to show that $\tilde{u}$ is an Eigenfunction.

- $\mathrm{div} q = \partial_x q_x + \partial_y q_y = \lambda \tilde{u}$
- $q_x n_x = 0$, $q_y n_y = 0$, with n_x and n_y denoting the normals of q_x and q_y in x- and y-direction, respectively
- $\|q\|_{L^\infty([-L,L]^2)} = \max(|q_x|, |q_y|) = 1$
- $$\begin{aligned} \langle \mathrm{div} q, \tilde{u} \rangle_{L^2([-L,L]^2;\mathbb{R}^2)} &= 16/\left(L^2\right) \left(\int_{-L/2}^{L/2} \int_{-L/2}^{L/2} 1 \, dx \, dy + \int_{-L}^{-L/2} \int_{-L}^{-L/2} 1 \, dx \, dy \right. \\ &\quad \left. + \int_{L/2}^{L} \int_{-L}^{-L/2} 1 \, dx \, dy + \int_{-L}^{-L/2} \int_{L/2}^{L} 1 \, dx \, dy + \int_{L/2}^{L} \int_{L/2}^{L} 1 \, dx \, dy \right) \\ &= 32 = \mathrm{TV}(\tilde{u}) \end{aligned}$$

Hence, $\tilde{u}$ is an Eigenfunction of anisotropic TV. Note that the factor $4/L$ has been chosen to guarantee $\lambda = 1$. We could have also considered a function with a different factor, denoted by β, and would have proved this function to be an Eigenfunction, but with Eigenvalue $\lambda = 4/(\beta L)$.

6.3.3 TV^2

After considering a few intuitive Eigenfunction examples for the total variation semi-norm, we now want to investigate second-order total variation, as introduced in Section 4.1.5. The subdifferential of TV^2 can be characterized via (4.7).

For the sake of simplicity we want to focus on the one-dimensional setting; extensions to anisotropic or isotropic higher-dimensional settings are comparable to the way one-dimensional

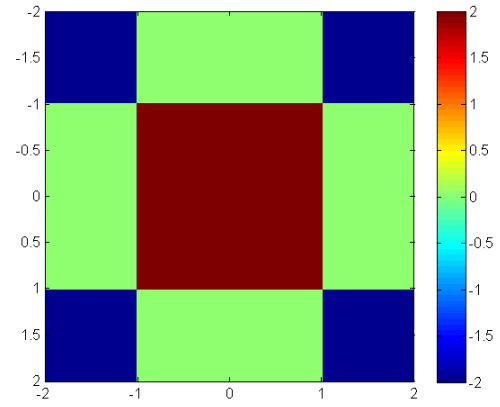

(a) On-top view of $\tilde{u}$

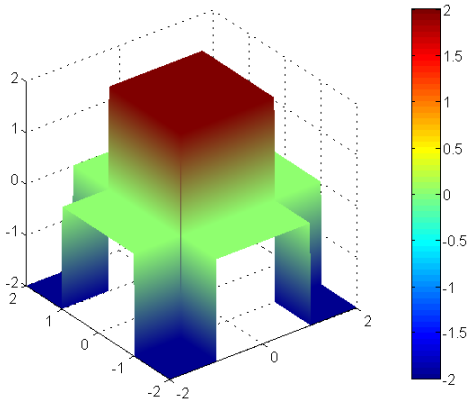

(b) 3d view of $\tilde{u}$

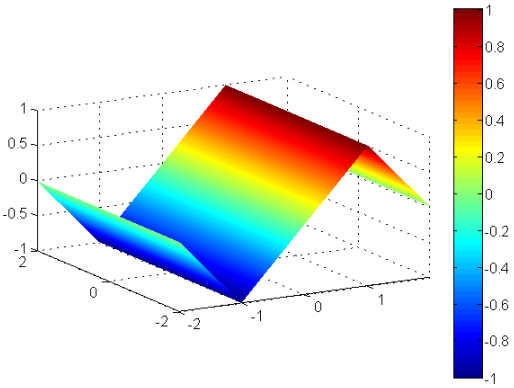

(c) Dual variable q_x

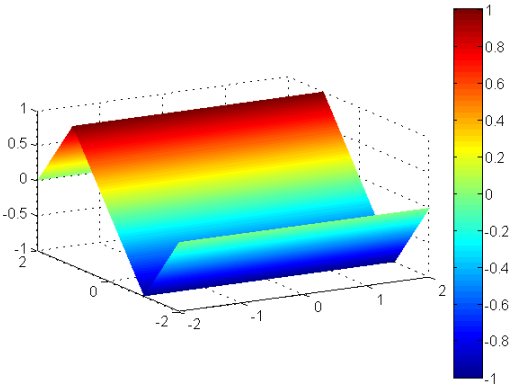

(d) Dual variable q_y

Figure 6.4: The figure shows an on-top view of the function $\tilde{u}$ as defined in (6.2), a three-dimensional view and the corresponding dual variables $(q_x, q_y) \in \partial \mathrm{TV}(\tilde{u})$ on the interval $[-2, 2]^2$.

TV-Eigenfunctions extend to higher dimensions. The subdifferential (4.7) in one dimension simplifies to

$$\partial \mathrm{TV}^2(u) = \left\{ p'' \mid p \in L_0^\infty([a,b]),\ \|p\|_{L^\infty([a,b])} = 1,\ \left\langle p'', u \right\rangle_{L^2([a,b])} = \mathrm{TV}^2(u) \right\},$$

for $b > a$, $a, b \in \mathbb{R}$.

Example 6.9 (The Hat)**.** As a first example, we want to consider the hat-function $\tilde{u}(x) = L/2 - |x|$ on the interval $[-L, L]$ again. In Example 6.7 we have seen that $\tilde{u}$ is not an Eigenfunction of the total-variation semi-norm, as expected. We would indeed expect, that $\tilde{u}$ is an Eigenfunction of TV^2 (with Eigenvalue $\lambda = 12/\left(L^3\right)$); in order to verify this assumption let us therefore define the function q with

$$q(x) := \frac{3}{L^2} x^2 - \frac{2}{L^3} |x|^3 - 1\,.$$

Examining the subdifferential properties yields

- $q'' = 6/(L^2) - (12/(L^3))|x| = \lambda\tilde{u}$,
- $q(L) = q(-L) = 0$,
- $q'(L) = q'(-L) = 0$
- $\|q\|_{L^\infty([-L,L])} = |q(0)| = 1$,
- $\langle q'', \tilde{u}\rangle_{L^2([-L,L])} = (12/(L^3)) \int_{-L}^{L} (L/2 - |x|)^2 \ dx = 2 = \mathrm{TV}^2(\tilde{u})$,

therefore we have $q'' \in \partial\mathrm{TV}^2(\tilde{u})$ and thus, $\tilde{u}$ is an Eigenfunction of TV^2.

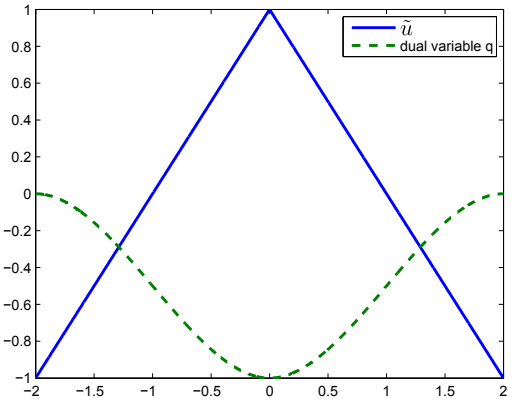

Figure 6.5: The function $\tilde{u} = 1 - |x|$ and the corresponding TV^2-dual variable $q \in \partial\mathrm{TV}^2(\tilde{u})$ on the interval $[-2, 2]$.

Example 6.10 (The Edge)**.** Intuitively it is obvious that piecewise constant functions cannot be Eigenfunctions of TV^2. With the edge-function $\tilde{u} = \mathrm{sign}(x)$ on the interval $[-L, L]$ of Example 6.5 as a counter example we are going to support this intuition. Let us therefore make an attempt and define a function q with

$$q(x) := \frac{1}{2}\mathrm{sign}(x)|x|^2 + \text{constant}$$

in order to guarantee $q''(x) = \mathrm{sign}(x)$. However, ensuring $q(L) = q(-L) = 0$ such that q is continuous is impossible and hence, $\tilde{u}$ is not an Eigenfunction of TV^2, since there does not exist a function q satisfying both $q'' = \tilde{u}$ and $q'' \in \partial\mathrm{TV}^2(\tilde{u})$.

Example 6.11 (The Cylinder)**.** In Example 6.10 we have seen that the piecewise constant function $\tilde{u}(x) = \mathrm{sign}(x)$ is not an Eigenfunction of TV^2, mainly because of wrong boundary conditions. That the wrong boundary conditions are not the only obstacle for piecewise constant functions to become TV^2-Eigenfunctions can be seen from the cylinder function of Example 6.6, i.e. $\tilde{u}(x) = 2H(L/2 - |x|) - 1$. For this function it is easy to construct a dual variable that meets the desired boundary conditions, since the cylinder-function changes it's sign twice. However, the TV^2-value of a piecewise constant function is given in terms of the derivative of a distribution, which is not a valid Radon-measure any more. Hence, $\mathrm{TV}^2(\tilde{u})$ does not exist. However, the integral $\langle q'', \tilde{u}\rangle_{L^2([-L,L])}$ takes a finite value and therefore the subgradient condition $\langle q'', \tilde{u}\rangle_{L^2([-L,L])} = \mathrm{TV}^2(\tilde{u})$ is never met for any piecewise constant function $\tilde{u}$.

6.3.4 Infimal Convolution

As we have seen in the two previous sections, there exist piecewise constant TV-Eigenfunctions, which are no TV^2-Eigenfunctions, and piecewise linear TV^2-Eigenfunctions that are no TV-Eigenfunctions. For infimal convolution regularization based on TV and TV^2 as presented in Section 4.1.6, we are going to see that there exist Eigenfunctions that are either just TV- or TV^2-Eigenfunctions, but at the same time both ICTV_β-Eigenfunctions.

For the sake of simplicity we consider the one-dimensional case only. In 1D the subdifferential (4.10) simplifies to

$$\partial \mathrm{ICTV}_\beta(u) = \left\{ q'' \mid p, q \in L_0^\infty([a,b]),\ \|p\|_{L^\infty([a,b])} = 1,\ \|q\|_{L^\infty([a,b])} = \beta, \right. \\ \left. q'' = p',\ \left\langle q'', u \right\rangle_{L^2([a,b])} = \mathrm{ICTV}_\beta(u) \right\} .$$

Note that both p and q need to have Dirichlet-boundary, due to the derivation of ICTV_β. In accordance to this definition, from a distributional point of view we see from

$$\left\langle u, q'' \right\rangle_{L^2([a,b])} = \int_a^b uq''\ dx = uq'\big|_a^b - \int_a^b u'q'\ dx = uq'\big|_a^b - u'q\big|_a^b + \int_a^b u''q\ dx \tag{6.3}$$

that

$$\left\langle u, q'' \right\rangle_{L^2([a,b])} = \left\langle u'', q \right\rangle_{L^2([a,b])}$$

is only satisfied for any twice-differentiable u if either $q(a) = q(b) = 0$ and $q'(a) = q'(b) = 0$ holds. However, for u with Neumann-boundary, i.e. $u'(a) = u'(b) = 0$, we see that the demand for Neumann-boundaries on q would be enough in order to guarantee that all boundary terms in (6.3) vanish. Nevertheless we assume the dual variable to have Dirichlet-boundary anyways.

Example 6.12 (The Hat)**.** Again, we consider $\tilde{u}(x) = L/2 - |x|$ on the interval $[-L, L]$. We are going to show that $\tilde{u}$ is an Eigenfunction of $\mathrm{ICTV}_{\frac{2}{3}L}$ with Eigenvalue $\lambda = 8/\left(L^2\right)$. For that reason we want to define q and p as

$$q(x) := \frac{2}{L}x^2 - \frac{4}{3L^2}|x|^3 - \frac{2}{3}L$$

and

$$p(x) := \frac{4}{L}x - \frac{4}{L^2}\mathrm{sign}(x)|x|^2 .$$

By taking a closer look we see that q and p satisfy the properties

- $q''(x) = 4/L - (8|x|)/\left(L^2\right) = (8\tilde{u})/\left(L^2\right) = \lambda\tilde{u}$,
- $q'' = p'$,
- $q(L) = q(-L) = 0$,
- $p(L) = p(-L) = 0$,
- $\|q\|_{L^\infty([-L,L])} = (2L)/3 = \beta$,
- $\|p\|_{L^\infty([-L,L])} = 1$,

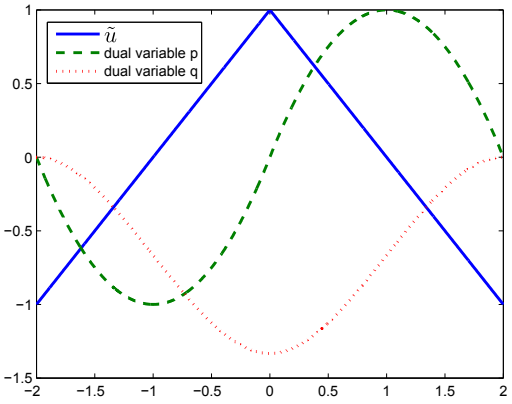

Figure 6.6: The function $\tilde{u}(x) = 1 - |x|$ and the corresponding dual variables $p, q \in \partial \mathrm{ICTV}_{\frac{4}{3}}(\tilde{u})$ on the interval $[-2, 2]$.

- $\langle q'', \tilde{u} \rangle_{L^2([-L,L])} = \langle p', \tilde{u} \rangle_{L^2([-L,L])} = 8/\left(L^2\right) \int_{-L}^{L} (L/2 - |x|)^2 \ dx = (4/3)L = \mathrm{ICTV}_{\frac{2}{3}L}(\tilde{u})$,

and therefore we have $q'' \in \partial \mathrm{ICTV}_{\frac{2}{3}L}(\tilde{u})$ and hence, $\tilde{u}$ is an Eigenfunction.

Example 6.13 (The Cylinder)**.** Considering the cylinder function of Example 6.6, i.e. $\tilde{u}(x) = 2H(L/2 - |x|) - 1$, for $x \in [-L, L]$, we want to show that $\tilde{u}$ is an Eigenfunction of $\mathrm{ICTV}_{\frac{1}{2}L}$ with Eigenvalue $\lambda = 2/L$. We therefore define

$$p(x) := \frac{2}{L} \begin{cases} x & x \in [-L/2, L/2[\\ L - x & x \in [L/2, L] \\ -L - x & x \in [-L, -L/2[\end{cases}$$

in analogy to Example 6.6, and

$$q(x) := \frac{2}{L} \begin{cases} \frac{1}{2}x^2 - \frac{1}{4}L^2 & x \in [-L/2, L/2[\\ Lx - \frac{1}{2}x^2 - \frac{1}{2}L^2 & x \in [L/2, L] \\ -Lx - \frac{1}{2}x^2 - \frac{1}{2}L^2 & x \in [-L, -L/2[\end{cases}.$$

It is easy to see that q and p satisfy the properties

- $q'' = (2\tilde{u})/L = \lambda \tilde{u}$,
- $q'' = p'$,
- $q(L) = q(-L) = 0$,
- $p(L) = p(-L) = 0$,
- $\|q\|_{L^\infty([-L,L])} = 2/L = \beta$,
- $\|p\|_{L^\infty([-L,L])} = 1$,

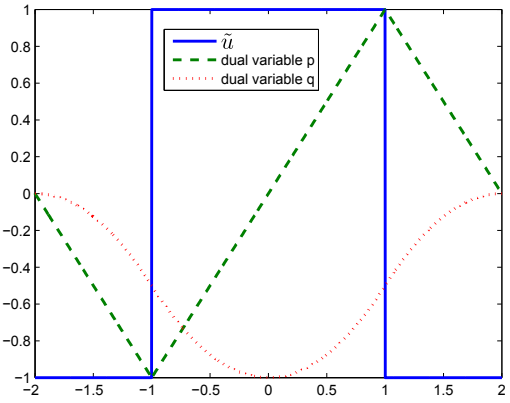

Figure 6.7: The function $\tilde{u}(x) = 2H(1-|x|) - 1$ and the corresponding dual variables $p, q \in \partial \mathrm{ICTV}_1(\tilde{u})$ on the interval $[-2, 2]$.

- $\langle q'', \tilde{u} \rangle_{L^2([-L,L])} = \langle p', \tilde{u} \rangle_{L^2([-L,L])} = 2/(L) \int_{-L}^{L} 1 \, dx = 4 = \mathrm{ICTV}_{\frac{1}{2}L}(\tilde{u})$.

Hence, $\tilde{u}$ is an Eigenfunction of $\mathrm{ICTV}_{\frac{1}{2}L}$ with Eigenvalue $\lambda = 2/L$.

From Example 6.13 we have seen that the function $u(x) = 2H(L/2 - |x|) - 1$, which is a TV-Eigenfunction (Example 6.6), but not a TV^2-Eigenfunction (Example 6.11), is a $\mathrm{ICTV}_{\frac{1}{2}L}$-Eigenfunction. In Example 6.12 we have shown that the function $u(x) = L/2 - |x|$ is an Eigenfunction of $\mathrm{ICTV}_{\frac{2}{3}L}$; moreover, u is an Eigenfunction of TV^2 (Example 6.9), but not of TV (Example 6.7). Hence, we have found two functions that are Eigenfunctions of ICTV_β, but not Eigenfunctions of both TV and TV^2. Unfortunately, TV- and TV^2-Eigenfunctions are not always ICTV_β-Eigenfunctions in general, as we are about to see with the following example.

Example 6.14 (The Edge)**.** As a last ICTV_β-example we want to discuss the edge-function $\tilde{u}(x) = \mathrm{sign}(x)$ again, for $x \in [-L, L]$. If we define q and p as

$$q(x) = \frac{1}{L}\left(\frac{1}{2}\mathrm{sign}(x)|x|^2 - Lx\right)$$

and

$$p(x) = \frac{1}{L}\left(|x| - L\right),$$

we can verify that the conditions

- $q''(x) = \mathrm{sign}(x)/L = \lambda \tilde{u}(x)$,
- $q'' = p'$,
- $q'(L) = p(L) = q'(-L) = p(-L) = 0$,
- $\|q\|_{L^\infty([-L,L])} = L/2$,
- $\|p\|_{L^\infty([-L,L])} = 1$,

- $\langle q'', \tilde{u} \rangle_{L^2([-L,L])} = \langle p', \tilde{u} \rangle_{L^2([-L,L])} = 1/L \int_L^L 1 \, dx = 2 = \mathrm{ICTV}_{\frac{L}{2}}(\tilde{u})$,

hold. Almost all conditions that have to be satisfied in order to guarantee that $\tilde{u}$ is an Eigenfunction are met, except for $q(L) = q(-L) = 0$, since we have
$q(L) = -L/2$ and $q(-L) = L/2$. As a consequence, $\tilde{u}$, which is a TV-Eigenfunction, is not an Eigenfunction of $\mathrm{ICTV}_{\frac{1}{2}L}$.

The main difference between $\mathrm{sign}(x)$ and $2H(L/2 - |x|) - 1$ on the interval $[-L, L]$ is that $\mathrm{sign}(x)$ is not orthogonal to the Ground States of ICTV_β, i.e. $\langle x, \mathrm{sign}(x) \rangle_{L^2([-L,L])} = 2L \neq 0$, while $2H(L/2 - |x|) - 1$ is orthogonal to the Ground States, since we have
$\langle x, 2H(L/2 - |x|) - 1 \rangle_{L^2([-L,L])} = 0$ and $\langle c, 2H(L/2 - |x|) - 1 \rangle_{L^2([-L,L])} = 0$ for any constant factor c.

We could assume that though $\tilde{u}(x) = \mathrm{sign}(x)$ is not an Eigenfunction, the solution of (2.9) with $J(u) = \mathrm{ICTV}_\beta(u)$ is still producing a preferable result. However, for $f = \tilde{u}$ we can actually compute that the solution of (2.9) with $J(u) = \mathrm{ICTV}_\beta(u)$ for $\beta \geq (4L)/27$ and $\alpha < L/4$ on the interval $[-L, L]$ is given as

$$u(x) = \begin{cases} \frac{6\alpha}{L^2} x - \frac{4\alpha}{L} + 1 & \text{for } x \geq 0 \\ \frac{6\alpha}{L^2} x + \frac{4\alpha}{L} - 1 & \text{else} \end{cases},$$

This result is actually not desirable, since homogeneous regions are tipped. An exemplary plot for $L = 1$ and $L = 2$ can be seen in Figure 6.8.

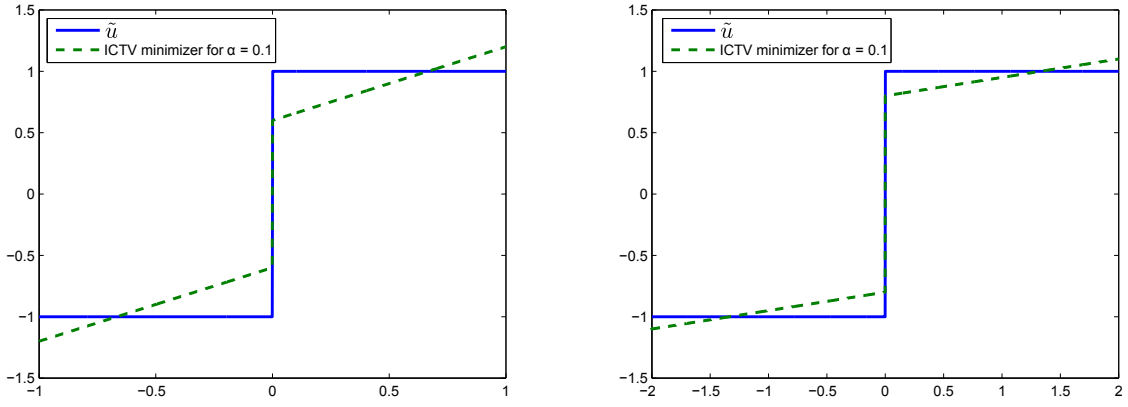

(a) $L = 1$ (b) $L = 2$

Figure 6.8: The function $\tilde{u}(x) = \mathrm{sign}(x)$, which is a TV-Eigenfunction, but not an ICTV_β-Eigenfunction, and two exemplary $\mathrm{ICTV}_{\frac{4}{27}L}$ reconstructions with $f = \tilde{u}$ and $\alpha = 1/10$ on the intervals $[-1, 1]$ and $[-2, 2]$, respectively.

6.3.5 Generalized Total Variation

Generalized Total Variation regularization has very similar characteristics as the Infimal Convolution regularization. As it has been pointed out in [118] the main advantages with respect to ICTV_β appear in dimensions higher than one; however, since a characterization of Eigenfunctions

in two or more dimensions is very complicated, we still want to focus on the one-dimensional setting. In 1D the subdifferential (4.12) simplifies to

$$\partial \mathrm{GTV}_\beta(u) = \big\{ p'' \mid p \in L_0^\infty([a,b]),\ \|p\|_{L^\infty([a,b])} = \beta,\ \|\mathrm{div} p\|_{L^\infty([a,b])} = 1, \\ \langle p'', u \rangle_{L^2([a,b])} = \mathrm{GTV}_\beta(u) \big\} .$$

It is easy to see that the Eigenfunction-examples of Section 6.3.4 and their results can easily be transferred to the one-dimensional Generalized Total Variation. Hence, GTV_β has the same advantages towards TV and TV^2 as ICTV_β, e.g. the fact that both TV- and TV^2-Eigenfunctions can simultaneously be Eigenfunctions of GTV_β. It also inheres the same problematic nature as ICTV_β that only those TV-Eigenfunctions are GTV_β-Eigenfunctions that are orthogonal to the TV^2-Groundstates. In recent work on GTV_β (cf. [18, 118]) it has been very popular to use a piecewise linear block image to demonstrate superiority of GTV_β towards ICTV_β. However, we want to show that a 1D profile of this image basically is not an Eigenfunction of GTV_β.

Example 6.15 (Counter-Linearity)**.** We want to consider the function

$$\tilde{u}(x) := \begin{cases} -x & x \in [-L/2, L/2] \\ x & \text{else} \end{cases}$$

on the interval $[-L, L]$. The problem with $\tilde{u}$ is that it is not orthogonal to the Ground States, since we have $\langle x, \tilde{u} \rangle_{L^2([-L,L])} = L^3/2 \neq 0$. If we modify $\tilde{u}$ by subtracting $(3x)/4$, then we obtain the function

$$\tilde{u}(x) := \begin{cases} -\frac{7}{4}x & x \in [-L/2, L/2] \\ \frac{1}{4}x & \text{else} \end{cases} ,$$

for which we can compute $\langle c, \tilde{u} \rangle_{L^2([-L,L])} = 0$ and $\langle x, \tilde{u} \rangle_{L^2([-L,L])} = 0$, for any constant c. Nevertheless, we want to show that $\tilde{u}$ is not an Eigenfunction of GTV_β. We make the attempt for the dual variable by defining $q \in C_0^2([-L, L])$ as

$$q(x) := \frac{1}{L^2} \begin{cases} -\frac{7}{3}x^3 + L^2 x & x \in [-L/2, L/2] \\ \frac{1}{3}x^3 - L^2 x + \frac{2}{3}L^3 & x \in\ ]L/2, L] \\ \frac{1}{3}x^3 - L^2 x - \frac{2}{3}L^3 & x \in [-L, -L/2[\end{cases} .$$

We can easily compute that q satisfies the properties

- $q'' = \lambda \tilde{u}$,
- $q(L) = q(-L) = 0$,
- $q'(L) = q'(-L) = 0$,
- $\|q\|_{L^\infty([-L,L])} = q(L/\sqrt{7}) = (2\sqrt{7}L)/21 = \beta$,
- $\|q'\|_{L^\infty([-L,L])} = q'(0) = 1$,

and hence, we would obtain $q \in \partial \mathrm{GTV}_{\frac{2\sqrt{7}}{21}L}(\tilde{u})$ with $\lambda = 8/(L^2)$ if we in addition could guarantee $\langle q'', \tilde{u} \rangle_{L^2([-L,L])} = \mathrm{GTV}_{\frac{2\sqrt{7}}{21}L}(\tilde{u})$. Computing the dual product actually yields $\langle q'', \tilde{u} \rangle_{L^2([-L,L])} =$

$(7L)/3$. We want to show that this value does not equal the value $\mathrm{GTV}_{\frac{2\sqrt{7}}{21}L}(\tilde{u})$ and therefore consider the decomposition $\tilde{u}(x) = \tilde{v}(x) + \tilde{w}(x)$ with

$$\tilde{v}(x) = \begin{cases} 0 & x \in [-L/2, L/2] \\ L & x \in \ ]L/2, L] \\ -L & x \in [-L, -L/2[\end{cases}$$

and

$$\tilde{w}(x) = \begin{cases} -\frac{7}{4}x & x \in [-L/2, L/2] \\ \frac{1}{4}x - L & x \in \ ]L/2, L] \\ \frac{1}{4}x + L & x \in [-L, -L/2[\end{cases}.$$

We easily see that for these two functions we obtain $\mathrm{TV}(\tilde{v}) = 2L$ and $\mathrm{TV}^2(\tilde{w}) = L$. From the underlying infimal convolution point of view we would expect $\mathrm{GTV}_{\frac{2\sqrt{7}}{21}L}(\tilde{u})$ to equal $\mathrm{TV}(\tilde{v}) + \beta\mathrm{TV}^2(\tilde{w})$ (cf. (4.8)), which would imply $\mathrm{GTV}_{\frac{2\sqrt{7}}{21}L}(\tilde{u}) = 2L + (2\sqrt{7}L^2)/21 \neq (7L)/3$. Hence, $\tilde{u}$ is not an Eigenfunction of GTV_β.

Example 6.16 (The Cylinder-Hat)**.** By taking a closer look at the decomposition of $\tilde{u}$ from the previous Example 6.15 we see that we indeed have orthogonality of $\tilde{u}$ to the Ground States of generalized TV, while for $\tilde{v}$ and $\tilde{w}$ we can easily compute $\langle x, \tilde{v}\rangle_{L^2([-L,L])} = (3L^3)/4 \neq 0$ and $\langle x, \tilde{w}\rangle_{L^2([-L,L])} = (3L^3)/4 \neq 0$. As a consequence, $\tilde{v}$ is an Eigenfunction of TV but $\tilde{w}$ is not an Eigenfunction of TV^2. We may assume that an additive composition of a TV-Eigenfunction and a TV^2-Eigenfunction that are both GTV_β-Eigenfunctions will allow us to discover an Eigenfunction of GTV_β that is neither an Eigenfunction of TV nor of TV^2. Let us therefore define $\tilde{u}(x) := \tilde{v}(x) + \tilde{w}(x)$ with $\tilde{v}(x) := 2H(L/2 - |x|) - 1$ (which is an Eigenfunction of either TV and ICTV_β due to Example 6.6 and Example 6.13) and $\tilde{w}(x) := L/2 - |x|$ (which is an Eigenfunction of either TV^2 and ICTV_β due to Example 6.9 and Example 6.12), i.e.

$$\tilde{u}(x) = \begin{cases} (L/2 + 1) - |x| & x \in [-L/2, L/2] \\ (L/2 - 1) - |x| & \text{else} \end{cases}.$$

We are going to show that $\tilde{u}$ is an Eigenfunction of $\mathrm{GTV}_{\frac{L^2+3L}{6+\frac{3}{2}L}}$ with Eigenvalue $\lambda = 1/(L(1/2 + L/8))$ and therefore define the dual variable q with

$$q(x) := \frac{1}{L\left(\frac{1}{2} + \frac{L}{8}\right)} \begin{cases} \frac{1}{2}\left(\frac{L}{2} + 1\right)x^2 - \frac{1}{6}|x|^3 - \frac{L^2}{12}(L+3) & x \in [-L/2, L/2] \\ \frac{1}{2}\left(\frac{L}{2} - 1\right)x^2 - \frac{1}{6}x^3 + Lx - \frac{L^2}{12}(L+6) & x \in]L/2, L] \\ \frac{1}{2}\left(\frac{L}{2} - 1\right)x^2 + \frac{1}{6}x^3 - Lx - \frac{L^2}{12}(L+6) & x \in [-L, -L/2[\end{cases}.$$

For these functions we can verify the properties

- $q''(x) = \tilde{u}/(L(1/2 + L/8)) = \lambda\tilde{u}(x)$,
- $q(L) = q(-L) = 0$,
- $q'(L) = q'(-L) = 0$,

- $\|q\|_{L^\infty([-L,L])} = \left(L^2+3L\right)/\left(6+(3L)/2\right) = \beta,$
- $\|q'\|_{L^\infty([-L,L])} = 1,$
- $$\begin{aligned}\left\langle q'', \tilde{u}\right\rangle_{L^2([-L,L])} &= \left(4\left((L+3)^2+3\right)\right)/\left(3\left(4+L\right)\right)\\ &= \mathrm{TV}(2H(L/2-|x|)-1) + \beta\mathrm{TV}^2(L/2-|x|) = \mathrm{GTV}_{\frac{L^2+3L}{6+\frac{3}{2}L}}(\tilde{u}),\end{aligned}$$

and as a consequence the sum of the Eigenfunctions $2H(L/2-|x|)-1$ and $L/2-|x|$ indeed is an Eigenfunction of $\mathrm{GTV}_{\frac{L^2+3L}{6+\frac{3}{2}L}}$ with Eigenvalue $\lambda = 1/(L(1/2+L/8))$.

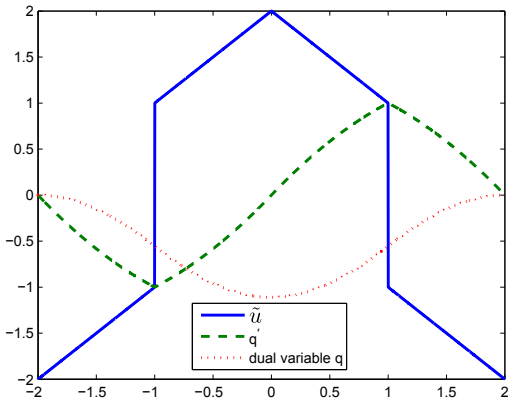

Figure 6.9: The function $\tilde{u}(x) = 2H(1-|x|)-|x|$ and the corresponding dual variable $q \in \partial\mathrm{GTV}_{\frac{10}{9}}(\tilde{u})$ and its derivative q' on the interval $[-2,2]$.

6.4 Exact Reconstruction of Eigenfunctions

In this section we are going to see that the recovery of Eigenfunctions is closely related to Bregman distances. First of all, we want to recall a criterion that has been shown by Meyer in [90] in order to derive trivial Eigenfunctions for the ROF-model. These considerations can be generalized by the use of Bregman distances as it can be seen by the following theorem.

Theorem 6.2. *Let $J : \mathrm{dom}(J) \subseteq L^2(\Omega) \to \mathbb{R}\cup\{+\infty\}$ be a convex functional and let $K : L^2(\Omega) \to L^2(\Sigma)$ be a linear operator. If the condition*

$$\frac{1}{\alpha}K^*f \in \partial J(0) \tag{6.4}$$

is satisfied, the minimizer of (2.8) *is given as $\hat{u} \equiv 0$.*

Proof. We can rewrite (2.8) to

$$\hat{u} = \operatorname*{arg\,min}_{u\in\mathrm{dom}(J)} \left\{ \frac{1}{2}\|Ku\|^2_{L^2(\Sigma)} + \alpha\left(J(u) - \left\langle \frac{1}{\alpha}K^*f, u\right\rangle_{L^2(\Omega)}\right) + \frac{1}{2}\|f\|^2_{L^2(\Sigma)}\right\}$$

Since (6.4) is satisfied, we can define $q := (K^*f)/\alpha$ such that

$$D_J^q(u,0) = J(u) - J(0) - \langle q, u\rangle_{L^2(\Omega)}$$

is a non-negative Bregman distance. Hence, ignoring the constant part $1/2\|f\|_{L^2(\Sigma)}$ we have

$$\hat{u} = \operatorname*{arg\,min}_{u\in\mathrm{dom}(J)} \left\{ \frac{1}{2}\|Ku\|^2_{L^2(\Sigma)} + \alpha D_J^q(u,0) \right\}$$

for which the obvious minimizer is given via $\hat{u} = 0$, since both terms are non-negative and vanish for $u = 0$. □

Remark 6.3. Note that if (6.4) is satisfied for a specific $\tilde{\alpha}$ and J being positive (which is a natural assumption for regularization functionals), then (6.4) is automatically guaranteed for every $\alpha \geq \tilde{\alpha}$, since $(K^*f)/\tilde{\alpha} \in \partial J(0)$ implies

$$J(v) \geq \left\langle \frac{1}{\tilde{\alpha}} K^*f, v \right\rangle_{L^2(\Omega)},$$

for all $v \in \mathrm{dom}(J)$. If we multiply both sides of the inequality with $\tilde{\alpha}$ we obtain

$$\tilde{\alpha}J(v) \geq \langle K^*f, v\rangle_{L^2(\Omega)},$$

since $\tilde{\alpha}$ is positive. Due to the positivity of J we even have

$$\alpha J(v) \geq \tilde{\alpha}J(v)$$

for all $v \in \mathrm{dom}(J)$ and $\alpha \geq \tilde{\alpha}$, and hence, (6.4) is guaranteed for all $\alpha \geq \tilde{\alpha}$.

Theorem 6.2 gives us an explicit condition on the regularization parameter α to enforce the solution of (2.9) to be zero. Furthermore, according to the following Lemma for Eigenfunctions $\tilde{u}$ of one-homogeneous functionals there even have to exist parameters α such that (6.4) is fulfilled for $f = K\tilde{u}$.

Lemma 6.1. *Let $J : \mathrm{dom}(J) \subseteq L^2(\Omega) \to \mathbb{R} \cup \{+\infty\}$ be a convex, nonnegative and one-homogeneous functional and let $K : L^2(\Omega) \to L^2(\Sigma)$ be a linear operator. If $u \in \mathrm{dom}(J) \cap \mathrm{dom}(K)$ is a function such that Theorem 6.2 is never valid for any $\alpha \in \mathbb{R}_{>0}$ with data $f = Ku$, i.e.*

$$\frac{1}{\alpha}K^*Ku \notin \partial J(0) \quad \forall \alpha \in \mathbb{R}_{>0},$$

then, u is not a non-trivial Eigenfunction with Eigenvalue $\lambda \neq 0$.

Proof. We want to prove the statement by contradiction. We therefore assume that on the one hand, u is an Eigenfunction with non-zero Eigenvalue λ, i.e. $\lambda K^*Ku \in \partial J(u)$. Taking a duality product of $\lambda K^*Ku = p$, $p \in \partial J(u)$, with u yields the equality

$$\lambda\|Ku\|^2_{L^2(\Sigma)} = J(u), \tag{6.5}$$

due to the one-homogeneity of J (see Lemma 2.4). Moreover, from the definition of the subdifferential, the Eigenvalue property yields

$$J(v) \geq J(u) + \lambda \langle K^*Ku, v - u\rangle_{L^2(\Omega)} \quad \forall v \in \mathrm{dom}(J). \tag{6.6}$$

On the other hand, we know due to $(K^*Ku)/\alpha \notin J(0)$ for all $\alpha \in \mathbb{R}_{>0}$ that there has to exist a function $v \in \mathrm{dom}(J)$ with

$$\langle Ku, Kv\rangle_{L^2(\Sigma)} > \alpha J(v)\,. \tag{6.7}$$

If we insert (6.6) into (6.7), for the particular choice of v we therefore obtain

$$\begin{aligned} &\langle Ku, Kv\rangle_{L^2(\Sigma)} > \alpha\left(J(u) + \lambda\langle Ku, Kv\rangle_{L^2(\Omega)} - \lambda\|Ku\|^2_{L^2(\Sigma)}\right) \\ \Leftrightarrow\ &(1-\lambda\alpha)\langle Ku, Kv\rangle_{L^2(\Sigma)} > \alpha\left(J(u) - \lambda\|Ku\|^2_{L^2(\Sigma)}\right)\,. \end{aligned} \tag{6.8}$$

Equation (6.8) is supposed to be true for every $\alpha \in \mathbb{R}_{>0}$, especially for the particular choice $\alpha = 1/\lambda$. In this case, (6.8) reads as

$$\lambda\|Ku\|^2_{L^2(\Sigma)} > J(u)\,,$$

for $\lambda > 0$, and therefore is a contradiction to (6.5). □

The reverse statement of Lemma 6.1 therefore is that for every data f given in terms of an Eigenfunction, i.e. $f = K\tilde{u}$, there exists a parameter $\tilde{\alpha}$ such that Theorem 6.2 is valid for $\alpha \geq \tilde{\alpha}$.

Moreover, condition (6.4) guarantees that the data f needs to satisfy certain properties in order to vanish for a large regularization parameter α, e.g. f does need to have zero mean for $K = I$ in the case of TV-regularization.

Remark 6.4. Note that, however, it is possible for a particular function f that there does not exist a parameter α such that (6.4) is fulfilled, though f is a trivial Ground-State-Eigenfunction with Eigenvalue $\lambda = 0$, e.g. for $f \not\equiv 0$ being a constant function and J being the total variation regularizer.

In the following we are going to investigate the reconstruction of Eigenfunctions with given data $f = K\tilde{u}$, while $\tilde{u}$ represents an Eigenfunction, in the absence and presence of noise.

6.4.1 Clean Data

In case of clean data $f = \gamma K\tilde{u}$, $\gamma > 0$ and $\tilde{u}$ being a non-trivial Eigenfunction, we are interested in finding a solution of (2.8) that can be expressed in terms of this Eigenfunction, i.e. $\hat{u} = c\tilde{u}$ for a positive constant c. We want to call such a function *almost exact solution*. The following theorem gives us the conditions on α needed for recovering a multiple of $\tilde{u}$.

Theorem 6.3. *Let $J : \mathrm{dom}(J) \subseteq L^2(\Omega) \to \mathbb{R}\cup\{+\infty\}$ be a convex and one-homogeneous functional and let $K : L^2(\Omega) \to L^2(\Sigma)$ be a linear operator. Furthermore, let $\tilde{u}$ be an Eigenfunction with corresponding Eigenvalue λ. Then, if the data f is given via $f = \gamma K\tilde{u}$ for a positive constant γ, the solution of (2.8) is $\hat{u} = c\tilde{u}$ for*

$$c = \gamma - \alpha\lambda\,,$$

if $\gamma > \alpha\lambda$ is satisfied.

Proof. Again, we rewrite (2.8) in terms of a Bregman distance. Inserting $f = \gamma K\tilde{u}$ yields

$$\begin{aligned}\hat{u} &= \operatorname*{arg\,min}_{u\in\mathrm{dom}(J)} \left\{ \frac{1}{2} \|Ku - \gamma K\tilde{u}\|^2_{L^2(\Sigma)} + \alpha J(u) \right\} \\ &= \operatorname*{arg\,min}_{u\in\mathrm{dom}(J)} \left\{ \frac{1}{2} \|Ku - cK\tilde{u}\|^2_{L^2(\Sigma)} + \alpha J(u) + \alpha J(c\tilde{u}) - \frac{\gamma - c}{\lambda} \langle \lambda K^*K\tilde{u}, u\rangle_{L^2(\Omega)} \right. \\ &\qquad \left. + \frac{1}{2} \left(\langle \gamma K\tilde{u}, \gamma K\tilde{u}\rangle_{L^2(\Sigma)} + \langle cK\tilde{u}, cK\tilde{u}\rangle_{L^2(\Sigma)} \right) - \alpha J(c\tilde{u}) \right\} .\end{aligned}$$

By ignoring the constant part, for $\gamma > \alpha\lambda$ and $c = \gamma - \alpha\lambda > 0$ we therefore obtain

$$\hat{u} = \operatorname*{arg\,min}_{u\in\mathrm{dom}(J)} \left\{ \frac{1}{2} \|Ku - cK\tilde{u}\|^2_{L^2(\Sigma)} + \alpha D^q_J(u, c\tilde{u}) \right\} ,$$

with

$$q = \lambda K^*K\tilde{u} \in \partial J(\tilde{u}) \overset{J \text{ one-homogeneous}}{=} \partial J(c\tilde{u}) .$$

The obvious minimizer is $\hat{u} = c\tilde{u}$. □

6.4.2 Noisy Data

The multivaluedness of the subdifferential ∂J allows to obtain almost exact solutions even in the presence of noisy data, i.e. $f = \gamma K\tilde{u} + n$, though the case of noisy data is slightly more complicated to prove. If the most significant features of $\tilde{u}$ with respect to the regularization energy J are left unaffected by the noise, then the following theorem guarantees almost exact recovery of the Eigenfunction $\tilde{u}$.

Theorem 6.4. *Let $J : \mathrm{dom}(J) \subseteq L^2(\Omega) \to \mathbb{R}\cup\{+\infty\}$ be a convex and one-homogeneous functional and let $K : L^2(\Omega) \to L^2(\Sigma)$ be a linear operator. Furthermore, let $\tilde{u}$ be an Eigenfunction with corresponding Eigenvalue λ. The data f is assumed to be corrupted by noise n, i.e. $f = \gamma K\tilde{u} + n$ for a positive constant γ, such that there exist positive constants μ and η with*

$$\mu K^*K\tilde{u} + \eta K^*n \in \partial J(\tilde{u}) . \tag{6.9}$$

Then, the solution of (2.8) *is given via $\hat{u} = c\tilde{u}$ for*

$$c = \gamma - \alpha\lambda + \frac{\lambda - \mu}{\eta} ,$$

if γ satisfies the SNR-condition

$$\gamma > \frac{\mu}{\eta} ,$$

and if $\alpha \in [1/\eta, \gamma/\lambda + 1/\eta[$ holds.

Proof. Similar to the proof of Theorem 6.3 we rewrite (2.8) to

$$\begin{aligned}\hat{u} &= \operatorname*{arg\,min}_{u\in\mathrm{dom}(J)} \left\{ \frac{1}{2} \left\| Ku - \gamma K\tilde{u} - n \right\|^2_{L^2(\Sigma)} + \alpha J(u) \right\} \\ &= \operatorname*{arg\,min}_{u\in\mathrm{dom}(J)} \left\{ \frac{1}{2} \left\| Ku - cK\tilde{u} \right\|^2_{L^2(\Sigma)} + \alpha J(u) - \alpha \left\langle \frac{\gamma - c}{\alpha} K^*K\tilde{u} + \frac{1}{\alpha} K^*n, u \right\rangle_{L^2(\Omega)} \right\} \\ &= \operatorname*{arg\,min}_{u\in\mathrm{dom}(J)} \left\{ \frac{1}{2} \left\| Ku - cK\tilde{u} \right\|^2_{L^2(\Sigma)} + \alpha D_J^q(u, c\tilde{u}) \right\},\end{aligned}$$

with obvious minimizer $\hat{u} = c\tilde{u}$, if we neglect the constant parts and if we can manage to choose c such that

$$\frac{\gamma - c}{\alpha} K^*K\tilde{u} + \frac{1}{\alpha} K^*n \in \partial J(\tilde{u}) = \partial J(c\tilde{u}) \,.$$

Note that since $\partial J(\tilde{u})$ is a convex set not only $\lambda K^*K\tilde{u}$ and (6.9) are elements of $\partial J(\tilde{u})$, but also any convex-combination, i.e.

$$\left((1-\beta)\,\lambda + \beta\mu \right) K^*K\tilde{u} + \beta\eta K^*n \in \partial J(\tilde{u}) \,,$$

for each $\beta \in [0,1]$.

Hence, we need to choose $c > 0$ and $\beta \in [0,1]$ such that $1/\alpha = \beta\eta$ and $(\gamma - c)/\alpha = (1-\beta)\lambda + \beta\mu$. Therefore, the unique solutions for β and c are

$$\beta = \frac{1}{\alpha\eta}$$

and

$$c = \gamma - \alpha\lambda + \frac{\lambda - \mu}{\eta} \,.$$

In order to satisfy $\beta \leq 1$ and $c > 0$, α has to be chosen such that α is bounded via

$$\frac{1}{\eta} \leq \alpha < \frac{\gamma}{\lambda} + \frac{1}{\eta} + \frac{\mu}{\lambda\eta} \,.$$

This condition can only be satisfied, if $\gamma > \mu/\eta$ holds. □

6.5 Subdifferential-Invariant Transforms

Under particular circumstances, the definition of Eigenfunctions actually allows us to easily compute analytic solutions of certain variational models for input data, which is not given in terms of an Eigenfunction. We are going to see that these particular circumstances can be expressed via subdifferential-invariant transforms. Prior to that, we would like to give a short example as a motivation first.

Let us therefore consider the ROF-model (4.6). We assume that $\tilde{u}$ is an Eigenfunction of TV with Eigenvalue λ, i.e. $\lambda\tilde{u} \in \partial\mathrm{TV}(\tilde{u})$, and that the data f is given in terms of that Eigenfunction, but shifted by a constant factor $s \in \mathbb{R} \setminus \{0\}$. We immediately see that, due to Theorem 6.1, $f = \gamma\,(\tilde{u} + s)$ is not an Eigenfunction, since Theorem 6.2 is not satisfied. However, we make the

attempt that the solution of the ROF-model is given via $u = (\gamma - \alpha\lambda)\tilde{u} + \gamma s$. Considering the optimality condition of (4.6) actually yields

$$\hat{p} = \frac{1}{\alpha}\left(f - \hat{u}\right),$$

for $\hat{p} \in \partial\mathrm{TV}(\hat{u})$. Inserting $f = \gamma(\tilde{u} + s)$ and $\hat{u} = (\gamma - \alpha\lambda)\tilde{u} + \gamma s$ leads to

$$\hat{p} = \lambda\tilde{u}\,.$$

If we can guarantee $\partial\mathrm{TV}(\hat{u}) = \partial\mathrm{TV}(\tilde{u})$, then the optimality condition is fulfilled and $\hat{u}$ is the true and unique solution. We therefore have to check if $\partial\mathrm{TV}((\gamma - \alpha\lambda)\tilde{u} + \gamma s) = \partial\mathrm{TV}(\tilde{u})$, which can be verified via

$$\begin{aligned}\partial\mathrm{TV}((\gamma - \alpha\lambda)\tilde{u} + \gamma s) = \Bigg\{ \mathrm{div}p \;\Bigg|\; & p \in L_0^\infty(\Omega;\mathbb{R}^n),\ \|p\|_{L^\infty(\Omega;\mathbb{R}^n)} \leq 1, \\ & \underbrace{\langle \mathrm{div}p, (\gamma - \alpha\lambda)\tilde{u} + \gamma s\rangle_{L^2(\Omega)}}_{=(*)} = \underbrace{\mathrm{TV}((\gamma - \alpha\lambda)\tilde{u} + \gamma s)}_{=(**)} \Bigg\} \\ = \partial\mathrm{TV}(\tilde{u})\end{aligned}$$

with

$$(\gamma - \alpha\lambda)\left(\langle \mathrm{div}p, \tilde{u}\rangle_{L^2(\Omega)} + \underbrace{\left\langle \mathrm{div}p, \frac{\gamma s}{\gamma - \alpha\lambda}\right\rangle_{L^2(\Omega)}}_{=0}\right) = (\gamma - \alpha\lambda)\langle \mathrm{div}p, \tilde{u}\rangle_{L^2(\Omega)}\,, \tag{*}$$

and

$$(\gamma - \alpha\lambda)\mathrm{TV}\left(\tilde{u} + \frac{\gamma s}{\gamma - \alpha\lambda}\right) = (\gamma - \alpha\lambda)\mathrm{TV}(\tilde{u}). \tag{**}$$

The subdifferential $\partial\mathrm{TV}$ therefore is invariant with respect to constant translations. We want to establish the notion of subdifferential invariance.

Definition 6.3. *Let $J : \mathrm{dom}(J) \to \mathbb{R} \cup \{\infty\}$ be a convex functional with non-empty subdifferential ∂J. Then, ∂J is called invariant under the transformation $T : \mathrm{dom}(J) \to \mathrm{dom}(J)$, if*

$$\partial J(u) = \partial J(T(u))$$

is true for all $u \in \mathrm{dom}(J)$.

Remark 6.5. Note that for any one-homogeneous functional J the corresponding subdifferential ∂J is invariant under multiplication with a positive constant $s > 0$, i.e. $\partial J(su) = \partial J(u)$.

For the introductory example the transformation T simply was given via $T_{s,\mu}(u) := su + \mu$. In the following we want to investigate a few more interesting examples that even allow us to analytically compute solutions of variational schemes with non quadratic fidelities.

6.5.1 TV^2 and Affine-Linear Transformations

In analogy to the TV-example of the previous section we would expect any subdifferential of a particular regularization functional to be invariant with respect to the Ground States of this functional. In case of $J(u) = \mathrm{TV}^2(u)$ this would suggest subdifferential-invariance with respect to affine-linear functions. Therefore, we would like to consider the transformation

$$T_{\mu,s_1,s_2}(u(x)) := s_1 u(x) + s_2 x + \mu\,.$$

We immediately see that the affine-linear part would vanish either in the definition of TV^2 and in the integral representation $\langle \mathrm{div}^2 p, u\rangle_{L^2(\Omega)}$, due to the second-order divergence term. Hence, we can conclude $\partial\mathrm{TV}^2(T_{\mu,s_1,s_2}(\tilde{u})) = \partial\mathrm{TV}^2(\tilde{u})$ for any TV^2-Eigenfunction $\tilde{u}$ with Eigenvalue λ. Consequently we can compute the analytical TV^2-solution for a function $f = \gamma(\tilde{u} + sx + \mu)$ via

$$\hat{u}(x) = (\gamma - \alpha\lambda)\tilde{u}(x) + \gamma(sx + \mu)\,.$$

6.5.2 ℓ^1 and Positive Diagonal Operators

In case of the ℓ^1 functional we want to show that the subdifferential $\partial\|\cdot\|_{\ell^1}$ is invariant with respect to positive diagonal operators. If $D : \ell^1 \to \ell^1$ represents a positive diagonal operator, i.e. $(Du)_n = u_n v_n$ for $v \geq 0$, then we want to define the transformation $T_{s_1,s_2}(u) : \ell^1 \to \ell^1$ with

$$T_{s_1,s_2}(u) := (s_1 D - s_2 I)\, u\,, \tag{6.10}$$

such that $s_1 v_n > s_2$ for all n. We immediately see that the last condition guarantees $\mathrm{sign}(u) = \mathrm{sign}\,(T_{s_1,s_2}(u))$ and hence, the subdifferential is invariant with respect to (6.10). As a consequence, for input data $f = \gamma K D\tilde{u}$ the solution of (2.8) with $J(u) = \|u\|_{\ell^1}$ can be computed as

$$\hat{u} = (\gamma D - \alpha\lambda I)\,\tilde{u}\,, \tag{6.11}$$

if $\tilde{u}$ is an Eigenfunction with Eigenvalue λ and if γ and α are chosen such that $(\gamma D - \alpha\lambda I)$ is positive. This can – in analogy to the proof of Theorem 6.3 – be seen by

$$\begin{aligned}\hat{u} &= \operatorname*{arg\,min}_{u\in\ell^1}\left\{\frac{1}{2}\|Ku - \gamma KD\tilde{u}\|^2_{L^2(\Sigma)} + \alpha J(u)\right\}\\ &= \operatorname*{arg\,min}_{u\in\ell^1}\left\{\frac{1}{2}\|Ku - K(\gamma D - \alpha\lambda I)\tilde{u}\|^2_{L^2(\Sigma)} + \alpha D_J^{\lambda K^*K\tilde{u}}(u, (\gamma D - \alpha\lambda I)\tilde{u})\right\}\,,\end{aligned}$$

for which the obvious minimizer is (6.11), as long as $\mathrm{sign}(\hat{u}) = \mathrm{sign}(\tilde{u}) = \lambda K^*K\tilde{u}$ holds.

6.5.3 KL-TV

Up to now we have only considered affine-linear transformations and their use in computing analytical solutions of (2.8) with changing regularization terms. Another interesting question that arises is the effect of different fidelity terms on the solution. We therefore want to investigate the total variation semi-norm as a regularizer again, but in combination with the Kullback-Leibler fidelity as introduced in Section 4.2.3. We are going to see that we will be able to compute analytical solutions for this setup by considering a non-linear subdifferential-invariant transformation.

We want to investigate the following setup. We assume $\tilde{u}$ to be an Eigenfunction of TV with Eigenvalue λ. Moreover, the input data is given as $f = \gamma(\tilde{u} + \mu)$ with $\mu \in \mathbb{R}_{>0}$ such that $f > 0$.

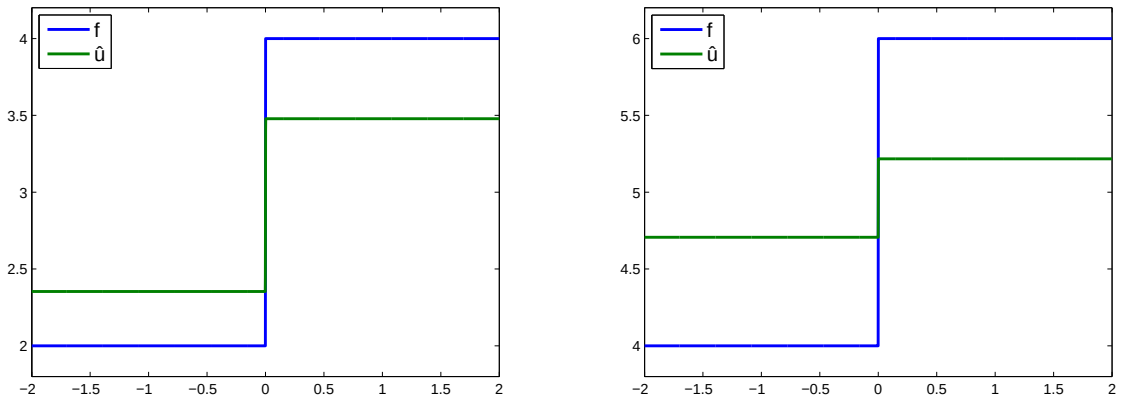

(a) $\mu = 3$ (b) $\mu = 5$

Figure 6.10: The comparison of data f, given in terms of $f(x) = \text{sign}(x) + 3$ (Figure 6.10(a)) and $f(x) = \text{sign}(x) + 5$ (Figure 6.10(b)), and computational reconstructions $\hat{u}$ for $\alpha = 3/10$, on the interval $[-2, 2]$. The reconstructions exactly behave as predicted by (6.12).

We make the attempt that the solution of (2.9) with $H_f(u) = \text{KL}(f, u)$ and $J(u) = \text{TV}(u)$ is given by $\hat{u} = T_{\mu,\gamma,\alpha\lambda}(\tilde{u})$, with

$$T_{\mu,s_1,s_2}(u) = \frac{s_1\,(u+\mu)}{1+s_2 u}\,.$$

Inserting $\hat{u}$ and f in the optimality condition of (4.25) yields $\hat{p} = \lambda\tilde{u}$ for $p \in \text{TV}(\tilde{u})$. Again it remains to prove $\partial\text{TV}(T_{\mu,s_1,s_2}(\tilde{u})) = \partial\text{TV}(\tilde{u})$, which however is not trivial since the transformation T_{μ,s_1,s_2} is non-linear. The important feature is that the transformation does not affect the edge-set of the input function, which is all that matters in case of ∂TV.

In the following we are going to consider the particular Eigenfunction $\tilde{u}(x) = \text{sign}(x)$ on the interval $x \in [-L, L]$. The transformed function $\hat{u}(x) = T_{\mu,\alpha\lambda,\gamma}(\tilde{u}(x))$ in that case reads as

$$\hat{u}(x) = \begin{cases} \frac{\mu+\gamma}{1+\frac{\alpha}{L}} & x \geq 0 \\ \frac{\mu-\gamma}{1-\frac{\alpha}{L}} & \text{else} \end{cases}\,. \tag{6.12}$$

We easily see that the total variation value simply equals the difference of the constant values, i.e.

$$\text{TV}(\hat{u}) = \frac{\mu+\gamma}{1+\frac{\alpha}{L}} - \frac{\mu-\gamma}{1-\frac{\alpha}{L}} = \frac{2L(\gamma L - \alpha\mu)}{L^2-\alpha^2}\,,$$

for $\alpha < (L\gamma)/\mu < L$, in order to be positive (the last inequality is true since $\mu > \gamma$ has to hold for $\hat{u}$ to be positive). Moreover, the total variation value actually equals the integral value $\langle \hat{u}, q' \rangle_{L^2([-L,L])}$ for $q(x) = (|x| - L)/L$ and as a consequence, both $\tilde{u}$ and $\hat{u}$ have the same corresponding subgradient $\lambda\tilde{u}$. Hence, for this particular Eigenfunction the subdifferential indeed is invariant under this non-linear transformation.

This example supports the view that in contrast to the standard L^2-fidelity for the Kullback-Leibler-fidelity the intensity of the input data also controls the amount of smoothing and therefore the loss of contrast. For fixed regularization parameter α, length $L > 0$ and scaling factor γ the total variation value gets smaller for growing μ. This has been illustrated in Figure 6.10 for different values of μ.

6.6 Relation to the Strong Source Condition

For the quadratic L^2-fidelity $F(Ku - f) = \frac{1}{2}\|Ku - f\|^2_{L^2(\Sigma)}$ the strong source condition (SC2) can be written as

$$\exists\, \xi \in \partial J(\tilde{u}),\, \exists\, v \in \mathcal{U}(\Omega) \setminus \{0\} : \quad \xi = -K^*Kv\,,$$

and therefore appears to be very related to the Eigenfunction condition $\lambda K^*K\tilde{u} \in \partial J(\tilde{u})$ of Definition 6.2. We would therefore assume that we are able to improve the error estimate (5.4) of Theorem 5.3, i.e.

$$D^{\xi}(\hat{u}, \tilde{u}) \leq D^{\xi}(\hat{u} - \alpha v, \tilde{u})\,,$$

which can actually be seen by the following theorem.

Theorem 6.5. *Let $J : \mathrm{dom}(J) \subseteq L^2(\Omega) \to \mathbb{R} \cup \{+\infty\}$ be a convex functional and let $K : L^2(\Omega) \to L^2(\Sigma)$ be a linear operator. Furthermore, let there exist a regularization parameter $\alpha > 0$ and two functions $\tilde{u} \in \mathrm{dom}(K) \cap \mathrm{dom}(J)$ and $v \in \mathrm{dom}(J) \setminus \{0\}$ that satisfy*

$$K^*Kv \in \partial J(\tilde{u} - \alpha v)\,.$$

Then, for input data $g = K\tilde{u}$ the minimizer of (4.14) with $F(Ku - g) = \frac{1}{2}\|Ku - g\|^2_{L^2(\Sigma)}$ is given by

$$\hat{u} = \tilde{u} - \alpha v\,.$$

Proof. We can rewrite (4.14) to

$$\begin{aligned}
\hat{u} &= \operatorname*{arg\,min}_{u \in \mathrm{dom}(J)} \left\{ \frac{1}{2}\|Ku - K\tilde{u}\|^2_{L^2(\Sigma)} + \alpha J(u) \right\} \\
&= \operatorname*{arg\,min}_{u \in \mathrm{dom}(J)} \left\{ \frac{1}{2}\|Ku - K\tilde{u}\|^2_{L^2(\Sigma)} + \alpha \langle Ku, Kv \rangle_{L^2(\Sigma)} + \alpha J(u) - \alpha \langle Ku, Kv \rangle_{L^2(\Sigma)} \right\} \\
&= \operatorname*{arg\,min}_{u \in \mathrm{dom}(J)} \left\{ \frac{1}{2}\|Ku - K\tilde{u} + \alpha Kv\|^2_{L^2(\Sigma)} + \alpha D_J^{K^*Kv}(u, \tilde{u} - \alpha v) \right\}.
\end{aligned}$$

The obvious minimizer is given via $\hat{u} = \tilde{u} - \alpha v$. □

Chapter 7

Unbiased Recovery

In Chapter 6 we have introduced the concept of Ground States and Eigenfunctions for the variational framework (2.9) in order to examine, under which conditions we can recover these Eigenfunctions almost exactly with a loss of contrast. In this chapter we want to extend this topic to the question of exact recovery without a loss of contrast, in the absence and presence of noise. Therefore, we are going to investigate the concept of Bregman iterations and its analytical counterpart, the inverse scale space flow.

7.1 Bregman Iteration

The goal of this section is to show that for one-homogeneous functionals the discrete Bregman iteration as introduced in Section 3.3 allows to converge to the exact solution in finitely many iteration steps. In analogy to Section 6.4.1 we want to investigate the noise-free setup first, i.e. we consider input data of the form $f = \gamma K\tilde{u}$, with $\tilde{u}$ denoting an Eigenfunction as defined in Definition 6.2. Subsequently we want to shortly examine a two-homogeneous counter-example, for which we can prove convergence in infinitely many iterations, in order to support the importance of one-homogeneity. Finally, we want to investigate the setup for noisy data similar to Section 6.4.2.

7.1.1 Clean Data

With the following Theorem we want to prove finite convergence of the Bregman iteration in case of L^2-fidelity, one-homogeneous regularization functional and input data given in terms of an Eigenfunction, i.e. $f = \gamma K\tilde{u}$.

Theorem 7.1. *Let $J : \mathrm{dom}(J) \subseteq L^2(\Omega) \to \mathbb{R}\cup\{+\infty\}$ be a convex and one-homogeneous functional and let $K : L^2(\Omega) \to L^2(\Sigma)$ be a linear operator. Furthermore, let $\tilde{u}$ be an Eigenfunction with corresponding Eigenvalue λ. Then, if the data f is given via $f = \gamma K\tilde{u}$ and if α is large enough such that the conditions of Theorem 6.2 are satisfied, the solution $u_{j+1} = \gamma\tilde{u}$ of the Bregman iteration scheme (3.5) is achieved for finite $j \in \mathbb{N}$. Furthermore, the solution remains $u_k = \gamma\tilde{u}$ for $k > j + 1$.*

Proof. Since the conditions of Theorem 6.2 are met, the first iterate simply is $u_1 \equiv 0$. Depending on the choice of α there exists a finite index $j > 1$ for which all previous Bregman iterations equal zero. Hence, the formula for the update for v reads as $v_{j-1} = (j-1)f = (j-1)\gamma K\tilde{u}$. Without loss of generality we assume j to be large enough such that $\frac{j\gamma}{\alpha}K^*K\tilde{u} \notin \partial J(0)$ holds. Hence, the

solution of the Bregman update for u reads as $u_j = c\tilde{u}$ for $c = j\gamma - \alpha\lambda$, due to Theorem 6.3. As a consequence, the Bregman update for v becomes

$$v_j = v_{j-1} - (Ku_j - f) = (j-1)\gamma K\tilde{u} - (cK\tilde{u} - \gamma K\tilde{u}) = \alpha\lambda K\tilde{u}$$

and hence, the update for u has to be computed via

$$u_{j+1} = \underset{u\in\mathrm{dom}(J)}{\arg\min} \left\{ \frac{1}{2} \left\| Ku - (\gamma + \alpha\lambda)K\tilde{u} \right\|^2_{L^2(\Sigma)} + \alpha J(u) \right\} .$$

Because of Theorem 6.3 the solution is given as $u_{j+1} = c\tilde{u} = \gamma\tilde{u}$, since we have $c = \gamma + \alpha\lambda - \alpha\lambda$. Moreover, we inductively see that for every further iteration the update for v remains $v_k = \alpha\lambda K\tilde{u}$ and hence, $u_k = \gamma\tilde{u}$ is valid for all $k > j + 1$. □

Remark 7.1. Theorem 7.1 is only valid for one-homogeneous functionals, which can be seen from the fact that we have used $\partial J(\tilde{u}) = \partial J(c\tilde{u})$ in the proof of Theorem 6.3. Moreover we can construct a very simple counter example by considering (2.9) with $J(u) = 1/2\|u\|^2_{L^2(\Omega)}$ and $K = I$. Since the Bregman distance for this particular functional J simply reads as $D_J^{u_{k-1}}(u, u_{k-1}) = 1/2\|u - u_{k-1}\|^2_{L^2(\Omega)}$, the Bregman iteration scheme becomes

$$u_k = \underset{u\in L^2(\Omega)}{\arg\min} \left\{ \frac{1}{2} \left\| u - f \right\|^2_{L^2(\Omega)} + \frac{\alpha}{2} \left\| u - u_{k-1} \right\|^2_{L^2(\Omega)} \right\} .$$

If we consider the optimality condition and assume the input data $f = \tilde{u}$ to be an Eigenfunction of J, the Bregman update can be written as

$$u_k = \tilde{u} + \frac{\alpha^k}{(1+\alpha)^k}(u_0 - \tilde{u}) .$$

On the one hand we see that for $\alpha < 1$ we have $\lim_{k\to\infty} u_k = \tilde{u}$. On the other hand we also see that there is no convergence in a finite number of steps for $u_0 \neq \tilde{u}$, in contrast to convergence in a finite number of iterations for one-homogeneous functionals, due to Theorem 7.1.

7.1.2 Noisy Data

In the case of noisy data we can, in analogy to Theorem 6.4, find criteria such that the Bregman iteration converges to the Eigenfunction before adding back the noise to the solution.

Theorem 7.2. *Let $J : \mathrm{dom}(J) \subseteq L^2(\Omega) \to \mathbb{R}\cup\{+\infty\}$ be a convex and one-homogeneous functional and let $K : L^2(\Omega) \to L^2(\Sigma)$ be a linear operator. Furthermore, let $\tilde{u}$ be an Eigenfunction with corresponding Eigenvalue λ. The data f is assumed to be corrupted by noise n, i.e. $f = \gamma K\tilde{u} + n$, for a positive constant γ, such that there exists an α large enough in order to satisfy the conditions of Theorem 6.2, positive constants μ, η, ϕ and ψ, and an iteration index $j > 1$, with*

$$\mu K^*K\tilde{u} + \eta j K^*n \in \partial J(\tilde{u}) \tag{7.1}$$

and

$$\phi K^*K\tilde{u} + \psi(j+1)K^*n \in \partial J(\tilde{u}) . \tag{7.2}$$

Then, the solution $u_{j+1} = \gamma\tilde{u}$ of the Bregman iteration scheme (3.5) is achieved for finite $j \in \mathbb{N}$.

Proof. In analogy to the proof of Theorem 7.1 we know that $u_k \equiv 0$ for $k < j$, due to Theorem 6.2. Hence, we have $v_{j-1} = (j-1)f$. The upcoming Bregman update then computes as

$$u_j = \operatorname*{arg\,min}_{u \in \mathrm{dom}(J)} \left\{ \frac{1}{2} \left\| Ku - jf \right\|^2_{L^2(\Sigma)} + \alpha J(u) \right\} .$$

Due to Theorem 6.4 u_j is given via $u_j = c\tilde{u}$ for $c = \gamma j - \alpha\lambda + (\lambda - \mu)/\eta$. The update for v therefore reads as

$$v_j = v_{j-1} - (Ku_j - f) = \left(\alpha\lambda - \frac{\lambda - \mu}{\eta} \right) K\tilde{u} + jn$$

and again by applying Theorem 6.4 we obtain $u_{j+1} = \gamma\tilde{u}$. □

Remark 7.2. Note that it is important to choose α large enough in order to find an appropriate index j to guarantee the conditions (7.1) and (7.1).

7.2 Inverse Scale Space Methods

The analytic counterpart to Bregman iteration is the inverse scale space flow as introduced in Section 3.4. Similar to the discrete case of Bregman iteration we are going to prove for which times t Eigenfunctions can be reconstructed exactly, even in the presence of noise.

Moreover we are briefly going to address the converse question, under which circumstances for any given data-function f the image $u(t_*)$ with corresponding time t_*, for which $u(t_*)$ is no longer a trivial Ground State, is an Eigenfunction.

7.2.1 Clean Data

Similar to Chapter 6, Section 6.4.1, we are going to consider data of the type $f = \gamma K\tilde{u}$, with $\tilde{u}$ denoting an Eigenfunction. For this setup we are able to derive the following result.

Theorem 7.3. *Let $J : \mathrm{dom}(J) \subseteq L^2(\Omega) \to \mathbb{R} \cup \{+\infty\}$ be a convex and one-homogeneous functional and let $K : L^2(\Omega) \to L^2(\Sigma)$ be a linear operator. Furthermore, let $\tilde{u}$ be an Eigenfunction with corresponding Eigenvalue λ. Then, if the data f is given via $f = \gamma K\tilde{u}$ for a positive constant γ, the solution of the inverse scale space flow (3.9) at time $t > t_* = \lambda/\gamma$ is $u(t) = \gamma\tilde{u}$.*

Proof. Due to Lemma 6.1 we know that there exists a parameter $\tilde{\alpha}$ to guarantee $(K^*f)/\alpha = (\gamma K^*K\tilde{u})/\alpha \in \partial J(0)$ for $\alpha \geq \tilde{\alpha}$. Hence, in the limiting case $\alpha \to \infty$ we can apply Theorem 6.2 and obtain $u(t) \equiv 0$ for $t < t_*$, and therefore

$$\frac{\partial}{\partial t} p(t) = K^*f = \gamma K^*K\tilde{u} \,.$$

Integrating with respect to t yields

$$p(t) = t\gamma K^*K\tilde{u} \,,$$

because $p(0) = 0$ holds. Since p is continuous in t we can continuously extend $p(t)$ to $p(t_*)$ and hence, for $t_* = \lambda/\gamma$ we obtain $p(t_*) \in \partial J(\tilde{u}) = \partial J(\gamma\tilde{u})$. Due to Section 3.4 the ISS is convergent and thus the unique ISS solution for $t \geq t_*$ is given via $u = \gamma\tilde{u}$ and $p = \lambda K^*K\tilde{u}$. □

7.2.2 Noisy Data

Similar as in the case of Bregman iteration the case of noisy data is a little bit more complicated. In order to recover an Eigenfunction exactly despite the contamination of the data f with noise, we basically need the signal ratio μ as introduced in Theorem 6.4 to equal the Eigenvalue λ. More precisely we obtain the following result.

Theorem 7.4. *Let $J : \mathrm{dom}(J) \subseteq L^2(\Omega) \to \mathbb{R} \cup \{+\infty\}$ be a convex and one-homogeneous functional and let $K : L^2(\Omega) \to L^2(\Sigma)$ be a linear operator. Furthermore, let $\tilde{u}$ be an Eigenfunction with corresponding Eigenvalue λ. The data f is assumed to be corrupted by noise n, i.e. $f = \gamma K\tilde{u} + n$ for a positive constant γ, such that there exist positive constants μ and η that satisfy (6.9). Then, the solution of the Inverse Scale Space Flow (3.9) for time $t_* \leq t < t_{**}$ is given via $u(t) = c\tilde{u}$ for*

$$c = \gamma + \frac{\lambda - \mu}{\eta}\,. \tag{7.3}$$

Proof. With a similar argumentation as in the proof of Theorem 7.3 we obtain

$$p(t_*) = t_*\gamma K^*K\tilde{u} + t_*K^*n$$

as the corresponding subgradient to the first non-zero u. Analogous to the proof of Theorem 6.4 we can treat the equation above as a convex combination of λK^*K and (6.9) for any $\beta \in [0, 1]$ and hence, we obtain

$$\beta = \frac{\lambda}{\lambda + \gamma\eta - \mu}$$

and

$$t_* = \frac{\lambda\eta}{\lambda + \gamma\eta - \mu}\,.$$

Moreover, we get a solution $u(t_*) = c\tilde{u}$ to the corresponding subgradient $p(t_*)$ and assume that $u(t)$ remains constant over time as long as $t \in [t_*, t_{**}[$ holds, for some t_{**}. The subgradient of $u(t)$, $p(t)$, then needs to satisfy $p(t_*) = t_*K^*f$ and $\partial_t p(t) = K^*(f - cK\tilde{u})$ and can be described via

$$\begin{aligned} p(t) &= tK^*f - (t - t_*)cK^*K\tilde{u} \\ &= tK^*(\gamma K\tilde{u} + n) - (t - t_*)cK^*K\tilde{u} \\ &= tK^*n + (\gamma t - c(t - t_*))K^*K\tilde{u}\,. \end{aligned}$$

If we compare this equation with (6.9) we need to choose c such that

$$t = \eta$$

and

$$\mu = \gamma t - c(t - t_*)$$

hold. Substituting $t_* = (\lambda\eta)/(\lambda + \gamma\eta - \mu)$ then yields (7.3). □

Remark 7.3. Note that for the particular choice $\gamma = 1$ the Eigenfunction $\tilde{u}$ can be recovered perfectly if the Eigenvalue λ equals the signal amount μ, no matter which value η takes (as long as μ and η satisfy (6.9)). However, naturally $\mu \neq \lambda$ holds, as we are going to discover in Section 9.1.2.

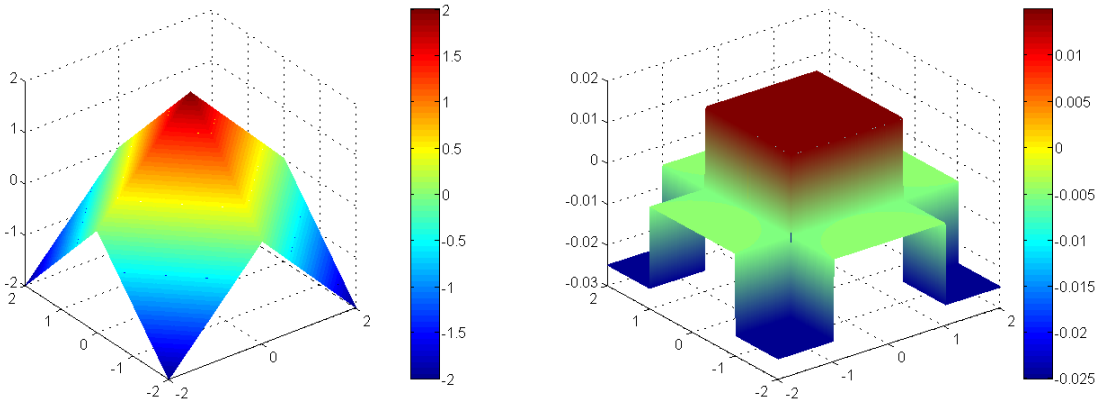

(a) f (b) u_4

Figure 7.1: The input data $f(x, y) = 2 - |x| - |y|$ and the first non-trivial Bregman iterate $u_4(x, y)$ in case of anisotropic total variation regularization, for $\alpha = 2$. It is obvious that $u_4(x, y)$ is given in terms of the Eigenfunction $\tilde{u}(x, y)$ of Section 6.3.2, Example 6.8.

7.3 Decomposition into Eigenfunctions

Despite the fact that Eigenfunctions can be recovered perfectly with the use of ISS, an interesting question that arises is the converse question: is the first non-zero solution of the ISS for arbitrary data f satisfying (6.4) an Eigenfunction? If so, the ISS would allow a decomposition of arbitrary data into Eigenfunctions of a particular functional J, since we could recursively subtract the Eigenfunction from the data and repeat the ISS application to this modified data. Unfortunately, the general answer to the converse question is no, which we will prove with the following counter example.

Lemma 7.1. *For the one-homogeneous functional* $J : L^2([a, b]) \to \mathbb{R} \cup \{\infty\}$ *with* $J(u) = \|u'\|_{L^2([a,b])}$ *the first non-zero ISS solution for* $K = I$ *and data* f*, satisfying* (6.4) *for* $\alpha \geq \hat{\alpha}$ *for a specific parameter* $\hat{\alpha}$*, that is not given in terms of an Eigenfunction, is not an Eigenfunction of* J*.*

Proof. We proof the statement by contradiction. Let t^* denote the time for which $u(t_*) \not\equiv 0$ is true, while $u(t) \equiv 0$ for $t < t^*$ holds. We assume $u(t_*)$ to be an Eigenfunction, i.e. there exists a parameter λ with $\lambda u(t_*) = \partial \|u'(t_*)\|_{L^2([a,b])} = (u''(t_*)) / \|u'(t_*)\|_{L^2([a,b])}$ (note that since $u(t_*)$ is a non-trivial Eigenfunction we have $u'(t_*) \neq 0$ and therefore the functional J is Fréchet-differentiable). From the ISS-definition we know that $p(t^*) = t^* f \in \partial \|u'(t^*)\|_{L^2([a,b])}$ also needs to be satisfied. Hence, we obtain the relation $t^* f = \lambda u(t_*)$, which is a contradiction to the assumption that f is not given in terms of an Eigenfunction. □

Though the converse is not true in general there do exist interesting cases in which the first non-trivial ISS-solution is indeed an Eigenfunction of the particular regularization functional. Let us for example consider the ℓ^1-functional $J(u) = \|u\|_{\ell^1}$. The inverse scale space in that particular case reads as

$$\frac{\partial}{\partial t} p(t) = K^* \left(f - K u(t) \right) ,$$

for $p \in \partial J(u(t)) = \operatorname{sign}(u(t))$. We easily see that for every $p(t)$ we have $\|p(t)\|_{\ell^\infty} = 1$. Let t_* denote the time for which $u(t) \equiv 0$ for $t < t_*$ and $u(t_*) \not\equiv 0$ is fulfilled. We immediately see that due to continuous extension we obtain $t_* = 1/\|K^* f\|_{\ell^\infty}$. Hence, the subgradient $p(t_*)$ is given via $p(t_*) = (K^* f)/\|K^* f\|_{\ell^\infty}$. Now assume $K = I$ to be the identity and f to be arbitrary data $f \not\equiv 0$ with unique and existing $\sup_x |f(x)|$, then $p(t_*)$ is exactly one or minus one at one specific position j. Hence, the corresponding primal variable $u(t_*)$ is $u(t_*) = \mu\delta_j$ for a parameter $\mu \in \mathbb{R}$ and therefore is an Eigenfunction of the ℓ^1-functional, according to Section 6.1, Example 6.1.

That the converse question seems to be true not only for rather simple examples (as for the ℓ^1-functional) can be seen by considering two-dimensional anisotropic total variation ISS. If we consider the function

$$f(x, y) := 2 - |x| - |y|$$

on the interval $[-2, 2]^2$, and compute Bregman iterates for $\alpha = 2$, we discover that the iterates u_1, u_2 and u_3 all equal zero, while the fourth iterate $u_4(x, y)$ equals the function $\tilde{u}(x, y)$ of Section 6.3.2, Example 6.8, up to a constant factor. Hence, the first non-zero ISS-solution indeed seems to be an Eigenfunction of the anisotropic total variation. The plots of f and u_4 can be seen in Figure 7.1.

A detailed analysis on when recovery of Eigenfunctions via ISS for arbitrary input data f and an associated Eigenfunction-decomposition is possible is beyond the scope of this thesis and will be part of future work. However, from the above examples it seems to be likely that for ℓ^1- or L^1-type polyhedral norms (as e.g. anisotropic total variation) the first ISS solution appears to be an Eigenfunction of the corresponding functional, while for norms for which the shapes have a continuous boundary (as e.g. L^2-norms or isotropic total variation) this does not seem to be the case.

Chapter 8

Algorithms

With this chapter we want to provide algorithms that allow the computational solution of applications discussed in the next chapter. First of all we want to give an overview on various existing methods we are going to use in the following. Subsequently, we will present a novel algorithm for the compressed sensing setup (4.3) as introduced in [27], which is based on the ISS-concept presented in Section 3.4.

8.1 State-of-the-Art-Methods

In the following we want to present state-of-the-art methods to solve variational schemes of the type (2.9), or even algorithms that attempt to solve a constrained minimization problem with constraint (2.4). The basic concept is the splitting of a given separable problem into subproblems. Hence, we are going to focus on so-called splitting methods in the upcoming section. Subsequently we will point out the relation to primal-dual problems and present alternative methods for the computational realization in comparison to splitting methods. Afterwards, we are going to extend the concept of Bregman iteration as described in Section 3.3 to the Kullback-Leibler fidelity instead of the standard L^2-fidelity. Finally, we will recall the orthogonal matching pursuit (OMP) algorithm (cf. [96, 88, 124]) that basically finds its applications in compressed sensing.

8.1.1 Splitting Methods

In this section we want to focus on so-called splitting methods. As already mentioned, the concept of splitting methods is to exploit the fact that operators or functionals inhere a separable structure. Splitting methods split the original problem into subproblems, solve these subproblems, and iteratively produce a solution for the original problem. The reason for splitting up a problem into subproblems lies in the effort that is needed to solve a problem. Most of the variational schemes presented in Chapter 4 cannot be solved directly and therefore have to be split up into problems that can be solved easily. In the following we are going to present different variants of one of the most simple splitting strategies called Forward-Backward-Splitting. Subsequently we will present the concept of augmented Lagrangian methods that suits very well to variational schemes with quadratic fidelity and singular regularization term.

Forward-Backward Splitting

One of the most simple and intuitive splitting strategy is Forward-Backward-Splitting (FBS). For a given problem

$$u \in \operatorname*{arg\,min}_{u \in \mathrm{dom}(L)} \{L(u) = F(u) + G(u)\},$$

that can be split up additively into two separate functionals F and G, the idea of FBS is to introduce an additional variable and to iteratively solve

$$\begin{aligned} u_{k+\frac{1}{2}} &\in \left\{ u_k - \tau_k \, \partial_u F(u_k) \right\} \\ u_{k+1} &\in \left\{ u_{k+\frac{1}{2}} - \tau_k \, \partial_u G(u_{k+1}) \right\} \end{aligned},$$

with a positive stepsize-sequence $\tau_k > 0$. It is easy to see that if we insert $u_{k+\frac{1}{2}}$ into the formula for u_{k+1} we end up with

$$\frac{u_{k+1} - u_k}{\tau_k} = -\left(F(u_k) + G(u_{k+1})\right).$$

FBS is a simple strategy to split a problem into an explicit (the forward step) and an implicit problem (the backward step). It seems to be obvious that this strategy is suitable for variational problems of the type (2.9); in particular for problems with L^2-fidelity (2.8). In the latter case we obtain the two subproblems

$$\begin{aligned} u_{k+\frac{1}{2}} &= u_k - \tau_k \, K^*(Ku_k - f) \\ u_{k+1} &\in \operatorname*{arg\,min}_{u \in \mathrm{dom}(J)} \left\{ \frac{1}{2\tau_k} \left\| u - u_{k+\frac{1}{2}} \right\|^2_{L^2(\Omega)} + \alpha J(u) \right\} \end{aligned},$$

which offer the advantage that the iterative computation of the minimizer can be done without inverting K^*K and that the implicit subproblem reduces to a simple L^2-denoising problem for which efficient algorithms are supposed to exist. The obvious drawback is that this iteration scheme can become very slow depending on the ill-posedness of the operator K, respectively the ill-conditioning of the matrix representing the discretization of K. Finally, in case of the variational framework (2.8) the FBS algorithm can be summarized as follows.

Algorithm 2 FBS with L^2-Fidelity

1. **Parameters:** $K,\ f,\ \alpha > 0,\ \mathrm{maxiter},\ (\tau_k)_{k \in \{0,\ldots,\mathrm{maxiter}-1\}}$
2. **Initialization:** $u_0 = 0$

for $k = \{0, \ldots, \mathrm{maxiter} - 1\}$ **do**

Compute $u_{k+\frac{1}{2}} = u_k - \tau_k \, K^*(Ku_k - f)$

Solve $u_{k+1} \in \arg\min_{u \in \mathrm{dom}(J)} \left\{ \frac{1}{2\tau_k} \left\| u - u_{k+\frac{1}{2}} \right\|^2_{L^2(\Omega)} + \alpha J(u) \right\}$

end for

return u_{maxiter}

In order to achieve a significant speedup the choice of the adaptive stepsize τ has to be done in an "optimal way". In case of quadratic fidelity and quadratic regularization energy the optimal

choice of τ is straightforward. If we define the function

$$s(\tau) := \frac{1}{2}\left\|K(u+\tau v)-f\right\|^2_{L^2(\Omega)} + \frac{\alpha}{2}\left\|D(u+\tau v)\right\|^2_{L^2(\Omega)}$$

for $u, v \in \mathrm{dom}(K) \cap \mathrm{dom}(D)$, and compute $\overline{\tau}$ that satisfies the optimality condition $s'(\overline{\tau}) = 0$, we end up with

$$\overline{\tau} = \frac{-\langle v, r\rangle}{\alpha\|Dv\|^2 + \|Kv\|^2}\,,$$

with r denoting the residual function $r = K^*(Ku-f)+\alpha D^*Du$. If we insert the gradient descent for v, i.e. $v = -r$, we obtain

$$\overline{\tau} = \frac{\|r\|^2}{\alpha\|Dr\|^2 + \|Kr\|^2}\,,$$

which is a strategy known as *exact stepsize*, see for instance [2, Section 4.5.1].

We easily see that an optimal choice for the algorithmic stepsize τ is difficult or probably impossible to find if either the fidelity term or the regularization term is not quadratic. The latter is of particular relevance in case of singular regularization energies. Moreover, in practice often line-search methods are considered instead of the exact stepsize strategy.

However, in the following we are going to discuss how to choose an optimal algorithmic stepsize in case of the compressed sensing setup (4.3), i.e. quadratic fidelity and ℓ^1-regularization. Subsequently, we are going to present a FBS technique for the Kullback-Leibler instead of the quadratic L^2 fidelity.

Forward-Backward Splitting with Quadratic Fidelity and ℓ^1-Regularization

In [60] the authors have reformulated the variational scheme (4.3) to a low-rank problem. If we suppose to have two successive iterates u^{k-1} and u^k of the FBS method for (4.3) with the same support (i.e. $\mathrm{sign}(u^{k-1}) = \mathrm{sign}(u^k)$) and if we assume D to be the diagonal matrix with $D_{ii} = 1$ if $u^{k-1} \neq 0$ and $D_{ii} = 0$ otherwise, then, obtaining u^k from u^{k-1} via FBS is equivalent to

$$u^k = \operatorname*{arg\,min}_{u\in\ell^1}\left\{\|KDu - f\|_2^2 + \alpha\langle u, s\rangle\right\}\,, \tag{8.1}$$

with $s = \alpha\ \mathrm{sign}(u^{k-1})$. Hence, if we have the same support for two successive iterates we have to solve a simple quadratic problem for which in analogy to the overall quadratic problem in the previous section we can find an optimal algorithmic stepsize for FBS via

$$\tau_k = \frac{\|r_k\|_2^2}{\|Kr_k\|_2^2} \tag{8.2}$$

with r denoting the residual of (8.1). If $\mathrm{sign}(u^{k-1}) \neq \mathrm{sign}(u^k)$ holds, still standard FBS needs to be applied on (4.3). Consequently, in [60] the residual has been rewritten to

$$r_k = D_kK^T\left(KD_ku_k - f\right) + \alpha\ \mathrm{sign}(u_k) + (I - D_k)\ \mathrm{shrink}\left(K^T\left(Ku_k - f\right), \alpha\right)\,. \tag{8.3}$$

With this reformulation of problem (4.3) to a low-rank problem the FBS with adaptive stepsize reads as follows.

Algorithm 3 CS-FBS with Adaptive Stepsize

1. **Parameters:** $K,\ f,\ \alpha > 0,\ \text{maxiter}$
2. **Initialization:** $u_0 = 0$

for $k = \{0, \dots, \text{maxiter} - 1\}$ **do**

Compute $g_k = K^T (K u_k - f)$

Define D_k as the diagonal matrix with $D_{ii} = \begin{cases} 1 & (u_k)_i \neq 0 \\ 0 & (u_k)_i = 0 \end{cases}$.

Compute r_k via (8.3)

Update τ_k via (8.2)

Compute $u_{k+1} = \text{shrink}\left(u_k - \tau_k g_k, \alpha \tau_k\right)$

end for

return u_{maxiter}

Forward-Backward Splitting with Kullback-Leibler Fidelity

In order to compute numerical solutions of a variational framework with Kullback-Leibler Fidelity without inverting the operator K, in [111, 21, 22] a specific FBS-approach has been proposed in case of total variation regularization, which can also be generalized to other regularization energies.

First of all we want to recall that a very popular approach for minimizing $\text{KL}(f, Ku)$ with respect to $u \geq 0$ is the standard Expectation Maximization (EM) algorithm, based on the optimality condition of $\hat{u} \in \arg\min_{\hat{u} \in L^1_{\geq 0}(\Omega)} \text{KL}(f, Ku)$, which is

$$0 = \hat{u} \left(1 - K^* \frac{f}{K\hat{u}}\right) . \tag{8.4}$$

The corresponding standard EM algorithm (cf. [92]) is the simple iterative scheme

$$u^{k+1} = \frac{u^k}{K^*\mathbf{1}} K^* \left(\frac{f}{K u^k}\right) , \tag{8.5}$$

for which convergence to the solution of (8.4) can be proved under approriate assumptions on the operator and the data f. The standard EM algorithm can be summarized as follows.

Algorithm 4 Standard EM Algorithm

1. **Parameters:** $K,\ f,\ \text{maxiter}$
2. **Initialization:** $u_0 > 0$

for $k = \{0, \dots, \text{maxiter} - 1\}$ **do**

Compute u_{k+1} via (8.5)

end for

return u_{maxiter}

If we assume to have given a variational minimization problem with Kullback-Leibler fidelity, convex regularization energy and positivity constraint, i.e.

$$u \in \underset{\substack{u \in \text{dom}(J) \\ u \geq 0}}{\arg\min} \left\{\text{KL}(f, Ku) + \alpha J(u)\right\} , \tag{8.6}$$

the particular FBS idea is to compute

$$\begin{aligned} u_{k+\frac{1}{2}} &= u_k - \sigma_k \partial_u \mathrm{KL}(f, u_k) \\ u_{k+1} &= u_{k+\frac{1}{2}} - \sigma_k \alpha p_{k+1} \ , \ p_{k+1} \in \partial J(u_{k+1}) \end{aligned}$$

with adaptive stepsize $\sigma_k = \tau_k \frac{u_k}{K^*\mathbf{1}}$, $\tau_k > 0$. The idea behind this special choice of σ is to reduce (8.6) to an iterate (8.5) of Algorithm 4 (in the following denoted by u_{EM}) and a regularized weighted-L^2-problem. Inserting σ_k yields

$$\begin{aligned} u_{k+\frac{1}{2}} &= u_k - \tau_k \left(u_k - \underbrace{\frac{u_k}{K^*\mathbf{1}} K^* \left(\frac{f}{K u_k} \right)}_{= u_{\mathrm{EM}}} \right) \\ u_{k+\frac{1}{2}} &= (1 - \tau_k) u_k + \tau_k u_{\mathrm{EM}} \, . \end{aligned}$$

Hence, u_{k+1} is the solution of the weighted-L^2-problem

$$u_{k+1} \in \operatorname*{arg\,min}_{\substack{u \in \mathrm{dom}(J) \\ u \geq 0}} \left\{ \frac{1}{2} \langle w_k (u - u_{k+\frac{1}{2}}), u - u_{k+\frac{1}{2}} \rangle_{L^2(\Omega)} + \alpha \tau_k J(u) \right\} \tag{8.7}$$

with weight $w_k := \frac{K^*\mathbf{1}}{u_k}$. Note that if J is one-homogeneous and can therefore be written as $J(u) = \langle u, p \rangle$ for $p \in \partial J(u)$ due to Lemma 2.4, we can rewrite (8.7) to

$$u_{k+1} \in \operatorname*{arg\,min}_{\substack{u \in \mathrm{dom}(J) \\ u \geq 0}} \left\{ \frac{1}{2} \left\| u - u_{k+\frac{1}{2}} \right\|^2_{L^2(\Omega)} + \alpha \tau_k \langle u, w_k^{-1} p \rangle \right\} .$$

This can be helpful especially when dealing with ℓ^1- and L^1-type regularizations, since the notation allows the modification of existing denoising schemes for the particular regularization energy simply by introducing a weight in the regularization term. In [111, 21, 22] the authors have analyzed the computational scheme above in the case of $J(u) = \mathrm{TV}(u)$. In case of total variation regularization it has been shown that the solution of (8.7) is positive if the input data $u_{k+\frac{1}{2}}$ is positive, due to a proved maximum-principle [21, Section 5.4.3]. Furthermore, for appropriate conditions on τ_k (cf. [21, Section 5.4.4, Theorem 5.4.12]) it has been shown that the iteration scheme converges to the exact minimizer of (8.6) for $J(u) = \mathrm{TV}(u)$.

We want to summarize the recent considerations to the following algorithm.

Algorithm 5 Regularized EM Algorithm

1. **Parameters:** $K,\ f,\ \alpha > 0,\ \text{maxiter},\ (\tau_k)_{k\in\{0,\dots,\text{maxiter}-1\}}$
2. **Initialization:** $u_0 > 0$

for $k = \{0, \dots, \text{maxiter} - 1\}$ **do**

Compute $u_{k+\frac{1}{2}} = \frac{u_k}{K^*\mathbf{1}} K^* \left(\frac{f}{Ku_k}\right)$ (EM-iterate)

Set $\overline{u}_k := (1-\tau_k)u_k + \tau_k u_{k+\frac{1}{2}}$

Define $\omega_k := u_k/(K^*\mathbf{1})$

Solve $u_{k+1} \in \arg\min_{\substack{u\in\text{dom}(J)\\ u\geq 0}} \left\{ \frac{1}{2} \left\| \frac{u-\overline{u}_k}{\sqrt{\omega_k}} \right\|^2_{L^2(\Omega)} + \alpha\tau_k J(u) \right\}$

end for

return u_{maxiter}

We want to mention that there exist various other methods that aim at solving (8.6) for various choices of regularization terms. In [41, 100, 99] (parallel) proximal-point algorithms have been investigated to solve (2.9) for different fidelities (for instance $H_f(Ku) = \text{KL}(f, Ku)$) and multiple regularization terms for different domains, by efficiently splitting the whole variational framework up into subproblems.

In [14, 13] a scaled projective gradient method and an inexact interior point method have been considered to minimize (8.6) in image deblurring applications. However, the application of these methods require the considered functionals to be differentiable.

In [65] the Kullback-Leibler fidelity has been approximated by its second-order Taylor linearization. More precisely, a simple FBS-strategy as in Algorithm 2 was performed, for which the stepsize has specifically been chosen via a Barzilai-Borwein-related criterion, based on the second derivative of the Kullback-Leibler fidelity.

Augmented-Lagrangian-Type Methods

Other popular splitting schemes originate in the consideration of saddle-point problems. A saddle-point problem is defined as follows.

Definition 8.1 (Primal-Dual Saddle-Point Problem)**.** *Let $\mathcal{L} : \mathcal{U} \times \mathcal{V} \to \mathbb{R} \cup \{\infty\}$ be a functional that is convex in $u \in \mathcal{U}$ and concave in $p \in \mathcal{V}$, for Banach spaces $\mathcal{U}$ and $\mathcal{V}$. Then, the saddle-point problem is defined as*

$$\inf_{u\in\mathcal{U}} \sup_{p\in\mathcal{V}} \mathcal{L}(u;p)\,, \tag{8.8}$$

with u denoting the primal, and p denoting the dual variable.

Typical convex-concave functionals are Lagrange-functionals, that transform constrained optimization problems into unconstrained problems.
Finding a saddle-point pair $(\bar{u}, \bar{p})$ is equivalent to finding a pair that satisfies

$$\mathcal{L}(\bar{u}, p) \leq \mathcal{L}(\bar{u}, \bar{p}) \leq \mathcal{L}(u, \bar{p})\ ,\ \ \forall (u,p) \in \mathcal{U} \times \mathcal{V}\,.$$

It is easy to see that problems like (8.8) can be split into two separate problems, which are $\inf_{u\in\mathcal{U}} F(u)$ for $F(u) := \sup_{p\in\mathcal{V}} \mathcal{L}(u;p)$; or, equivalently, $\sup_{p\in\mathcal{V}} G(p)$ for $G(p) := \inf_{u\in\mathcal{U}} \mathcal{L}(u;p)$, since inf and sup can be interchanged in specific cases, see for instance [91, Section 3.2, Theorem 3.1] in case of the ROF model (4.6).

In the following we want to discuss two typical constrained minimization problems that result from the variational frameworks we are interested in. The first problem can be defined as follows.

Problem 8.1.

$$u \in \underset{u \in \mathrm{dom}(J)}{\arg\min}\, J(u)$$

subject to

$$Ku = f$$

In order to turn Problem 8.1 into an unconstrained minimization problem, we can define the Lagrange functional

$$\mathcal{L}(u;\mu) := J(u) + \langle \mu, Ku - f \rangle_{L^2(\Sigma)}$$

with Lagrange multiplier μ, and rewrite Problem 8.1 to the saddle-point problem

$$(u,\mu) \in \underset{u \in \mathrm{dom}(J)}{\arg\min} \underset{\mu \in L^2(\Sigma)}{\arg\max}\, \mathcal{L}(u;\mu)\,. \tag{8.9}$$

In case of a quadratic functional J the system of equations derived from the Karush-Kuhn-Tucker (KKT) conditions, i.e. the optimality conditions, of (8.9) can be solved easily. In case of a singular regularization energy, (8.9) is not that easy or even impossible to solve. Therefore we want to introduce the augmented Lagrange functional of Problem 8.1, i.e.

$$\mathcal{L}_{\mathcal{A}}(u;\mu) = J(u) + \langle \mu, Ku - f \rangle_{L^2(\Sigma)} + \frac{\delta}{2} \left\| Ku - f \right\|^2_{L^2(\Sigma)}\,. \tag{8.10}$$

As we see the only modification of the standard Lagrange multiplier is an additional squared L^2-term of the constraint, balanced by a positive relaxation parameter δ. The ALM goes back to [66, 98] and has been originally introduced as the *method of multipliers*. In [57, 58, 72] an extensive overview of the ALM can be found. It can be seen that a saddle-point of the standard Lagrange functional is also a saddle-point of the augmented Lagrange functional, since the additional L^2-term does on the one hand not affect the optimality condition for μ and on the other hand vanishes for $Ku = f$. The basic algorithmic idea in order to split the overall problem into subproblems is to apply the standard Uzawa algorithm without preconditioning ([3, Chapter 10]) on (8.10). Furthermore the stepsize of the gradient ascent on the dual variable (which is the Lagrange multiplier) is set to the relaxation parameter. Hence, we obtain the following algorithm, called method of multipliers ([66, 98]) or the augmented Lagrangian method (ALM).

Algorithm 6 Augmented Lagrangian Method for Problem 8.1

1. **Parameters:** $K,\ f,\ \alpha > 0,\ \mathrm{maxiter},\ (\delta_k)_{k \in \{0,\dots,\mathrm{maxiter}-1\}}$
2. **Initialization:** $u_0 \in \mathrm{dom}(J),\ \mu_0 \in L^2(\Sigma)$

for $k = \{0, \dots, \mathrm{maxiter} - 1\}$ **do**

Compute

$$\begin{aligned} u_{k+1} &\in \underset{u \in \mathrm{dom}(J)}{\arg\min}\, \mathcal{L}_{\mathcal{A}}(u;\mu_k) \\ &= \underset{u \in \mathrm{dom}(J)}{\arg\min} \left\{ J(u) + \langle \mu_k, Ku - f \rangle_{L^2(\Sigma)} + \frac{\delta_k}{2} \left\| Ku - f \right\|^2_{L^2(\Sigma)} \right\} \end{aligned}$$

Update $\mu_{k+1} = \mu_k + \delta_k \left(K u_{k+1} - f \right)$

end for

return u_{maxiter}

The second problem we want to discuss is a variational minimization framework with additional equality constraint.

Problem 8.2.

$$(u, v) \in \arg\min_{u,v} \{H_f(Ku) + \alpha J(v)\}$$

subject to

$$v = Bu$$

A typical problem that can be reformulated to be of the type of Problem 8.2 is the computation of a ROF-minimizer (4.6). Computing a ROF-minimizer can be rewritten to

$$\begin{aligned} (u, v) \in & \underset{\substack{u \in \mathrm{BV}(\Omega) \\ v \in \mathcal{M}(\Omega;\mathbb{R}^n)}}{\arg\min} \left\{ \frac{1}{2} \|Ku - f\|^2_{L^2(\Sigma)} + \alpha \|v\|_{\mathcal{M}(\Omega;\mathbb{R}^n)} \right\} \\ & \text{subject to } v = \nabla u \,, \end{aligned} \tag{8.11}$$

with $\mathcal{M}(\Omega;\mathbb{R}^n)$ being the space of Radon measures on Ω. In analogy to Problem 8.1 we can define the augmented Lagrange functional for Problem 8.2 and iteratively compute the separate optimality conditions. The ALM for Problem 8.2 reads as follows.

Algorithm 7 Augmented Lagrangian Method for Problem 8.2

1. **Parameters:** $K,\ f,\ \alpha > 0,\ \text{maxiter},\ (\delta_k)_{k\in\{0,\dots,\text{maxiter}-1\}}$
2. **Initialization:** u_0 with $Bu_0 \in \mathrm{dom}(J)$, $\mu_0 \in L^2(\Sigma)$

for $k = \{0, \dots, \text{maxiter} - 1\}$ **do**

Compute $u_{k+1} \in \arg\min_{u\in\mathrm{dom}(J(B\cdot))} \left\{ H_f(Ku) + \langle \mu_k, Bu - v_k \rangle_{L^2(\Omega)} + \frac{\delta_k}{2} \|Bu - v_k\|^2_{L^2(\Omega)} \right\}$

Solve $v_{k+1} \in \arg\min_{v\in\mathrm{dom}(J)} \left\{ \alpha J(v) + \langle \mu_k, Bu_{k+1} - v \rangle_{L^2(\Omega)} + \frac{\delta_k}{2} \|Bu_k - v\|^2_{L^2(\Omega)} \right\}$

Update $\mu_{k+1} = \mu_k + \delta_k \left(Bu_{k+1} - v_{k+1} \right)$

end for

return u_{maxiter}

For problems like (8.11) the ALM approach offers the advantage to separate the nonlinear problem into two linear problems and a nonlinear problem that can be solved analytically. If we consider (8.11) the ALM reads as

$$u_{k+1} = \underset{u\in\mathrm{BV}(\Omega)}{\arg\min} \left\{ \frac{1}{2} \|Ku - f\|^2_{L^2(\Omega)} + \langle \mu_k, \nabla u - v_k \rangle_{L^2(\Omega)} + \frac{\delta_k}{2} \|\nabla u - v_k\|^2_{L^2(\Omega)} \right\} , \tag{8.12}$$

$$v_{k+1} = \underset{v\in\mathcal{M}(\Omega;\mathbb{R}^n)}{\arg\min} \left\{ \alpha \|v\|_{\mathcal{M}(\Omega;\mathbb{R}^n)} + \langle \mu_k, \nabla u_{k+1} - v \rangle_{L^2(\Omega)} + \frac{\delta_k}{2} \|\nabla u_{k+1} - v\|^2_{L^2(\Omega)} \right\} , \tag{8.13}$$

$$\mu_{k+1} = \mu_k + \delta_k \left(\nabla u_{k+1} - v_{k+1} \right) , \tag{8.14}$$

for which equation (8.12) and (8.13) can be solved via

$$(K^*K - \delta_k \Delta)\, u_{k+1} = K^* f - \delta_k \mathrm{div}\left(v_k - \frac{1}{\delta_k}\mu_k\right), \tag{8.15}$$

and

$$v_{k+1} = \mathrm{shrink}\left(\nabla u_{k+1} - \frac{1}{\delta_k}\mu_k, \frac{\alpha}{\delta_k}\right), \tag{8.16}$$

respectively. We see that we have to solve iteratively the two linear equations (8.15) and (8.14) of which only (8.15) involves a matrix inversion. If K is the identity operator (8.15) can even be solved directly since Δ is diagonalizable with respect to a certain basis depending on the boundary conditions. For $K = \mathrm{I}$ and Neumann boundary conditions on Δ we can use the Cosine transform for diagonalization, which is briefly explained in Appendix A.1. The computation of (8.16) is a direct, pointwise operation as well, which makes the ALM a very suitable algorithmic scheme for problems like (8.11).

The computational scheme (8.11) in order to solve (4.6) has been introduced in [59] as the *Split Bregman method*. Many works (cf. [115, 116] together with [52, 54]) yet have pointed out the relation between ALM, Split Bregman and other splitting methods. Moreover, further developments of ALM especially in the context of imaging and total variation regularization can be found in [52, 54, 53, 139, 140, 133, 71, 21]. In the following we briefly want to highlight the connection between ALM and Bregman Distances. If we consider the primal minimization problem of ALM for Problem 8.1 in Algorithm 6, i.e.

$$\begin{aligned} u_k &\in \operatorname*{arg\,min}_{u \in \mathrm{dom}(J)} \left\{ J(u) + \langle \mu_{k-1}, Ku - f \rangle_{L^2(\Sigma)} + \frac{\delta_{k-1}}{2} \|Ku - f\|^2_{L^2(\Sigma)} \right\} \\ &= \operatorname*{arg\,min}_{u \in \mathrm{dom}(J)} \left\{ \frac{1}{\delta_{k-1}} J(u) + \frac{1}{2} \left\| Ku - \left(f - \frac{1}{\delta_{k-1}} \mu_{k-1} \right) \right\|^2_{L^2(\Sigma)} \right\} \end{aligned},$$

we can set $\delta_{k-1} = 1/\alpha$ for all k and a fixed positive constant α and substitute $v_{k-1} := -\alpha \mu_{k-1}$ to obtain

$$u_k \in \operatorname*{arg\,min}_{u \in \mathrm{dom}(J)} \left\{ \alpha J(u) + \frac{1}{2} \|Ku - (f + v_{k-1})\|^2_{L^2(\Sigma)} \right\}.$$

The update for the Lagrange multiplier μ_{k-1},

$$\mu_k = \mu_{k-1} + \delta_{k-1} (Ku_k - f),$$

modifies to

$$v_k = v_{k-1} - (Ku_k - f),$$

and hence, the ALM Algorithm 6 for Problem 8.1 and the Bregman Iteration Algorithm 1 are equivalent for constant stepsize of the gradient ascent on the Lagrange multiplier.

8.1.2 Direct Methods

In this section we want to discuss alternative concepts for the computational solution of (8.8), for the particular problem

$$\inf_u \sup_{\|p\|_\infty \leq 1} \left\{ \frac{1}{2} \|u - f\|^2_{L^2(\Omega)} + \alpha \langle u, B^* p \rangle_{L^2(\Omega)} \right\} . \tag{8.17}$$

One concept is based on a projected gradient descent method applied to the dual problem, while the other concept is founded on a quasi-Newton approach.

Dual Gradient-Descent Methods

In [37] a primal-dual gradient-descent method has been presented in order to find computational solutions of the ROF-model (4.6). In this section we want to briefly recall the algorithm in case of an arbitrary linear operator B. The basic idea is to compute the dual problem of (4.6) instead of the primal problem. If we consider

$$\inf_{u \in \mathrm{BV}(\Omega)} \sup_{\|p\|_\infty \leq 1} \left\{ \frac{1}{2} \|u - f\|^2_{L^2(\Omega)} + \alpha \langle B^* p, u \rangle_{L^2(\Omega)} \right\} ,$$

we can at least in case of $B = \nabla$ interchange inf and sup due to [91, Section 3.2, Theorem 3.1] to obtain the minimization problem

$$\inf_{u \in \mathrm{BV}(\Omega)} \frac{1}{2} \|u - f\|^2_{L^2(\Omega)} + \alpha \langle B^* p, u \rangle_{L^2(\Omega)} .$$

The function u that minimizes this expression is simply given via $u = f - \alpha B^* p$. Hence, we end up with the dual optimization problem

$$\sup_{\|p\|_\infty \leq 1} \left\{ -\frac{1}{2} \|\alpha B^* p\|^2_{L^2(\Omega)} + \alpha \langle B^* p, f \rangle_{L^2(\Omega)} \right\} = \inf_{\|p\|_\infty \leq 1} \left\{ \frac{1}{2} \|\alpha B^* p - f\|^2_{L^2(\Omega)} \right\} ,$$

for which the optimality condition is

$$B B^* p = \frac{1}{\alpha} B f , \tag{8.18}$$

subject to $\|p\|_\infty \leq 1$. The idea of the algorithm presented in [37] in case of $B = \nabla$ is to solve (8.18) via a projected gradient descent method, i.e. p is approximated via

$$p_{k+1} = \frac{p_k - \tau B \left(B^* p_k - \frac{1}{\alpha} f \right)}{\left\| p_k - \tau B \left(B^* p_k - \frac{1}{\alpha} f \right) \right\|_\infty} . \tag{8.19}$$

If p_k has converged up to a certain tolerance, the primal variable can be obtained via the relation $u = f - \alpha B^* p$. If we summarize the different algorithmic steps we end up with the following algorithm.

Algorithm 8 Chambolle Algorithm

1. **Parameters:** $f,\ \alpha > 0,\ \tau > 0,\ \text{maxiter}$
2. **Initialization:** $p_0 \in \mathrm{dom}(B^*)$, with $\|p_0\|_\infty \leq 1$

for $k = \{0, \ldots, \text{maxiter} - 1\}$ **do**

Compute p_{k+1} via (8.19)

end for

return p_{maxiter}, $u_{\text{maxiter}} = f - \alpha B^* p_{\text{maxiter}}$

Primal-Dual Quasi-Newton Methods

In the previous section we have presented a projected gradient descent method in order to solve (8.17). In this section we want to consider the same problem but we want to discuss an alternative method that has originally been proposed in [125] (in order to solve the ROF model, i.e. $B = \nabla$). For this method a nonlinear problem needs to be split up into a linear and a nonlinear part, while the nonlinear part has to be linearized and subsequently both parts have to be merged together into a linearized iterative scheme.

We want to approximate the dual characterization of the L^1 regularization of Bu, i.e. $\sup_{\substack{p\in C_0^\infty(\Omega;\mathbb{R}^n)\\ \|p\|_\infty\leq 1}} \langle u, B^*p\rangle$, by a nonlinear penalty term. Precisely, we want to consider Lagrange functionals of the type

$$\mathcal{L}_{\mathcal{P}}(u;p) := \frac{1}{2}\|Ku-f\|^2_{L^2(\Omega)} + \alpha\,\langle u, B^*p\rangle_{L^2(\Omega)} - \frac{\epsilon}{2}\|\max(|p|-1,0)\|^2_{L^2(\Omega)}\,. \tag{8.20}$$

The optimality conditions of (8.20) are

$$\partial_u \mathcal{L}_{\mathcal{P}}(u;p) = 0 = K^*(Ku-f) + \alpha B^*p \tag{8.21}$$
$$\partial_p \mathcal{L}_{\mathcal{P}}(u;p) = 0 = \alpha Bu - \epsilon H(p) \tag{8.22}$$

with $H(p)$ being defined as

$$H(p) := \operatorname{sign}(p)\max(|p|-1,0)\,. \tag{8.23}$$

We have a linear (8.21) and a nonlinear (8.22) equation as our optimality system. We now want to linearize (8.22) by approximating (8.23) via its first order Taylor approximation, i.e.

$$H(p_{k+1}) \approx H(p_k) + H'(p_k)(p_{k+1}-p_k)\,, \tag{8.24}$$

with

$$H'(p) = \begin{cases} 1 & \text{if } |p|>1 \\ 0 & \text{else} \end{cases}\,.$$

If we replace $H(p)$ via its linearization (8.24) and add a damping term with respect to the dual variable p we end up with the iterative Quasi-Newton-scheme

$$\begin{aligned} 0 &= K^*(Ku_{k+1}-f) + \alpha B^*p_{k+1}\,,\\ 0 &= \alpha Bu_{k+1} - \epsilon H(p_k) - \epsilon H'(p_k)(p_{k+1}-p_k) - \tau_k(p_{k+1}-p_k)\,, \end{aligned}$$

for a sequence of positive damping parameters τ_k, which we can rewrite to

$$K^*Ku_{k+1} + \alpha B^*p_{k+1} = K^*f\,, \tag{8.25}$$
$$\alpha Bu_{k+1} + M_k p_{k+1} = v_k\,, \tag{8.26}$$

with

$$M_k := -\epsilon H'(p_k) - \tau_k \mathrm{I}\,, \tag{8.27}$$

and

$$v_k := \epsilon(H(p_k) - H'(p_k)p_k) - \tau_k p_k \,. \tag{8.28}$$

By applying a Schur-Complement strategy the system of equations (8.25) and (8.26) can be reduced to one equation. If we solve (8.26) for p_{k+1} we obtain

$$p_{k+1} = M_k^{-1}\left(v_k - Bu_{k+1}\right) . \tag{8.29}$$

Note that M_k^{-1} is easy to invert (for $\tau_k \neq 0$), since M_k^{-1} is a diagonal operator. Inserting p_{k+1} into (8.25) yields

$$u_{k+1} = \left(K^*K + \alpha B^* M_k^{-1} B\right)^{-1}\left(K^* f - B^* M_k^{-1} v_k\right) . \tag{8.30}$$

If K^*K is easily invertible, the solution of u_{k+1} and subsequent insertion into (8.26) could be an alternative option. The above considerations lead to the following algorithm.

Algorithm 9 Primal Dual Quasi-Newton Method

1. **Parameters:** $f,\ \alpha > 0,\ \epsilon > 0,\ \text{maxiter},\ (\tau_k)_{k\in\{0,\dots,\text{maxiter}-1\}}$
2. **Initialization:** $p_0 \in \text{dom}(B^*)$, with $\|p_0\|_\infty \leq 1$

for $k = \{0, \dots, \text{maxiter} - 1\}$ **do**

Define M_k via (8.27)
Set v_k as in (8.28)
Solve u_{k+1} via (8.30)
Update p_{k+1} via (8.29)

end for
return u_{maxiter}, p_{maxiter}

In [91] the Primal-Dual Quasi-Newton method has been parallelized and optimized for computing ROF-minimizers, i.e. $K = \text{I}$ and $B = \nabla u$. In more than one dimensions implementing the Primal-Dual Quasi-Newton method for ROF-minimization can become more complicated. The anisotropic case is straight forward. The dual variables in the different dimensions are not linked as they are in the isotropic case. Therefore additional penalty terms are all independent of each other, and hence, computations can be done in an analogous way as in the one dimensional case. For isotropic total variation regularization the extension of the computational scheme is much more complicated, since the dual variables are linked via the condition $\sqrt{p_1^2 + p_2^2 + \dots + p_n^2} \leq 1$.

8.1.3 Bregman-Iteration for the Kullback-Leibler Fidelity

The concept of Bregman iteration as introduced in Section 3.3 can be transferred to other data fidelities. In [21, Section 5.6.1] a computational scheme for the solution of

$$u^l \in \underset{u\in\text{dom}(J)}{\arg\min}\left\{\text{KL}(f, Ku) + \alpha D_J^{p^{l-1}}(u, u^{l-1})\right\} \tag{8.31}$$

has been presented and analyzed in case of $J(u) = \text{TV}(u)$. Considering the optimality condition of (8.31) yields

$$0 = K^*\left(\mathbf{1} - \frac{f}{Ku^l}\right) + \alpha\left(p^l - p^{l-1}\right) .$$

If we substitute $p^l := \left(K^*\mathbf{1}v^l\right)/\alpha$ we obtain the update formula

$$v^l = v^{l-1} - \left(1 - \frac{1}{K^*\mathbf{1}} K^*\left(\frac{f}{Ku^l}\right)\right). \tag{8.32}$$

In analogy to the derivation of Algorithm 1 the idea of substituting v for p is to shift the Bregman update for v into the data fidelity. If we consider Algorithm 5 again, our goal is to replace (8.7) with

$$u_{k+1}^l \in \operatorname*{arg\,min}_{\substack{u\in\mathrm{dom}(J)\\ u\geq 0}} \left\{ \frac{1}{2}\int_\Omega \frac{K^*\mathbf{1}\left(u - \left((1-\tau_k)u_k^l + \tau_k u_{k+\frac{1}{2}}^l\right)\right)^2}{u_k^l}\, d\mu(x) + \tau_k \alpha D_J^{p^{l-1}}(u, u^{l-1}) \right\}.$$

If we replace p^{l-1} by v^{l-1} with $\left(K^*\mathbf{1}v^{l-1}\right)/\alpha = p^{l-1}$ we can shift v^{l-1} into the fidelity term to obtain

$$u_{k+1}^l \in \operatorname*{arg\,min}_{\substack{u\in\mathrm{dom}(J)\\ u\geq 0}} \left\{ \frac{1}{2}\int_\Omega \frac{K^*\mathbf{1}\left(u - \left((1-\tau_k)u_k^l + \tau_k u_{k+\frac{1}{2}}^l + \tau_k v^l u_k\right)\right)^2}{u_k^l}\, d\mu(x) + \tau_k \alpha J(u) \right\}. \tag{8.33}$$

The whole procedure can be summarized into the following algorithm.

Algorithm 10 Bregmanized EM Algorithm

1. **Parameters:** K, f, $\alpha > 0$, maxiter, bregiter, $(\tau_k)_{k\in\{1,\dots,\mathrm{maxiter}\times\mathrm{bregiter}\}}$
2. **Initialization:** $u_0^l > 0$, $v^0 = 0$

for $l = \{0, \dots, \mathrm{bregiter} - 1\}$ **do**
  for $k = \{1, \dots, \mathrm{maxiter}\}$ **do**
    Solve $u_{k+\frac{1}{2}}^l = \frac{u_k^l}{K^*\mathbf{1}} K^*\left(\frac{f}{Ku_k^l}\right)$
    Compute u_{k+1}^l via (8.33)
  end for
  Update v^l via (8.32)
end for
return $u_{\mathrm{maxiter}}^{\mathrm{bregiter}}$

8.1.4 Orthogonal Matching Pursuit

The efficient computation of sparse solutions for underdetermined linear systems of equations (LES) is of high relevance, since many applications (especially those related to the terminology of compressed sensing) can be described as problems for which the desired solution has a sparse representation with respect to a certain basis. This representation therefore allows recovery of this sparse pattern if the rank of the LES is still high enough in contrast to the level of sparsity.

A very simple and intuitive algorithm to solve underdetermined LES for solutions with sparse patterns is the orthogonal matching pursuit (OMP) algorithm (cf. [96, 88, 124]) as summarized in Algorithm 11. Note that P_I denotes the projection on I.

Algorithm 11 Orthogonal Matching Pursuit

1. **Parameters:** $K,\ f,\ \text{threshold} > 0$
2. **Initialization:** $r_0 = f,\ I_0 = \emptyset$

while $\|r_k\| > \text{threshold}$ **do**

Compute $I_k = I_{k-1} \cup i$ with i such that $\left|(K^T r_k)_i\right| = \|K^T r_k\|_\infty$

Compute $u_k = \arg\min_u \left\{\|KP_{I_k} u - f\|^2\right\}$

Update $r_{k+1} = f - KP_{I_k} u_k$

end while

return u_k

The idea behind OMP is to iteratively consider the coefficients that represent most of the data, to subsequently project the data on these coefficients and to subtract the result from the data, until a specified threshold has been reached. The features that make the algorithm very attractive is its simplicity and the fact that only low-dimensional LES have to be solved in each iteration. Moreover, for matrices K that have special properties it can even be proved that OMP converges to the sparsest possible solution (cf. [121, 85]). However, for rather difficult or ill-conditioned matrices OMP is not producing desirable results, which is the motivation for the upcoming section to investigate a new OMP-related algorithm based on the ISS (3.9) in case of the compressed sensing setup (4.3), which has been proposed in [27].

8.2 Adaptive Inverse Scale Space Methods

Inspired by the ISS method as introduced in Section 3.4, and greedy methods such as OMP considered in the previous section, we want to present a novel algorithm that, in analogy to OMP, iteratively solves small least-squares problems in order to recover the sparse set of coefficients that represents given data best. In contrast to OMP we are going to see that the novel algorithm is guaranteed to converge to at least the ℓ^1-minimizing solution that solves the LES.

8.2.1 Inverse Scale Space Methods for Compressed Sensing

In the following we are going to investigate the behaviour of inverse scale space methods in the compressed sensing setup

$$\partial_t p(t) = K^T(f - Ku(t)), \qquad p(t) \in \partial\|u\|_{\ell^1}. \tag{8.34}$$

Similar to the Eigenfunction-decomposition example for $J(u) = \|u\|_{\ell^1}$ in Section 7.3 we want to start with a rather general statement related to Theorem 6.2 in case of $\alpha \to \infty$.

Lemma 8.1. *For*

$$t < t_1 := \frac{1}{\|K^T f\|_{\ell^1}}$$

a solution (u, p) *of the inverse scale space flow* (8.34) *is given by*

$$u(t) = 0, \qquad p(t) = tK^T f.$$

Proof. We immediately see

$$\partial_t p(t) = K^T f = K^T(f - Ku(t))$$

and

$$\|p(t)\|_{\ell^1} = t\|K^T f\|_{\ell^1} < t_1\|K^T f\|_{\ell^1} = 1,$$

thus

$$p(t) \in \partial\|0\|_{\ell^1} = \partial\|u(t)\|_{\ell^1}.$$

□

The observation in Lemma 8.1 is the basis for further characterizing the inverse scale space flow for larger times. We expect changes in the primal variable u only to occur at some discrete time steps, when some $|p_i(t)|$ reaches the value one and that p behaves linearly in the intermediate times. It remains to characterize u at the discrete time steps t_k. This can be understood from the limit of the Bregman iteration

$$\frac{1}{2}\|Ku - f\|_{\ell^2}^2 + \alpha(\|u\|_{\ell^1} - p \cdot u)$$

as $\alpha \to \infty$. In order to obtain a minimum we expect the Bregman distance to go to zero, i.e. $p \cdot u = \|u\|_{\ell^1}$ (thus $p \in \partial\|u\|_{\ell^1}$), and the squared norm to be minimized subject to this constraint. In this way we can indeed compute the detailed behaviour of the inverse scale space flow:

Theorem 8.1. *There exists a sequence of times*

$$0 = t_0 < t_1 < t_2 < \dots$$

such that

$$u(t) = u(t_k), \qquad p(t) = p(t_k) + (t - t_k)K^T(f - Ku(t_k)) \tag{8.35}$$

for $t \in [t_k, t_{k+1})$ is a solution of the inverse scale space flow (8.34), where $u(t_k)$ is a solution of

$$\|Ku - f\|_{\ell^2} \to \min_{u, p(t_k) \in \partial\|u\|_{\ell^1}}. \tag{8.36}$$

Moreover $t_{k+1} = \infty$ if and only if $K^T K u(t_k) = K^T f$.

Proof. Due to Lemma 8.1 the assertion clearly holds for $k = 0$ (with $t_0 = 0$), noticing that

$$p(0) = 0 \in \partial\|u(0)\|_{\ell^1} = \partial\|0\|_{\ell^1}.$$

Now we proceed inductively. Given $u(t_k)$ and $p(t_k)$ we compute

$$t_{k+1} = \min\{t \mid t > t_k, \exists j : |p_j(t)| = 1, u_j(t_k) = 0, p_j(t) \neq p_j(t_k)\}, \tag{8.37}$$

where

$$p_j(t) = p_j(t_k) + (t - t_k)e_j \cdot K^T(f - Ku(t_k)) \tag{8.38}$$

holds.

Now $u(t_k)$ minimizes $\|Ku - f\|_{\ell^2}$ subject to the constraint $p(t_k) \in \partial\|u\|_{\ell^1}$, which we can rewrite as a linearly constrained quadratic problem of minimizing $\|Ku - f\|_{\ell^2}^2$ subject to

$$\begin{aligned} u_j &\geq 0 \qquad \text{if } p_j = 1 \\ u_j &\leq 0 \qquad \text{if } p_j = -1 \\ u_j &= 0 \qquad \text{if } -1 < p_j < 1. \end{aligned}$$

From the optimality condition we obtain:

- $u_j(t_k) > 0$ or $u_j(t_k) < 0$ implies $e_j \cdot K^T(Ku(t_k) - f) = 0$, hence $p_j(t) = p_j(t_k) = \pm 1$.
- $u_j(t_k) = 0$ and $p_j(t_k) = 1$ implies $e_j \cdot K^T(Ku(t_k) - f) \geq 0$, hence $-1 \leq p_j(t) \leq p_j(t_k) = 1$ for t small.
- $u_j(t_k) = 0$ and $p_j(t_k) = -1$ implies $e_j \cdot K^T(Ku(t_k) - f) \leq 0$, hence $1 \geq p_j(t) \geq p_j(t_k) = -1$ for t small.
- $u_j(t_k) = 0$ and $p_j(t_k) \in]-1, 1[$ implies $p_j(t) \in [-1, 1]$ for t small.

Hence the construction yields a solution in $[t_k, t_{k+1})$ and t_{k+1} is well-defined. The existence of $u(t_{k+1})$ follows from a standard result for quadratic programs. □

Theorem 8.1 provides a direct way to formulate the inverse scale space method as an adaptive scheme for compressed sensing. We will refer to this method as adaptive inverse scale space method (aISS):

Algorithm 12 Adaptive Inverse Scale Space Method

1. **Parameters:** $K,\ f,$ threshold ≥ 0
2. **Initialization:** $t_1 = 1/\left\|K^T f\right\|_\infty,\ p(t_1) = t_1\ K^T f,\ I_1 = \{i \mid |p_i(t_1)| = 1\}$

while $\|Ku(t_k) - f\|_{\ell^2} >$ threshold **do**

Compute $u(t_k) = \arg\min_u \left\{\|KP_{I_k}u - f\|_{\ell^2}^2\right\}$ subject to $u(t_k)p(t_k) \geq 0$
Obtain t_{k+1} as the minimal time for which (8.37) holds
Update the dual variable $p(t)$ via (8.38) with $t = t_{k+1}$
Compute $I_{k+1} = \{i \mid |p_i(t_{k+1})| = 1\}$

end while
return $u(t_k)$

We want to mention that the solution of the quadratic programming problem in each step is a very low-dimensional one, since we can directly set $u_j(t_k) = 0$ for $|p_j(t_k)| < 1$. Hence we can minimize the problem on the lower-dimensional index set I_k of components where $|p_j(t_k)| = 1$. In most cases we expect the solution to be the same as $(KP_{I_k})^\dagger f$, hence we might try to solve the low-dimensional least-squares problem first and then check the signs of the solution.

The resulting characterization of the inverse scale space method is reminiscent to greedy methods for compressed sensing, in particular orthogonal matching pursuit (see Algorithm 11). We can easily see the differences concerning the structure of the algorithm

- OMP restricts the index set similar to the inverse scale space method, but does not enforce a sign constraint.
- OMP only adds single indices in each iteration, while it is possible to change the index set arbitrarily in inverse scale space methods (practical observations confirm however a change of only one index in a vast majority of cases).
- OMP – brought to the inverse scale space notation – uses the supremum norm of $K^T(f - Ku(t_k))$ to select relevant indices, while the inverse scale space method uses $sp(t_k) + K^T(f - Ku(t_k))$ for varying s (related to $t - t_k$).

We expect the last point to be the major change from OMP to inverse scale space methods. The update of the dual variable encodes some history and improves the convergence behaviour. In

situations where OMP performs well, the first two points are probably no major differences, since we expect to automatically find correct signs by solving the unconstrained least-squares problem and we expect the index set to increase by one in each step also in the inverse scale space method. The sign constraint and the different update of the index set (in particular also the chance to make it smaller) are expected to yield improved behaviour in situations where OMP does not perform well (see also the numerical examples in Section 9.1.4), it also reflects the convergence of the inverse scale space method in arbitrary situations.

In analogy to Theorem 8.1 and Algorithm 12 we can derive similar results for the regularized inverse scale space flow (3.10). The major modification is that the update of the dual variable (8.38) changes to

$$\begin{aligned} p_j(t) = &\left(p_j(t_k) - \frac{1}{\alpha} e_j \cdot K^T \left(f - Ku(t_k)\right)\right) \exp\left(-\alpha \left(t - t_k\right)\right) \\ &+ \frac{1}{\alpha} e_j \cdot K^T \left(f - Ku(t_k)\right) . \end{aligned} \tag{8.39}$$

The related regularized-aISS-algorithm reads:

Algorithm 13 Adaptive Regularized Inverse Scale Space Method

1. **Parameters:** $K,\ f,\ \text{threshold} \geq 0$
2. **Initialization:** $t_1 = -\log\left(1 - \alpha / \left\|K^T f\right\|_\infty\right)/\alpha,\ p(t_1) = \left(K^T f\right)\left(1 - \exp(\alpha t_1)\right)/\alpha,\ I_1 = \{i \mid |p_i(t_1)| = 1\}$

while $\|Ku(t_k) - f\|_{\ell^2} >$ threshold **do**

Compute $u(t_k) = \arg\min_u \left\{\|KP_{I_k} u - f\|_{\ell^2}^2 + \alpha \left(P_{I_k} u \cdot p(t_k)\right)\right\}$ subject to $u(t_k)p(t_k) \geq 0$

Obtain t_{k+1} as the minimal time for which (8.37) holds

Update the dual variable $p(t)$ via (8.39) with $t = t_{k+1}$

Compute $I_{k+1} = \{i \mid |p_i(t_{k+1})| = 1\}$

end while

return $u(t_k)$

8.2.2 Further Convergence Analysis

In the following we provide some additional analysis confirming the favorable properties of the method in typical setups for compressed sensing. We shall assume that

$$f = K\tilde{u}, \quad P_I \tilde{u} = \tilde{u}, \quad \tilde{u} \cdot e_i \neq 0, i \in I. \tag{8.40}$$

where $\tilde{u}$ is the sparsest solution of $Ku = f$. Here I denotes an index set, and P_I the projection onto the elements supported on this index set. Hence, the above condition ensures that I is the index set of nonzero entries of the sparsest solution. In addition we shall assume a normalization condition on the columns of the matrix K, i.e.,

$$\|Ke_i\|_{\ell^2} = 1, \qquad \forall\ i\,. \tag{8.41}$$

First of all, we can see that each iteration improves the approximation accuracy of the data:

Proposition 8.1. *The approximation error $\|Ku(t) - f\|_{\ell^2}$ of the inverse scale space flow is strictly decreasing at the times t_k, i.e.*

$$\|Ku(t_{k+1}) - f\|_{\ell^2} < \|Ku(t_k) - f\|_{\ell^2}$$

Proof. We will prove the above Proposition in two steps

1. Show that $\|Ku(t_{k+1}) - f\|_{\ell^2} < \|Ku(t_k) - f\|_{\ell^2}$ if $p(t_k) \notin \partial\|u(t_{k+1})\|_{\ell^1}$.
2. Show that $p(t_k) \notin \partial\|u(t_{k+1})\|_{\ell^1}$ is always satisfied.

First part: Let us assume that $p(t_k) \notin \partial\|u(t_{k+1})\|_{\ell^1}$. In this case we have

$$D^{p(t_k)}_{\|\cdot\|_{\ell^1}}(u(t_{k+1}), u(t_k)) > 0. \tag{8.42}$$

Notice that $u(t_{k+1})$ is a minimizer of

$$Q(u) = \frac{1}{2}(t_{k+1} - t_k)\|Ku - f\|^2_{\ell^2} + D^{p(t_k)}_{\|\cdot\|_{\ell^1}}(u, u(t_k)),$$

which can easily be verified by confirming that the formula for $p(t_{k+1})$ coincides with the optimality condition of the above functional. Using (8.42) this yields the conclusion

$$\begin{aligned} \frac{1}{2}(t_{k+1} - t_k)\|Ku(t_{k+1}) - f\|^2_{\ell^2} &< Q(u(t_{k+1})) \\ &\leq Q(u(t_k)) \\ &= \frac{1}{2}(t_{k+1} - t_k)\|Ku(t_k) - f\|^2_{\ell^2}, \end{aligned}$$

and since $(t_{k+1} - t_k) > 0$ we have shown $\|Ku(t_{k+1}) - f\|_{\ell^2} < \|Ku(t_k) - f\|_{\ell^2}$.

Second part: By construction, more specific by the choice of t_{k+1}, there exists an index i such that $|p_i(t_{k+1})| = 1$ and $|p_i(t_k)| < 1$. Let us assume $p_i(t_{k+1}) = 1$, $p_i(t_k) < 1$, and i is – without restriction of generality – the only index at which the value of the subgradient becomes 1 (the negative case is similar and so is the case of multiple indices). We will show that $u_i(t_{k+1}) > 0$ which then (by the characterization of the subdifferential (4.2)) allows the conclusion $p_i(t_k) \notin \partial\|u(t_{k+1})\|_{\ell^1}$.
Given $p_i(t_{k+1}) = 1$, $p_i(t_k) < 1$ we know that

$$[K^T(f - Ku(t^k))]_i = \frac{1}{t_{k+1} - t_k}\left(p_i(t_{k+1}) - p_i(t_k)\right) > 0$$

Now we can prove $u_i(t_{k+1}) > 0$ by contradiction. If we had $u_i(t_{k+1}) = 0$, we already knew that $u(t_{k+1}) = u(t_k)$. Based on our previous calculation, this would mean that also $[K^T(f - Ku(t_{k+1}))]_i > 0$. However, $u(t_{k+1})$ is determined as the minimizer of

$$\frac{1}{2}\|KP_{I_{k+1}}u - f\|^2_{\ell^2} + \lambda \cdot u, \tag{8.43}$$

with Lagrange multipliers λ that enforce the constraint $u_j \geq 0$, if $p_j = 1$, $u_j \leq 0$, if $p_j = -1$, which means that $\lambda_j \leq 0$ if $p_j = 1$, $\lambda_j \geq 0$ if $p_j = -1$. Now the optimality condition of (8.43) in the i^{th} coefficient tells us that

$$0 \geq \lambda_i = [K^T(f - Ku(t_{k+1}))]_i,$$

which is a contradiction to $[K^T(f - Ku(t_{k+1}))]_i > 0$. Therefore, our assumption must have been wrong and thus $u_i(t_{k+1}) > 0$, which means $p_i(t_k) \notin \partial\|u(t_{k+1})\|_{\ell^1}$. □

The previous proposition allows us to conclude the finite time convergence of aISS to an ℓ^1 minimizing solution:

Theorem 8.2. *Let (u,p) be a solution of the adaptive inverse scale space method as above, then there exists a $M>0$ such that $t_{M+1}=\infty$ and $u(t)$ is an ℓ^1-minimizing solution for $t\geq t_M$.*

Proof. Let us denote

$$\begin{aligned} I_1^k &= \{i \,:\, p_i(t_k)=1\} \\ I_2^k &= \{i \,:\, p_i(t_k)=-1\} \\ I_3^k &= \{i \,:\, |p_i(t_k)|<1\} \end{aligned}$$

Notice that the solution $u(t_k)$ and therefore the ℓ^2 error $\|Ku(t_k)-f\|_{\ell^2}$ only depend on the index sets I_1^k, I_2^k, I_3^k. If there exists an $l\neq k$ such that $I_1^k=I_1^l$, $I_2^k=I_2^l$, $I_3^k=I_3^l$, then obviously

$$\|Ku(t_k)-f\|_{\ell^2}=\|Ku(t_l)-f\|_{\ell^2}.$$

However, Proposition 8.1 shows that this cannot happen, i.e.

$$\|Ku(t_k)-f\|_{\ell^2}<\|Ku(t_l)-f\|_{\ell^2}$$

for $k>l$. Since in finite dimensions there are only finitely many possibilities for I_1^k, I_2^k, I_3^k to be different we can conclude that the method has to converge in a finite number of iterations, i.e. there exists a $M>0$ such that $t_{M+1}=\infty$.

As we have seen in Theorem 8.1, $t_{M+1}=\infty$ implies $K^TKu(t_M)=K^Tf$ and since in (8.40) we have assumed that f is in the range of K, we obtain $Ku(t^k)=f$. To show that $u(t_k)$ indeed is an ℓ^1-minimizing solution, let $\hat{u}$ be another solution to $Ku=f$. Then the Bregman distance between $\hat{u}$ and $u(t_k)$ is

$$\begin{aligned} 0 &\leq D_{\|\cdot\|_{\ell^1}}^{p(t_M)}(\hat{u},u(t_M)) \\ &= \|\hat{u}\|_{\ell^1}-\|u(t_M)\|_{\ell^1}-\langle p(t_M),\hat{u}-u(t_M)\rangle \\ &= \|\hat{u}\|_{\ell^1}-\|u(t_M)\|_{\ell^1}-\left\langle \sum_{i=1}^{M}(t_i-t_{i-1})K^T(f-Ku(t_{i-1})),\hat{u}-u(t_M)\right\rangle \\ &= \|\hat{u}\|_{\ell^1}-\|u(t_M)\|_{\ell^1}-\Bigg\langle \sum_{i=1}^{M}(t_i-t_{i-1})(f-Ku(t_{i-1})),\underbrace{\underbrace{K\hat{u}}_{=f}-\underbrace{Ku(t_M)}_{=f}}_{=0}\Bigg\rangle \\ &= \|\hat{u}\|_{\ell^1}-\|u(t_M)\|_{\ell^1}, \end{aligned}$$

which shows that $u(t_M)$ is an ℓ^1 minimizing solution. □

The above proof of Theorem 8.2 yields finite time convergence but not much information about the complexity needed to reach the desired solution. In a reasonable setup we expect convergence with low complexity, i.e. few iteration steps with small support of the iterates. We shall obtain further information on the complexity by the following analysis. We start with a simple property for only one nonzero entry:

Proposition 8.2. *If $|I|=1$ and let (u,p) be a solution of the adaptive inverse scale space method as above. Then $u=\tilde{u}$ for $t\geq t_1$.*

Proof. Let k be the index of the nonzero entry of $\tilde{u}$. For $t < t_1$ we have

$$\partial_t p_i = (Ke_i) \cdot f = \tilde{u}_k (Ke_i) \cdot (Ke_k).$$

From (8.41) and the Cauchy-Schwarz inequality we see

$$p_k(t) = t\tilde{u}_k$$

and for $i \neq k$

$$|p_i(t)| = t|\tilde{u}_k||(Ke_i) \cdot (Ke_k)| < t|\tilde{u}_k| = |p_k(t)|.$$

Hence for $t = t_1$ we have $|p_i(t_1)| < 1$ for $i \neq k$ and $p_k(t_1)$ equals the sign of $\tilde{u}_k$. Consequently, $u(t_1)$ is determined by minimizing $\|Ku - f\|_{\ell^2}$ over all u such that only the k-th component is nonzero and has the same sign of $\tilde{u}_k$, thus $\tilde{u}$ is the obvious minimizer. Since $K^T(Ku - f) = 0$ we obtain $\partial_t p = 0$ for $t \geq t_1$, thus u remains unchanged. □

For more than one nonzero entry we need further properties of the matrix K, several of which are regularly used in compressed sensing. The most prominent example is the *restricted isometry property* (RIP) due to Candes and Tao [34], for which equivalence of ℓ^0 and ℓ^1 minimization can be shown. Here we shall use a weaker property due to Tropp [122], the so-called *exact recovery condition* (ERC), which can be used to show that also in the noisy case the exact support can be reconstructed: In [122, 123] J. A. Tropp has introduced a condition that guarantees recovery of the true support of a solution for the compressed sensing setup (4.3), namely the exact recovery condition (ERC). The exact recovery condition is defined as

$$\left\| (KP_I)^\dagger Ke_j \right\|_{\ell^1} < 1 \ \forall j \in I^c \,, \tag{ERC}$$

for I denoting the index set of the true solution $\tilde{u}$, I^c representing the complement of I, $P_I : \ell^2 \to \ell^2$ being the projection of a vector onto the index set and with $(KP_I)^\dagger$ denoting the generalized Moore-Penrose inverse of (KP_I). Before we continue to verify that for K satisfying (ERC) the inverse scale space method only operates on the support of the exact solution, we first want to highlight how (ERC) is connected to the source condition (SC1). Actually, (ERC) implies (SC1), which we will prove with the following Lemma.

Lemma 8.2. *Let $\tilde{u}$ denote the exact solution of* (2.3) *with support-set I, for a linear operator $K : \ell^2 \to \mathcal{V}(\Sigma)$. Then, if KP_I is injective (with P_I denoting the projection on I), the exact recovery condition* (ERC) *implies the source condition* (SC1) *for $J(\tilde{u}) = \|\tilde{u}\|_{\ell^1}$.*

Proof. The source condition in case of $J(u) = \|u\|_{\ell^1}$ reads as

$$\exists\, \xi_n \in \operatorname{sign}(\tilde{u}_n),\ \exists\, q \in \mathcal{V}(\Sigma)^* \setminus \{0\} : \quad \xi_n = (K^* q)_n \,.$$

If we define

$$q := ((KP_I)^*)^\dagger \operatorname{sign}(P_I \tilde{u})$$

we see that for this particular choice of q we have $\xi_n = ((KP_I)^* q)_n = \operatorname{sign}(P_I \tilde{u}_n)$ on the index set I, since KP_I is assumed to be injective. Hence, the source condition (SC1) is already fulfilled on the index set I. It remains to show that (SC1) is also valid on the complement of I. Therefore the only thing left that needs to be shown is

$$|\langle K^* q, e_j \rangle| < 1$$

for $j \in I^c$. We obtain

$$\begin{aligned}|\langle K^* q, e_j\rangle| = |\langle q, Ke_j\rangle| &= |\langle ((KP_I)^*)^\dagger \operatorname{sign}(P_I\tilde{u}), Ke_j\rangle| \\ &= |\langle \operatorname{sign}(\tilde{u}), (KP_I)^\dagger Ke_j\rangle| \leq \|(KP_I)^\dagger Ke_j\|_{\ell^1} < 1\,,\end{aligned}$$

due to (ERC) and hence, (SC1) is valid. □

Using the exact recovery condition we can verify that the inverse scale space method only operates on the support of the exact solution:

Proposition 8.3. *Let $f = KP_I\tilde{u}$ and let condition* (ERC) *be satisfied. Moreover let $(u(t), p(t))$ be the solution of the inverse scale space method as above. Then $|p_j(t)| < 1$ for all $j \notin I$ and all $t > 0$.*

Proof. We look for a solution $u = P_I u$ and project the equation

$$\partial_t p = K^T(f - Ku) = K^T K P_I(\tilde{u} - u)$$

onto I and with the regularity of $(KP_I)^T KP_I$ we find

$$P_I(\tilde{u} - u) = (P_I K^T K P_I)^{-1} \partial_t P_I p$$

and hence

$$KP_I(\tilde{u} - u) = K(P_I K^T K P_I)^{-1} \partial_t P_I p = ((KP_I)^\dagger)^T \partial_t P_I p.$$

Now let $j \notin I$, then

$$\partial_t p_j(t) = e_j \cdot K^T K P_I(\tilde{u} - u) = (Ke_j) \cdot ((KP_I)^\dagger)^T \partial_t P_I p.$$

Since all initial values are zero we can integrate this identity to obtain

$$p_j(t) = ((KP_I)^\dagger Ke_j) \cdot P_I p.$$

Now (ERC) and $\|P_I p\|_\infty \leq 1$ imply $|p_j(t)| < 1$ for all t. □

With (ERC) we can also obtain a result further confirming the optimal behaviour for a very small index set:

Proposition 8.4. *Assume $|I| = 2$,* (ERC)*, and let (u, p) be a solution of the adaptive inverse scale space method as above. Then $u = \tilde{u}$ for $t \geq t_2$.*

Proof. Without restriction of generality let $|\tilde{u}_1| \geq |\tilde{u}_2| > 0$ be the nonzero elements. We already know that $u_j(t) = 0$ for all $t > 0$ and $j > 2$, thus it suffices to consider the two-dimensional subspace. In the following, let K_i denote the i^{th} column of K. If $\tilde{u}_1 > 0$ then for $0 < t < t_1$ we have

$$\begin{aligned}\frac{1}{t} p_1(t) &= [K^T f]_1 = K_1 \cdot f = K_1 \cdot K\tilde{u} = K_1 \cdot (K_1\tilde{u}_1 + K_2\tilde{u}_2) \\ &= \underbrace{(K_1 \cdot K_1)}_{=1}\tilde{u}_1 + \underbrace{(K_1 \cdot K_2)}_{>-1}\tilde{u}_2 \\ &> \tilde{u}_1 - \tilde{u}_2 \geq 0\end{aligned}$$

while for $\tilde{u}_1 < 0$ we can show in a similar fashion that

$$p_1(t) < 0.$$

Hence, p_1 has the same sign as $\tilde{u}_1$ and by considering the different cases of signs for $\tilde{u}_1$ and $\tilde{u}_2$ one can easily verify that $|p_1(t)| \geq |p_2(t)|$. If equality holds, then it is easy to see that $|\tilde{u}_1| = |\tilde{u}_2|$ and thus, $u(t_1)$ is obtained by minimizing the residual on the two-dimensional subspace with indices I. Since the signs of $u_i(t_1)$, $i = 1, 2$, are the same as the signs of $\tilde{u}_i$, we obviously have $u(t_1) = \tilde{u}$ and thus $u(t) = \tilde{u}$ for all $t \geq t_1$.

If $|p_1(t)| > |p_2(t)|$, the residual is minimized over the one-dimensional subspace with index 1 and sign constraint. It is easy to verify that $u_1(t_1) = 0$ cannot be the minimizer, thus

$$K_1 \cdot (Ku(t_1) - f) = 0$$

and consequently p_1 remains constant in (t_1, t_2). Due to Proposition 8.3 we must have $|p_2(t_2)| = 1$ and it is easy to check that the sign of p_2 equals the sign of $\tilde{u}_2$. Hence, the minimization of the residual at time t_2 is carried out over the two-dimensional subspace I with same signs as $\tilde{u}$, which implies $u(t_2) = \tilde{u}$ and thus, $u(t) = \tilde{u}$ for $t \geq t_2$. □

Chapter 9

Applications

This chapter is all about applications that involve methods that have been subject of this thesis so far. We start supporting some of the rather theoretic results of the Chapters 5, 6 and 7 by computational examples. Moreover, we want to compare different computational scenarios for the aISS algorithm introduced in Section 8.2 and the OMP algorithm, to point out the strengths and weaknesses of the two algorithms. Subsequently we want to consider two real world applications, namely Positron Emission Tomography (PET) and Bioluminiscence Tomography (BLT), and present complex computational schemes that allow us to approximate solutions of these inverse problems very well.

9.1 Synthetic Examples

In this section we are going to discuss a few synthetic, computational examples to support the general error estimates of Chapter 5 for the L^1- and the Kullback-Leibler fidelity. Subsequently, we want to present computational results that confirm the statements of Theorem 6.3 and Theorem 6.4 and even fail, if the necessary assumptions are not fulfilled. Finally, we want to point out the advantages and disadvantages of the aISS Algorithm 12 in comparison to the OMP Algorithm 11.

9.1.1 Error Estimates

In this section we particularly want to demonstrate that in case the assumptions of Theorem 5.5 or Theorem 5.6 are fulfilled, computational examples will verify these results and will not violate the estimates. Moreover, in case of Theorem 5.5 we are even going to show that in case of violated assumptions the error in the solution can become arbitrary large.

We want to start with a little Salt'n'Pepper-denoising example to support Theorem 5.5 in case of the considered norm fidelity being the L^1-fidelity. Afterwards we want to create a compressed sensing setup for data being corrupted by Poisson-distributed noise in order to examine the capability of Theorem 5.6.

Salt'n'Pepper Noise Removal

In order to validate the asymptotic exactness or non-exactness in case of Laplacian noise we investigate a denoising approach with quadratic regularization, i.e. the minimization

$$\int_\Omega |u - f| \, dx + \frac{\alpha}{2} \int_\Omega (|\nabla u|^2 + u^2) \, dx \to \min_{u \in H^1(\Omega)}, \tag{9.1}$$

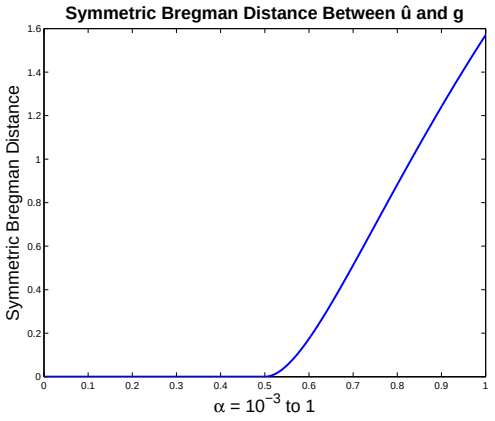

Figure 9.1: The Bregman distance error between $\hat{u}$ and g for $\alpha \in [10^{-3}, 1]$. As soon as $\alpha \leq \frac{1}{2}$, the error equals zero.

whose optimality condition is

$$-\alpha\Delta u + \alpha u + s = 0, \qquad s \in \operatorname{sign}\,(u - f).$$

A common approach to the numerical minimization of functionals like (9.1) is a smooth approximation of the L^1-norm, e.g. by replacing $|u - f|$ with $\sqrt{(u-f)^2 + \epsilon^2}$ for small ϵ. Such an approximation will however alter the asymptotic properties and destroy the possibility to have asymptotic exactness. Hence we shall use a dual approach as an alternative, comparable to Algorithm 8 but with fidelity and regularization term changed. Again, we derive the algorithm from the dual characterization of the one-norm:

$$\begin{aligned}
&\inf_u \left[\int_\Omega |u - f|\ dx + \frac{\alpha}{2}\int_\Omega (|\nabla u|^2 + u^2)\ dx\right] \\
=&\inf_u \sup_{|s|\leq 1} \left[\int_\Omega (u - f)s\ dx + \frac{\alpha}{2}\int_\Omega (|\nabla u|^2 + u^2)\ dx\right] \\
=&\sup_{|s|\leq 1} \inf_u \left[\int_\Omega (u - f)s\ dx + \frac{\alpha}{2}\int_\Omega (|\nabla u|^2 + u^2)\ dx\right].
\end{aligned}$$

Again, exchanging infimum and supremum in the last formula can easily be justified with standard methods in convex analysis (cf. [91, 50]). The infimum can be calculated exactly from solving

$$-\alpha\Delta u + \alpha u = -s$$

with homogeneous Neumann boundary conditions, and hence we obtain after a simple manipulation the dual problem (with the notation $A := (-\Delta \cdot + \cdot)$)

$$\frac{1}{2}\int_\Omega s(A^{-1}s)\ dx + \alpha\int_\Omega fs\ dx \to \min_{\substack{s\in L^\infty(\Omega)\\ \|s\|_\infty \leq 1}}.$$

This bound-constrained quadratic problem can be solved with efficient methods, we simply use a projected gradient approach, i.e.,

$$s^{k+1} = \mathbf{P}_1\left(s^k - \tau\left(A^{-1}s^k + \alpha f\right)\right),$$

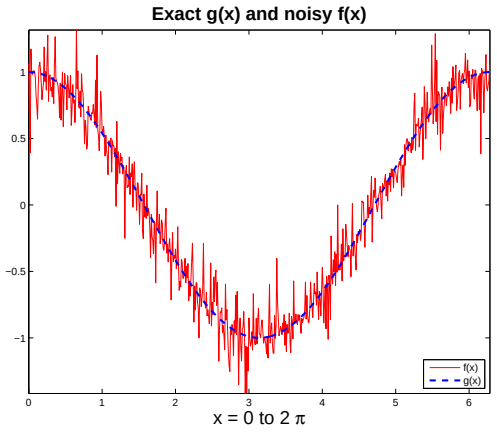

Figure 9.2: The exact function $g(x) = \cos(x)$, and the noisy function $f(x)$, corrupted by Laplace noise with mean zero, $\sigma = 0.1$ and $\delta \approx 0.1037$.

where $\tau > 0$ is a damping parameter and $\mathbf{P}_1$ is the pointwise projection operator

$$\mathbf{P}_1(v)(x) = \begin{cases} v(x) & \text{if } |v(x)| \leq 1 \\ \frac{v(x)}{|v(x)|} & \text{else} \end{cases} .$$

Due to the quadratic H^1 regularization we obtain

$$D_{H^1}^{\text{symm}}(\hat{u}, g) = 2D_{H^1}(\hat{u}, g) = \|\hat{u} - g\|_{H^1(\Omega)}^2 , \tag{9.2}$$

and the source condition becomes

$$\begin{aligned} q(x) &= -\Delta g(x) + g(x) , \quad \text{for } x \in \Omega \text{ and } q \in H^1(\Omega), \\ \frac{\partial q}{\partial n} &= 0 , \quad \text{for } x \in \partial\Omega. \end{aligned} \tag{SCH^1}$$

In the following we want to present two examples and their related error estimates.

Example 9.1. For our first data example we choose $g(x) = \cos(x)$, for $x \in [0, 2\pi]$. Since $g \in C^\infty([0, 2\pi])$ and $g'(0) = g'(2\pi) = 0$, the source condition (SCH^1) is fulfilled. Hence, the derived error estimates in Section 5.2 should work.

First of all we check (5.12) and (5.13) numerically for noise-free data, i.e. $f = g$ and $\delta = 0$. The estimates predict that as soon as $\alpha \leq \frac{1}{2}$ holds (note that $\|q\|_{L^\infty([0,2\pi])} = 2\,\|\cos(x)\|_{L^\infty([0,2\pi])} = 2$), the regularized solution $\hat{u}$ should be identical to the exact solution g in the Bregman distance setting (9.2). This is also found in computational practice, as Figure 9.1 confirms.

In the following we want to illustrate the sharpness of (5.13) in case of non-zero δ. For that reason, we have generated Laplace-distributed random variables and have added them to g, to obtain f. We have generated random variables with different values for the variance of the Laplace distribution, to obtain different noise levels δ in the L^1-measure. Figure 9.2 shows g and an exemplarily noisy version of g with $\delta \approx 0.1037$. In the following, we have computed δ as the L^1-norm over $[0, 2\pi]$, to adjust the dimension of δ to the H^1-norm (in the above example δ then approximately becomes $\delta \approx 0.6$).

In order to validate (5.13) we have produced many noisy functions f with different noise levels δ in the range of 0 to 2. For five fixed α values ($\alpha = 0.2$, $\alpha = 0.4$, $\alpha = 0.52$, $\alpha = 0.6$ and $\alpha = 1$)

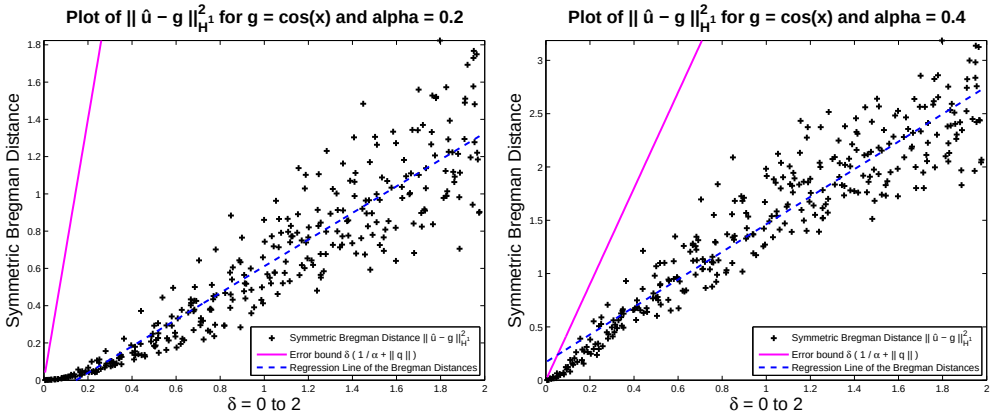

(a) $\alpha = 0.2$

(b) $\alpha = 0.4$

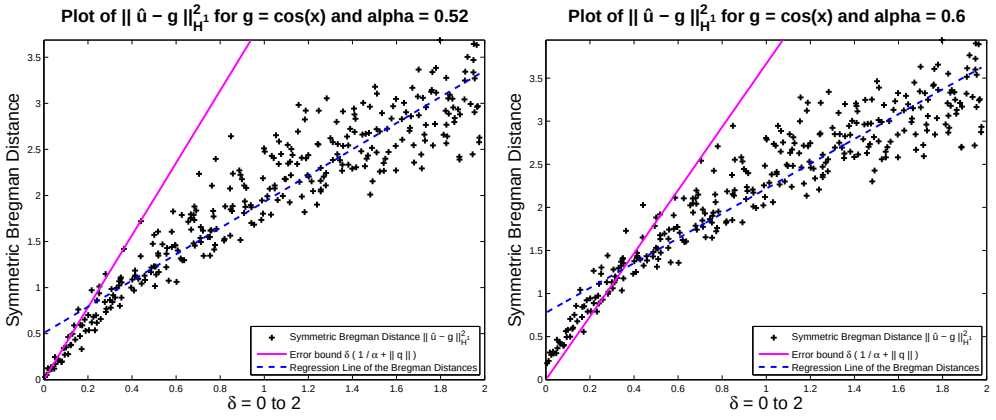

(c) $\alpha = 0.52$

(d) $\alpha = 0.6$

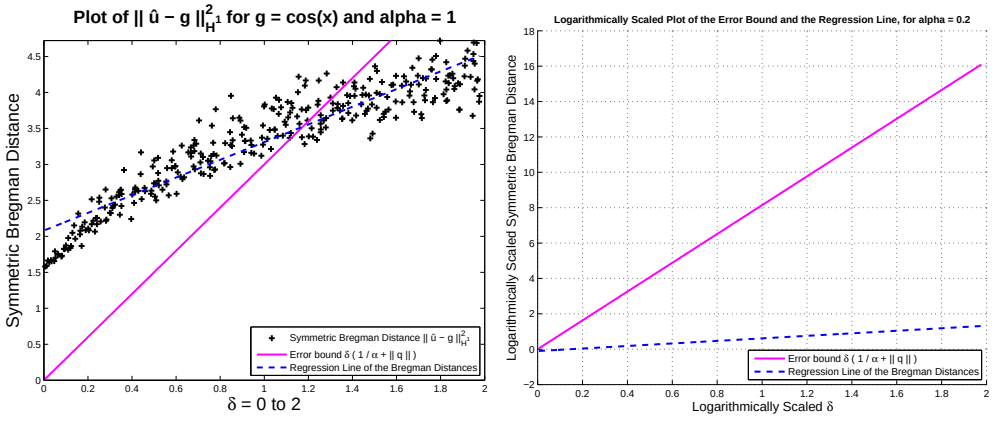

(e) $\alpha = 1$

(f) $\alpha = 0.2$

Figure 9.3: The plots of computed symmetric Bregman distances for $\alpha = 0.2,\ 0.4,\ 0.52,\ 0.6$ and $\alpha = 1$, against $\delta = 0$ to $\delta = 2$. It can be seen that in 9.3(a) and 9.3(b) the computed Bregman distances lie below the error bound derived in (5.13), while the distances in 9.3(c), 9.3(d) and 9.3(e) partly violate this bound. Figure 9.3(f) shows the logarithmically scaled error bound in comparison to the logarithmically scaled regression line of the Bregman distances for $\alpha = 0.2$. It can be observed, that the slope of the regression line is smaller than the slope of the error bound. Hence, for the particular choice of $g(x) = \cos(x)$ there might exist an even stronger error bound than (5.13).

we have plotted the symmetric Bregman distances between the regularized solutions $\hat{u}$ and g, the regression line of these distances and the error bound given via (5.13); the results can be seen in Figure 9.3. It can be observed that for $\alpha = 0.2$ and $\alpha = 0.4$ the computed Bregman distances lie below that bound, while for $\alpha = 0.52$, $\alpha = 0.6$ and $\alpha = 1$ the error bound is violated, which seems to be a good indicator of the sharpness of (5.13).

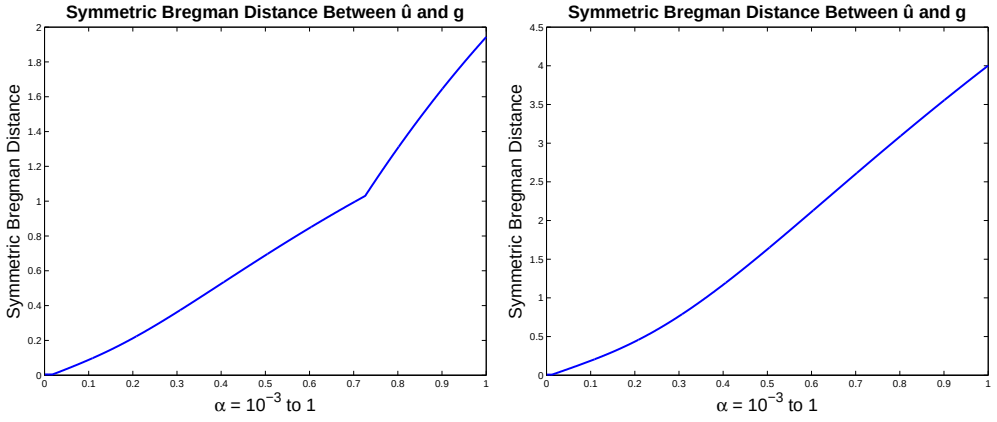

(a) $D_{H^1}^{\text{symm}}(\hat{u}, g_1)$ vs α (b) $D_{H^1}^{\text{symm}}(\hat{u}, g_2)$ vs α

Figure 9.4: The symmetric Bregman distances $D_{H^1}^{\text{symm}}(\hat{u}, g_1)$ 9.4(a) and $D_{H^1}^{\text{symm}}(\hat{u}, g_2)$ 9.4(b), for $\alpha \in [10^{-3}, 1]$.

Example 9.2. In order to validate the need for the source condition (SCH^1) we want to consider two more examples; $g_1(x) = \sin(x)$ and $g_2(x) = |x - \pi|$, $x \in [0, 2\pi]$. Both functions do violate (SCH^1); g_1 does not fulfill the Neumann boundary conditions, while the second derivative of g_2 is a δ-distribution centered at $\pi/2$ and therefore is not integrable. In case of g_2 there does not exist a q such that there could exist an α to guarantee (5.13). Nevertheless, in order to visualize that there exists no such error bound, we want to introduce a reference bound $\delta\left(1/\alpha + \|w\|_{L^\infty([0,2\pi])}\right)$ with $w(x) := -\Delta g_2(x) + g_2(x)$, $x \in ([0, \pi[) \cup (]\pi, 2\pi])$, which yields $\|w\|_{L^\infty([0,2\pi])} = \pi$.

As in Example 9.1 we want to begin with the case of exact data, i.e. $f = g$. If we plot the symmetric Bregman distance against α we obtain the graphs displayed in Figure 9.4. It can be seen that for g_1 as well as for g_2 the error tends to be zero only if α gets very small. To illustrate the importance of the source condition in the noisy case with non-zero δ we have proceeded as in Example 9.1. We have generated Laplace-type noise and added it to g_1 and g_2 to obtain f_1 and f_2 for different error values δ. Figure 9.5 shows the Bregman distance error in comparison to the error bound given via (5.13) and in comparison to the reference bound as described above, respectively. It can be seen that in comparison to Example 9.1 the error and reference bounds are completely violated, even for small α. Furthermore, in the worst case of g_2 for $\alpha = 1$ the slope of the logarithmically scaled regression line is equal to the slope of the reference bound, which indicates that the error assumingly will in general never get beyond this reference bounds. The results support the need for the source condition to find quantitative error estimates.

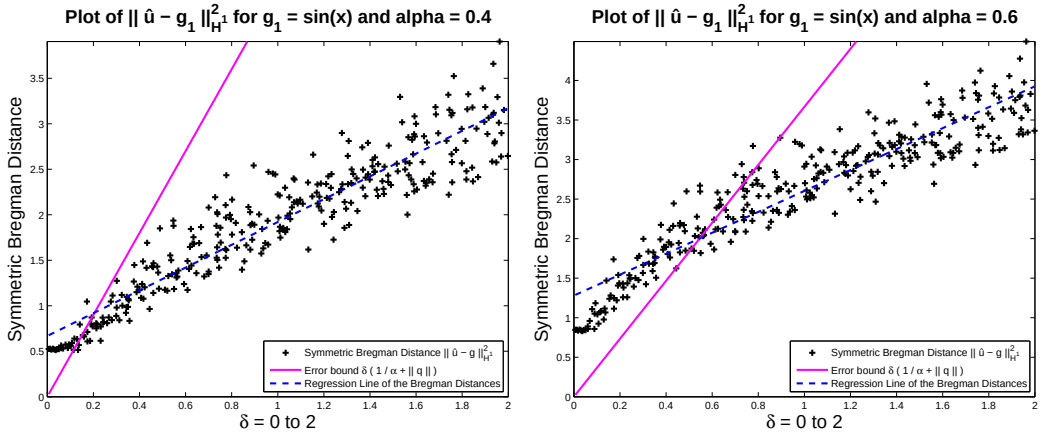

(a) $\alpha = 0.4$

(b) $\alpha = 0.6$

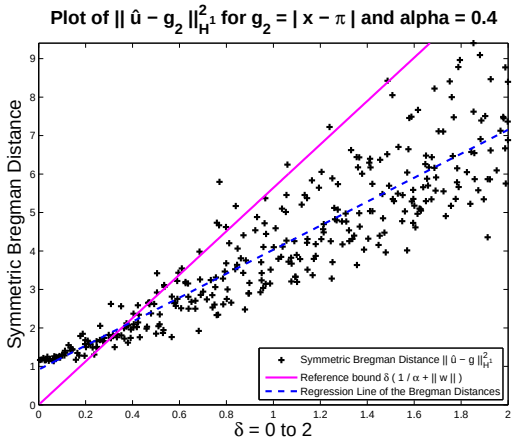

(c) $\alpha = 0.4$

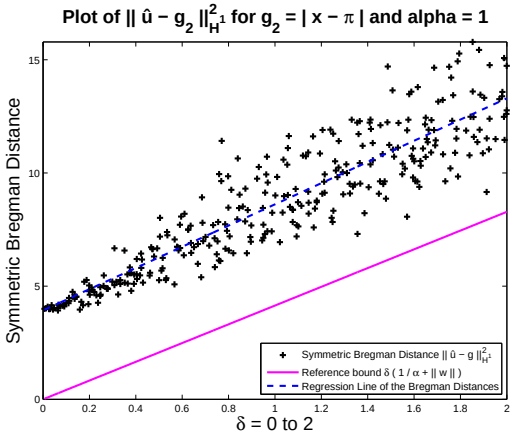

(d) $\alpha = 1$

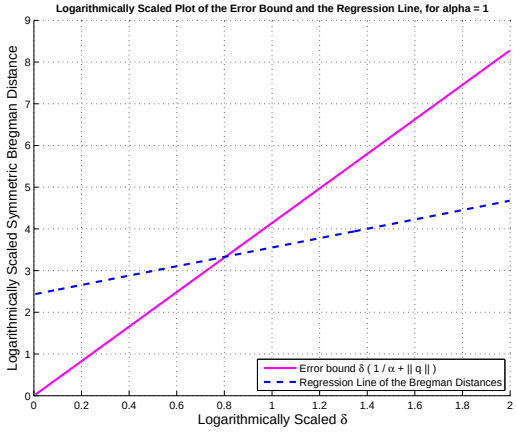

(e) $\alpha = 1$

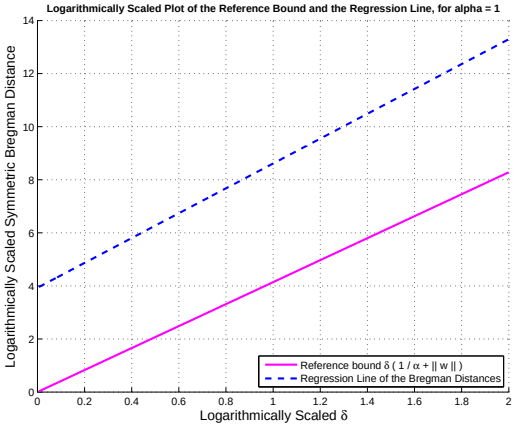

(f) $\alpha = 1$

Figure 9.5: The plots of the computed Bregman distances with violated (SCH^1). Figure 9.5(a) and Figure 9.5(b) show the Bregman distances $D_{H^1}^{\text{symm}}(\hat{u}, g_1)$ for $\alpha = 0.4$ and $\alpha = 0.6$, respectively. Figure 9.5(c) and Figure 9.5(d) represent the Bregman distances $D_{H^1}^{\text{symm}}(\hat{u}, g_2)$ for $\alpha = 0.4$ and $\alpha = 1$. Furthermore, Figure 9.5(e) and Figure 9.5(f) show the logarithmically scaled versions of the error/reference bound in comparison to a line regression of the Bregman distances for $\alpha = 1$.

Compressed Sensing with Poisson-Distributed Noise

For the validation of the error estimates in the Poisson case we want to consider the two-dimensional, fully discrete compressed sensing setup

$$\hat{u} \in \operatorname*{arg\,min}_{u \in \mathrm{dom}(\|W\cdot\|_{\ell^1})} \left\{ \sum_{l=1}^{k} \left[f_l \log\left(\frac{f_l}{(Ku)_l} \right) + (Ku)_l - f_l \right] + \alpha \|(Wu)\|_{\ell^1} \right\}, \tag{9.3}$$

with $W \in \mathbb{R}^{(mn)\times(mn)}$ being a level-6 Haar-wavelet transform matrix, $K \in \{0,1\}^{k\times(mn)}$ being a sensing matrix with $k \ll (mn)$ and $K^T\mathbf{1} = \mathbf{1}$, and for m and n being the dimensions of the 2D-variable u. In order to generate a specific example we set $m = n = 64$ and define an exact

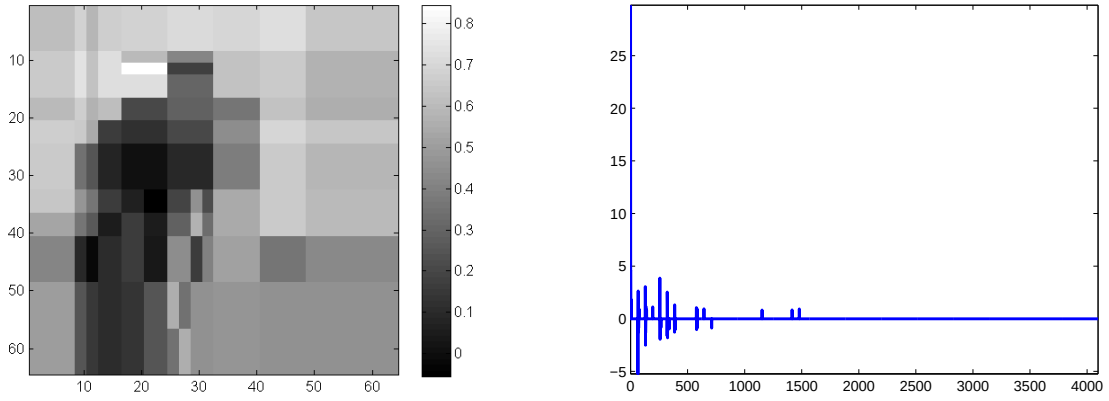

(a) $\tilde{u}$ (b) $W\tilde{u}$

Figure 9.6: The function $\tilde{u}$ and its 2D level-6 Haar-wavelet transform.

solution $\tilde{u}$ that can bee seen in Figure 9.6. The exact solution inheres a remarkable similarity to Matlabs famous camera man image, and moreover has a sparse representation with respect to the level-6 Haar-wavelet transform. Only 44 of the 4096 discrete values are non-zero values, while all other values equal zero. In the following we want to denote the index set of non-zero indices with I.

For the sensing matrix K we set $k = 1024$ and simply construct a matrix that randomly samples 1024 of the 4096 data points, i.e. each row of K consists of a single one and 4095 zeros. In addition we randomly add ones to each column if $K^T\mathbf{1} = \mathbf{1}$ is violated, in order to guarantee $K^T\mathbf{1} = \mathbf{1}$. The exact data g therefore is defined as the sensing $g = K\tilde{u}$. Conclusively, we corrupt the data g by Poisson distributed noise; we replace every data point g_l by a Poisson random variable with expected value $\lambda = g_l$.

In order to validate the error estimate (5.14) computationally, we want to find the vector q among all vectors q satisfying (SC1) with minimal supremum-norm $\|q\|_\infty$. The source condition for this setup reads

$$\xi = W^{-1}K^T q\,, \xi \in \mathrm{sign}(W\tilde{u})\,,$$

since W is invertible. Hence, we have to compute functions q and ξ such that $\xi = W^{-1}K^T q$ holds, and for which $\mathrm{sign}(P_I\xi) = \mathrm{sign}(P_I W\tilde{u})$ as well as $P_{I^c}\xi \in [-1,1]$ is guaranteed, with P_I denoting

the projection on I and with I^c representing the complement of I. Figure 9.7 shows the solutions q and ξ among all possible solutions for which q has the smallest supremum norm $\|q\|_\infty = 2$. Consequently, the error estimate (5.14) for this particular computational example reads as

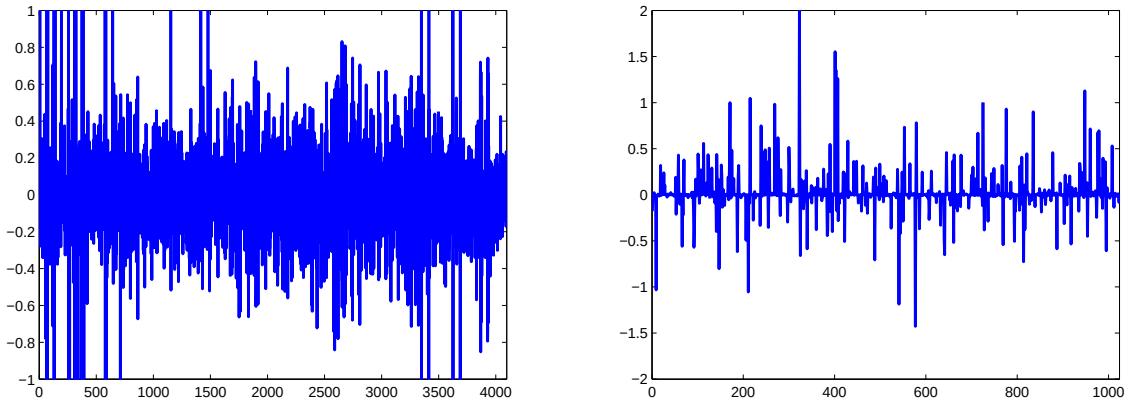

(a) ξ (b) q with $\|q\|_\infty = 2$

Figure 9.7: The vectors ξ and q that satisfy the source condition and for which q is the vector among all vectors q that satisfy (SC1) that has the smallest supremum norm, which is $\|q\|_\infty = 2$.

$$\begin{aligned}(1-c)KL(f,K\hat{u}) + \alpha D^{\text{symm}}_{\|W\cdot\|_{\ell^1}}(\hat{u},\tilde{u}) &\leq (1+c)\delta - c\left(\sum_{l=1}^{k} f_l\right)\left(\ln\left(1-4\frac{\alpha^2}{c^2}\right)\right) \\ &= (1+c)\delta - \gamma c\left(\ln\left(1-4\frac{\alpha^2}{c^2}\right)\right)\end{aligned}, \tag{9.4}$$

for $\alpha < c/2$ and $\gamma = \sum_{l=1}^{k} f_l$. Note that the factor γ has to be multiplied with the logarithm-term on the right-hand side, since we have not normed the data to ensure $\sum_{l=1}^{k} f_l = 1$ as it is necessary for the application of Theorem 5.6 without additional factor. We did several computations with different values for α and the constant $c \in]0,1[$ to support the error estimate (5.14). The results can be seen in Table 9.1. Note that the values of the symmetric Bregman distance $D^{\text{symm}}_{\|W\cdot\|_{\ell^1}}(\hat{u},\tilde{u})$ can easiliy be computed via

$$D^{\text{symm}}_{\|W\cdot\|_{\ell^1}}(\hat{u},\tilde{u}) = \sum_{i=1}^{mn}(\hat{p}_i - \xi_i)\left((W\hat{u})_i - (W\tilde{u})_i\right),$$

for $\hat{p} \in \text{sign}(W\hat{u})$.

The computational solution of (9.3) has been realized via Algorithm 5, while the subproblem has been solved with Algorithm 7 in case of $J(u) = \|Wu\|_{\ell^1}$. Since wavelet-regularization is not necessarily positivity preserving, we have furthermore added a projection step that ensures Wu to be positive.

9.1.2 Unbiased Recovery

In this section we want to support some of the results of Chapter 6 and Chapter 7 with computational examples. We therefore focus on L^1-type regularization functionals, namely TV and

		Left Hand Side		Right Hand Side	
c	α	$(1-c)\mathrm{KL}(f, K\hat{u})$	$D^{\mathrm{symm}}_{\|W\cdot\|_{\ell^1}}(\hat{u}, \tilde{u})$	$(1+c)\delta$	$-\gamma c\left(\ln\left(1-4\frac{\alpha^2}{c^2}\right)\right)$
0.99	0.494	0.6001	45.82	189.1	10390
0.99	0.329	0.3225	47.89	189.1	1099
0.99	0.164	0.0972	39.38	189.1	219.2
0.5	0.249	10.1	47.04	142.6	4599
0.5	0.1657	4.948	39.68	142.6	550.6
0.5	0.08233	1.396	23.68	142.6	109.3
0.1	0.049	0.9496	15.48	104.5	614.8
0.1	0.03233	0.4268	10.69	104.5	103.1
0.1	0.01567	0.1042	5.383	104.5	19.68
0.99	0.494	0.2782	5.663	40.61	10430
0.99	0.329	0.1981	6.964	40.61	1103
0.99	0.164	0.08013	9.872	40.61	220
0.5	0.249	7.14	8.846	30.61	4616
0.5	0.1657	4.068	9.856	30.61	552.6
0.5	0.08233	1.26	8.379	30.61	109.7
0.1	0.049	0.875	6.104	22.45	617.1
0.1	0.03233	0.3995	4.434	22.45	103.5
0.1	0.01567	0.09785	2.362	22.45	19.75
0.99	0.494	0.1853	7.357	20.41	10410
0.99	0.329	0.1353	2.513	20.41	1101
0.99	0.164	0.0665	4.044	20.41	219.5
0.5	0.249	5.4	1.723	15.38	4606
0.5	0.1657	3.371	4.005	15.38	551.4
0.5	0.08233	1.131	4.833	15.38	109.5
0.1	0.049	0.8154	3.761	11.28	615.8
0.1	0.03233	0.3774	2.852	11.28	103.3
0.1	0.01567	0.09396	1.581	11.28	19.71

Table 9.1: Comparison of the left hand and right-hand side of (9.4) for different parameters c, α and δ, and their consequent computations of f and $\hat{u}$. The right-hand side is always larger than the left hand side and hence, the results support the derived error estimate.

GTV_β, since they are one-homogeneous and do have a large multivalued subdifferential at the singular points, which will be of importance when applying the Theorems of Section 6.4, 7.1 and 7.2.

ROF Minimization

In case of ROF minimization we want to start with the sign-function of Example 6.5 again. For the sake of simplicity we are going to consider $\tilde{u}(x) = \mathrm{sign}(x)$ on the interval $x \in [-1, 1]$. As we have seen from Example 6.5, in that case $\tilde{u}$ is an Eigenfunction of TV with Eigenvalue $\lambda = 1$. Hence, for input data $f = \gamma\tilde{u}$, $\gamma \in \mathbb{R}_{>0}$, the solution of (4.6) for fixed α should be $\hat{u} = c\tilde{u}$, for $c = \gamma - \alpha$ and $\gamma > \alpha$, due to Theorem 6.3. In Figure 9.8 we actually see computational results of the ROF-model that have been realized with Algorithm 9 as described in Section 8.1.2, for

$\gamma = 1$ and the α-values $\alpha = 7/10$, $\alpha = 3/10$ and $\alpha = 1/20$. It can be seen that the computational

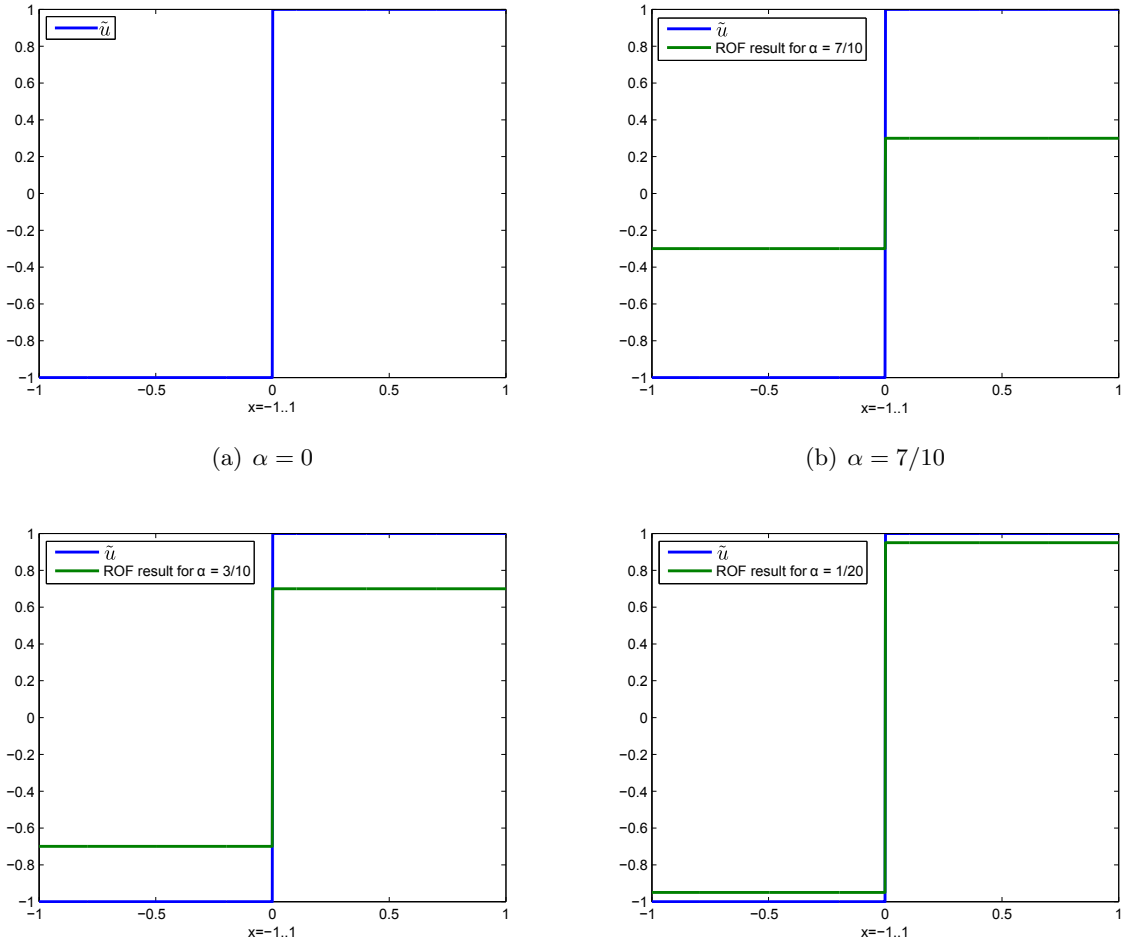

(a) $\alpha = 0$

(b) $\alpha = 7/10$

(c) $\alpha = 3/10$

(d) $\alpha = 1/20$

Figure 9.8: Exemplary ROF computations for $f(x) = \tilde{u}(x) = \text{sign}(x)$ on the interval $[-1, 1]$ and $\alpha = 7/10, 3/10, 1/20$. The data has been sampled with stepsize $h = 0.001$ at 2001 discrete points.

examples match with the analytical solution predicted by Theorem 6.3.

Obviously the case of exact data is rather trivial; more interesting is the case of noisy data $f = \tilde{u} + n$. For that reason we want to corrupt $\tilde{u}$ by a very specific noise n, given via

$$n(x) = A\cos(\varphi\pi x)\,,$$

with $A \in \mathbb{R}_{>0}$ and $\varphi \in \mathbb{Z}$ denoting the amplitude and the phase of the noise, respectively. The application of Theorem 6.4 states that for input data f the solution of (4.6) is given via $u = c\tilde{u}$ with $c = 1 - \alpha + (1 - \mu)/\eta$, if there exist constants μ and η that satisfy condition (6.9), i.e.

$$\mu\text{sign}(x) + \eta A\cos(\varphi\pi x) \in \partial\text{TV}(\text{sign}(x))\,. \tag{9.5}$$

In order to verify (9.5) we consider the function q with

$$q(x) = \mu(|x| - 1) + \frac{\eta A}{\varphi\pi}\sin(\varphi\pi x)$$

for which we want to show that it is a subgradient at $\tilde{u}$, i.e. $q' \in \partial \mathrm{TV}(\tilde{u})$. In analogy to the Eigenfunction examples of Section 6.3.2 we therefore have to prove that q fulfills the subdifferential properties. We easily check

- $q(-1) = q(1) = 0$,
- $\langle q', \tilde{u} \rangle_{L^2([-1,1])} = \mu \int_{-1}^{1} 1 \, dx = \mathrm{TV}(\tilde{u}) = 2$,

if we guarantee $\mu = 1$. In that case we can also ensure $|q(0)| = 1$ and, as an immediate consequence, the loss of contrast c simplifies to $c = 1 - \alpha$. The question that remains is: for which parameters can we guarantee $\|q\|_\infty < 1$ for $x \neq 0$? We will see that this condition is naturally satisfied if the amplitude of the noise is not too large and if the phase is not too small with respect to the regularization parameter α, which controls the bounds for η. If for instance we set $A = 1/10$ and $\varphi = 26$, and compute the ROF minimizers for the same values of α as we did for clean data, we discover that in order to apply Theorem 6.4 we need to ensure $\alpha \geq 1/\eta$. In particular, this means that for $\alpha = 7/10$ it follows that $\eta \geq 10/7$ needs to hold, while for $\alpha = 3/10$ we obtain the condition $\eta \geq 10/3$ and for $\alpha = 1/20$ the value of η even has to be larger or equal 20. However, for $\eta \geq 20$ we can compute $\|q\|_\infty > 1$ and hence, Theorem 6.4 is not applicable, while for $\eta = 10/7$ and $\eta = 10/3$ we obtain $\|q\|_\infty \leq 1$. From a theoretical point of view we can therefore ensure that for $\alpha = 7/10$ and $\alpha = 3/10$ the ROF minimum is $\hat{u} = c\tilde{u}$ with $c = 3/10$ and $c = 7/10$, respectively. But for $\alpha = 1/20$ we cannot conclude $c = 19/20$ as we did in the noise-free case. Moreover, computational results as shown in Figure 9.9 demonstrate that for $\alpha = 1/20$ the computed ROF solution indeed features parts of the noise.

Obviously, the considered noise has the specific structure that is does not affect the edge of $\tilde{u}$, which allows $\mu = \lambda$. If we would apply an ISS-related algorithm (e.g. Bregman iteration) on f with this specific type of noise we therefore could expect to recover $\tilde{u}$ perfectly despite the noise, since Theorem 7.4 states that there exists a time t_* such that $u(t_*) = \tilde{u}$ is the solution of the ISS.

However, realistically modeled noise usually affects the edge-set of an Eigenfunction and as a consequence, we have to face $\mu \neq \lambda$. More precisely, if for $x \in [-L, L]$ we assume $f(x) = \mathrm{sign}(x) + n(x)$ to be corrupted by noise $n(x)$ that satisfies $\int_{-L}^{L} n(x) \, dx = 0$ and $N(L) = N(-L) = 0$, for N being the primitive of n (i.e. $N'(x) = n(x)$), we observe the following. As an attempt to guarantee

$$\mu \mathrm{sign}(x) + \eta n(x) \in \partial \mathrm{TV}(\mathrm{sign}(x))$$

we define

$$q(x) = \mu \left(|x| - L \right) + \eta N(x) \,,$$

for which we obtain $q(L) = q(-L) = 0$ due to the definition of n. Moreover, we discover

$$\begin{aligned} \left\langle q', \mathrm{sign} \right\rangle_{L^2([-L,L])} &= \mu \int_{-L}^{L} 1 \, dx + \eta \left(\int_0^L n(x) \, dx - \int_{-L}^0 n(x) \, dx \right) \\ &= 2(\mu L - \eta N(0)) \,, \end{aligned} \tag{9.6}$$

which equals $\mathrm{TV}(\mathrm{sign}) = 2$ if η fulfills

$$\eta = \frac{\mu L - 1}{N(0)} \,. \tag{9.7}$$

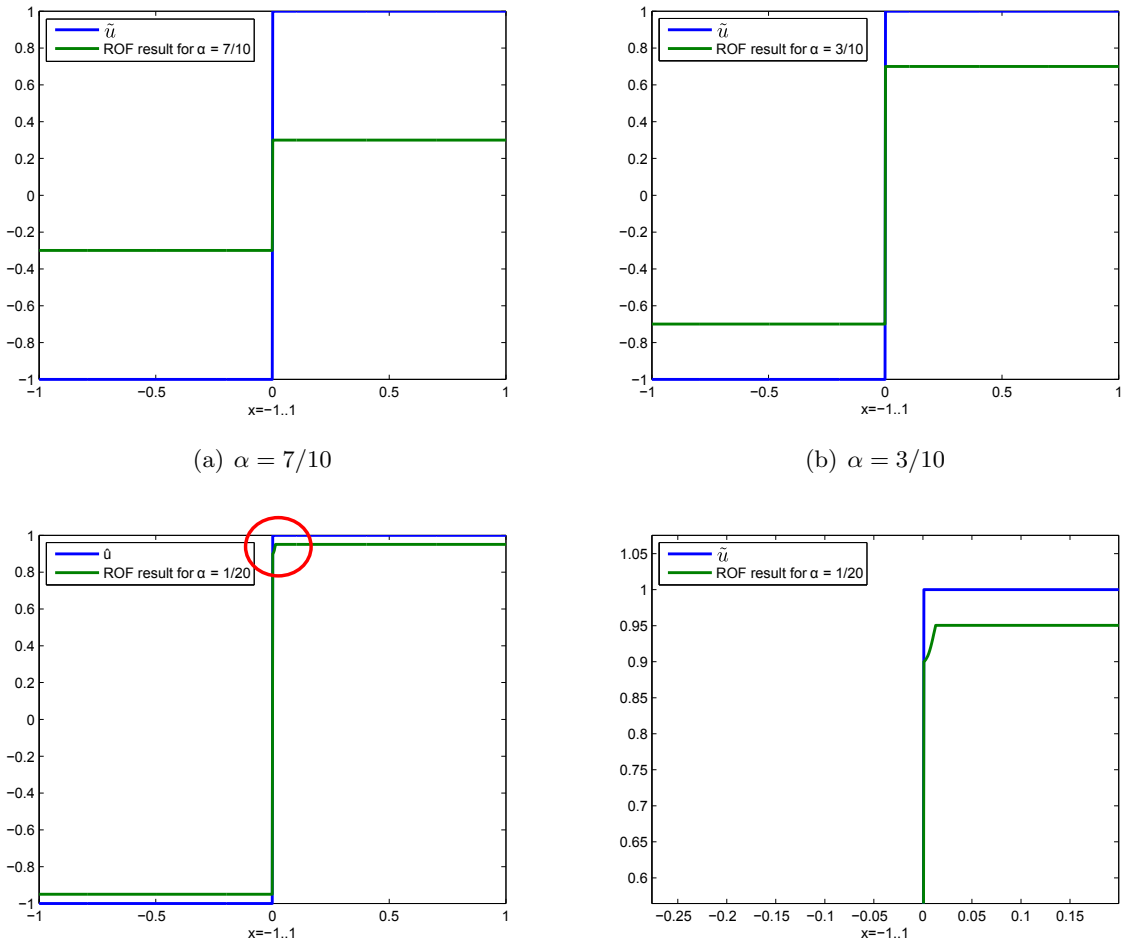

(a) $\alpha = 7/10$ (b) $\alpha = 3/10$

(c) $\alpha = 1/20$ (d) $\alpha = 1/20$

Figure 9.9: Exemplary ROF computations for $f(x) = \tilde{u}(x) + n(x)$ on the interval $[-1, 1]$ and $\alpha = 7/10, 3/10, 1/20$. The data has been sampled with stepsize $h = 0.001$ at 2001 discrete points. Figure 9.9(d) is a close-up of Figure 9.9(c).

From (9.6) and (9.7) we see that, in order to ensure $\eta > 0$, μ needs to be chosen such that

$$\begin{cases} \mu = \frac{1}{L} = \lambda & \text{if } N(0) = 0 \\ \mu > \frac{1}{L} = \lambda & \text{if } N(0) > 0 \\ \mu < \frac{1}{L} = \lambda & \text{if } N(0) < 0 \end{cases}$$

is guaranteed. Note that for the above noise-example $n(x) = A\cos(\varphi\pi x)$ the noise was defined to satisfy $N(0) = 0$. From Theorem 6.4 we know that η has to be large enough to guarantee $\eta \geq 1/\alpha$, consequently, in case of $N(0) > 0$, μ has to be chosen such that

$$\mu = \frac{1 + N(0)\eta}{L} \geq \frac{1 + \frac{N(0)}{\alpha}}{L} > \frac{1}{L}\,.$$

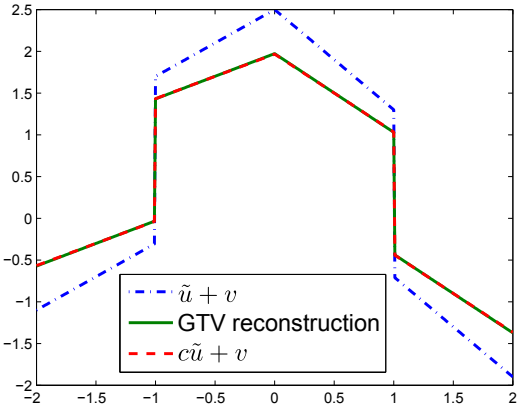

Figure 9.10: The functions $\tilde{u}+v$ and $c\tilde{u}+v$ for $c=11/15$, and a numerical reconstruction for $\alpha=2/5$ and $\beta=10/9$. The data has been sampled with stepsize $h=0.01$ at 401 discrete points.

The question if Theorem 6.4 is applicable again reduces to the question, for which regularization parameter α we still can ensure $\|q\|_\infty \leq 1$. In any case we obtain $q(0) = -\mu L + \eta N(0) = 0$, but if $\eta N(x)$ is too large in contrast to $\mu \operatorname{sign}(x)$ this likely yields $\|q\|_\infty > 1$. However, if Theorem 6.4 is applicable and if $N(0) > 0$, the loss of contrast can be computed via

$$c = 1 - \frac{\alpha}{L} + \frac{\frac{1}{L} - \frac{1+\frac{N(0)}{\alpha}}{L}}{\frac{1}{\alpha}} = 1 - \frac{\alpha + N(0)}{L},$$

for $L - N(0) > \alpha$.

Generalized Total Variation Regularization

Before we continue with the extensive investigation of the aISS Algorithm 12, we want to consider a brief example that describes the capability of subdifferential-invariant transforms in terms of an analytical computation of solutions of (2.8) for $J(u) = \mathrm{GTV}_\beta(u)$. Again, we want to consider the Eigenfunction Example 6.16 with $\tilde{u}(x) = 2H(1-|x|) - |x|$ on the interval $[-2,2]$. The corresponding Eigenvalue in that case reads as $\lambda = 2$ for $\beta = 10/9$. We want to perturb the function $\tilde{u}$ by a second, affine-linear function $v(x) = -x/5 + 1/2$, to obtain the input data $g(x) = \tilde{u}(x) + v(x)$. Since the subdifferential $\partial \mathrm{GTV}_{\frac{10}{9}}$ is invariant with respect to affine-linear transformations, we would expect a computational solution $\hat{u}$ to satisfy $\hat{u}(x) = c\tilde{u} + v(x)$ for $c = 1 - 2\alpha$. In Figure 9.10 we compare $\tilde{u}+v$, u and a solution of a computational realization of (2.8) for $J(u) = \mathrm{GTV}_\beta(u)$ and $\alpha = 2/5$. The computational realization of the GTV-model has been done via a Quasi-Newton approach similar to the one proposed in Section 8.1.2. Unlike Algorithm 9, an additional Lagrange multiplier ensuring $w = \mathrm{div} q$ and a second penalty term guaranteeing $\|w\|_\infty \leq \beta$ have been incorporated. Obviously the reconstruction and u coincide, demonstrating the ability of designing analytical solutions for variational schemes with singular regularization based on Eigenfunctions and subdifferential-invariant transformations.

9.1.3 AISS on a Random Matrix

To get a better understanding of the behavior of the adaptive inverse scale space flow of Algorithm 12, let us take a look at the simple case of generating a matrix $K \in \mathbb{R}^{m \times n}$, $n \ll m$, with random values between 0.5 and -0.5. We normalize each column with respect to the two-norm and generate a signal $\tilde{u}$ which has random values between -5 and 5 at s random indices, where the sparsity level s is small in comparison to the size n of the signal. The data is generated as $f = K\tilde{u}$. Figure 9.11 shows the aISS iterations as well as $\tilde{u}$ for an example of $n = 50$, $m = 1000$, and $s = 5$. We can see that on the first seven iterations aISS reconstructs one peak at a time. The first three peaks are indeed peaks of the true solution. The peaks reconstructed in iteration four and five are not part of the true solution. However, in the course of the iteration aISS does find the remaining two true peaks and immediately eliminates the three false peaks in the last iteration as the subgradient of the last missing peak (at index 310) reaches 1 and therefore is included in the support. In the following section we want to provide a detailed analysis on the differences,

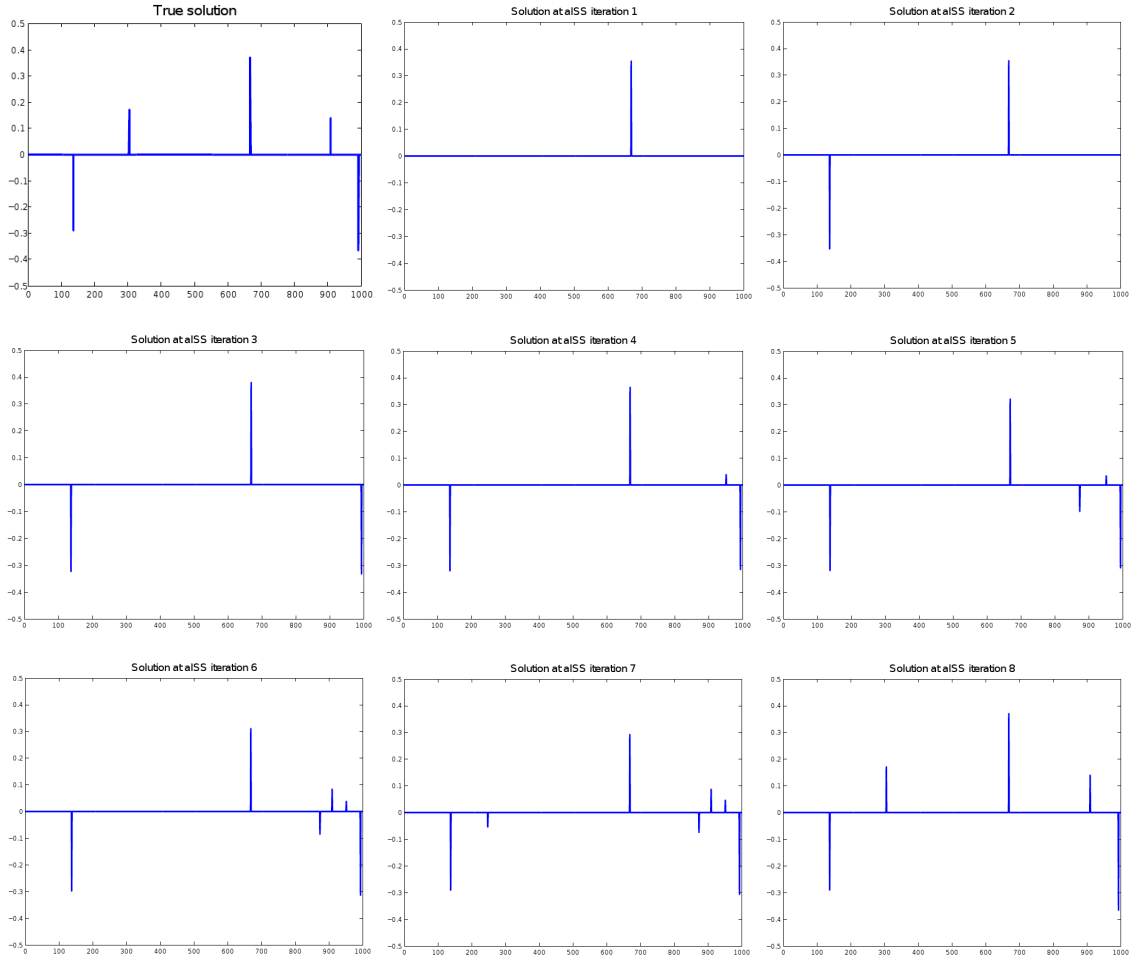

Figure 9.11: Example iteration of the aISS method for a random matrix. The true input signal is shown in the upper left.

advantages and disadvantages of either the OMP Algorithm 11 and the aISS Algorithm 12.

9.1.4 Comparison: OMP vs ISS

In this subsection we compare aISS and OMP in two steps. First, we will describe the problem of monotonic increase of the support of OMP and present an algorithm to construct a sensing matrix K and a signal f for which OMP fails. Second, we will compare aISS and OMP on different types of matrices including random matrices, combined wavelet matrices, and ill-conditioned matrices arising in dynamic Positron Emission Tomography (PET) to see how frequently the problem setup we present in the next subsection occurs in realistic, practical settings.

A counter example for OMP

As discussed before, a major difference between OMP and aISS is that OMP never decreases the support of the solution and (in the terminology of aISS) resets the dual variable/subgradient after each iteration, whereas aISS is able to decrease its support and to continuously evolve the subgradient, taking the information of all previous iterations into account. In this subsection we will show that this difference can have a major effect on the reconstruction results leading to arbitrarily non-sparse results of OMP while aISS can still recover the exact solution. We can construct an example for which OMP fails as follows: Assume we have data f which can be written as $f = c(v_1 + v_2)$ for two normalized vectors v_1, v_2 and a constant c. We will include v_1 and v_2 in our matrix K, since this will guarantee the sparsest solution of $Ku = f$ to be 2-sparse. We start the construction of K by choosing a small ϵ, setting $K^0 = \emptyset$, and define an $r_0 = f$, which will correspond to the residual in the construction. Let $f \in \mathbb{R}^n$, then we iteratively choose for $i = 1, ..., n$

1. $K^i = [K^{i-1}, r_{i-1} - \epsilon e_i]$
2. $r_i = f - K^i((K^i)^\dagger f)$,

where $(K^i)^\dagger$ denotes the generalized inverse of the current matrix K^i. The first step takes the current residual and deflects it by a small ϵ in the direction of the i^{th} unit normal vector. This will make OMP select this vector in the i^{th} step since for ϵ small enough, the correlation of this vector to the current residual will be maximal. However, the small disturbance will lead to OMP not having converged yet. Therefore, we compute the next residual r_i that will come up in the OMP algorithm and again provide a column in K^i that has a very high correlation to this residual but does not enable the method to solve $K^i u = f$ exactly. Iteratively, we construct n such vectors. Note that n is the least sparse vector one can get for the description of $f \in \mathbb{R}^n$, since any additional vector would automatically be linearly dependent. Finally, we add v_1 and v_2 as the last two columns to obtain the final $K = [K^n v_1 v_2]$, which we normalize afterwards.

Although v_1 and v_2 are sufficient to describe f they will likely not have the highest correlation to any residual of OMP. Figure 9.12 shows some iterations of the OMP algorithm on an K constructed as described above with $n = 50$ and $v_1 = e_n$, $v_2 = e_{n-1}$, $f = 0.5v_1 + 0.5v_2$, $\epsilon = 0.15$. As we can see OMP indeed adds one component after the other until at the 50^{th} iteration it finally has the maximum number of linearly independent vectors in $\mathbb{R}^n$ and can therefore reconstruct f exactly. The OMP answer is as non-sparse as possible although the input signal was 2-sparse (which is the sparsest possible without being reconstructed in 1 iteration by either of the two methods aISS or OMP).

Now let us take a look at the iteration of aISS for the same example. Figure 9.13 shows not only the solution at each iteration but also the corresponding subgradient since this is crucial for understanding the difference between the two methods. We can see that the first three iterations

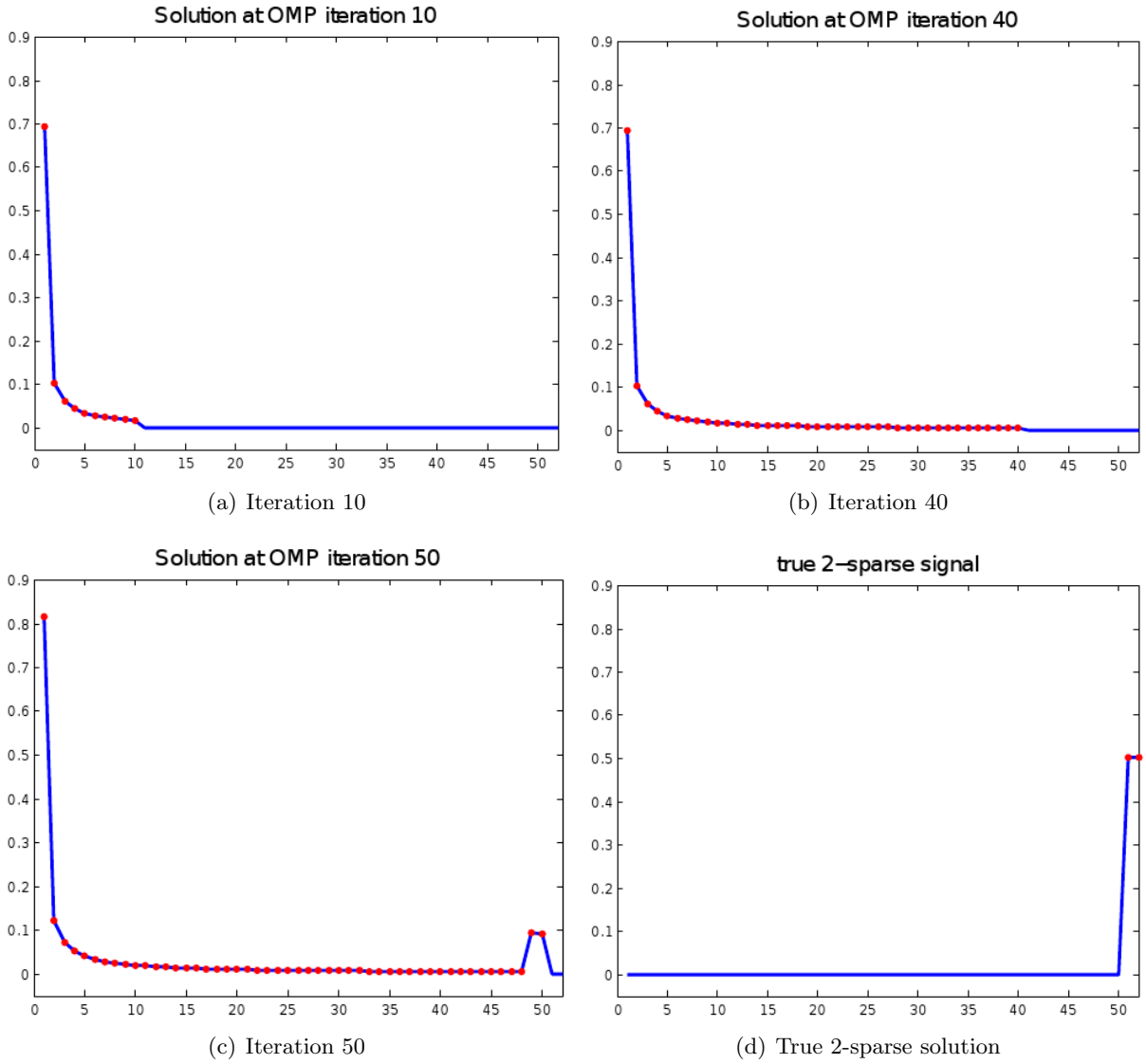

(a) Iteration 10

(b) Iteration 40

(c) Iteration 50

(d) True 2-sparse solution

Figure 9.12: Iterates of OMP on a constructed example. Red dots indicate the coefficients at which the current solution is non-zero.

coincide with the OMP method, and components corresponding to a high correlation with the residual are added to the set of non-zero elements. However, the subgradient shows that aISS 'sees' that the last two components in the matrix K also have a good correlation to the signal f. Their correlation is not as high as for the first columns of K which is why neither aISS nor OMP added them immediately. However, OMP basically resets the subgradient at each iteration and includes the vector with the highest correlation to the residual. aISS on the contrary, does not reset the subgradient and keeps adding to the correlation of the last 2 vectors until, at iteration 4, the subgradient of components 51 and 52 hits 1, which immediately leads to the right, 2-sparse answer. aISS converged in only 4 iterations to the correct answer while OMP converged in 50 iterations to the least sparse answer possible.

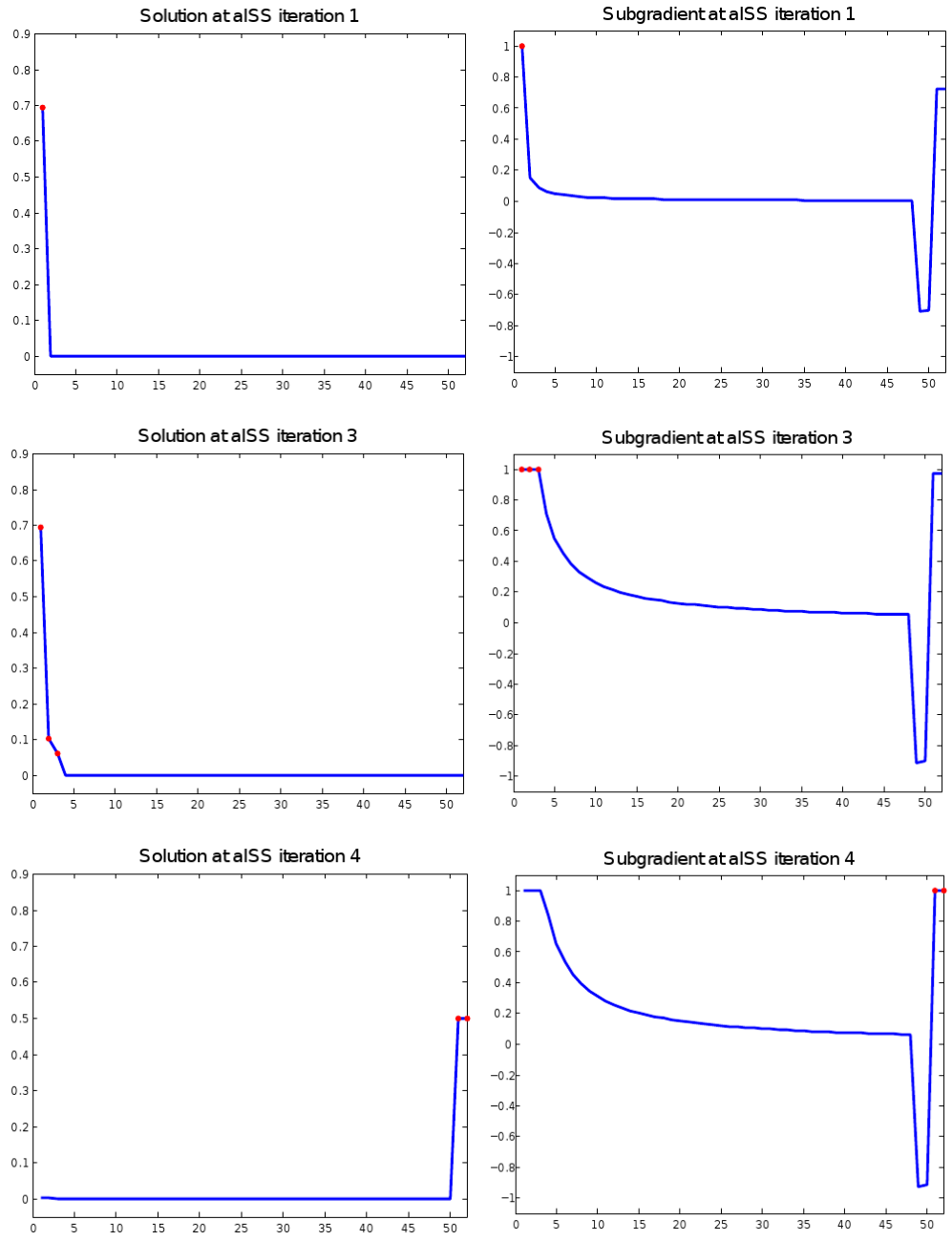

Figure 9.13: Iterates of aISS on constructed example. Red dots indicate the coefficients at which the current solution is non-zero.

Random Matrices and Combined Wavelet Basis

In this subsection we will investigate how aISS and OMP compare on noise free data. The criteria for our comparison will be

1. Frequency of exact recovery of the sparsest signal,

2. Sparsity of the solution each algorithm found, i.e. number of non-zero elements $\|u\|_{\ell^0}$,

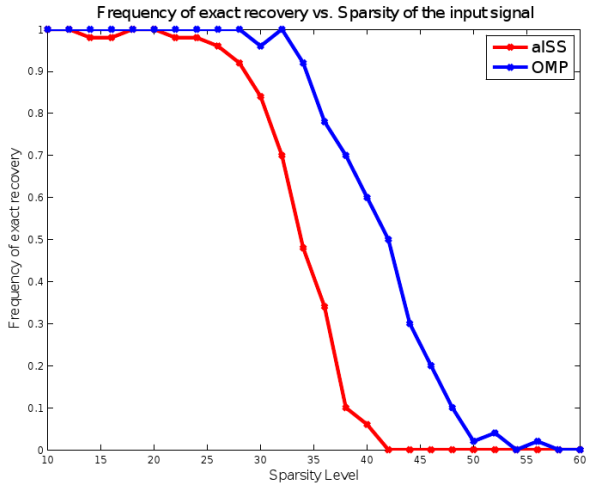

(a) Frequency of exact recovery

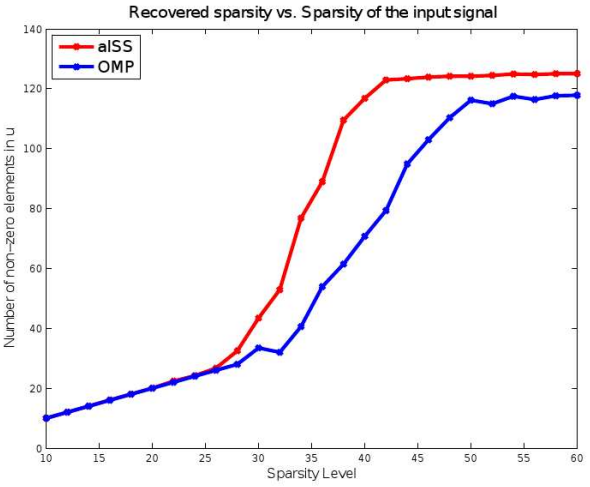

(b) Number of non-zero coefficients

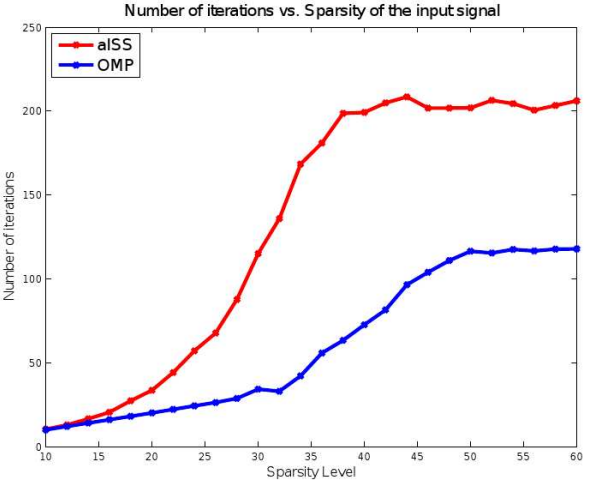

(c) Number of iterations

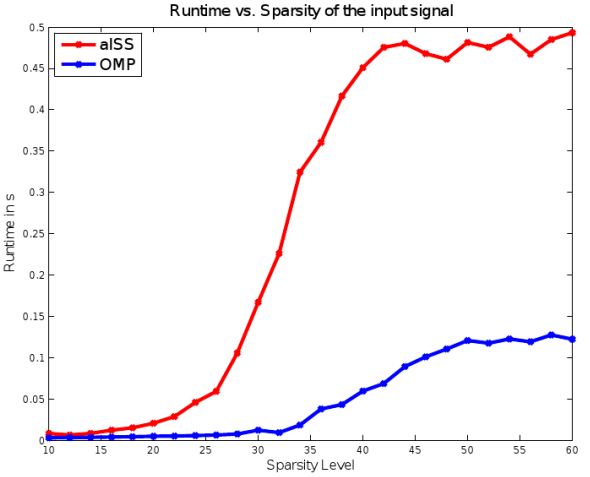

(d) Runtime

Figure 9.14: Comparison of OMP and aISS on random matrices and input signals with random values. The plots show the comparison metrics with respect to the sparsity level of the input signal.

3. Number of iterations each algorithm took,

4. Runtime of each algorithm.

The tests will be based on cases, where neither of the two algorithms is guaranteed to converge to the sparsest solution (for theoretical guarantees for this kind of convergence see for instance [93]). Notice, that aISS will always converge to the ℓ^1 minimizing solution of $Ku = f$. The criteria of frequency of exact recovery as well as sparsity of the solution are therefore rather based on the question whether the ℓ^1 minimizing solution coincides with the ℓ^0 minimizing solution than a convergence/quality property of our algorithm in particular. The examples where aISS does not reconstruct the sparsest solution are therefore a violation of the requirements we need for the ℓ^1 minimizing solution to be the sparsest solution.

In the first experiment we generate a matrix $K \in \mathbb{R}^{128\times512}$ with random entries between -0.5 and 0.5. Then, we normalize each column of K and generate a signal $\tilde{u}$ also with random values between -0.5 and 0.5 at s random indices. s is the sparsity level of the true, sparsest solution. We vary s from 10 to 60, run each algorithm 50 times per s, and record the comparison metrics described above. Figure 9.14 shows the results among all sparsity levels.

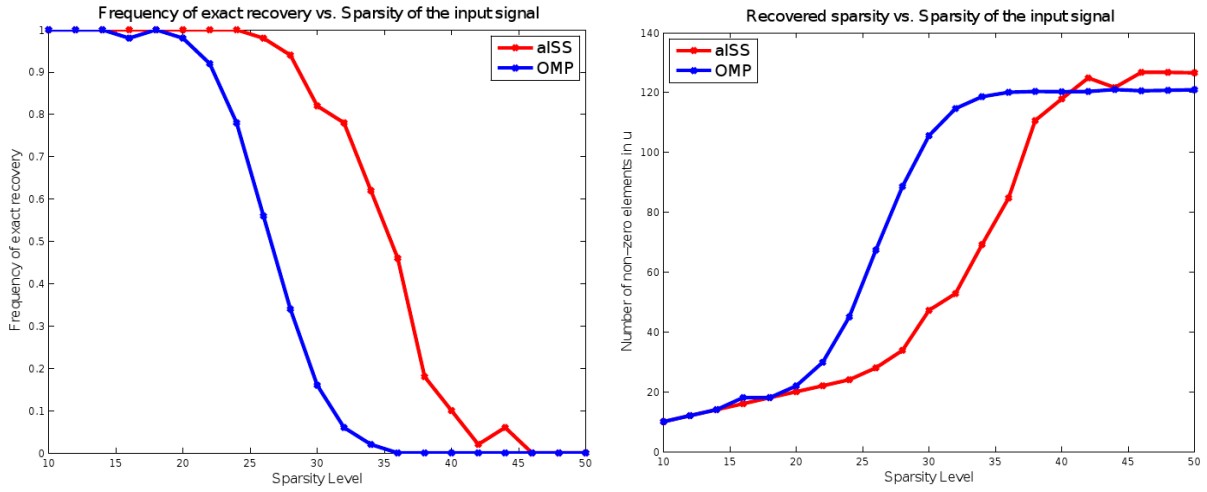

(a) Frequency of exact recovery

(b) Number of non-zero coefficients

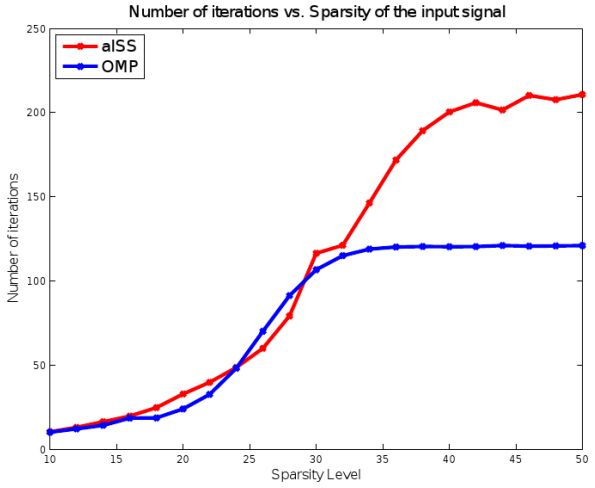

(c) Number of iterations

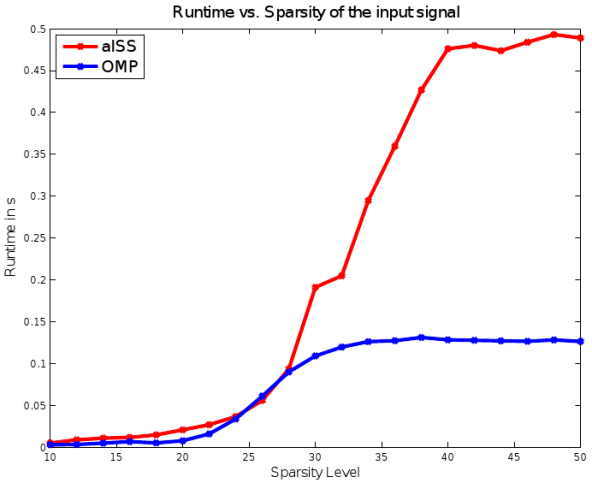

(d) Runtime

Figure 9.15: Comparison of OMP and aISS on random matrices and input signals with random $+1$ and -1 values. The plots show the comparison metrics with respect to the sparsity level of the input signal.

We can see that the greedy approach to ℓ^0 minimization works much better in this example. The frequency of exact recovery is higher, and even for the cases where the sparsest solution is not recovered exactly, the sparsity of the OMP solution is much better than for the aISS solution. Furthermore, OMP obtained its results in fewer iterations and less runtime.

Despite the very good results OMP gave in this example, we will see that this is not the case in general. In our second example, we create the random matrix K in the same fashion as in the previous experiment. The only change is that we generate the signal $\tilde{u}$ as a random sign function

at s coefficients, i.e. we set s values in $\tilde{u}$ randomly to -1 or $+1$. As we can see in Figure 9.15 this changes the results dramatically.

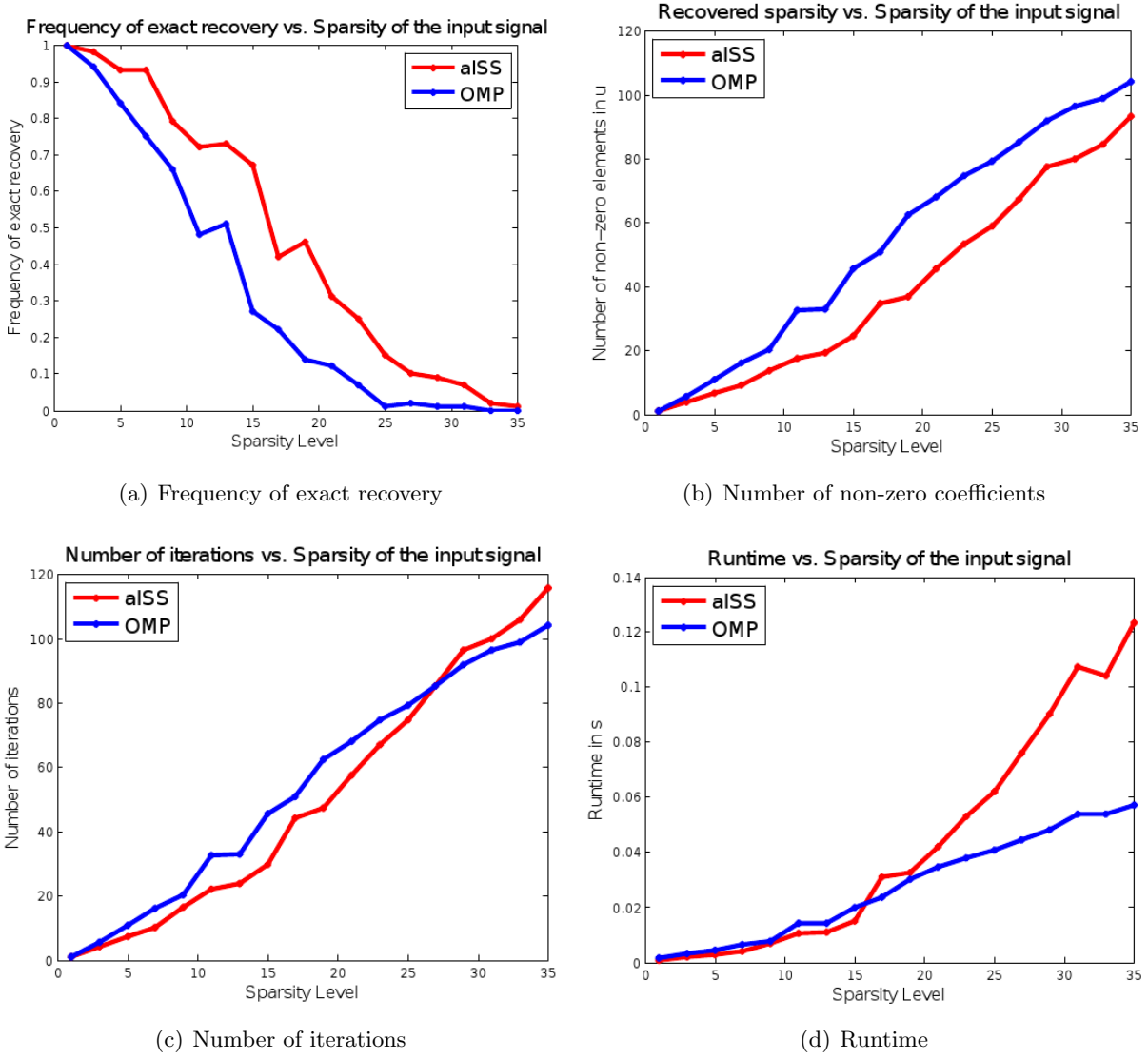

(a) Frequency of exact recovery

(b) Number of non-zero coefficients

(c) Number of iterations

(d) Runtime

Figure 9.16: Comparison of OMP and aISS on a matrix of combined 'Haar' and 'Daubechies4' wavelet basis and input signals with random values. The plots show the comparison metrics with respect to the sparsity level of the input signal.

In this case, aISS clearly outperforms OMP regarding the quality of the results, yielding better frequency of recovery and sparser solutions. It is interesting to see that the aISS recovery frequency stays almost the same as in the previous example, whereas the recovery frequency of OMP dropped significantly. Note that the number of iterations of OMP and aISS is very similar up to a sparsity of 32 of the input signal. The runtime is almost the same up to a sparsity of 28. After that, aISS pays for the higher accuracy and higher sparsity with more computational effort – however, even for the most complex example the runtime is below 0.5 seconds using a Laptop with 2Ghz dual core processor and 3GB memory.

We obtain similar results on more structured, over-complete bases like the combination of Matlabs 'Haar' and 'Daubechies4' bases for a level 6 decomposition. With K being generated as the normalized combination of those two bases, again using 128 to be the number of rows of K, we choose a signal $\tilde{u}$ also with random values between -0.5 and 0.5 at s random indices. Figure 9.16 shows the comparison of OMP and aISS in this test case. First of all we can see that

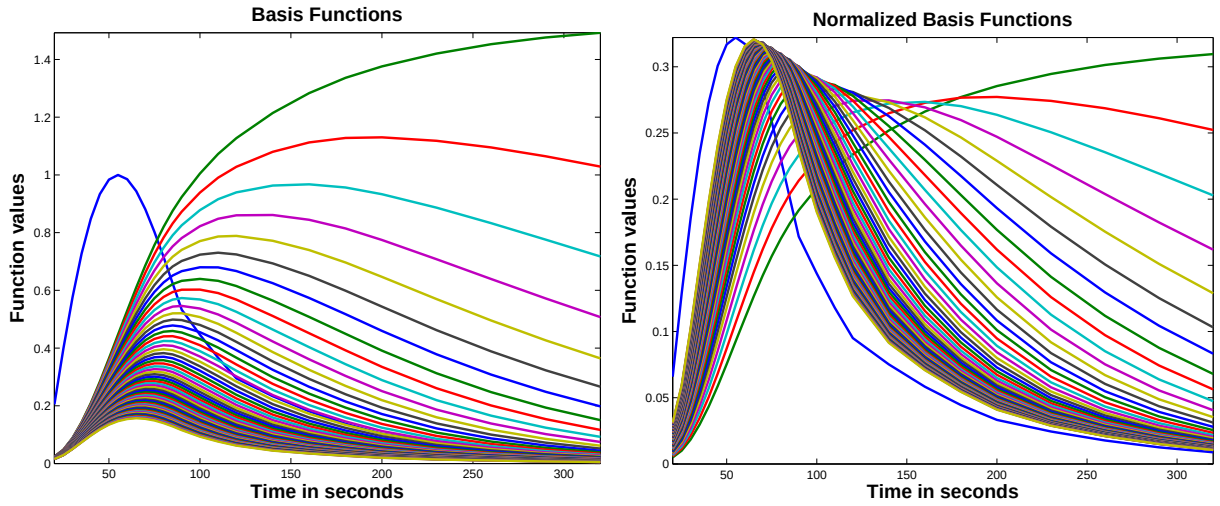

(a) Basis Functions (b) Normalized Basis Functions

Figure 9.17: The columns of K as defined in this section. The left-hand-side shows the columns, representing the basis functions (9.9). The right-hand-side shows the normalized columns with respect to the 2-norm.

this example was more challenging for both algorithms yielding a lower frequency of recovery at earlier iterations in comparison to the random matrices. Again, aISS outperforms OMP in terms of frequency of exact recovery and sparsity of the recovered signal. In this case, even the number of iterations is similar, whereas the runtime is similar up to iteration 20, then increasing stronger but still being relatively fast.

As mentioned earlier, aISS finds the ℓ^1 minimizer which might not be the sparsest solution. Thus, we could also compare two other cases: If among all examples mentioned above, we compare OMP and aISS only on the cases where both methods reconstruct the sparsest solution exactly, OMP gives the correct result faster only needing about 0.0045 seconds whereas aISS needs 0.027 seconds on average. This difference in speed is also due to the average number of iterations needed to find the solution which is 16.2 for OMP and 30.3 for aISS. Comparing the methods only for the cases where the ℓ^1 minimizing solution coincides with the ℓ^0 minimizing solution we have a sparsest signal recovery rate of 100% for aISS and about 75.8% for OMP. In these examples the average OMP solution is much more dense with an average number of non-zero coefficients of 32.4 opposed to 17.3 for the aISS solutions. To also compare OMP and aISS on matrices K used in practical applications we will discuss temporal basis functions for dynamic PET in the next subsection.

Temporal Basis Functions for Dynamic PET

In [102] an exponential basis operator has been introduced in order to improve dynamic Positron Emission Tomography (PET) images. For applications like e.g. myocardial perfusion quantifi-

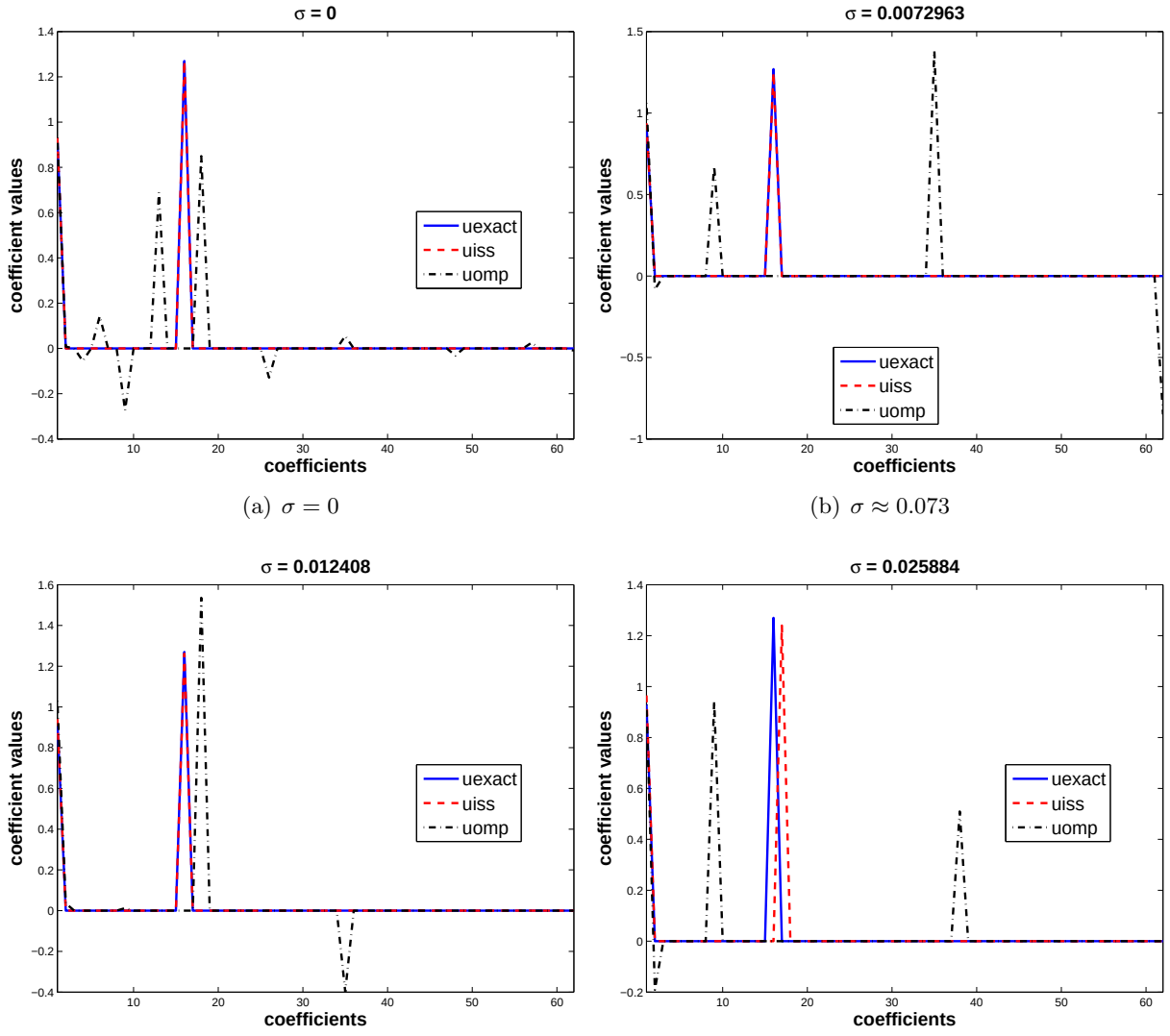

(a) $\sigma = 0$ (b) $\sigma \approx 0.073$

(c) $\sigma \approx 0.0124$ (d) $\sigma \approx 0.0260$

Figure 9.18: Comparison of particular aISS and OMP reconstructions with the true coefficients in the noise-free (Figure 9.18(a)) and in the noisy case (Figure 9.18(b) – 9.18(d)), for varying standard deviation σ.

cation (see for instance [10] and Section 9.2) it is a standard assumption that the measured dynamic signal is a composition of a so-called input function (which we assume to be known) and a Laplace-convolution of that input function with a specific exponential function. In this short computational example we therefore intend to solve the inverse problem $Ku = f$ with the operator K given as the linear combination

$$(Ku)(t) := u_0 h(t) + \sum_{n=1}^{N} u_n \tilde{b}_n(t)\,, \tag{9.8}$$

of basis functions $\tilde{b}_n(t)$ defined as

$$\tilde{b}_n(t) := \int_0^t h(\tau) \exp\left(-b_n\left(t-\tau\right)\right)\, d\tau\,, \tag{9.9}$$

for a given positive input function $h : [0,T] \to \mathbb{R}_{>0}$ and a given vector $b = (b_n)_{n\in\{1,\dots,N\}}$ containing non-negative real values.

For the sake of simplicity, we focus on a one-dimensional setting; To simulate input data realistically, we sample the time $t \in [0,T]$, with $T = 320$ seconds, at 26 discrete points $\{20, 25, 30, 35, 40, 45, 50, 55, 60, 65, 70, 75, 80, 85, 90, 100, 110, 120, 140, 160, 180, 200, 230, 260, 290, 320\}$. The basis functions $\tilde{b}_n$ were computed on a finer grid via a simple Euler-scheme, for $N = 61$ given values $b_n \in [0,6]$ with stepsize 0.1, and were subsequently sampled at the discrete temporal points. The underlying function h is defined as $h(t) := \frac{t}{64}\exp\left(-\frac{-t^2}{128}\right)$ and normalized with respect to the $\|\cdot\|_\infty$-norm.

Hence, we obtain a fully discrete matrix $K \in \mathbb{R}^{26\times 62}$, for which its columns (which are the discrete analogue of the basis functions $\tilde{b}_n$) can be seen in Figure 9.17. As in the previous examples we are going to normalize the columns of K in order to weight the basis functions correctly and not to distort reconstructions. Figure 9.17 makes already clear that the considered matrix is very ill-conditioned, since the columns appear to be very similar to each other. As described above it is very natural to assume the exact signal g to be a composition of the function h and one single basis function. We therefore define an example such that the true coefficients are given as the vector

$$\tilde{u}^j := \begin{cases} \approx 0.931 & \text{if } j = 0 \\ \approx 1.270 & \text{if } j = 15 \\ 0 & \text{else} \end{cases}$$

and the exact data $g = K\tilde{u}$. Moreover, we compute a set of noisy datum f, for which we disturb g with normal-distributed noise with mean zero and standard-deviation σ. In Table 9.2 we have

Noise Level	$\sigma = 0$		$\sigma = 0.0075$		$\sigma = 0.0125$		$\sigma = 0.03$	
Method	aISS	OMP	aISS	OMP	aISS	OMP	aISS	OMP
Runtime	0.004041	0.0008346	0.004103	0.0005302	0.004306	0.0005242	0.004577	0.0005098
ℓ^0-norm	2	12	2.27	4.971	2.099	4.611	2.073	4.152
ℓ^1-norm	2.201	3.198	2.199	3.473	2.198	3.378	2.189	3.217
$\frac{\|\hat{u}-\tilde{u}\|_{\ell^1}}{\|\tilde{u}\|_{\ell^1}}$	0	1.607	0.3493	1.744	0.5658	1.739	0.9673	1.721
$\|A\hat{u}-g\|_{\ell^2}$	0	0	0.002058	0.003509	0.00364	0.005829	0.009601	0.01206
$\|A\hat{u}-f\|_{\ell^2}$	0	0	0.007254	0.006916	0.01215	0.01158	0.02939	0.02789
No. of iter.	22	12	22.58	4.971	23.77	4.611	25.11	4.152

Table 9.2: Comparison of aISS and OMP for the matrix K as defined in (9.8) with normalized columns in terms of runtime, sparsity of $\hat{u}$ (ℓ^0), ℓ^1-norm, error to $\tilde{u}$, standard-deviation between $K\hat{u}$ and g and standard-deviation between $K\hat{u}$ and f. The results are average values for each σ-value. All computations have been made on a laptop with a 2.53 GHz dual core processor and 4 GB memory.

listed the results of several computations with metric values similar to the ones of the previous comparisons. We have compared the runtime, the total number of non-zero coefficients, the ℓ^1-norms as well as a normed ℓ^1-difference between $\hat{u}$ and $\tilde{u}$ (with $\hat{u}$ denoting the reconstruction), and the standard-deviations between $K\hat{u}$ and g and $K\hat{u}$ and f, respectively, for different noise

levels σ. The results are average values over 1000 computations for each value of σ. In case of $\sigma \neq 0$ we have stopped the aISS- and OMP-computations according to the discrepancy principle that if the standard-deviation between $\hat{u}$ and f is below σ the computation is stopped.

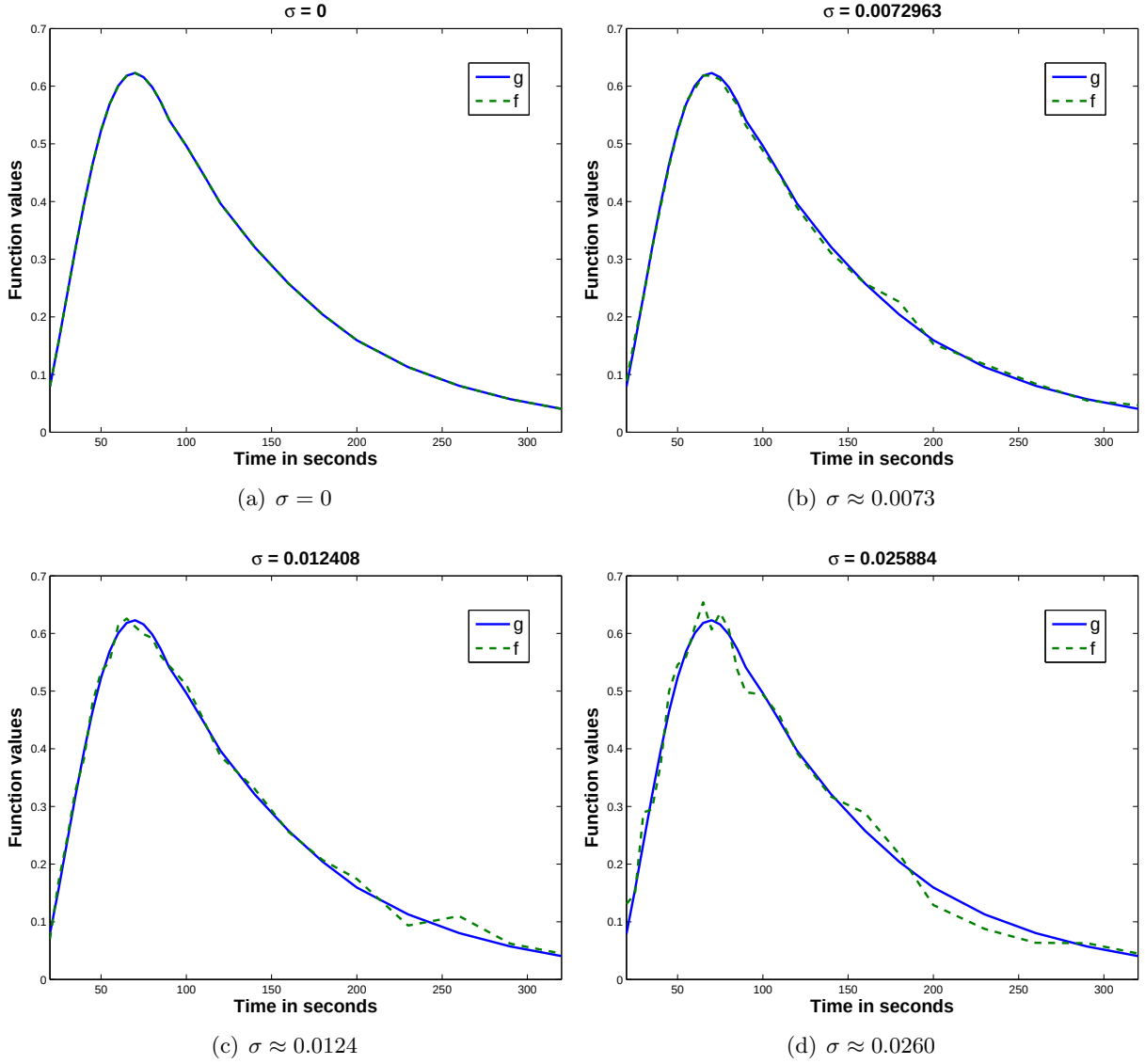

(a) $\sigma = 0$

(b) $\sigma \approx 0.0073$

(c) $\sigma \approx 0.0124$

(d) $\sigma \approx 0.0260$

Figure 9.19: The function g and different noisy functions f, for which the noise has standard deviation σ.

It can be seen that for any σ the OMP algorithm needs less iterations and therefore less runtime than the aISS algorithm. However, regarding the quality of the results aISS outperforms OMP for each σ-value, which we would also expect since the matrix is highly ill-conditioned. In the noise-free case aISS perfectly recovers the two desired coefficients after 21 iterations, while OMP recovers 12 coefficients in order to somehow approximate the exact data without reconstructing a sparse solution. In the presence of noise and by applying the discrepancy principle (which might not guarantee the algorithm to stop at the iteration that produces the best result) we see that

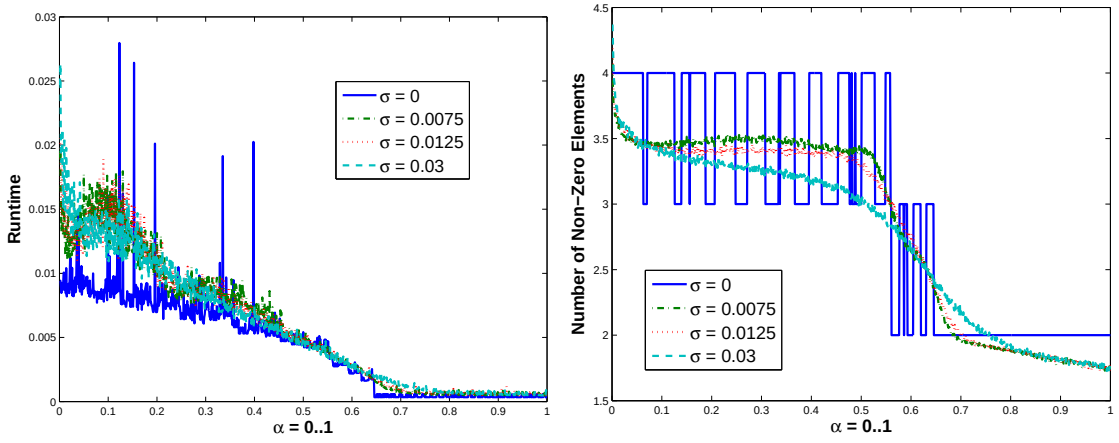

(a) Runtime

(b) ℓ^0-norm

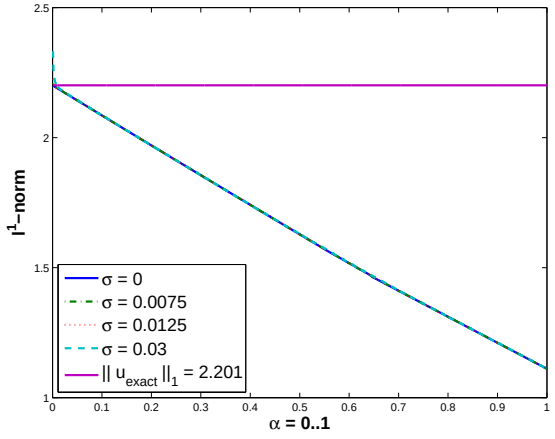

(c) ℓ^1-norm

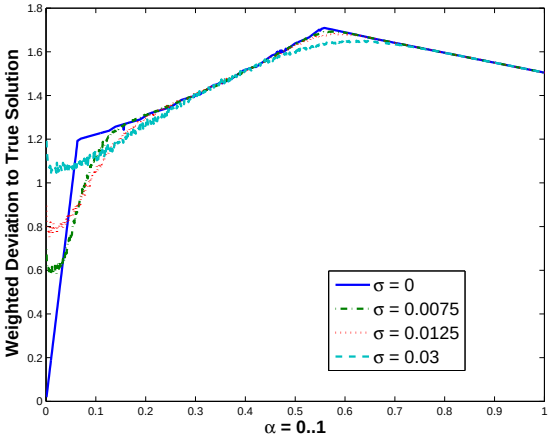

(d) $\frac{\|\tilde{u}-u\|_{\ell^1}}{\|\tilde{u}\|_{\ell^1}}$

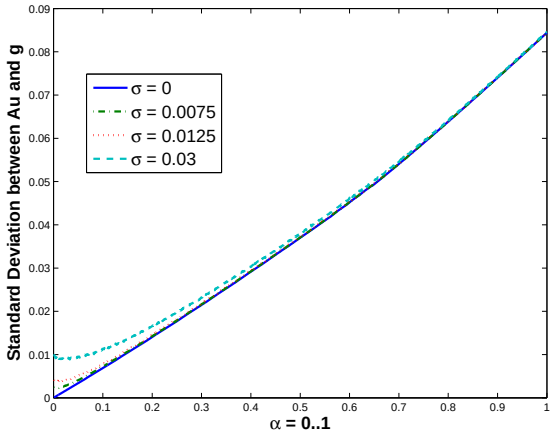

(e) std$(Au - g)$

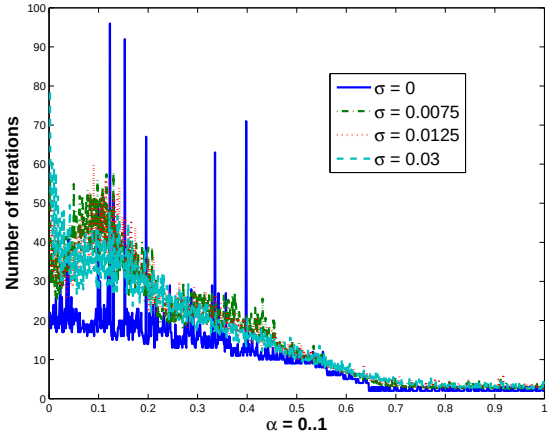

(f) Number of iterations

Figure 9.20: The average attributes runtime, ℓ^0-norm, ℓ^1-norm, weighted ℓ^1-deviation between $\hat{u}$ and $\tilde{u}$, standard deviation between Au and g and the number of iterations, over 1000 computations per α- and σ-value, for $\alpha \in [0.001, 1]$ and $\sigma \in \{0, 0.0075, 0.0125, 0.03\}$. All computations have been made on a computer with 2.83 GHz quad core processor with 8 GB memory.

aISS is not always computing the sparsest approximation, since the average ℓ^0-value is larger than two. But in comparison to OMP the results are significantly closer to two-sparsity as the results with OMP. The ℓ^1-norms of the computed aISS-solution are closer to the ℓ^1-norm of the true signal, and the weighted ℓ^1-norm between reconstruction and exact solution is also lower for aISS- than for OMP-computations. In addition, the standard-deviation of $K\hat{u}$ to $K\tilde{u}$ $(= g)$ is smaller in case of aISS than for OMP; the OMP solutions better approximate the noisy data f.

Moreover, we have plotted exemplary reconstructions in Figure 9.18 for particular noisy functions f that can be seen in Figure 9.19. For moderate noise aISS is able to recover the true support of the exact solution. Note that there is no additional positivity constraint in the computation of aISS. In the presence of severe noise neither OMP nor aISS can obtain the true support, which surely is a result of the severely ill-conditioned matrix K, but might also be a consequence of the early stopping due to the discrepancy principle.

Finally, we also run several tests for Algorithm 13, computing a solution of the regularized inverse scale space flow (3.10). We compute the average values over 1000 reconstructions for α varying between 0.001 and 1, for different noise levels with standard deviation σ. In Figure 9.20 we plot almost the same attributes as we have compared in Table 9.2 (except for the standard deviation between $K\hat{u}$ and f, which is rather similar to the standard deviation between $K\hat{u}$ and g), for varying α and the different noise levels. Obviously the runtime as well as the number of iterations decreases for increasing α, which seems to be natural since a more regularized solution should become sparser. This is indeed the case if we take a look at Figure 9.20(b). Moreover, the ℓ^1-norm (which is ≈ 2.201 for $\tilde{u}$) is monotonically decreasing for increasing α, which we also would expect. The weighted ℓ^1-difference reveals interesting insights, since for increasing α in the noiseless case the difference first increases (up to an α-value of about 0.57) and then decreases again; in case of noisy data, the behavior is similar, except for a slight decrease for small α, indicating that the optimal α seems to be somewhere inbetween 0.001 and 0.05. The standard deviation between $K\hat{u}$ and g is almost monotonically increasing, which is not surprising but rather expectable.

9.2 Positron Emission Tomography

Positron Emission Tomography (PET) is an imaging technique that produces 2D- or 3D-images of physiological processes in human or animal bodies. It therefore differs from imaging techniques as e.g. *Computerized Tomography (CT)*, which basically produce morphological information. In PET imaging a specific radionuclide (a so-called *tracer*) is injected into the human or animal body that is being placed in a so-called *PET-scanner*. Within the body, the tracer interacts with the body's molecules depending on its specific molecular structure (radioactive glucose for example locates in areas with high metabolic activity, e.g. tumors). Furthermore, the tracer emits positrons, which annihilate with the body's electrons into pairs of gamma rays. These pairs (*coincidences*) are collected by detectors in the PET-scanner architecture, and are subsequently stored by a processing unit in a certain data format. Finally, image reconstruction techniques are performed on the collected data in order to produce the desired images.

There are different ways the data can be stored by the processing unit. The data is either stored as list-mode data, which is basically a collection of all coincidences and the time each coincidence has been collected. However, in order to perform reconstruction algorithms on these list-mode datasets, the data needs to be organized in a way a reconstruction algorithm is able to produce a satisfactory image or a sequence of images (so-called *frames*). This data organization is called *binning*. Typically, the data is organized in a set of different slices with the use of advanced

mathematical methods (e.g. Fourier Rebinning, [45, 46]). For each slice the coincidences are parameterized as lines with parameters s and θ, where s represents the smallest distance between the line and the origin of the coordinate system, and θ denotes the angle with respect to the coordinate axes. The parameterized data is called *sinogram*-data.

The data does not only need to be binned in geometric slices, but also into temporal slices. The size of these temporal bins clearly affects the quality of the image reconstruction. The more events stored in one temporal bin, the higher the image quality of the corresponding frame of this particular temporal bin should become after image reconstruction. Often, the overall data is stored into one single temporal bin in order to achieve the best possible image quality. However, the power of PET lies in the interaction between the tracer and the body's molecules. Recent research has focused on studying the behavior of the interacting tracer over time. Hence, the goal, in order to make dynamic studies of the tracer interaction, is to split the data into as many temporal bins as possible. The amount and the size of the temporal bins has to be chosen to obtain an optimal trade-off between frame quality and frame quantity.

There are several other approaches of reorganizing list-mode data, e.g. the organization into so-called *gates* to overcome the problem of motion blur (see for instance [42, 44, 43]). Basically, the data is not organized into temporally consecutive bins but rather into bins of different motion phases.

In the course of this chapter we are only going to focus on data that has been parameterized as sinograms and that has been organized into one single or several temporally consecutive bins.

From a mathematical point of view, the process of PET imaging for one particular temporal bin of sinogram data can be described as the inverse problem of recovering u from f via

$$\wp(Ku) = f\,, \tag{9.10}$$

with

$$(Ku)(s,\theta) = \int_{x\cdot\theta=s} u(x)\ dx \tag{9.11}$$

being the Radon-transform (in two dimensions), for $\theta \in S^{n-1}$ and $s \in \mathbb{R}$, respectively with

$$(Ku)(\theta,x) = \int_{\mathbb{R}} u(x+t\theta)\ dx \tag{9.12}$$

being the X-ray transform in higher dimensions, for $\theta \in S^{n-1}$ and $x \in \theta^{\perp}$. The data f is a collection of randomly sampled intensities along the lines $x\cdot\theta = s$ or $x + t\theta$ respectively, which suits well as a model for the detected gamma ray annihilations. The random sampling process is denoted by $\wp$, to highlight that this sampling process is a Poisson process.

The mathematical setup that has been introduced is rather simple and neglects many effects that occur in PET, as e.g. scattering (cf. [81, 130, 89]) or partial volume effects (cf. [16]). Basically, most of these effects can be modeled by linear operators that can easily be integrated into (9.10). We continue focusing on the above setup though, for the sake of simplicity.

It is well known that the inverse problem (9.10) is ill-posed (cf. [92]); furthermore, the data is corrupted by Poisson-distributed noise. Hence, in order to recover u from (9.10) with given data f we need to consider a specific variational regularization scheme to obtain suitable solutions in the following section.

Moreover, we want to focus on the dynamic PET problem and will present a modification of (9.10) with respect to the dynamic behavior of the tracer. We are going to explain the computational realization of this model and will show computational results on both artificial and real PET data.
For more information on PET we refer to [131, 62].

9.2.1 Static PET

In order to find a function $\hat{u}$ close to the function $\tilde{u}$, which exactly solves $K\tilde{u} = g$, just from the single-frame sinogram data f, while g and $\tilde{u}$ are not available, we propose to use the variational scheme as introduced in Section 4.2.3, Equation (4.23), i.e.

$$\hat{u} \in \underset{\substack{u\in\mathrm{dom}(J)\\ u\geq 0}}{\arg\min} \left\{\mathrm{KL}(f, Ku) + \alpha J(u)\right\} ,$$

with $\alpha \in \mathbb{R}_{>0}$ and a regularization energy J.

In practice, instead of model (4.23) KL is often minimized without an additional regularization functional, but with an additional linear convolution operator R in order to improve image quality by modeling a deconvolution process, due to computational simplicity. The minimizer of $\mathrm{KL}(f, \tilde{K}u)$ with $\tilde{K} = KR$ under the positivity constraint $u \geq 0$ is given via (8.4). The most intuitive iteration scheme in order to solve (8.4) is Algorithm 4. Here, the use of a linear Gauss-filter as the convolution operator R to improve image quality of the solution is most prevalent in the application of PET.

However, we want to discuss the use of (4.23) with the typical singular regularization energy $\mathrm{TV}(u)$ and its algorithmic realization in order to show that singular energies represent good alternatives to linear filtering techniques and that they have superior behavior with respect to contrast enhancement via Bregman iteration.

As an example, we are going to discuss PET in the context of total variation regularization in the following.

EM-TV

The use of a combination of the Kullback-Leibler functional as a data fidelity and the total variation seminorm as a regularizer, i.e.

$$\hat{u} \in \underset{\substack{u\in\mathrm{BV}(\Omega)\\ u\geq 0}}{\arg\min} \left\{\mathrm{KL}(f, Ku) + \alpha\mathrm{TV}(u)\right\} ,$$

has extensively been studied in [21]. As a computational model the use of the forward-backward scheme presented in Algorithm 5 has been proposed. Due to the fact that the use of this scheme yields the alternating computation of either a standard EM algorithm step and a subsequent weighted-ROF-computation the scheme has been named *EM-TV*. The computation of the backward step can be done via efficient computational schemes for weighted-ROF-computation; in [21] the author chose a variant of Algorithm 8. Nevertheless, other schemes like e.g. Augmented Lagrangian based or Primal-Dual-type Quasi-Newton methods as presented in Section 8.1.1 and Section 8.1.2 might perform as well or even better. Moreover, as described in Section 8.1.3 the use of the Bregman distance $D_{\mathrm{TV}}(u, u^l)$ as a regularizer in order to produce a sequence of contrast-enhanced solutions u^{l+1} has been considered.

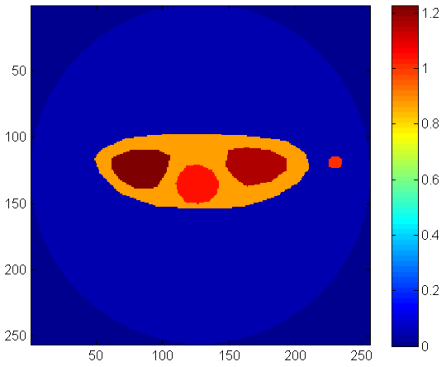

(a) $\tilde{u}$

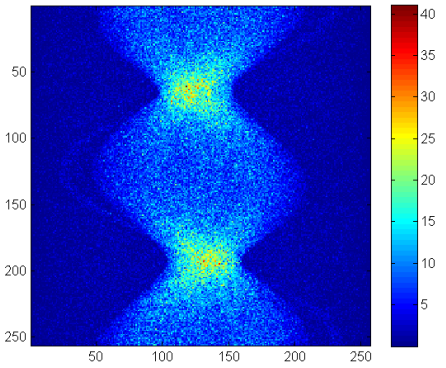

(b) f

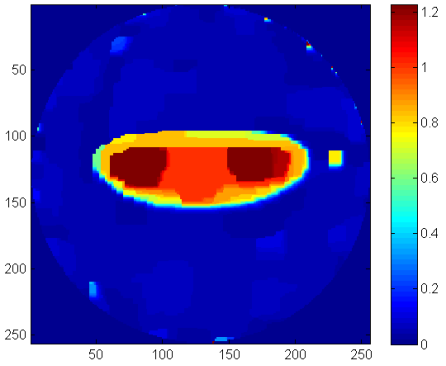

(c) u^5 for $\alpha = 0.5$

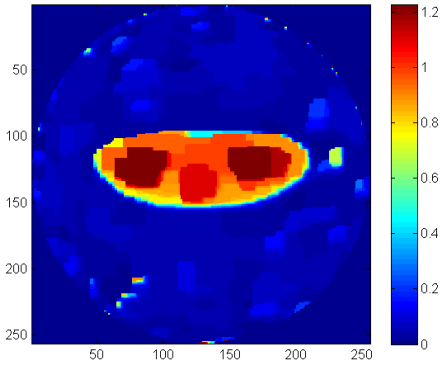

(d) u^7 for $\alpha = 0.5$

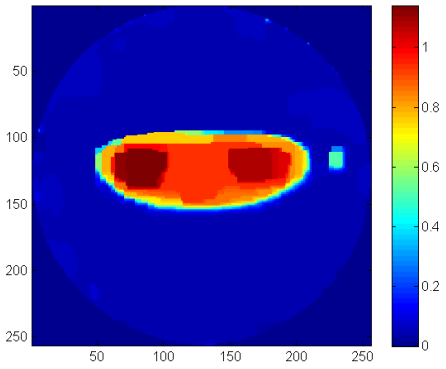

(e) u^1 for $\alpha = 0.1$

Figure 9.21: Exemplary EM-TV reconstructions with and without Bregman iteration. Figure 9.21(a) shows the exact image data $\tilde{u} \in \mathbb{R}^{256\times256}$, while Figure 9.21(b) shows the corresponding sinogram data $f \in \mathbb{R}^{256\times257}$, computed via a Monte-Carlo simulation. In Figure 9.21(c) and Figure 9.21(d) we can see two exemplary reconstructions of Algorithm 10, for $\alpha = 1/2$, $l = 5$ and $l = 7$, respectively. Figure 9.21(e) shows a standard EM-TV reconstruction without Bregman iteration for $\alpha = 1/10$.

Figure 9.21 shows EM-TV computations for synthetic 2D PET data $f \in \mathbb{R}^{256\times257}$, computed via a Monte-Carlo simulation for $s \in [-1, 1]$ sampled at 257 samples and $\theta \in [0, 2\pi]$ sampled at 256 samples, with the use of an augmented Lagrangian approach in order to solve the weighted-ROF-problem. Figure 9.22 shows computational results of real 3D PET data. The underlying data is a temporal bin containing five seconds of 2D-mode sinogram data approximately one minute after tracer injection. The tracer that has been used is radioactive water, $H_2{}^{15}O$. Radioactive water has a very short half-life and hence, the amount of events in the particular bin is very small.

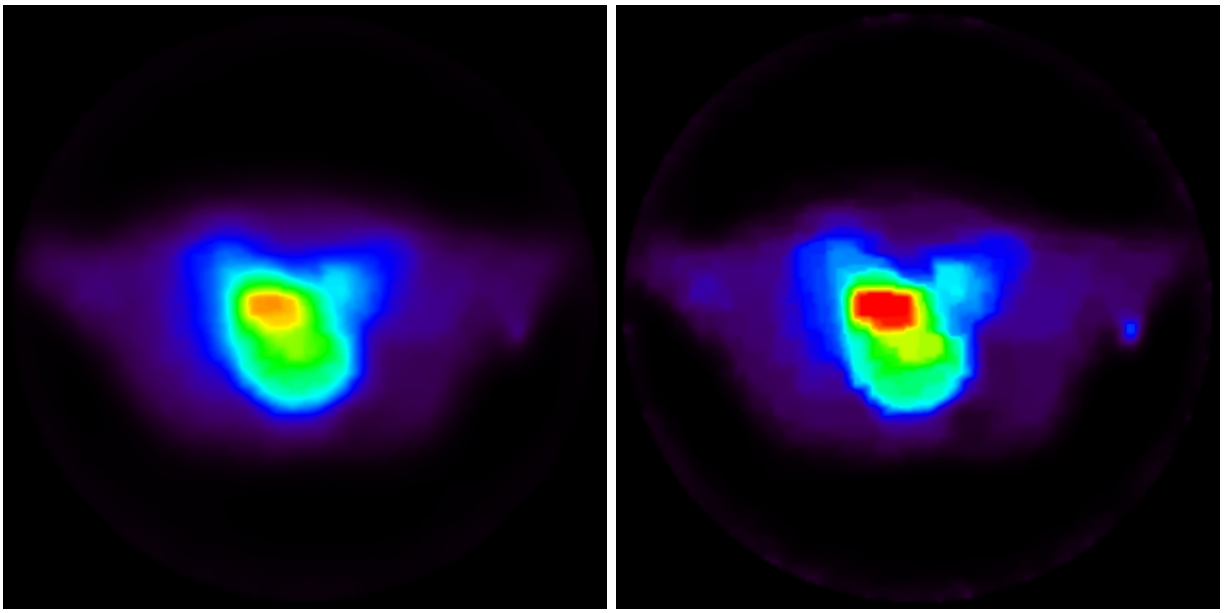

(a) Transversal View (b) Transversal View

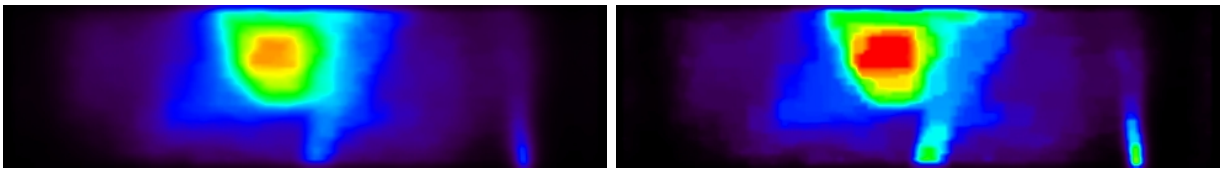

(c) Coronal View (d) Coronal View

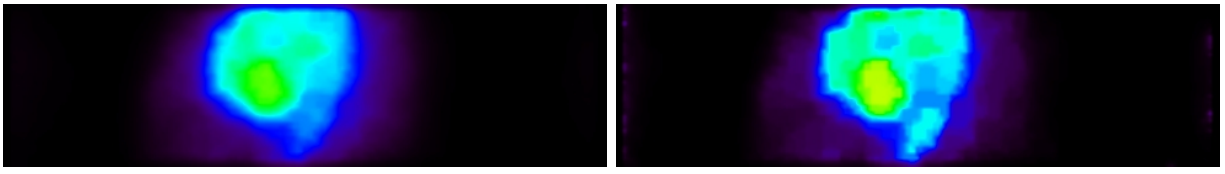

(e) Sagittal View (f) Sagittal View

Figure 9.22: EM-TV and Bregmanized EM-TV reconstructions of real $H_2{}^{15}O$-data. The images on the left hand side show a transversal, a coronal and a sagittal slice of a standard EM-TV reconstruction of dimension $175 \times 175 \times 47$, for $\alpha = 10$. The images on the right-hand side show the same slices for the 6-th EM-TV Bregman iteration with $\alpha = 100$.

9.2.2 Dynamic PET

In comparison to static PET, dynamic PET aims at producing a sequence of frames from a certain number of temporal bins of sinogram data. An easy image reconstruction approach would be the division of the sinogram data into a set of temporal bins and subsequent image reconstruction with a static method for each bin independently. The obvious drawback is that the temporal correlation between events in different bins is completely neglected. Furthermore, the image quality gets worse the less events are contained in an underlying bin. In the following, we therefore want to introduce an additional operator that temporarily correlates the PET frames.

Tracer Kinetics: Myocardial Perfusion Quantification as a Motivation

In order to motivate a reasonable operator that temporarily correlates dynamic PET frames we are going to briefly introduce compartment modeling and will illustrate the topic with the application of myocardial perfusion quantification (see for instance [11, 70, 112, 10]).

For this motivation we assume that the particular tracer that is being used is radioactive water $H_2{}^{15}O$. Radioactive water is used to examine how well tissue is provided with blood, or – with other words – how well tissue is perfused. The exchange between blood in the vessels and blood in tissue occurs in the capillaries; so does the exchange between $H_2{}^{15}O$ in blood and $H_2{}^{15}O$ in tissue. Assume that we are given a region that simply consists of tissue and a capillary vessel. The capillary vessel transports the radioactive water coming from an artery so that it can perfuse into tissue. This influx $J_{\mathcal{A}}$ can be described as a multiplication of the perfusion F with the arterial tracer concentration, denoted by h. Moreover, the capillary carries away the depleted blood from tissue back into a vein. Hence, we have an outflux $J_{\mathcal{V}}$ that equals the perfusion F and the venous tracer concentration, denoted by v. If we assume to have a fixed spatial region of capillary vessel for which the radioactive concentration only varies over time, we can describe this simplified setup as in Figure 9.23. With the same notation as above we can describe the process in Figure 9.23

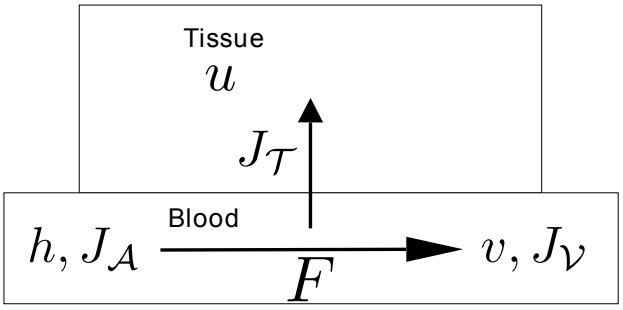

Figure 9.23: The one-compartment model with tracer in- and out-flux, for the modeling of a tracer exchange in the capillaries. The compartment consists of two regions, blood and tissue. The tracer concentration for the latter is described by the function $u(t)$. The tracer concentration in the blood depends on the capillary in- and outflux $J_{\mathcal{A}} = Fh(t)$ and $J_{\mathcal{A}} = Fv(t)$, respectively, with $h(t)$ denoting the tracer concentration in the arterial and with $v(t)$ representing the tracer concentration in the venous blood. The flux is controlled by the perfusion constant F.

via

$$\begin{aligned} \frac{d}{dt}u(t) &= F\left(h(t) - v(t)\right) , \\ u(0) &= 0 . \end{aligned} \tag{9.13}$$

The initial condition $u(0) = 0$ is rather natural, since we do not expect to observe radioactivity other than background activity within the body before the tracer is injected.

In case of radioactive water as a tracer, we can moreover assume that the tissue concentration quickly equilibrates with the venous outflow, since $H_2{}^{15}O$ is highly diffusible. We denote this equilibrium state as the partition coefficient $\lambda = u/v$. If we substitute $v(t)$ with $u(t)/\lambda$ in (9.13) we obtain the simple ODE

$$\begin{aligned} \frac{d}{dt}u(t) &= F\left(h(t) - \frac{u(t)}{\lambda}\right), \\ u(0) &= 0\,, \end{aligned} \tag{9.14}$$

or, by variation of parameters, the integral equation

$$u(t) = F\int_0^t h(\tau)\exp\left(-F(t-\tau)\right)\,d\tau\,, \tag{9.15}$$

which have been introduced in [11] first.

If we now assume (9.15) to hold for every spatial region x in a domain Ω, for spatially varying perfusion values $F(x)$, we can introduce the spatio-temporal operator G

$$\left(G(F,h)\right)(x,t) := F(x)\int_0^t h(\tau)\exp\left(-\frac{F(x)}{\lambda}(t-\tau)\right)\,d\tau\,, \tag{9.16}$$

as in [10], to modify the inverse problem (9.10) to

$$\wp(KG(F,h)) = f\,. \tag{9.17}$$

We now face to solve an inverse problem with an operator concatenation KG that spatially and temporally correlates every input frame. We therefore expect to obtain better image reconstructions by solving the inverse problem (9.17) instead of (9.10). Nevertheless there are certain drawbacks of this approach. First of all, the modeling can be argued to be unrealistic. For instance no underlying motion (breathing, heart-beating etc.) is modeled and conclusively these effects will affect the reconstruction results of the new model in a negative way. Furthermore, due to the lack of high-resolution, spillover effects are likely to occur, forcing spatial regions to contain mixtures of independent regions. To overcome at least the spillover problem a modification of (9.16) has been proposed in [70], including additional tissue fraction and spillover terms, i.e.

$$\left(G_{\mathcal{M}}(F,R,S,h)\right)(x,t) := R(x)\left(G(F,h)\right)(x,t) + S(x)h(t)\,, \tag{9.18}$$

with R denoting the tissue fraction per spatial region x and with S representing the arterial spillover per $x \in \Omega$. However, a challenging mathematical difficulty is that the operator equations (9.16) and (9.18) are at least nonlinear with respect to F and therefore lead to non-convex variational schemes.

To overcome the difficulties regarding the nonlinearity, a reasonable option is the linearization of the operator G, which yields an operator we have already examined in Section 9.1.4. We define a set of $n \in \mathbb{N}$ basis elements $b_i \in \mathbb{R}_{\geq 0}$ and introduce the operator

$$(B(a,h))(x,t) := \sum_{i=1}^{n} a_i(x)\tilde{b}_i(t)\,, \tag{9.19}$$

with basis functions

$$\tilde{b}_i(t) := \int_0^t h(\tau) \exp\left(-b_i(t-\tau)\right) \, d\tau \,,$$

a coefficient vector $(a_i(x))_{i\in\{1,\dots,n\}}$, $x \in \Omega$, and the arterial input curve h as input data. In order to allow a linearized approximation also for the myocardial perfusion model (9.18), including spillover and tissue fraction terms, we can define the additional basis function $\tilde{b}_0(t) := h(t)$, with $a_0(x)$ being the corresponding spillover coefficient. The operator (9.19) is not only linear in h but also linear in a, which makes the inverse problem much easier to solve if either one of the parameters is assumed to be fixed. However, often both parameters are unknown and hence, the inverse problem still might not have a unique solution. For simplicity, we assume the arterial input function to be given.

Originally, (9.19) has been derived in [102] as a multiple-compartment-model for the use of dynamic FDG-reconstructions. Hence, the model is much more versatile to use than just for myocardial perfusion quantification. Nevertheless, in the following we are going to focus on the application of myocardial perfusion quantification and present computational results for either synthetic 2D-/3D- and real 3D-/4D-data.

For more information and different variants of dynamic PET reconstruction we for instance may refer to [36, 134, 135, 101, 102, 103, 77].

9.2.3 Variational Model

In order to approximately solve the inverse problem

$$\wp(KBa) = f \,,$$

we need to find an appropriate variational model of the form (2.9) with its minimizer being close to the desired exact but unknown solution vector $\tilde{a}_n(x)$. From Section 4.2.3 we know that the Kullback-Leibler functional is supposed to be the right data fidelity term in order to incorporate the knowledge that the noise is Poisson distributed. As a regularizing term we would like to use a functional that allows to obtain a sparse solution for each spatial $x \in \Omega$, i.e. the vector $a_n(x)$ should be forced to become sparse. This sparsity assumption on the coefficients is rather natural, as we have introduced (9.19) as a linearization of (9.16). We therefore would like to obtain only two non-zero coefficients per spatial region; a_0 on the one hand, to recover the arterial spillover, and a_j for $j \neq 0$ on the other hand, to recover a particular perfusion and tissue fraction value. If we define the exemplary values $F(x) = 1.344$ (perfusion), $S(x) = 0.3$ (arterial spillover), $T(x) = 0.6$ (tissue fraction) at position x and a partition coefficient of $\lambda = 0.96$, then – if the j-th value of b is $b_j = 1.4$ – the j-th coefficient at position x ideally should equal $a_j(x) = 0.8064$, while $a_0(x) = 0.3$ and $a_i(x) = 0$ for $i \neq j \neq 0$ shall be satisfied. In order to promote sparsity in a variational setup with L^2 fidelity we know from Section 4.1.2 that the ℓ^1-norm is a suitable regularizer, since the variational model (4.3) is the convex relaxation of the ℓ^0-problem. However, in case of Kullback-Leibler as the fidelity term, the ℓ^1-norm does not necessarily promote sparsity of a solution, as we will discover in the following.

Example 9.3 (Kullback's and Leibler's Peak)**.** First of all, we want to argue why the natural scaling assumption (4.24) indeed is necessary in case we want to recover a single peak as in analogy to Example 6.4 for a Kullback-Leibler fidelity.

Theorem 9.1. *Let $K : \ell^1_{\geq 0} \to L^1(\Sigma)$ be a linear operator with $K^*\mathbf{1} = \mathbf{1}$. Then, $\hat{u} = c\delta_j$, with $c = 1/(1+\alpha)$ and δ representing the Kronecker-δ-function, is the solution of the variational scheme (2.9) with $H_f(Ku) = KL(f, Ku)$ and $J(u) = \|u\|_{\ell^1}$, for given input data $f = K\delta_j$.*

Proof. Considering the optimality condition of (2.9) with the particular functionals yields

$$\hat{p}_n = \frac{1}{\alpha}\left(K^*\left(\frac{f - K\hat{u}}{K\hat{u}}\right)\right)_n ,$$

for $\hat{p}_n \in \operatorname{sign}(\hat{u}_n)$. If we insert $f = K\delta_j$ and $\hat{u} = c\delta_j$ we end up with

$$\hat{p}_n = \frac{1-c}{\alpha c}\left(K^*\mathbf{1}\right)_n = 1 ,$$

for all n. In particular we therefore have $\hat{p}_j = 1$ and $\hat{p}_i \in \operatorname{sign}(\hat{u}_i)$ for $i \neq j$ and hence, the optimality condition is satisfied. □

Moreover, the proof of Theorem 9.1 points out that for an operator-scaling different than $K^*\mathbf{1} = \mathbf{1}$, the coefficient δ_i for which $(K^*\mathbf{1})_i$ is largest is returned as a solution of (2.9).

However, if we have an operator with large nullspace (which is natural in case of compressed sensing, and is also true for the operator B as defined in (9.19) for a large number of b_n's) and if we have only non-negative coefficients $u_n \geq 0$, then we easily see

$$\|u\|_{\ell^1} = \langle \mathbf{1}, u\rangle_{\ell^1} = \langle K^*\mathbf{1}, u\rangle_{\ell^1} = \langle \mathbf{1}, Ku\rangle_{L^1(\Sigma)} = \langle \mathbf{1}, f\rangle_{L^1(\Sigma)} .$$

Hence, with the scaling assumption $K^*\mathbf{1} = \mathbf{1}$ every non-negative solution of $Ku = f$ has the same ℓ^1-norm. As a consequence, the values of (2.9) with $H_f(Ku) = \mathrm{KL}(f, Ku)$ and $J(u) = \|u\|_{\ell^1}$ equal each other for every solution of $Ku = f$, no matter if u is sparse or not. Therefore, the ℓ^1-norm does not suit as a regularizer in case of our desired setup.

The development of a setup recovering sparse coefficients in the presence of the Kullback-Leibler fidelity would go beyond the scope of this thesis. We therefore decide not to pursue a setup as in [9], but rather to split up the process of sparse recovery into two steps. First of all, we are going to reconstruct the image sequence $u = Ba$ without assuring sparsity, but with ensuring a spatial smoothness of the coefficients. Subsequently, we are going to compute two-sparse coefficients for each pixel (consisting of one spillover and one perfusion coefficient) by comparing the least-squares values for each combination per pixel.
In order to realize the first step we want to propose the use of the Bregman-iteration-scheme

$$a^l = \operatorname*{arg\,min}_{a \in \mathrm{BV}(\Omega;\mathbb{R}^{n+1})} \left\{ \mathrm{KL}(f, KBa) + \alpha D^{p^{l-1}}_{\mathrm{TV}}(a, a^{l-1}) \right\} , \tag{9.20}$$

with the informal TV-definition

$$\mathrm{TV}(a) := \sum_{i=1}^{n} \int_\Omega \|a_i(x)\|_{\ell^p}\, dx ,$$

$p \in \{1, 2\}$, to ensure spatial smoothness for each single coefficient function without loss of contrast. The functional is minimized with the use of Algorithm 10 and Algorithm 5. The inner weighted ROF-problem of Algorithm 5 is solved via Algorithm 7.

For the second step we compute for every pixel $x \in \Omega$ and every combination $(0, j)$ for all $j \in \{1, \dots, n\}$ the coefficient combination with the minimal least-squares error, i.e.

$$\inf_{j\in\{1,\dots,n\}} \inf_{a_0(x),a_j(x)} \left\| u(x,\cdot) - \Big(a_0(x)h(\cdot) + a_j(x)\tilde{b}_j(\cdot)\Big) \right\|_{L^2([0,T])} \quad \forall x \in \Omega\,, \tag{9.21}$$

for $u(x,t) = (Ba^l)(x,t)$. In addition, we also check the (unlikely) case if a spatial region is being represented best by the input curve h only, i.e.

$$\inf_{a_0(x)} \|u(x,\cdot) - a_0(x)h(\cdot)\|_{L^2([0,T])} \quad \forall x \in \Omega\,. \tag{9.22}$$

In the following, we are going to present computational results on synthetic as well as on real $H_2{}^{15}O$-data.

9.2.4 Computational Results

In this section we want to investigate 2+1 dimensional synthetic and 3+1 dimensional real $H_2{}^{15}O$-data to demonstrate the capabilities and limitations of the proposed scheme. As in Section 9.1.4, for both synthetic and real data we sample the time $t \in [0, T]$, with $T = 320$ seconds, at the 26 discrete points $\{20, 25, 30, 35, 40, 45, 50, 55, 60, 65, 70, 75, 80, 85, 90, 100, 110, 120, 140, 160, 180, 200, 230, 260, 290, 320\}$. In both cases, after interpolating the data to a finer and equidistant temporal grid via bicubic interpolation, we compute the discrete approximations of the basis functions $\tilde{b}_j$ via a simple forward Euler strategy with stepsize $\Delta t = 0.001$, and apply a subsequent reinterpolation to the original temporal grid.

Synthetic Data

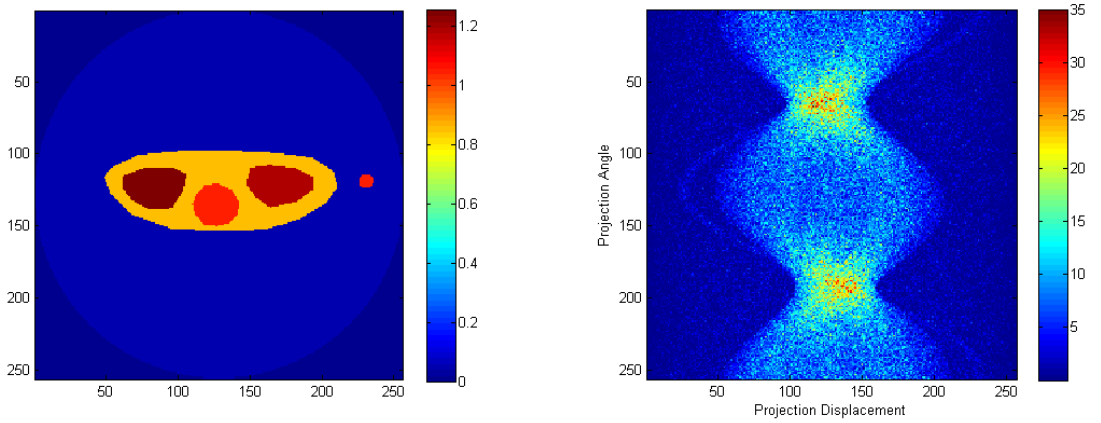

(a) Exact Data

(b) Sinogram Data

Figure 9.24: The 11-th frame of the exact data sequence $U \in \mathbb{R}^{256\times256\times26}$ and the corresponding sinogram data $Y \in \mathbb{R}^{256\times257\times26}$ of the same frame.

In case of fully synthetic data we consider a 2+1 dimensional image sequence $U \in \mathbb{R}^{256\times256\times26}$, for which the 11-th frame (time after 70 seconds) can be seen in Figure 9.24(a). This sequence

has been designed to attain spillover, tissue fraction and myocardial perfusion values as in Figure 9.25, for the input curve $h(t) := \tilde{h}(t)/\|\tilde{h}\|_\infty$, with $\tilde{h}(t) := \frac{t}{64}\exp\left(-\frac{-t^2}{128}\right)$. Subsequently, the frames of the sequence are processed to sinogram data $Y \in \mathbb{R}^{256\times257\times26}$ via a Monte-Carlo-simulation, generating 10000 photon counts in average per frame, for which the 11-th sinogram frame can be seen in Figure 9.24(b). The sinogram parameter s is sampled at 257 samples for $s \in [-1, 1]$, while

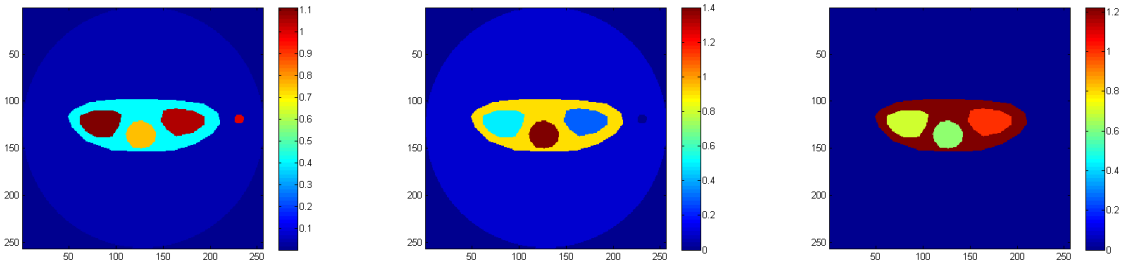

(a) Arterial Spillover (b) Myocardial Perfusion (c) Tissue Fraction

Figure 9.25: The per-pixel-values of arterial spillover, myocardial perfusion and tissue fraction that are attained by the designed image sequence U.

the angle $\theta \in [0, 2\pi]$ is sampled at 256 discrete points, leading to sinogram data $Y \in \mathbb{R}^{256\times257\times26}$. For the sinogram data Y as the input data we have computed 8 Bregman iterations of scheme (9.20) via Algorithm 10 for $\alpha = 10$. The considered dynamic PET matrix has been generated with the basis vector $b \in \mathbb{R}^{61}$ with $b_j \in [0, 6]$, sampled with stepsize 0.1, and subsequently normalized to ensure $B^T\mathbf{1} = \mathbf{1}$. The 11-th frame of the reconstruction can be seen in Figure 9.26(c), in comparison to the exact frame and the static PET reconstruction of Section 9.2.1. As expectable, the dynamic reconstruction appears to resemble the exact frame more than the static frame, due to the additional a-priori information of the exact input curve and the temporal correlation between the frames being embedded in the reconstruction process. In addition, Figure 9.27 shows the comparisons of the exact spillover, tissue fraction and myocardial perfusion values with the values reconstructed via (9.21) and (9.22). The values have been computed via the following

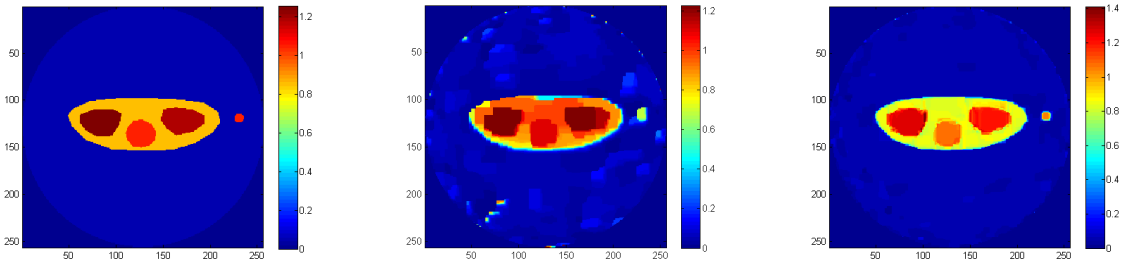

(a) Exact Data (b) Static Bregman Reconstruction (c) Dynamic Bregman Reconstruction

Figure 9.26: Comparison of the 11-th frame of exact data, static and dynamic pet reconstruction.

procedure. The spillover term $S(x)$ equals $a_0(x)$, while the myocardial perfusion $F(x)$ is being

set to $F(x) = b_j\lambda$, with j denoting the non-zero index and λ being the partition coefficient set to $\lambda = 0.96$. Finally, the tissue fraction value has been computed via $R(x) = a_j(x)/F(x)$.

It can be seen that despite the very bad signal-to-noise ratio the recovered spillover and tissue fraction values are quite close to the exact values. However, the quality of the recovered myocardial perfusion values is slightly worse, probably due to the fact that F can only attain the discrete values determined by $(b_j)_{\{1,\dots,n\}}$, or due to the nonlinearity of F in the original problem that cannot be handled by the linearization. Note that we have manually set all values of F for which R is almost zero to zero as well. Nevertheless, the quality of the reconstructions allows to draw quantitative conclusions on the observed values, although the quality of the data is limited.

Real $H_2{}^{15}O$ Data

In this section we want to consider results for real $H_2{}^{15}O$-sinogram data. We have collected 26 sinogram frames Y, sampled at the discrete timesteps defined in the introduction of this section, with a Siemens PET Scanner ECAT EXACT operating in 2D-mode, which means that only those events have been collected that were detected in perpendicular slices. Figure 9.28 shows the 11th frame of the sinogram data. The related image sequence data is reconstructed with the dimensions $175 \times 175 \times 47$ per frame. In order to handle the huge data matrices that therefore occur in the reconstruction process, we limit the number of basis elements to 29. More precisely we define b as the vector $b = \{0, 0.1, 0.2, 0.3, 0.4, 0.5, 0.6, 0.7, 0.8, 0.9, 1, 1.1, 1.2, 1.3, 1.4, 1.5, 1.6, 1.7, 1.8, 1.9, 2, 2.5, 3, 3.5, 4, 4.5, 5, 5.5, 6\}$. Again, the resulting dynamic PET matrix B is normalized to ensure $B^T\mathbf{1} = \mathbf{1}$ and rescaled after the first part of the parameter reconstruction process is finished.

Another problem we face is that in contrast to synthetic data for which we know the exact data we do not necessarily know the exact input curve in case of real data. Since we have already discovered in the previous section that in case of the exact input curve being given the method is capable to recover the desired parameters very well, in this section we do not claim to exactly recover these parameters. We rather choose a specific input curve and show that the method operates in a full 4D setup for real data as well as for the synthetic 3D setup. We therefore define the input curve as the spectral mean over all voxels in the field-of-view of the scanner of one single EM-iterate with initial value $u_0 = \mathbf{1}$. In Figure 9.29 this input curve is visualized for illustrative purposes.

For the computations we proceed analogously as in case of synthetic data. First, we compute five Bregman iterations of scheme (9.20) via Algorithm 10 for $\alpha = 10$. Subsequently, we compute the two-sparse solution via (9.21) and (9.22) for every voxel in order to determine the spillover, perfusion and tissue fraction values.

In Figure 9.30 three particular slices with different orientation (transversal, coronal and sagittal) of the 11-th frame of the static and the dynamic PET reconstruction have been compared. From a visual point of view the dynamic PET reconstruction appears to include more details and structures than the frame-independent static PET reconstruction.

In Figure 9.31 the results of the parameter identification step for the parameters S (spillover) and R (tissue fraction) that have been processed via the second least-squares step are visualized.

It is easy to see that the particular choice of h as described above and visualized in Figure 9.29 does not seem to be a good choice with respect to myocardial perfusion quantification. Most of the cardiac regions (including the tissue regions) can be represented by the input curve, leading to high spillover values but extremely low tissue fraction values. In contrast, the tissue fraction values grow large in areas below the cardiac and lung regions. Due to the high amount of areas for which the tissue fraction values are very small we refrain from visualizing the parameter F (myocardial perfusion), since in analogy to the synthetic data case the perfusion values cannot be

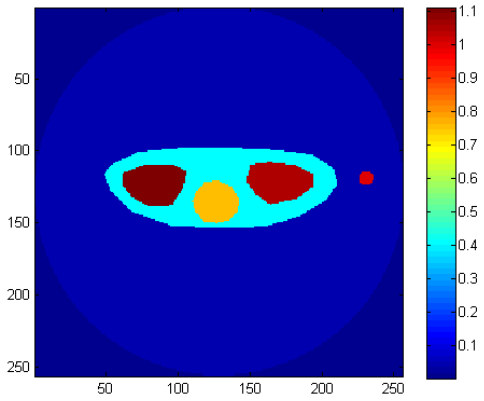

(a) Arterial Spillover

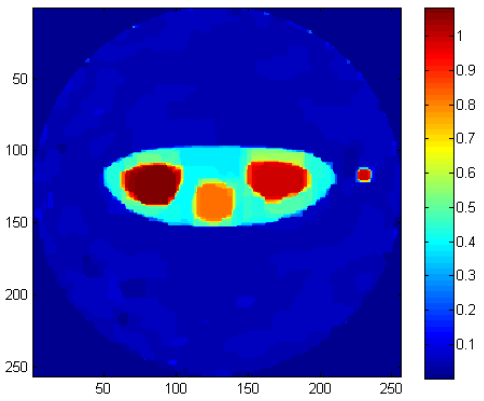

(b) Arterial Spillover Reconstruction

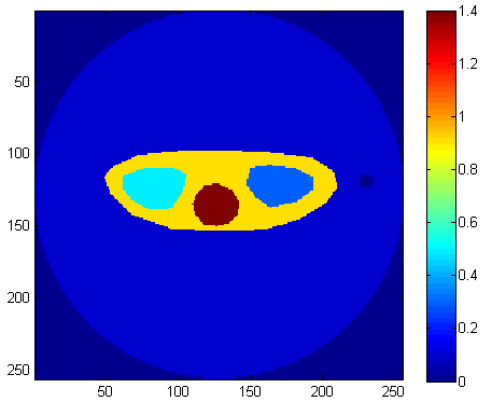

(c) Myocardial Perfusion

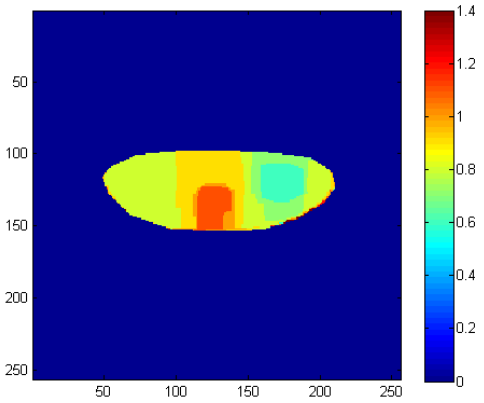

(d) Myocardial Perfusion Reconstruction

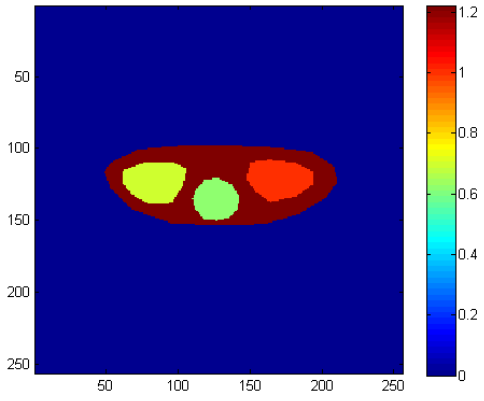

(e) Tissue Fraction

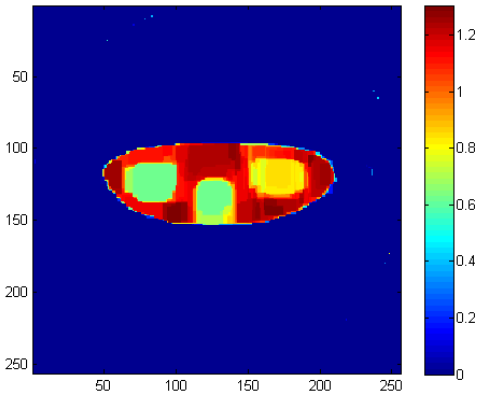

(f) Tissue Fraction Reconstruction

Figure 9.27: Comparison between exact and reconstructed values for arterial spillover $S(x)$, myocardial perfusion $F(x)$ and tissue fraction $R(x)$. Note that for illustrative purposes we have set $F(x) = 0$ if $R(x)$ is almost zero, since a small tissue fraction also implies a small perfusion value.

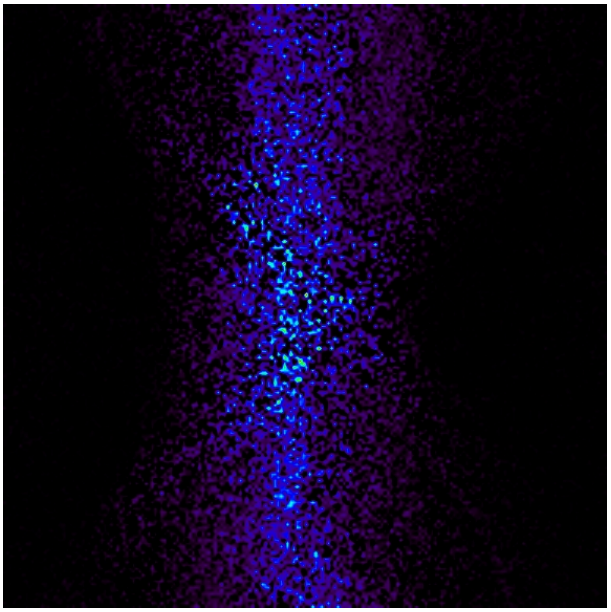

(a) Transversal View

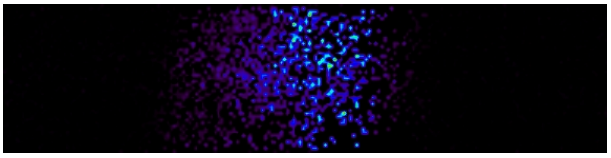

(b) Coronal View

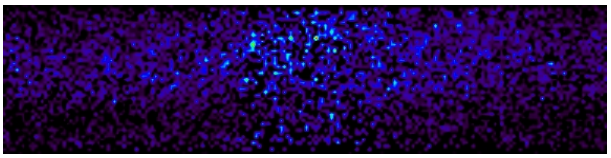

(c) Sagittal View

Figure 9.28: Three-dimensional sinogram data of the 11th frame of real dynamic $H_2{}^{15}O$ PET data collected with a Siemens PET Scanner ECAT EXACT.

recovered properly and indeed become very large. Alternatively, in Figure 9.32 the product FR is visualized, representing the coefficient values of the non-input-curve coefficients.

The dynamic reconstruction therefore seems to be very sensitive regarding the choice of the input curve. In order to draw quantitative conclusions from the dynamic PET reconstruction, the considered input curve needs to be very accurate. The method proposed for dynamic PET reconstruction therefore is only as good as the quality of the input curve is, with respect to the considered application. This suggests that both the coefficients as well as the input curve should be recovered simultaneously.

Nevertheless, if an accurate input curve is given, the use of Bregman iteration in combination with total variation regularization allows a quantitative analysis of dynamic PET data.

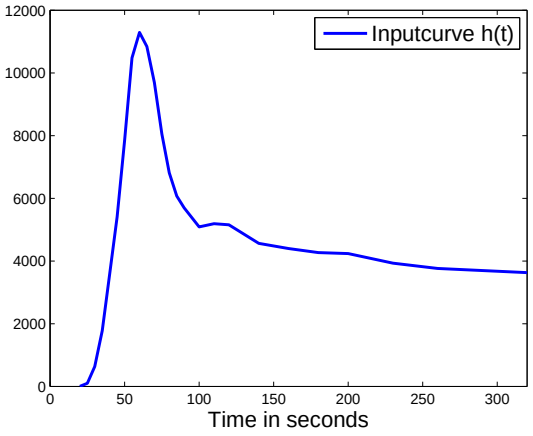

Figure 9.29: The input curve $h(t)$ that has been used for the dynamic PET reconstruction of real $H_2{}^{15}O$-data.

9.3 Bioluminescence Tomography

A very novel optical molecular imaging technique in order to make bioluminescent markers in small animals (particularly genetically engineered mice) visible is *Bioluminescence Tomography* (BLT), which has been developed in [128] and extensively studied in [129, 64, 126, 127]. According to [129], BLT "collects emitted photons from multiple 3-D directions with respect to a living mouse marked by bioluminescent reporter luciferases, and reconstructs an internal bioluminescent source distribution based on both the outgoing bioluminescent signals and a prescanned tomographic volume, such as a CT/micro-CT volume, of the same mouse". While transmitting through tissue the bioluminescent photons are exposed to scattering and absorption. These phenomena can accurately be described by the *Radiative Transfer Equation* (RTE) (cf. [92]). However, analysis and computational realization of the RTE based BLT is very difficult. For that reason most recent existing studies are limited to BLT with a diffusion approximation of the RTE (cf. [64]). Precisely, the goal is to recover a light source function p that obeys the diffusion equation

$$-\nabla \cdot (D\nabla u) + \mu u = p \text{ in } \Omega\,, \tag{9.23}$$

with the boundary conditions

$$D\frac{\partial u}{\partial \nu} = -f \text{ on } \Gamma\,, \tag{9.24}$$

and

$$2D\frac{\partial u}{\partial \nu} + = g^- \text{ on } \Gamma\,, \tag{9.25}$$

with $D = (3\,(\mu + \mu'))^{-1}$, μ and μ' being absorption and scattering coefficients, f denoting the measurements and g^- being the given influx function (which is typically zero for standard BLT applications), for the domain Ω with Lipschitz boundary Γ.

The recovery of p from (9.23), (9.24) and (9.25) is an ill-posed problem and therefore needs further regularization. In [64] the considered variational minimization problem was the classical

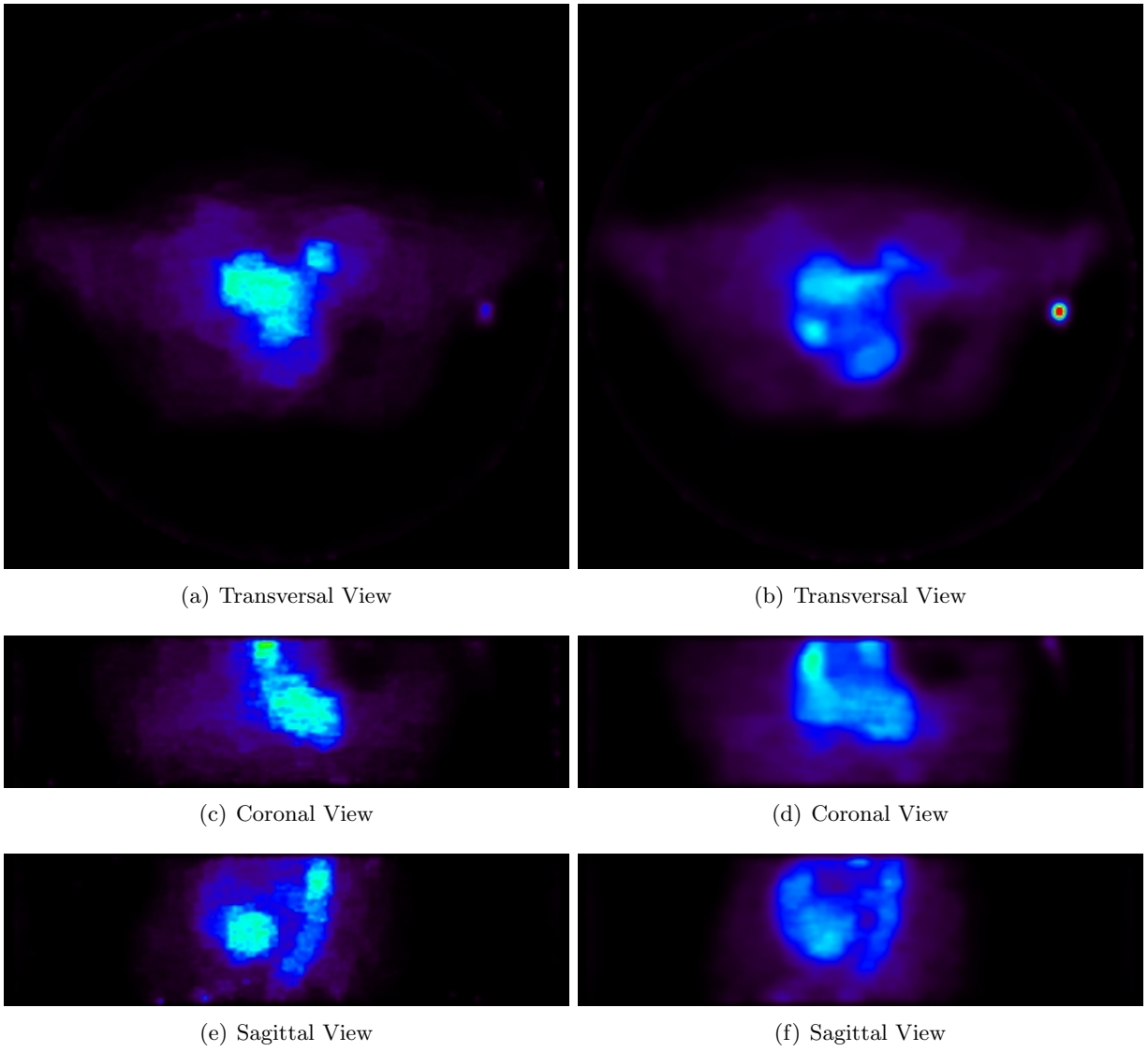

(a) Transversal View (b) Transversal View

(c) Coronal View (d) Coronal View

(e) Sagittal View (f) Sagittal View

Figure 9.30: Transversal, coronal and sagittal view of the 11th frame of the static PET reconstruction (left side) and the dynamic PET reconstruction (right side). The additional a-priori information allows a qualitative improvement of the reconstruction leading to more details and structures in the reconstructed frames.

Tikhonov regularization scheme with quadratic regularization term, i.e.

$$p \in \underset{p \in L^2(\Omega)}{\arg\min} \left\{ \frac{1}{2} \left\| Kp - f \right\|^2_{L^2(\Gamma)} + \frac{\alpha}{2} \left\| p \right\|^2_{L^2(\Omega)} \right\},$$

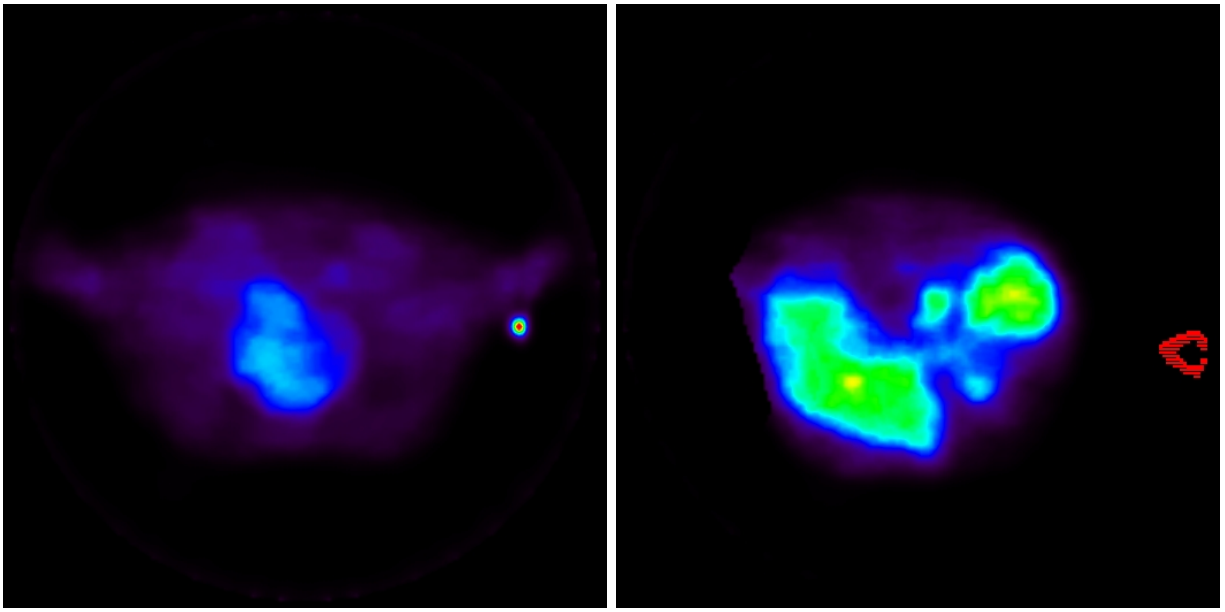

(a) Transversal View (b) Transversal View

(c) Coronal View (d) Coronal View

(e) Sagittal View (f) Sagittal View

Figure 9.31: Transversal, coronal and sagittal view of the recovered parameters S (spillover, left side) and R (tissue fraction, right side). Note that the transversal views of both parameters do not show the same slice, in order to visualize slices that contain high tracer activity. The coronal and sagittal views however show the same slides in both cases. The results demonstrate the bad choice of the input function. The input curve represents much of the coronary areas so well that the spillover in these regions is very high. The tissue fraction values in these regions tend to zero, while they appear to be relatively high in the lower areas. Note that the red dots in the tissue-fraction-reconstruction are outliers.

with K denoting the linear operator that relates p to the data f in terms of (9.23), (9.24) and (9.25). In common computational realizations the diffusion equation is approximated via a finite element scheme, leading to a fully discrete setup

$$p \in \operatorname*{arg\,min}_{p \in \ell^2} \left\{ \frac{1}{2} \|Kp - f\|_{\ell^2}^2 + \frac{\alpha}{2} \|p\|_{\ell^2}^2 \right\}. \tag{9.26}$$

The problem-formulation (9.26) has actually two drawbacks. In [87] it has been argued that the

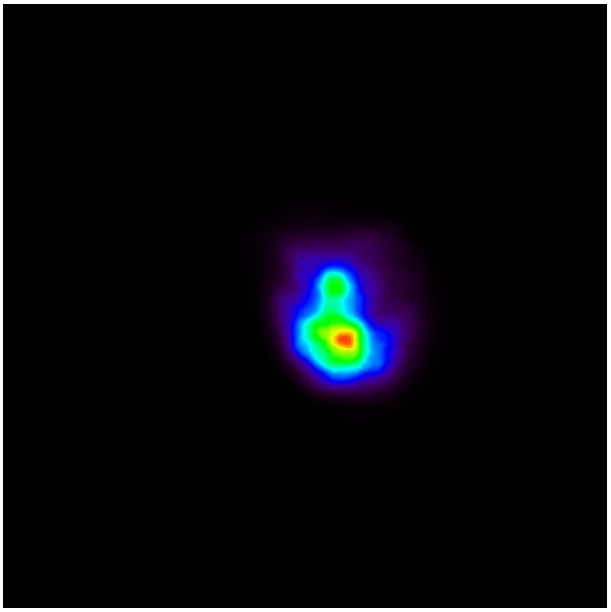

(a) Transversal View

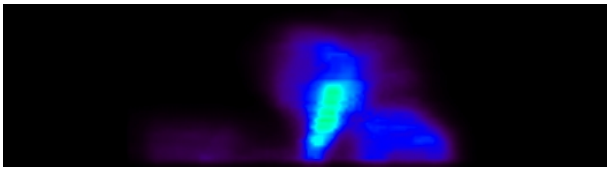

(b) Coronal View

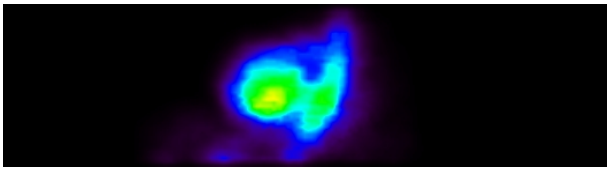

(c) Sagittal View

Figure 9.32: Transversal, coronal and sagittal view of FR, with F denoting the myocardial perfusion and R representing the tissue fraction.

ℓ^1-norm is a more suitable regularizer than the ℓ^2-norm, since the finite element approximation usually implies that the number of surface discretized points is significantly fewer than the number of discretized points in the inner domain. Thus, the finite-element-discretization leads to a matrix $K \in \mathbb{R}^{m \times n}$ with $m \ll n$ and therefore, K has a large nullspace. In order to find a suitable solution among all possible solutions the ℓ^1-norm-minimizing solution seems to be a preferable choice and has been realized in [87] in case of quadratic fidelity, i.e.

$$p \in \operatorname*{arg\,min}_{p \in \ell^2} \left\{ \frac{1}{2} \|Kp - f\|_{\ell^2}^2 + \alpha \|p\|_{\ell^1} \right\}. \tag{9.27}$$

The second drawback is that the noise the data is contaminated with is supposed to be Poisson-distributed photon count noise, similar to the application of PET. As a consequence, the choice

of a ℓ^2-fidelity does not seem to be the best option, since the a-priori information that the noise is Poisson-distributed is not incorporated into the reconstruction process. However, we have discovered in Section 9.2.3 that the combination of the Kullback-Leibler fidelity and ℓ^1-regularization might be a good alternative to (9.26), but will not produce sparse and satisfactory results and therefore will not represent a good alternative to (9.27).

In the following we want to present a different option, leading to qualitatively improved results. If we consider the general variational framework with Kullback-Leibler fidelity (i.e. (4.23)) again and compute the optimality condition with neglected positivity constraint, we obtain

$$0 = K^T \left(\frac{Kp - f}{Kp} \right) + \alpha q \ , \text{ with } q \in \partial J(p).$$

Approximating Kp in the denominator of the fraction via f yields the related ℓ^2-type problem

$$p \in \operatorname*{arg\,min}_{p \in \mathrm{dom}(J)} \left\{ \frac{1}{2} \left\| \frac{Kp - f}{\sqrt{f}} \right\|_{\ell^2}^2 + \alpha J(p) \right\} . \tag{9.28}$$

In case that we know the noise bound between noisy data f and exact data g in terms of

$$\frac{1}{2} \left\| \frac{g - f}{\sqrt{f}} \right\|_{\ell^2}^2 \leq \delta \, , \tag{9.29}$$

an alternative to minimizing (9.28) is to consider the ISS with discrepancy principle, i.e.

$$\frac{\partial}{\partial t} q(t) = K^T \left(f - Kp(t) \right) \text{ , for } q(t) \in \partial J(p(t)), \tag{9.30}$$

until we obtain

$$\frac{1}{2} \left\| \frac{Kp(t_*) - f}{\sqrt{f}} \right\|_{\ell^2}^2 \leq \delta \, ,$$

for $0 < t_* < \infty$, leading to better approximations without loss of contrast. In the following, we want to computationally realize (9.30) for $J(p) = \|p\|_{\ell^1}$ via Algorithm 12 and compare computations for synthetic data with different sparsity levels.

9.3.1 Computational Realization

As mentioned in the previous section we want to consider the setup

$$\frac{\partial}{\partial t} q(t) = A^T \left(f - Ap(t) \right) \text{ , for } q(t) \in \mathrm{sign}(p(t)), \tag{9.31}$$

with A denoting the matrix $A = DK$ for D being defined as the positive diagonal matrix

$$D_{i,j} = \begin{cases} \frac{1}{\sqrt{f_l}} & \text{for } (i,j) = (l,l) \\ 0 & \text{else} \end{cases} ,$$

for all l of the discrete domain of f that we want to denote with m. If we assume p to consist of n pixels (or voxels, respectively), we therefore have $K \in \mathbb{R}^{m \times n}$, $D \in \mathbb{R}^{m \times m}$ and $A \in \mathbb{R}^{m \times n}$. In

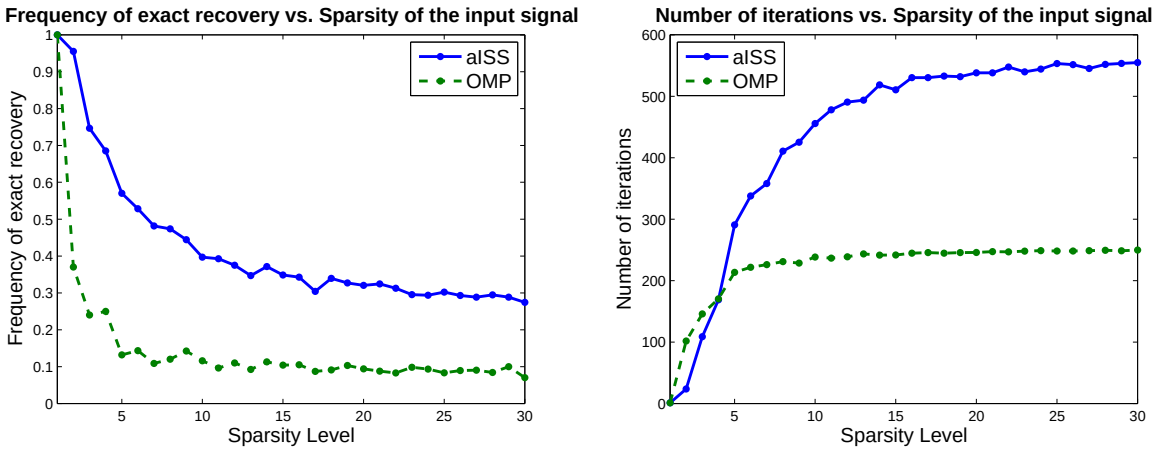

(a) Frequency of exact recovery

(b) Number of iterations

Figure 9.33: Comparison of OMP and aISS for the matrix A_1 and noise-free data, for varying sparsity level s. The plots show the comparison metrics with respect to the sparsity level of the input signal.

order to recover at least trivial peaks we furthermore normalize the columns of A with respect to the two-norm, due to Example 6.4. We therefore define another diagonal matrix $N \in \mathbb{R}^{n\times n}$ with

$$N_{i,j} = \begin{cases} \frac{1}{\|A_r\|_{\ell^2}} & \text{for } (i,j) = (r,r) \\ 0 & \text{else} \end{cases},$$

for $i, j, r \in \{1, \cdots, n\}$, with A_r denoting the r-th column of A, and define $\tilde{A} := AN$ as the matrix to consider in (9.31) instead of A. After computing iterations of (9.31) until $\frac{1}{2}\left\|\tilde{A}p(t_*) - \sqrt{g}\right\|_{\ell^2}^2 \leq \delta$ is satisfied, we can recover the original scaling of the coefficients via $p_{\text{scal}} = Np$. The computational realization of (9.31) is done with Algorithm 12 for parameters $\tilde{A}$ (the considered matrix), f (the input data) and δ (the threshold).

9.3.2 Computational Results

In the following we briefly want to show and compare numerical examples on exact and noisy synthetic data. The underlying matrices K are generated as in [87], by finite-element discretizations with different amounts of discretized surface points. More precisely, we consider two matrices $K_1 \in \mathbb{R}^{256\times 4096}$ and $K_2 \in \mathbb{R}^{1352\times 4096}$. In the following section, we want to run computational tests of either aISS and OMP on clean data for the two matrices in order to compare the performances of aISS and OMP as well as the ill-conditioning of the matrices.

Clean Data

First of all we investigate the aISS- and OMP-setup for K_1 and K_2 in case of noise-free data. We define matrices A_1 and A_2 as described in Section 9.3.1 and compare the frequency of exact recovery as well as the number of iterations needed for both aISS and OMP. The exact data is produced by applying the matrices A_1 and A_2 to random signals with sparsity level s. The procedure is repeated 50 times for each sparsity level, and obtained frequency and number of iterations are averaged. The results of the subsequent reconstructions can be seen in Figure 9.33 for sparsity levels $s = 1$ to $s = 30$.

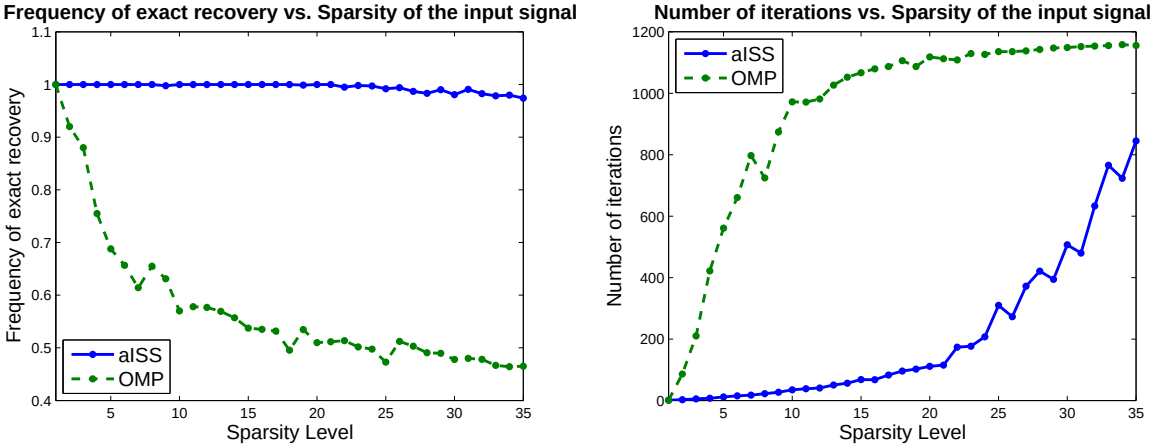

(a) Frequency of exact recovery

(b) Number of iterations

Figure 9.34: Comparison of OMP and aISS for the matrix A_2 and noise-free data, for varying sparsity level s. The plots show the comparison metrics with respect to the sparsity level of the input signal.

For matrix A_1 it can be seen that the problem is highly ill-conditioned. Only for signals with sparsity level $s = 1$ exact recovery can be guaranteed with a frequency of one. Then, with increasing sparsity level the frequency gets terribly worse. Despite the fact that the matrix A_1 is very ill-conditioned and therefore very impractical, in terms of frequency aISS does a better job than OMP. In analogy to the comparisons of Section 9.1.4 the improvements in frequency are at the expense of a higher number of iterations.

The same computational experiments as for A_1 have also been performed for A_2, for increasing sparsity level $s = 1$ to $s = 35$. The comparisons of frequency of exact recovery as well as the number of iterations for aISS and OMP are presented in Figure 9.34.

Both algorithms can at least handle low sparsity levels much better as in case of A_1, which is not surprising since for A_2 many more surface points are sampled. However, this time aISS is not only able to recover the true coefficients better than OMP, but also with fewer iterations needed.

In the following, we want to discuss whether the proposed model leads to improved reconstructions in case of Poisson-distributed noise, in contrast to the use of the standard ℓ^2-fidelity. For that purpose we want to focus on the underlying matrix K_2 only, since K_1 appears to be impractical for further use due to its high degree of ill-conditioning.

Noisy Data

In case of noisy data we compare the frequency of exact recovery, the number of iterations and the normed ℓ^1-difference between a reconstruction and the true solution, i.e. $\|\hat{p} - \tilde{p}\|_{\ell^1} / \|\tilde{p}\|_{\ell^1}$, with $\tilde{p}$ denoting the true and $\hat{p}$ representing the recovered solution. We do not only compare the different algorithms aISS and OMP, but also the use of the matrix A_2 and the matrix K_2, since we have assumed to obtain an extra benefit from the modeling of A_2 in case of data corrupted by Poisson distributed noise. The basic setup is as follows. We generate random signals with sparsity level s as our true solutions $\tilde{p}$, for s varying from one to 20. We compute the corresponding exact data $g = A_2\tilde{p}$ (and $g = K_2\tilde{p}$ respectively) and corrupt the data g by Poisson-noise bounded by δ in the sense of (9.29), to obtain the input data f. Subsequently we compute the first 150 ISS iterates via Algorithm 12 for the input data f to compute solutions $\hat{p}$ of which we pick the solution

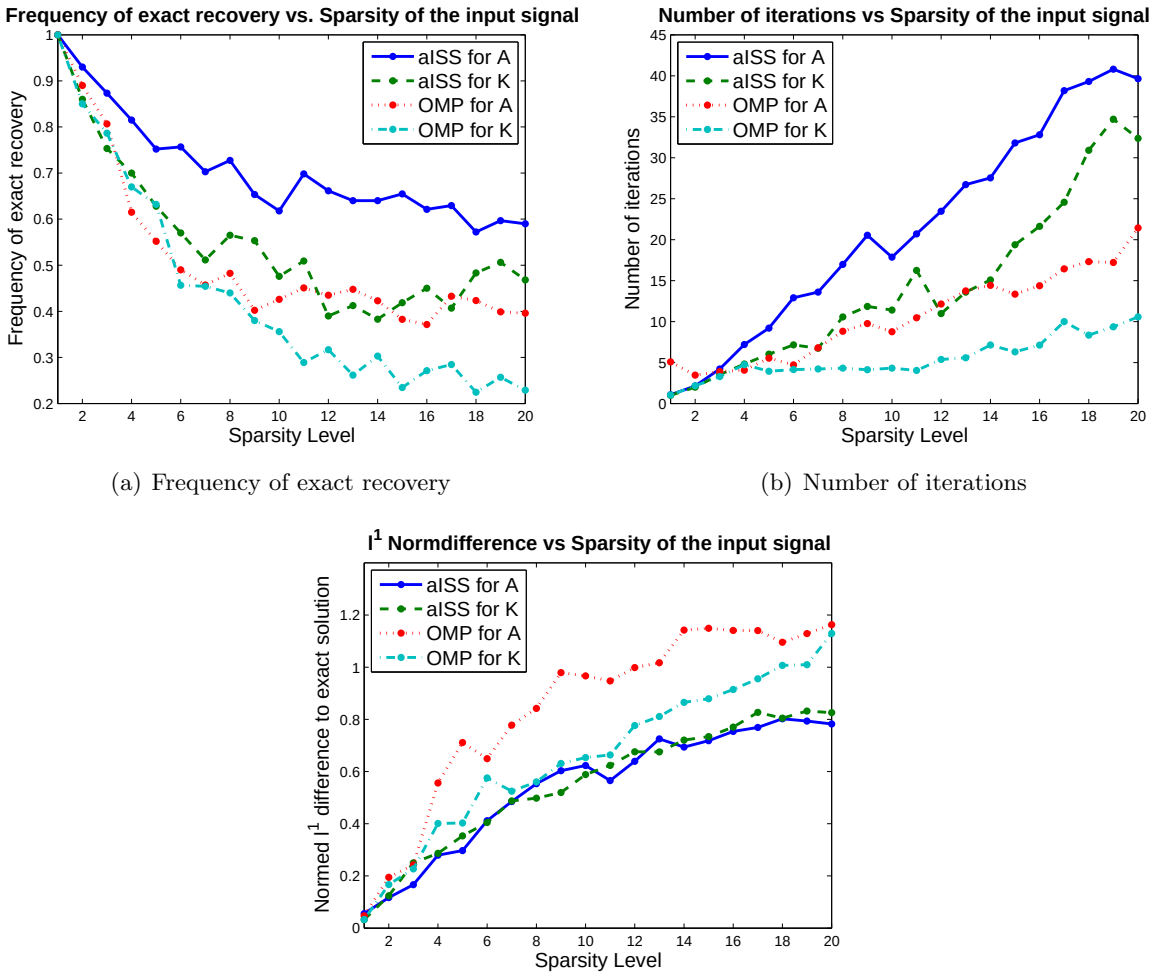

(a) Frequency of exact recovery

(b) Number of iterations

(c) Normed ℓ^1-difference to $\tilde{p}$

Figure 9.35: Comparison of OMP and aISS for noisy data and different matrices A_2 and K_2, for varying sparsity level s. The plots show the comparison metrics with respect to the sparsity level of the input signal.

with smallest ℓ^1-difference to $\tilde{p}$ among all 150 iterates. For every sparsity level s we repeat this procedure 50 times for different random signals $\tilde{p}$ to obtain reliable average values. The computed results are shown in Figure 9.35.

First of all it can be seen that the use of aISS in contrast to OMP brings a visible improvement for the reconstruction in case of noisy data, at the cost of more iterations until converging to the best possible solution. Moreover, in terms of frequency of exact recovery the use of A_2 instead of K_2 improves the frequency for both aISS and OMP. Considering A_2 instead of K_2 with OMP only leads to results that are almost qualitatively as good as they are for the use of aISS with matrix K_2. In terms of normed ℓ^1-differences however the considered combinations of algorithms and matrices used appear to lead to similar results, except in case of OMP with matrix A_2, which is significantly worse.

Appendix A

Computational Realization

In this chapter we briefly describe the computational realization of the discrete Laplace inversion, needed for some of the algorithms presented in Chapter 8, via the discrete Cosine transform.

A.1 Discrete Laplace Inversion via Cosine Transform

Assume that we face to solve the operator equation

$$-\Delta u = f\,, \tag{A.1}$$

with u satisfying Neumann boundary conditions. Then, a discrete finite differences approximation of (A.1) in two dimensions $\mathbb{R}^M \times \mathbb{R}^N$ is given via

$$f_{i,j} = 2\left(\frac{1}{h_x^2} + \frac{1}{h_y^2}\right) u_{i,j} - \frac{1}{h_x^2}\left(u_{i+1,j} + u_{i-1,j}\right) - \frac{1}{h_y^2}\left(u_{i,j+1} + u_{i,j-1}\right)\,, \tag{A.2}$$

with h_x and h_y denoting the stepsizes in x- and y-direction. Due to the Neumann boundary conditions, we can rewrite u and f in terms of the inverse cosine transform (IDCT), i.e.

$$u_{i,j} = \sum_{p=0}^{M-1}\sum_{q=0}^{N-1} \alpha_p^M \alpha_q^N \hat{u}_{p,q} \cos\left(\frac{\pi(2i+1)p}{2M}\right) \cos\left(\frac{\pi(2j+1)q}{2N}\right)\,,$$

with

$$\alpha_t^T = \begin{cases} \frac{1}{\sqrt{T}} & \text{if } t = 0 \\ \sqrt{\frac{2}{T}} & \text{if } 0 \le t \le T-1 \end{cases}\,,$$

for $0 \le i \le M-1$ and $0 \le j \le N-1$. Replacing u and f via the IDCT-representation yields

$$\begin{aligned} &2\left(\frac{1}{h_x^2} + \frac{1}{h_y^2}\right) \hat{u}_{p,q} \cos\left(\frac{\pi(2i+1)p}{2M}\right) \cos\left(\frac{\pi(2j+1)q}{2N}\right) \\ &- \frac{1}{h_x}\hat{u}_{p,q} \cos\left(\frac{\pi(2j+1)q}{2N}\right)\left(\cos\left(\frac{\pi(2i+3)p}{2M}\right) + \cos\left(\frac{\pi(2i-1)p}{2M}\right)\right) \qquad \text{(A.3)} \\ &- \frac{1}{h_y}\hat{u}_{p,q} \cos\left(\frac{\pi(2i+1)p}{2M}\right)\left(\cos\left(\frac{\pi(2j+3)q}{2N}\right) + \cos\left(\frac{\pi(2j-1)q}{2N}\right)\right) \qquad \text{(A.4)} \\ &= \hat{f}_{p,q} \cos\left(\frac{\pi(2i+1)p}{2M}\right) \cos\left(\frac{\pi(2j+1)q}{2N}\right)\,, \end{aligned}$$

for all $0 \leq p \leq M-1$ and $0 \leq q \leq N-1$. We can rewrite (A.3) and (A.4) to

$$-\frac{2}{h_x}\hat{u}_{p,q}\cos\left(\frac{\pi(2i+1)p}{2M}\right)\cos\left(\frac{\pi(2j+1)q}{2N}\right)\cos\left(\frac{\pi p}{M}\right)$$

and

$$-\frac{2}{h_y}\hat{u}_{p,q}\cos\left(\frac{\pi(2i+1)p}{2M}\right)\cos\left(\frac{\pi(2j+1)q}{2N}\right)\cos\left(\frac{\pi q}{N}\right),$$

due to the addition theorem $\cos(x \pm y) = \cos(x)\cos(y) \mp \sin(x)\sin(y)$. By defining

$$\hat{h}_{p,q} := 4\left(\left(\frac{\sin\left(\frac{\pi p}{2M}\right)}{h_x}\right)^2 + \left(\frac{\sin\left(\frac{\pi q}{2N}\right)}{h_y}\right)^2\right) \tag{A.5}$$

we obtain an equivalent represantation for (A.2) as

$$\hat{u}_{p,q} = \frac{\hat{f}_{p,q}}{\hat{h}_{p,q}}, \tag{A.6}$$

due to the relation $\cos(2x) = 1 - 2\sin^2(x)$. In analogy to the computations above the Laplace inversion can also be done for n-dimensional data, the only difference is that (A.5) changes to

$$\hat{h}_{\mathbf{p}} = 4\sum_{k=1}^{n}\left(\frac{\sin\left(\frac{\pi p_k}{2M_k}\right)}{h_k}\right)^2,$$

with M_k being the k-th dimension, h_k being the stepsize in the k-th dimension and with $\mathbf{p}$ denoting a multiindex that satisfies $0 \leq p_k \leq M_k - 1$, for all $k \in \{1, \ldots, n\}$.

A computational issue with (A.6) is that we have to divide by zero at $(p, q) = 1$. But usually, as we have seen in Chapter 8, Laplace inversions arise from optimality conditions of the form

$$(I - \delta\Delta)\, u = f\,. \tag{A.7}$$

With B denoting the cosine transform operator, we can rewrite this equation to

$$\begin{aligned} Bu - \delta B\Delta u &= Bf \\ Bu + \delta(Bu)\hat{h} &= Bf \\ u &= B^*\left(\frac{Bf}{1+\delta\hat{h}}\right), \end{aligned}$$

which is completely unproblematic to solve. Moreover, computing a discrete approximation of (A.7) by using the Bilaplace operator $\Delta\Delta$ instead of the Laplace operator Δ (with Neumann boundary conditions) can simply be done via

$$u = B^*\left(\frac{Bf}{1+\delta\hat{h}^2}\right).$$

Bibliography

[1] H. W. Alt. *Lineare Funktionalanalysis*. Springer, Berlin, 1999. 35

[2] W. Alt. *Nichtlineare Optimierung*. Vieweg, 2002. 131

[3] K. Arrow, L. Hurwicz, and H. Uzawa. *Studies in Linear and Non-Linear Programming*, volume 2 of *Stanford Mathematical Studies in the Social Sciences*. Stanford University Press, Stanford, California, 1958. With contributions by H. B. Chenery, S. M. Johnson, S. Karlin, T. Marschak, R. M. Solow. 135

[4] G. Aubert and J.-F. Aujol. A variational approach to remove multiplicative noise. *SIAM J. Appl. Math.*, 68:925–946, 2008. 74

[5] J.-F. Aujol, G. Aubert, L. Blanc-Féraud, and A. Chambolle. Image decomposition into a bounded variation component and an oscillating component. *Journal of Mathematical Imaging and Vision*, 22(1):71–88, January 2005. 69

[6] J.-F. Aujol and A. Chambolle. Dual norms and image decomposition models. *Journal of Computer Vision*, 63(1):85–104, 2005. 69

[7] A. Banerjee, S. Merugu, I. S. Dhillon, and J. Ghosh. Clustering with bregman divergences. *Journal of Machine Learning Research*, 6:1705–1749, 2005. 17, 58

[8] M. Benning and M. Burger. Error estimates for general fidelities. *Electronic Transactions on Numerical Analysis*, 38:44–68, 2011. 77

[9] M. Benning, P. Heins, and M. Burger. A solver for dynamic pet reconstruction based on forward-backward splitting. In *AIP ICNAAM Conference Proceedings*, pages 1967–1970, 2010. 184

[10] M. Benning, T. Kösters, F. Wübbeling, K. P. Schäfers, and M. Burger. A nonlinear variational method for improved quantification of myocardial blood flow using dynamic h215o pet. *IEEE Nuclear Science Symposium Conference Record*, pages 4472–4477, 2008. 172, 181, 182

[11] S. R. Bergmann, K. A. Fox, and A. L. Rand. Quantification of regional myocardial blood flow in vivo with h215o. *Circulation*, 70:724–733, 1984. 181, 182

[12] R. L. Bishop and S. I. Goldberg. *Tensor Analysis on Manifolds*. Dover Publications, December 1980. 35, 41

[13] S. Bonettini and T. Serafini. Nonnegatively constrained image deblurring with an inexact interior point method. *Journal of Computational and Applied Mathematics*, 231:236–248, 2009. 134

[14] S. Bonettini, R. Zanella, and L. Zanni. A scaled gradient projection method for constrained image deblurring. *Inverse Problems*, 25(1), 2009. 015002 doi:10.1088/0266-5611/25/1/015002. 134

[15] J. M. Borwein and A. S. Lewis. *Convex Analysis and Nonlinear Optimization: Theory and Examples (CMS Books in Mathematics)*. Springer, 2nd edition, November 2005. 49

[16] N. Boussion, C. Cheze Le Rest, M. Hatt, and D. Visvikis. Incorporation of wavelet-based denoising in iterative deconvolution for partial volume correction in whole-body pet imaging. *Eur J Nucl Med Mol Imaging*, 2009. DOI 10.1007/s00259-009-1065-5. 177

[17] S. Boyd and L. Vandenberghe. *Convex Optimization*. Cambridge University Press, March 2004. 49

[18] K. Bredies, K. Kunisch, and T. Pock. Total generalized variation. *SIAM Journal on Imaging Sciences*, 3(3):492–526, 2010. 35, 41, 69, 70, 111

[19] K. Bredies and H. K. Pikkarainen. Inverse problems in spaces of measures. Technical report, University Graz, November 2010. SFB-Report No. 2010-037. 67, 68

[20] L.M. Bregman. The relaxation method for finding the common point of convex sets and its application to the solution of problems in convex programming. *USSR Comp. Math. Math. Phys.*, 7:200–217, 1967. 55, 77

[21] C. Brune. *4D Imaging in Tomography and Optical Nanoscopy*. PhD thesis, University of Münster, Germany, July 2010. Reviewer: Prof. Dr. Martin Burger, Prof. Dr. Stanley Osher. 74, 132, 133, 137, 140, 178

[22] C. Brune, A. Sawatzky, F. Wübbeling, T. Kösters, and M. Burger. Forward backward em-tv methods for inverse problems with poisson noise. unpublished, 2011. 132, 133

[23] M. Burger. A note on sparse reconstruction methods. *J. Phys. Conference Series*, 2008. 012002. 55

[24] M. Burger and C. Brune. Variationsmethoden in der Biomedizinischen Bildgebung, 2010. Lecture Notes. 51

[25] M. Burger, K. Frick, S. Osher, and O. Scherzer. Inverse total variation flow. *SIAM Multiscale Modelling and Simulation*, 6:366–395, 2007. 55, 61

[26] M. Burger, G. Gilboa, S. Osher, and J. Xu. Nonlinear inverse scale space methods. *Comm. Math. Sci.*, 4:179–212, 2006. 55, 61

[27] M. Burger, M. Möller, M. Benning, and S. Osher. An adaptive inverse scale space method for compressed sensing. CAM Report 11-08, UCLA, 2011. 129, 142

[28] M. Burger and S. Osher. Convergence rates of convex variational regularization. *Inverse Problems*, 20:1411–1421, 2004. 55, 59, 77, 85, 86

[29] M. Burger and S. Osher. A guide to tv zoo 1: Models and analysis. In *Level Set and PDE-based Reconstruction Methods*. Springer, 2011. To appear. 35, 68

[30] M. Burger, E. Resmerita, and L. He. Error estimation for bregman iterations and inverse scale space methods in image restoration. *Computing*, 81:109–135, 2007. 55, 59, 60, 61, 62, 77, 85

[31] M. Burger, C. Schönlieb, and L. He. Cahn-hilliard inpainting and a generalization to gray-value images. *SIAM J. Imaging Sciences*, 2:1129–1167. 55, 77

[32] J. Cai, S. Osher, and Z.Shen. Convergence of the linearized bregman iteration for ℓ^1-norm minimization. *Math. Comp.*, 78:2127–2136, 2009. 55, 59

[33] J. Cai, S. Osher, and Z.Shen. Linearized bregman iterations for compressed sensing. *Math. Comp.*, 78:1515–1536, 2009. 55, 59

[34] E. J. Candes and T. Tao. Decoding by linear programming. *IEEE Transactions on Information Theory*, 51(12):4203–4215, December 2005. 66, 148

[35] E. J. Candes and T. Tao. Near-optimal signal recovery from random projections: universal encoding strategies? *IEEE Transactions on Information Theory*, 52(12):5406–5425, December 2006. 66

[36] R. E. Carson and K. Lange. A statistical model for positron emission tomography. *Journal of the American Statistical Association*, 80(389):20–22, 1985. 183

[37] A. Chambolle. An algorithm for total variation minimization and applications. *Journal of Mathematical Imaging and Vision*, 20:89–97, 2004. 138

[38] A. Chambolle and P.-L. Lions. Image recovery via total variation minimization and related problems. *Numerische Mathematik*, 76:167–188, 1997. 69

[39] R. Chan, C. Ho, and M. Nikolova. Salt-and-pepper noise removal by median-type noise detector and detail-preserving regularization. *IEEE Trans. on Image Processing*, 14(10):1479–1485, October 2005. 72

[40] T. F. Chan and S. Esedoglu. Aspects of total variation regularized l^1 function approximation. *SIAM J. Appl. Math.*, 65:1817–1837, 2005. 72

[41] C. Chaux, J.-C. Pesquet, and N. Pustelnik. Nested iterative algorithms for convex constrained image recovery problem. *SIAM Journal on Imaging Sciences*, 2(2):730–762, June 2009. 134

[42] M. Dawood, F. Büther, N. Lang, O. Schober, and K. P. Schäfers. Respiratory gating in positron emission tomography: A quantitative comparision of different gating schemes. *Med Phys*, 34(7):3067–3076, 2007. 177

[43] M. Dawood, T. Kösters, M. Fieseler, F. Büther, X. Jiang, F. Wübbeling, and K. P. Schäfers. Motion correction in respiratory gated cardiac pet/ct using multi-scale optical flow. LNCS. 177

[44] M. Dawood, N. Lang, X. Jiang, and K. P. Schäfers. Lung motion correction on respiratory gated 3d pet/ct images. *IEEE Trans Med Imaging*, 25(4):476–485, 2006. 177

[45] M. Defrise, P. E. Kinahan, D. W. Townsend, C. Michel, M. Sibomana, and D. F. Newport. Exact and approximate rebinning algorithms for 3-d pet data. *IEEE Transactions on Medical Imaging*, 16(2):145–158, April 1997. 177

[46] M. Defrise and X. Liu. A fast rebinning algorithm for 3d positron emission tomography using john's equation. *Inverse Problems*, 15(4), 1999. 1047 doi: 10.1088/0266-5611/15/4/314. 177

[47] D. L. Donoho. Compressed sensing. *IEEE Transactions on Information Theory*, 52(4):1289–1306, April 2006. 65, 66

[48] D. L. Donoho and M. Elad. Optimally sparse representation in general (nonorthogonal) dictionaries via l-minimization. *PNAS*, 100(5):2197–2202, March 2003. 66

[49] P. P. B. Eggermont. Maximum entropy regularization for fredholm integral equations of the first kind. *SIAM J. Math. Anal.*, 24:1557–1576, 1993. 77

[50] I. Ekeland and R. Temam. *Convex analysis and variational problems*. Corrected Reprint Edition. SIAM, 1999. 32, 46, 48, 49, 53, 152

[51] H. W. Engl, M. Hanke, and A. Neubauer. *Regularization of Inverse Problems*. Kluwer Academic Publishers, paperback edition 2000 edition, 1996. 29, 77

[52] E. Esser. Applications of lagrangian-based alternating direction methods and connections to split bregman. Technical report, UCLA, April 2009. CAM Report 09-31. 137

[53] E. Esser. *Primal Dual Algorithms for Convex Models and Applications to Image Restoration, Registration and Nonlocal Inpainting*. PhD thesis, UCLA, Department of Mathematics, June 2010. 137

[54] E. Esser, X. Zhang, and T. Chan. A general framework for a class of first order primal-dual algorithms for tv minimization. Technical report, UCLA, August 2009. CAM Report 09-67. 137

[55] A.G. Fakeev. A class of iterative processes for solving degenerate systems of linear algebraic equations. *USSR Computational Mathematics and Mathematical Physics*, 21:15–22, 1981. 55

[56] O. Forster. *Analysis III: Integralrechnung im $\mathbb{R}^n$ mit Anwendungen*. Vieweg, 1981. 33

[57] M. Fortin and R. Glowinski. Augmented lagrangian methods: Applications to the numerical solution of boundary-value problems. In *Studies in Mathematics and its Applications*. Elsevier Science Publishers B.V., Amsterdam, 1983. 135

[58] R. Glowinski and P. Le Tallec. *Augmented Lagrangian and Operator-Splitting Methods in Nonlinear Mechanics*. SIAM, Studies in Applied Mathematics, 1989. 135

[59] T. Goldstein and S. Osher. The split bregman method for l1-regularized problems. *SIAM J. Imaging Sci.*, 2:323–343, 2009. 55, 137

[60] T. Goldstein and S. Setzer. High-order methods for basis pursuit. Technical report, UCLA, July 2010. CAM Report 10-41. 131

[61] M. Grasmair. The equivalence of the taut string algorithm and bv-regularization. *Journal of Mathematical Imaging and Vision*, 27:59–66, 2007. 10.1007/s10851-006-9796-4. 103

[62] G. T. Gullberg, B. W. Reutter, A. Sitek, J. S. Maltz, and T. F. Budinger. Dynamic single photon emission computed tomographybasic principles and cardiac applications. *Physics in Medicine and Biology*, 55(20):R111, 2010. 178

[63] J. Hadamard. Sur les problèmes aux dérivés partielles et leur signification physique. *Princeton University Bulletin*, 13:49–52, 1902. 28

[64] W. Han, W. Cong, and G. Wang. Mathematical theory and numerical analysis of bioluminescence tomography. *Inverse Problems*, 22:1659–1675, 2006. 190

[65] Z. T. Harmany, R. F. Marcia, and R. M. Willett. This is spiral-tap: Sparse poisson intensity reconstruction algorithms - theory and practice. *IEEE Transactions on Image Processing*, 2010. Submitted, arXiv:1005.4274v1. 134

[66] M. R. Hestenes. Multiplier and gradient methods. *Journal of Optimization Theory and Applications*, 4:303–320, 1969. 135

[67] M. Hinze, R. Pinnau, M. Ulbrich, and S. Ulbrich. *Optimization with PDE Constraints*. Mathematical Modelling: Theory and Applications Volume 23. Springer, Netherlands, 2009. 27, 35

[68] B. Hofmann, B. Kaltenbacher, C. Pöschl, and O. Scherzer. A convergence rates result for tikhonov regularization in banach spaces with non-smooth operators. *Inverse Problems*, 23:987–1010, 2007. 55, 77

[69] Y. M. Huang, M. K. Ng, and Y. W.Wen. A new total variation method for multiplicative noise removal. *SIAM J. Imaging Sciences*, 2:20–40, 2009. 74

[70] H. Iida, I. Kanno, A. Takahashi, S. Miura, M. Murakami, K. Takahashi, Y. Ono, F. Shishido, A. Inugami, and N. Tomura. Measurement of absolute myocardial blood flow with h215o and dynamic positron-emission tomography. strategy for quantification in relation to the partial-volume effect [published erratum appears in circulation 1988 oct;78(4):1078]. *Circulation*, 78(1):104–115, 1988. 181, 182

[71] K. Ito and K. Kunisch. An active set strategy based on the augmented lagrangian formulation for image restoration. *M2AN Math. Model. Numer. Anal.*, 33(1):1–21, 1999. 137

[72] K. Ito and K. Kunisch. *Lagrange Multiplier Approach to Variational Problems and Applications*, volume 15 of *Advances in Design and Control*. SIAM, Philadelphia, PA, 2008. 135

[73] H. Jarchow. *Locally Convex Spaces*. Teubner, Stuttgart, 1981. 38

[74] Z. Jin and X. Yang. A variational model to remove the multiplicative noise in ultrasound images. *J. Math. Imaging Vis.*, 39:62–74, 2011. 75

[75] J. Jost. *Postmodern Analysis*. Springer, Berlin, 1998. 35

[76] M. Jung, E. Resmerita, and L. A. Vese. Dual norm based iterative methods for image restoration. Technical report, UCLA, 2009. CAM Report 09-88. 74

[77] M. E. Kamasak, C. A. Bouman, E. D. Morris, and K. Sauer. Direct reconstruction of kinetic parameter images from dynamic pet data. *IEEE Transactions on Medical Imaging*, 24:636–650, 2005. 183

[78] J. T. King and D. Chillingworth. Approximation of generalized inverses by iterated regularization. *Numerical Functional Analysis and Optimization*, 1:499–513, 1979. 55

[79] K.C. Kiwiel. Proximal minimization methods with generalized bregman functions. *SIAM J. Cont. Optim.*, 35:1142–1168, 1997. 77

[80] F. Knoll, K. Bredies, T. Pock, and R. Stollberger. Second order total generalized variation (tgv) for mri. *Magnetic Resonance in Medicine*, 65(2):480–491, 2011. 69

[81] T. Kösters. *Derivation and analysis of scatter correction algorithms for quantitative positron emission tomography.* PhD thesis, University of Münster, 2010. 177

[82] K. Krissian, R. Kikinis, C. F. Westin, and K. Vosburgh. Speckleconstrained filtering of ultrasound images. *IEEE Comput. Vis. Pattern Recogn.*, pages 547–552, 2005. 74

[83] A. V. Kryanev. An iterative method for solving incorrectly posed problems. *USSR Computational Mathematics and Mathematical Physics*, 14:24–33, 1974. 55

[84] D. A. Lorenz. Convergence rates and source conditions for tikhonov regularization with sparsity constraints. *J. Inverse Ill-Posed Problems*, 16:463–478, 2008. 55, 77

[85] D. A. Lorenz, S. Schiffler, and D. Trede. Beyond convergence rates: Exact inversion with tikhonov regularization with sparsity constraints. 2010. submitted for publication. 142

[86] D. A. Lorenz and D. Trede. Optimal convergence rates for tikhonov regularization in besov scales. *Inverse Problems*, 24, 2008. 055010. 55, 77

[87] Y. Lu, X. Zhang, A. Douraghy, D. Stout, J. Tian, T. F. Chan, and A. F. Chatziioannou. Source reconstruction for spectrally-resolved bioluminescence tomography with sparse a priori information. *Opt. Express*, 17:8062–8080, 2009. 192, 193, 195

[88] S. G. Mallat and Z. Zhang. Matching pursuits with time-frequency dictionaries. *IEEE Transactions on Signal Processing*, 12:3397–3415, 1993. 129, 141

[89] P. J. Markiewicz et al. High accuracy multiple scatter modelling for 3d whole body pet. *Phys Med Biol*, 52:829–847, 2007. 177

[90] Y. Meyer. *Oscillating patterns in image processing and nonlinear evolution equations.* The Fifteenth Dean Jacquelines B. Lewis Memorial Lectures. American Mathematical Society, 2001. 73, 113

[91] J. Müller. Parallel total variation minimization. Diploma thesis, University of Münster, WWU, November 2008. 50, 134, 138, 140, 152

[92] F. Natterer and F. Wübbeling. *Mathematical Methods in Image Reconstruction.* SIAM, 2001. 73, 132, 177, 190

[93] D. Needell, J. A. Tropp, and R. Vershynin. Greedy signal recovery review. *Proc. 42nd Asilomar Conf. Signals, Systems and Computers*, 2008. 168

[94] A. Neubauer. On converse and saturation results for tikhonov regularization of linear ill-posed problems. *SIAM J. Numer. Anal.*, 34:517–527, 1997. 87

[95] S. Osher, M. Burger, D. Goldfarb, J. Xu, and W. Yin. An iterative regularization method for total variation based image restoration. *Multiscale Model. and Simul.*, 4:460–489, 2005. 55, 59, 60

[96] Y. C. Pati, R. Rezaiifar, and P. S. Krishnaprasad. Orthogonal matching pursuit: Recursive function approximation with applications to wavelet decomposition. *Proceedings of the 27 th Annual Asilomar Conference on Signals, Systems, and Computers*, pages 40–44, 1993. 129, 141

[97] C. Pöschl. *Tikhonov Regularization with General Residual Term.* PhD thesis, Leopold-Franzens-Universität Innsbruck, Austria, October 2008. 77

[98] M. J. D. Powell. A method for nonlinear constraints in minimization problems. In *Optimization*, pages 283–298, New York, 1969. Academic Press London. 135

[99] N. Pustelnik, C. Chaux, and J.-C. Pesquet. Parallel proximal algorithm for image restoration using hybrid regularization. *IEEE Transactions on Image Processing*, 2011. Accepted. 134

[100] N. Pustelnik, C. Chaux, J.-C. Pesquet, and C. Comtat. Parallel algorithm and hybrid regularization for dynamic pet reconstruction. In *IEEE Medical Imaging Conference*, Knoxville, Tennessee, 30, Oct - 6, Nov. 2010. 5p. 134

[101] A. Rahmim, Y. Zhou, and D. F. Wong. Direct 4d parametric image reconstruction with plasma input and reference tissue models in reversible binding imaging. *IEEE Nuclear Science Symposium Conference Record*, pages 2516–2522, 2009. 183

[102] A. J. Reader, J. C. Matthews, F. C. Sureau, C. Comtat, R. Trébossen, and I. Buvat. Fully 4d image reconstruction by estimation of an input function and spectral coefficients. *IEEE Nuclear Science Symposium Conference Record*, pages 3260–3267, 2007. 171, 183

[103] A. J. Reader, F. C. Sureau, C. Comtat, R. Trébossen, and I. Buvat. Joint estimation of dynamic pet images and temporal basis functions using fully 4d ml-em. *Physics in Medicine and Biology*, 51(21):5455–5474, 2006. 183

[104] M. Renardy and R. C. Rogers. *An Introduction to Partial Differential Equations.* Springer, Berlin, 1993. 35

[105] E. Resmerita. Regularization of ill-posed problems in banach spaces: Convergence rates. *Inverse Problems*, 21(4):1303, 2005. 78, 82, 83, 84

[106] E. Resmerita and R. S. Anderssen. Joint additive kullback-leibler residual minimization and regularization for linear inverse problems. *Mathematical Methods in the Applied Sciences*, 30(13):1527–1544, 2007. 74

[107] E. Resmerita and O. Scherzer. Error estimates for non-quadratic regularization and the relation to enhancing. *Inverse Problems*, 22:801–814, 2006. 55, 77

[108] R. T. Rockafellar. *Convex Analysis (Princeton Mathematical Series).* Princeton University Press. 46, 49

[109] R. T. Rockafellar and R. J. B. Wets. *Variational Analysis.* Springer-Verlag, New York, 1997. 49

[110] L. Rudin, S. Osher, and E. Fatemi. Nonlinear total variation based noise removal algorithms. *Physica D*, 60:259–268, 1992. 55, 68

[111] A. Sawatzky, C. Brune, F. Wübbeling, T. Kösters, K. P. Schäfers, and M. Burger, editors. *Accurate EM-TV Algorithm in PET with Low SNR*, 2008 IEEE Nuclear Science Symposium Conference Record, November 2008. DOI: 10.1109/NSSMIC.2008.4774392. 132, 133

[112] K. P. Schäfers, T. J. Spinks, P. G. Camici, P. M. Bloomfield, C. G. Rhodes, M. P. Law, C. S. R. Baker, and O. Rimoldi. Absolute quantification of myocardial blood flow with h215o and 3-dimensional pet: An experimental validation. *J Nucl Med*, 43(8):1031–1040, 2002. 181

[113] O. Scherzer, M. Grasmair, H. Grossauer, M. Haltmeier, and F. Lenzen. *Variational Methods in Imaging (Applied Mathematical Sciences)*. Springer, 1 edition, October 2008. 35

[114] O. Scherzer and C. Groetsch. Inverse scale space theory for inverse problems. In M. Kerckhove, editor, *Scale-space and morphology in computer vision*, Proc. 3rd Int. Conf. Scale-space, pages 317–325, Berlin, 2001. Springer. 61

[115] S. Setzer. *Splitting methods in image processing*. PhD thesis, University of Mannheim, 2009. 137

[116] S. Setzer. Operator splittings, bregman methods and frame shrinkage in image processing. *International Journal of Computer Vision*, 2010. Accepted. 137

[117] S. Setzer and G. Steidl. Variational methods with higher order derivatives in image processing. In M. Neamtu and L. L. Schumaker, editors, *Approximation XII*, pages 360–386, Brentwood, 2008. Nashboro Press. 69, 70

[118] S. Setzer, G. Steidl, and T. Teuber. Infimal convolution regularizations with discrete ℓ^1-type functionals. *Communications in Mathematical Sciences*, 9(3):797–872, 2011. 69, 70, 110, 111

[119] J. Shi and S. Osher. A nonlinear inverse scale space method for a convex multiplicative noise model. *SIAM Journal on Imaging Sciences*, 1(3):294–321, 2008. 74

[120] J. L. Starck, M. Elad, and D. L. Donoho. Image decomposition: separation from texture from piecewise smooth content. *IEEE Transactions on Image Processing*, 14(10):1570–1582, 2005. 69

[121] D. Trede. *Inverse problems with sparsity constraints: Convergence rates and exact recovery*. PhD thesis, University of Bremen, Germany, April 2010. 142

[122] J. A. Tropp. Just relax: Convex programming methods for identifying sparse signals in noise. *IEEE Trans. Inform. Theory*, 52:1030–1051, 2006. 148

[123] J. A. Tropp. Corrigendum in just relax: Convex programming methods for identifying sparse signals in noise. *IEEE Transactions on Information Theory*, 55(2):917–918, 2009. 148

[124] J. A. Tropp and A. C. Gilbert. Signal recovery from random measurements via orthogonal matching pursuit. *IEEE Trans. Inf. Theory*, 53:46554666, 2007. 129, 141

[125] C. R. Vogel and M. E. Oman. Iterative methods for total variation denoising. *SIAM J. Sci. Comput*, 17(1):227–238, 1996. 139

[126] G. Wang, W. Cong, D. Kumar, X. Qian, H. Shen, P. Sinn, E. Hoffman, G. McLennan, and M. Henry. In vivo mouse studies with bioluminescence tomography. *Optics Express*, 14:7801–7809, 2006. 190

[127] G. Wang, W. Cong, H. Shen, X. Qian, M. Henry, and Y. Wang. Overview of bioluminescence tomography-a new molecular imaging modality. *Frontiers in Bioscience*, 13:1281–1293, 2008. 190

[128] G. Wang, E. A. Hoffman, G. McLennan, L. V. Wang, M. Suter, and J. F. Meinel. Development of the first bioluminescence ct scanner. *Radiology*, 566:229, 2003. 190

[129] G. Wang, Y. Li, and M. Jiang. Uniqueness theorems in bioluminescence tomography. *Med. Phys.*, 31:2289–2299, 2004. 190

[130] C. C. Watson. New, faster, image-based scatter correction for 3d pet. *IEEE TNS*, 47(4):1587–1594, 2000. 177

[131] M. N. Wernick and J. N. Aarsvold. *Emission Tomography: The Fundamentals of PET and SPECT*. Academic Press, 2004. 178

[132] J. Wloka. *Funktionalanalysis und ihre Anwendungen*. De Gruyter, 1971. 35

[133] C. Wu, J. Zhang, and X. Tai. Augmented lagrangian method for total variation restoration with non-quadratic fidelity. Technical report, UCLA, October 2009. CAM Report 09-82. 72, 137

[134] J. Yan, B. Planeta-Wilson, and R. E. Carson. Direct 4d list mode parametric reconstruction for pet with a novel em algorithm. *IEEE Nuclear Science Symposium Conference Record*, pages 3625–3628, 2008. 183

[135] J. Yan, B. Planeta-Wilson, J. D. Gallezot, and R. E. Carson. Initial evaluation of direct 4d parametric reconstruction with human pet data. *IEEE Nuclear Science Symposium Conference Record*, pages 2503–2506, 2009. 183

[136] W. Yin, S. Osher, D. Goldfarb, and J. Darbon. Bregman iterative algorithms for ℓ^1-minimization with applications to compressed sensing. *SIAM J. Imaging Sci.*, 1:143–168, 2008. 55, 59

[137] K. Yosida. *Functional Analysis*. Springer, Berlin, 1980. 35

[138] E. Zeidler. *Nonlinear Functional Analysis and Its Applications III: Variational Methods and Optimization*. Springer, 1984. 34

[139] X. Zhang, M. Burger, X. Bresson, and S. Osher. Bregmanized nonlocal regularization for deconvolution and sparse reconstruction. Technical report, UCLA, January 2009. CAM Report 09-03. 137

[140] X. Zhang, M. Burger, and S. Osher. A unified primal-dual algorithm framework based on bregman iteration. Technical report, UCLA, November 2009. CAM Report 09-99. 137